Gradient-Constrained Flow-Dependent Networks for Underground Mine Design

Marcus Volz

Submitted in total fulfilment of the requirements of the degree of

Doctor of Philosophy

Department of Electrical and Electronic Engineering
THE UNIVERSITY OF MELBOURNE

August 2008

Abstract

A NETWORK is called *gradient-constrained* if the absolute value of the instantaneous gradient at each differentiable point on the edges in the network is no more than a given positive constant [13]. A *flow-dependent* network is a network in which flow demands are assigned between given pairs of vertices, and the cost per unit length of an edge in the network is a function of the total flow through the edge [34].

An application of gradient-constrained flow-dependent networks is to underground mine design. In an underground mining operation, ore is extracted from fixed underground points, called *draw points*, and transported to a common facility, such as the base of a vertical hoisting shaft or a fixed portal at the surface. The set of tunnels interconnecting the draw points and the facility can be modelled by a mathematical network, where the draw points correspond to fixed vertices and the tunnels correspond to edges. The gradient constraint ensures that a tunnel is navigable by haulage trucks, since the maximum grade at which these vehicles can operate is typically 1:7.

Fundamental properties of *length-minimising* gradient-constrained networks have been well-studied [13]. Properties of *flow-dependent* networks subject to the gradient constraint are, however, less well understood, and in this work we provide a thorough treatment of such networks. Two problems are considered: the *Fermat-Weber problem*, which asks for a point minimising the sum of weighted distances to a set of given points, and the *Gilbert arborescence problem*, which asks for a minimum-cost flow-dependent network interconnecting given sources and a unique sink.

Initially, we investigate flow-dependent networks in two settings without the gradient constraint. First, we examine networks in Euclidean space. Euclidean networks provide valuable insights into gradient-constrained networks, and are applicable to un-

derground mining in their own right. Second, we explore flow-dependent networks in *Minkowski spaces*, which are real finite-dimensional normed spaces. The importance of studying networks in Minkowski spaces is made apparent by the connection that a gradient-constrained network is a special example of a network in a Minkowski space.

We demonstrate the application of flow-dependent networks to underground mining via an industry case study, in which aspects from the Fermat-Weber problem and the Gilbert arborescence problem are used to mathematically determine an optimum location and depth of a vertical hoisting shaft in the Callie underground mine.

Declaration

This is to certify that

1. the thesis comprises only my original work towards the PhD,
2. due acknowledgement has been made in the text to all other material used,
3. the thesis is less than 100,000 words in length, exclusive of tables, maps, bibliographies and appendices.

Marcus Volz, August 2008

Acknowledgements

First and foremost, I thank my supervisors Doreen Thomas and Marcus Brazil. From the beginning of my PhD candidature, when they proposed the topic which forms the basis of this research, through to submission of the thesis, they provided invaluable advice and encouragement and always set aside time for weekly meetings.

For their comments and advice I thank other members of the Network Research Group: Peter Grossman, David Lee, Hyam Rubinstein, Jia Weng and Nick Wormald. The group's collective research provided a solid basis on which to formulate a meaningful body of work, and their software product UNO provided a valuable tool for studying gradient-constrained networks.

I thank Newmont Australia Limited and the Australian Research Council for their joint sponsorship of my research via an ARC Linkage Grant. I also thank Newmont for suggesting and formulating the Callie shaft location study, which forms an integral part of this thesis. A simplified version of study was originally proposed by Steven Harvey, and the detailed investigation was proposed and commissioned by Andrew Fox and Ian Suckling. I thank Robert Parr and Nadine Wetzel for their time and effort collecting and preparing data and for their constructive feedback.

The appearance and layout of this thesis is based largely on the excellent template designed and developed by John Papandriopoulos. I also thank Dawn Volz for her careful review of the thesis for grammar and style. Finally, I thank my partner Rebekah for her constant support and encouragement.

Contents

List of Figures

List of Tables

Chapter 1
Introduction

MINING is a significant industry worldwide. Reducing the cost of mining operations is an important issue for mining companies in an extremely competitive marketplace. For many years there have been well-developed methods for modelling and optimising the operation of open-cut mines. Commercial optimisation mine planning software packages have been developed based on a technique developed in 1965 by Lerchs and Grossmann [57]. These packages have revolutionised the design of open-pit mines, allowing mining engineers and planners to manipulate and visualise data associated with optimal designs.

Until recently, a comprehensive optimisation tool for the design and planning of underground mining operations had not been available to the mining industry. The design process is typically facilitated by planning software packages (see, for example, *Vulcan* [59]) which require high levels of user intuition and experience. The usefulness of these programs lies in their ability to efficiently generate a range of potential designs, from which the 'best' feasible solution can be selected and refined. However, since these programs do not harness the benefits of optimisation, there is no guarantee that the final solution is in fact the best possible one.

The *Network Research Group*, based at the University of Melbourne, is in the process of designing and developing an optimisation tool for the design of underground mines, called *Decline Optimisation Tool* (DOT). Currently at Version 4.1, with Version 4.2 in development, the application efficiently determines an optimal (least-cost) or near-optimal underground mining network servicing a given set of points associated with an ore body [7].

Several constraints are imposed on the geometry of the tunnels in the network, to

ensure that the tunnels are navigable by haulage trucks. One such constraint is that the slope (steepness or grade) of a tunnel cannot be too large, since the maximum grade at which haulage vehicles can operate is typically 1:7. A network satisfying this constraint is called *gradient-constrained*.

Gradient-constrained networks were introduced by the Network Research Group, who initially studied them in a vertical plane [17], and later in three dimensions [13]. An algorithm for computing least-cost gradient-constrained networks was implemented into a second software product [10], called *Underground Network Optimiser* (UNO). Although this application does not account for other practical constraints, such as truck turning circle navigability, UNO is especially useful for efficiently determining optimal layouts for large-scale mining networks where the effects of constraints other than the gradient constraint on the optimal layout of the mine are not significant.

Until recently, research on gradient-constrained networks has focused on networks which minimise length. While length-minimising networks optimise the total development (or infrastructure) cost associated with an underground mine, they do not account for the effects of haulage on the optimal design of the mine. Haulage costs can have a significant impact on the structure and layout of an underground mine, and considerable savings can be achieved by including both cost components in the objective function. A network facilitating flows between given pairs of vertices in the network is called a *flow-dependent network*. In the mining context, these networks incorporate both development and haulage costs in the objective function.

The principal aim of this research is to obtain a comprehensive understanding of minimum-cost gradient-constrained flow-dependent networks. In particular, we are interested in the geometric structures possible in such networks. These properties can play a crucial role in improving the efficiency of heuristic algorithms for computing gradient-constrained networks. Such improvements would be of great benefit to programs like DOT and UNO which, for large complex networks, have huge computational demands. Before formally introducing this research, we provide some background on the use of mathematical networks to model underground mines.

1.1 Underground mining networks

This background is taken primarily from [2]. An underground mine consists of a series of interconnecting tunnels, ore passes (near-vertical chutes down which ore is dropped) and vertical shafts (used to hoist ore up to the surface). Its purpose is to allow extraction of ore containing valuable minerals (such as gold, silver, lead, zinc and copper) from underground locations to a predetermined surface portal (or breakout point), from where it is transported to a processing mill.

Ore zones (or stopes) are identified by geological tests such as surface and infill drilling. From this information, mining engineers can determine suitable draw points, which are the locations on the boundary of each stope from which the ore is accessed. The ore is then excavated using a number of mining methods (such as stoping, caving, room and pillar, etc.) and is transported to the surface via large haulage trucks.

Given that these laden trucks must be able to traverse the ramps, the following important constraints must be imposed on the mine:

- Ramps must have absolute gradient not greater than some constant m. This constant is typically in the range 1:9 to 1:7 depending on equipment specifications.
- Ramps must satisfy a minimum turning radius (typically in the range 15-30 m), so that they are navigable by the trucks.
- Ramps must avoid certain no-go regions such as the interior of an ore body or other ramps in the mine.

A set of tunnels satisfying these constraints and interconnecting the draw points and a point at the surface can be modelled by a mathematical network T, where the draw points correspond to fixed vertices and the tunnels correspond to edges. The cost C associated with a network with a set E of edges is typically modelled by a function of the form

$$C(T) = \sum_{e \in E} (d + ht_e) l_e$$

where d is a development cost rate (typically \$3000/m), h is a haulage cost rate (typically \$0.75/t.km), t_e is the total quantity of ore to be transported along an edge e over the life of the mine, and l_e is the length of e. We can view the first term $\sum dl_e$ as the total development

cost of the mine, and the second component $\sum ht_e l_e$ as the total haulage cost associated with the mine over its life. If h is set to zero, then the cost of the network is proportional to its length, and a network with this objective function is a *length-minimising network*.

1.1.1 Networks applied to underground mine design

Until recently, only a few papers had investigated the use of network theory in underground mine design. Lizotte and Elbrond [58] reported an early application of network theory to some underground mine layout problems, but limited their work to network techniques in a horizontal plane. Brimberg [21] considered a network model to minimise the cost of an underground mine with a vertical hoisting shaft connected to ore deposits by a series of horizontal tunnels.

By far the most significant contribution to the use of network theory in underground mine design is by the Network Research Group. Their investigation of underground mining networks began in the late 1990s, although Lee [55] first raised the problem of setting up and optimising a three-dimensional network modelling the infrastructure costs of an underground mine layout in 1989. Since then, a significant body of research has been developed and implemented into the aforementioned software products, UNO and DOT. The following is a summary of this research to date.

- [2], [8], [9], [15], [18] A network optimisation model for minimising development and haulage costs in underground mines was first proposed. The possibility of modelling the haulage cost of an edge as a function of the slope of the edge was also facilitated in the cost function, and conditions under which the cost function is convex were discussed. Application of the model was demonstrated via a prototype network interconnecting draw points and a vertical hoisting shaft, and several case studies in which the model was applied to mines at Pajingo and Kanowna Belle.
- [17] The gradient-constrained Steiner problem (in a vertical plane) was introduced. The problem asks for a shortest network interconnecting a set of points, called *terminals*, in a vertical plane such that no part of the network has absolute gradient greater than a given positive constant m satisfying $m \leq 1$. Geometric structures

of these networks were used construct a finite algorithm for solving the problem which, when suitably discretised, was shown to be NP-complete.

- [13] The study of the gradient-constrained Steiner problem was extended to three dimensions. The *gradient metric* was introduced to measure the lengths of edges in gradient-constrained networks, and the terms *flat*, *maximum* and *bent* were introduced to label edges whose respective gradients are less than, equal to or greater than m. It was shown that a Steiner point, which is a vertex in the network not among the given set of terminals, has either three or four incident edges, and Steiner points were classified in terms of the labellings of their incident edges. The UNO software product was concurrently developed with this work.
- [16], [76] The terms *labelled-minimal* and *locally-minimal* were introduced to describe Steiner points for which a label-preserving perturbation and, respectively, *any* perturbation of the Steiner point, cannot shorten the length of the network. Properties of labelled-minimal Steiner points were studied, and necessary and sufficient conditions for Steiner points to be locally-minimal were obtained. A formula for computing labelled-minimal degree-three Steiner points was derived, and an algorithm for computing locally minimal Steiner points was developed.
- [63], [64] The *Steiner ratio* for gradient-constrained networks connecting three points in three dimensions was investigated. The Steiner ratio is the smallest ratio of the length of a Steiner tree to the length of a minimum spanning tree when the two networks interconnect the same set of given points. It was shown that this minimum ratio for gradient-constrained networks tends to 0.75 as the value of m tends to zero.
- [7], [10], [11], [74] A method for optimising *declines* in underground mines was developed, a decline being a gradient-constrained, turning-circle-constrained path connecting level access points to a surface portal while avoiding certain no-go regions. A procedure for finding an optimal decline was implemented into the DOT software product, which was applied to several case studies including a decline servicing the Jandam gold mine at Pajingo, and an access decline at Olympic Dam. The software was further developed to handle networks of declines.

The future direction of this expanding body of research focuses on integrating the use of network models, and the DOT software product, into the context of a complete mining operation, so that interactions with other aspects of the operation are modelled. This forms part of an *AMIRA International* research project called *Planning and Rapid Integrated Mine Optimisation* (PRIMO), in which the expertise of key researchers is pooled to develop complete integrated solutions to large mining projects with complex infrastructure.

1.1.2 Motivation for studying flow-dependent networks

While work undertaken by the Network Research Group has continued to progress with great success, there are aspects of the research that, until recently, had not received detailed attention. One area that was not well understood was the effect of weighted edges on the optimal design of gradient-constrained networks. Indeed, work undertaken in [13], [16], [17], [63], [64] and [76] has focused exclusively on length-minimising gradient-constrained networks, and other references have not addressed weighted networks specifically.

While UNO and DOT handle the effects of edge weights induced by flows, their underlying algorithms are based on properties of unweighted networks. It is expected that implementing properties of weighted networks into the algorithms will improve their computational performance, and this becomes an increasingly important consideration as the problem becomes more complex.

In this work our goal is to gain a comprehensive understanding of gradient-constrained flow-dependent networks. We do not consider the turning-circle constraint, or any of the other constraints incorporated into DOT. However, it is expected that results uncovered here can be implemented into the algorithms independently.

In our investigation of gradient-constrained flow-dependent networks, we consider two related problems. The first is the *Fermat-Weber problem*, which asks for a point minimising the sum of weighted distances to a set of given points. The second is the *Gilbert arborescence problem*, which asks for a minimum-cost flow-dependent network interconnecting given sources and a unique sink.

Initially, we investigate flow-dependent networks in two settings without the gra-

dient constraint. First, we examine networks in Euclidean space. Euclidean networks provide valuable insights into gradient-constrained networks, and are applicable to underground mining in their own right.

Second, we explore flow-dependent networks in *Minkowski spaces*, which are real finite-dimensional normed spaces. The importance of studying networks in Minkowski spaces is made apparent by the connection that a gradient-constrained network is a special example of a network in a Minkowski space. Moreover, by studying networks in Minkowski spaces, we introduce an approach not previously utilised in the study of gradient-constrained networks, since results to date have been obtained using the variational argument [67] and geometric techniques.

We now discuss each of the two problems in turn.

1.2 The Fermat-Weber problem

Part I of this thesis is dedicated to a famous problem of mathematics called the *Fermat-Weber problem* (FW problem). The problem asks for a point, called a *Fermat-Weber point* (FW point), minimising the sum of weighted distances to a set of given points. We introduce the *gradient-constrained FW problem*, which is the FW problem in which distance is measured by the gradient metric. The problem is formulated as follows:

- **GIVEN**: A set $N = \{p_1, \ldots, p_k\}$ of points in Euclidean space with respective positive weights $w_1, \ldots, w_k$, and a gradient bound m satisfying $0 < m \leq 1$.
- **FIND**: A point x_0 minimising the sum of weighted distances from x_0 to the points in N such that each distance is the minimum length of a piecewise-smooth curve whose gradient at each differentiable point is no more than m.

In the mining context, $p_1, \ldots, p_k$ represent draw points with associated tonnages $t_1, \ldots, t_k$. Material is hauled from the draw points via independent paths to the FW point, x_0, which might represent, for instance, the base of a vertical hoisting shaft. The total cost of the mine can be minimised by positioning the facility at an optimal location.

The weight on the path from p_i to x_0 is given by $w_i = d + ht_i$, where d and h are development and haulage cost rates respectively. Since the t_i can take on any value, there

are no restrictions on the values of the weights associated with the points in N. This is in contrast to the Gilbert arborescence problem described shortly, in which edge weights in the network satisfy certain implicit conditions resulting from the flow structure in the network.

Initially in Chapter 2, we examine the problem in Euclidean space. We provide a brief history of the problem, from its origin in the 17th century to the present, and state a known geometric characterisation of FW points [53], the characterisation being in terms of weighted unit vectors to the given points. We use this result to derive a geometric construction [85] for solving the three-point problem. We identify special instances of the FW problem that can be solved with very little computational effort, and present new results for the case where the given points form the vertices of a convex polygon and certain pairs of weights are equal.

We state Weiszfeld's famous algorithm [86] for solving the FW problem iteratively, and demonstrate its use via an example. We introduce a variation of the FW problem in the plane whereby one of the given points is allowed to lie anywhere on a straight line in the plane, and show how Weiszfeld's algorithm can be amended to suit this case. We demonstrate the application of this new problem to underground mining by using it to solve a subproblem of an industry case study presented in Chapter 9.

In Chapter 3, we investigate the FW problem in n-dimensional real normed spaces, or Minkowski spaces. Martini et al. [60] provided a minitheory of this problem for the case where all the weights equal one, and established a range of geometric results. Our main goal is to generalise some of these results to the weighted case. We provide background relating to Minkowski spaces and functional analysis, including a method for constructing the dual ball for a given unit ball. We state a known geometric characterisation of FW points in Minkowski spaces [31], the characterisation being in terms of weighted norming functionals associated with the given points.

We then provide several properties of the set of solutions to the FW problem, and identify special instances of the problem that can be solved exactly with very little computational effort. The notions of double-clusters, ρ-concurrent ρ-segments, collinear and cogeodesic sets are generalised to the weighted case, and corresponding theorems and

proofs are provided. Finally, we generalise a geometric result originally posed in [22] for the three-point unweighted problem, to the weighted case.

In Chapter 4, we formally introduce the gradient-constrained FW problem. We concentrate on two- and three-dimensional spaces, which are natural contexts for underground mining problems. We begin by outlining the gradient metric, deriving its unit ball and dual ball in two and three dimensions, and demonstrating how to compute the set of norming functionals associated with a point in gradient-constrained space. We then present an iterative scheme for solving the gradient-constrained FW problem numerically, and prove convergence for the two- and three-dimensional cases. Finally, we demonstrate the application of the problem to the optimal design of underground mines by using it to solve a simplified version of the case study presented in Chapter 9.

1.3 The Gilbert arborescence problem

Part II of this thesis is dedicated to the *Gilbert arborescence problem*, which asks for a minimum-cost flow-dependent network interconnecting given sources and a unique sink. The gradient-constrained version of the problem in three-space is formulated as follows:

- **GIVEN**: A set of points $N = \{p_1, \ldots, p_k\}$ in Euclidean three-space, where $p_1, \ldots, p_{k-1}$ are sources with respective positive flows $t_1, \ldots, t_{k-1}$, and p_k is a unique sink, a gradient bound satisfying $0 < m \leq 1$, and positive constants d and h.
- **FIND**: A minimum-cost network T interconnecting N which provides flow paths from the sources to the sink, such that the cost of an edge e in T is given by $(d + ht_e)l_e$, where t_e is the total flow through e, and l_e is the length of e under the gradient metric.

A network satisfying the above conditions is called a *minimum Gilbert arborescence* (MGA). Vertices in T not in N are called *Steiner points* and, as we will show, a Steiner point is an FW point with respect to its adjacent vertices in T. A key difference between the two problems is that a Steiner point s in a Gilbert arborescence has *source edges*, which are directed into s, and a unique *sink edge*, directed outward from s, whereas all incident paths connected to an FW point are directed toward that point.

As for the FW problem, we initially investigate the Gilbert arborescence problem in two settings without the gradient constraint. First, in Chapter 5, we examine the problem in Euclidean space. This problem has applications to drainage [56] and gas pipeline [4] networks. We present many new properties of MGAs, and provide a characterisation of the local structure of their Steiner points, generalising a known result for unweighted networks. We use this characterisation to investigate the maximum degree of Steiner points in MGAs in the Euclidean plane and in Euclidean three-space. We then briefly discuss how some known algorithms can be applied to the problem. In particular, we look at a generalised Melzak algorithm which provides exact solutions, and an angle-splitting heuristic for obtaining approximate solutions.

In Chapter 6, we study the Gilbert arborescence problem in Minkowski spaces. A geometric characterisation of Steiner points and terminals in MGAs in Minkowski spaces is established, generalising a result for Steiner minimum trees in such spaces [73]. We use these characterisations to derive additional geometric properties of MGAs in Minkowski spaces.

In Chapters 7 and 8, we study gradient-constrained MGAs in a vertical plane and in three dimensions. We provide many new geometric properties of gradient-constrained MGAs in a vertical plane and in three dimensions, and use these properties to provide a classification of Steiner points, extending work done in [13] for gradient-constrained SMTs. The classification of a Steiner point is in terms of the *labels* of its incident edges, a label indicating whether the absolute value of the gradient of the Euclidean straight line between the endpoints of an edge is less than, equal to, or greater than m. We show that the degree of a Steiner point in MGA in a vertical plane is either three or four, and we conjecture that there is no upper bound on the degree of a Steiner point in an MGA in three-space.

We conclude the thesis in Part III (Chapter 9) with an industry case study that draws on material presented in Parts I and II. In the case study, we examine the Callie underground mine, which is located in the Tanami Desert in the Northern Territory. It includes two parallel declines accessing a large orebody extending some two kilometres below the surface. As part of the strategic mine planning, it was proposed to incorporate a vertical

hoisting shaft and an ore pass as an alternative to trucking material to the surface along the declines.

We use network optimisation techniques developed in Parts I and II to investigate the feasibility of the proposed system, and to mathematically determine the optimum positions and geometry of the shaft, ore pass and surrounding infrastructure. We propose a modelling procedure taking aspects from the FW and Gilbert arborescence problems, and describe the implementation of the procedure into a computer program for solving the problem exactly. We present results over a range of infrastructure and haulage costs, decline gradients and life-of-mine schedules, and analyse the effects of changing various parameters on the optimal design of the mine.

We conclude the thesis in Chapter 10 by summarising the new contributions we have made to flow-dependent networks in Euclidean, Minkowski and gradient-constrained spaces. We also suggest some possible extensions of this work which would make good topics for future research.

In Appendix A we provide a list of mathematical symbols used throughout this thesis, and in Appendix B we provide some useful trigonometric identities relating maximum gradients and angles.

1.4 Summary of new contributions

In this section we list the new contributions of this thesis. Contributions are listed in order of appearance, with section numbers indicating where the point is first discussed in the thesis. Published, submitted and forthcoming papers are shown in parentheses.

1.4.1 The Fermat-Weber problem

Euclidean space

1. A new characterisation of Fermat-Weber points for collinear sets of given points is developed (Section 2.3).

2. New results are derived for the case where the given points form the vertices of a convex polygon, and certain pairs of weights are equal (Section 2.5).
3. A previously unstudied variant of the Fermat-Weber problem in the plane is introduced, whereby one of the given points is allowed to lie anywhere on an infinite line in the plane. The problem is applied to a subproblem of the Callie shaft location study (Section 2.7).

Minkowski spaces [84]

1. Practical methods are developed for determining the dual ball for a given unit ball (Section 3.2.1).
2. The term *balanced double cluster* is introduced to depict weighted sets of given points satisfying special properties. It is shown that if a Fermat-Weber point for a set N of given points lies outside the convex hull of N, then N is a balanced double cluster (Section 3.4.2).
3. The term *balanced concurrent segments* is introduced to depict weighted sets of given points satisfying special properties. It is shown that if a set N of given points can be matched up to form balanced concurrent segments, then the intersection of these segments is the set of Fermat-Weber points for N (Section 3.5.1).
4. The study of the Fermat-Weber problem for a given set of weighted *cogeodesic* points is initiated. A new characterisation of Fermat-Weber points for weighted collinear and cogeodesic sets is developed (Section 3.5.2).
5. A new geometric property of the solution to the weighted three-point problem in the plane is discovered (Section 3.6).

Gradient-constrained space [14], [84]

1. The *gradient-constrained Fermat-Weber problem* is introduced (Section 4.1).
2. For the first time, gradient-constrained space is treated as a Minkowski space. The unit ball, dual ball and dual norm are derived, and a practical method for determining sets of norming functionals is developed (Section 4.2).

3. A new gradient descent algorithm is developed for solving the problem iteratively. The algorithm is implemented into a software product (Section 4.3).
4. Convergence is proved for the two- and three-dimensional cases (Section 4.4).
5. The problem is applied to a simplified version of the Callie shaft location study (Section 4.5).

1.4.2 The Gilbert arborescence problem

Euclidean space [81]

1. A new title, the *Gilbert arborescence problem*, is given to the special case of the Gilbert network problem in which flows are from given sources to a unique sink. At present, this problem has been studied only in a handful of papers (Section 5.1).
2. It is shown that a minimum Gilbert arborescence has a tree topology, i.e. it has no cycles or crossing edges (Section 5.3).
3. Necessary and sufficient conditions for a Steiner point to be locally minimal with respect to its adjacent vertices are established (Section 5.4).
4. It is shown that the degree of all Steiner points in minimum Gilbert arborescences in the Euclidean plane is three (Section 5.5).
5. Good progress is made on proving the conjecture that the degree of Steiner points in minimum Gilbert arborescences in Euclidean three-space is three (Section 5.6).
6. Expressions for the optimum angles between edges incident to a Steiner point are determined. The notions of *critical and absorbing angles* are generalised to the Gilbert arborescence problem (Section 5.7).
7. Exact and approximate algorithms for solving the Gilbert arborescence problem in Euclidean space are discussed (Section 5.8).

Minkowski spaces [80]

1. The study of the Gilbert arborescence problem is in Minkowski spaces is initiated. (Section 6.1).

2. Concepts of parenthesisations, abstract Steiner trees and reduced Minkowski addition are generalised to the weighted case (Section 6.3).
3. Necessary and sufficient conditions for a terminal to be locally minimal with respect to its adjacent vertices are established (Section 6.4).
4. Necessary and sufficient conditions for a Steiner point to be locally minimal with respect to its adjacent vertices are established (Section 6.5).

Gradient-constrained vertical plane [82]

1. The *gradient-constrained Gilbert arborescence problem* (in a vertical plane) is introduced (Section 7.1).
2. A range of fundamental properties of gradient-constrained minimum Gilbert arborescences (in a vertical plane) is established. In particular, it is shown that the degree of Steiner points is either three or four (Section 7.3).
3. It is shown that a degree-three Steiner point has seven feasibly optimal labellings: (fff), (ffm), (ffb), (fmm), (fmb), (mmm) and (mmb) (Section 7.4).
4. It is shown that a degree-four Steiner point has three feasibly optimal labellings: (ffmm), (fmmm) and (mmmm) (Section 7.5).
5. The *reduced hull* of a set N of terminals is defined. It is shown that all Steiner points lie in the reduced hull of N (Section 7.6).

Gradient-constrained three-space [82]

1. The *gradient-constrained Gilbert arborescence problem* (in three-space) is introduced (Section 8.1).
2. A range of fundamental properties of gradient-constrained minimum Gilbert arborescences (in three-space) is established (Section 8.3).
3. It is shown that a degree-three Steiner point has seven feasibly optimal labellings: (fff), (ffm), (ffb), (fmm), (fmb), (mmm) and (mmb) (Section 8.4).
4. It is shown that a degree-four Steiner point has four feasibly optimal labellings: (fffm), (ffmm), (fmmm) and (mmmm) (Section 8.5).

5. It is shown that there is no upper bound on the degree of Steiner points (Section 8.6).

1.4.3 Callie shaft location study [83]

1. Aspects from the Fermat-Weber problem and the Gilbert arborescence problem are used to develop a network model for the Callie underground mine (Section 9.1).
2. An algorithm is developed to mathematically determine an optimum location and depth of a vertical hoisting shaft in the Callie underground mine. The algorithm is implemented into a software product. (Section 9.3).
3. Results are analysed over a range of infrastructure and haulage costs, decline gradients and life-of-mine schedules (Section 9.5).

Part I

The Fermat-Weber Problem

Introduction to Part I

IN Part I of this thesis we investigate the Fermat-Weber problem in three settings. First, in Chapter 2, we study the problem in its classical environment, Euclidean space. This is a good starting point as the Euclidean problem provides insight into the problem in other spaces. In particular, there exists a geometric characterisation of Fermat-Weber points that has a natural physical interpretation in terms of weighted vectors from the Fermat-Weber point to the given points. Moreover, the Euclidean problem is applicable to underground mining in its own right.

Next, in Chapter 3, we study the Fermat-Weber problem in *Minkowski spaces*, which are real finite-dimensional vector spaces. We show that the characterisation of Steiner points for the Euclidean case generalises to Minkowski spaces, where now the orientations and lengths of the vectors associated with the given points are determined by the unit ball and the dual ball associated with the space.

Finally, in Chapter 4, we introduce the *gradient-constrained Fermat-Weber problem*, which is the Fermat-Weber problem where distance is measured by the *gradient metric*. This metric ensures that the distance between two points is the minimum length of a piecewise smooth curve connecting the points such that the absolute value of the instantaneous gradient at each differentiable point on the curve is no more than a given upper bound. We show that the vectors associated with given points depend on the gradient of the line from the minimum point to the given point, and devise a numerical procedure for solving the problem iteratively.

Chapter 2

The Fermat-Weber Problem in Euclidean Space

In this chapter we investigate the Fermat-Weber problem, which asks for a point, called a Fermat-Weber point, minimising the sum of weighted distances to a set of given points in Euclidean space. We provide a brief history of the problem, from its origin in the 17th century to the present. We state a known geometric characterisation of Fermat-Weber points [53], the characterisation being in terms of weighted unit vectors to the given points. We use this result to derive a geometric construction [85] for solving the three-point problem. We identify special instances of the Fermat-Weber problem that can be solved with very little computational effort, and present new results for the case where the given points form the vertices of a convex polygon and certain pairs of weights are equal.

We state Weiszfeld's famous algorithm [86] for solving the Fermat-Weber problem iteratively, and demonstrate its use via an example. We introduce a variation of the Fermat-Weber problem in the plane whereby one of the given points is allowed to lie anywhere on a straight line in the plane, and show how Weiszfeld's algorithm can be amended to suit this case. We demonstrate the application of this new problem to underground mining by using it to solve a subproblem of an industry case study presented in Chapter 9.

2.1 Introduction

LET $N = \{p_1, \ldots, p_k\}$ be a set of given points in Euclidean n-space, and suppose that each point $p_i \in N$ has a given weight $w_i > 0$. Consider the following problem: find a point, $x_0 \in \mathbb{R}^n$, that minimises

$$f(x) = \sum_{i=1}^{k} w_i |p_i - x| \tag{2.1}$$

where $|\cdot|$ denotes the Euclidean norm. Although this problem has many variants and names, when used in the context of location theory it is often called the *Fermat-Weber problem* (FW problem)[1], and x_0 is called a *Fermat-Weber point* (FW point). The first name is that of Pierre de Fermat (1601-1665), who is thought to have first posed the problem in the 17th century [51] for the case where $k = 3$, $n = 2$ and $w_1 = w_2 = w_3 = 1$. The second name is that of Alfred Weber (1868-1958), who applied the problem to locate industries to minimise transportation costs [85].

The importance of the FW problem lies not only in the mathematical challenges it presents, but also in its application to practical problems in engineering, location theory and economics. One such application is to underground mining. Suppose we are given a number of fixed underground points, called *draw points*, from which ore is to be extracted. Mined material is to be trucked via tunnels from each draw point to a common underground facility, such as the base of a vertical shaft, before being hoisted to the surface. The development and haulage costs associated with the mine can be minimised by positioning the facility at an FW point.

While in practice additional constraints are required for the mining problem (most notably the gradient constraint, which will be discussed in detail in Chapter 4), the Euclidean problem is applicable in its own right, as demonstrated in Section 2.7. Moreover, properties of FW points are extremely important in Chapter 5, where we examine the more complex Gilbert arborescence problem in Euclidean space.

The structure of this chapter is as follows. In Section 2.2, we provide a brief history of the FW problem, from its origin in the 17th century to the present. Then in Section 2.3, we state a known geometric characterisation of FW points [53], the characterisation being in terms of weighted unit vectors to the given points. We use this result in Section 2.4 to derive a geometric construction [85] for solving the three-point problem. In Section 2.5 we identify special instances of the FW problem that can be solved with very little computational effort, and present new results for the case where the given points form the vertices of a convex polygon and certain pairs of weights are equal.

In Section 2.6 we state Weiszfeld's famous algorithm [86] for solving the FW prob-

[1] In a purely mathematical setting, the problem is often called the *Fermat-Torricelli problem* for the unweighted case, and the *generalised Fermat-Torricelli problem* for the weighted case [53].

lem iteratively, and demonstrate its use via an example. We introduce a variation of the FW problem in the plane in Section 2.7, whereby one of the given points is allowed to lie anywhere on a straight line in the plane. We show how Weiszfeld's algorithm can be amended to suit this case. Finally, we demonstrate the application of this new problem to underground mining by using it to solve a subproblem of an industry case study presented in Chapter 9.

2.2 Historical background

The following is a brief history of the FW problem, based largely on a historical exposition by Kuhn [51]. A more detailed account is given by Kupitz and Martini [53], and another good general reference is [28].

Early in the 17th century, Fermat posed the following problem: given three points in the plane, find a fourth point such that the sum of its distances to the three given points is a minimum. Torricelli proposed a geometric solution to the problem (Figure 2.1). He asserted that the three circles circumscribing the equilateral triangles constructed on the sides of, and outside the triangle $\triangle p_1 p_2 p_3$ with vertices at the given points p_1, p_2, p_3, intersect at the required point x_0. Cavalieri showed that the three lines from x_0 to p_1, p_2, p_3 make angles of 120° with each other. Simpson then showed that the three lines joining the outside vertices of the equilateral triangles to the opposite vertices of the given triangle intersect at x_0. The three lines, shown dashed in Figure 2.1, are called *Simpson lines*. Heinen proved that the lengths of the three Simpson lines are each equal to the sum of distances from x_0 to p_1, p_2, p_3. He also proved that, if one of the angles in $\triangle p_1 p_2 p_3$ is at least 120°, then x_0 coincides with the vertex of that angle. Fasbender proved that the perpendiculars to the Simpson lines through p_1, p_2, p_3 form the sides of the largest equilateral triangle circumscribing these points. He also proved that the altitude of this triangle equals the sum of distances from x_0 to p_1, p_2, p_3.

In 1909, Weber used a *weighted* three-point version of the problem to depict industrial location minimising transportation costs. A mathematical appendix to Weber's book [85], written by Georg Pick, gives a geometrical construction procedure similar to the one

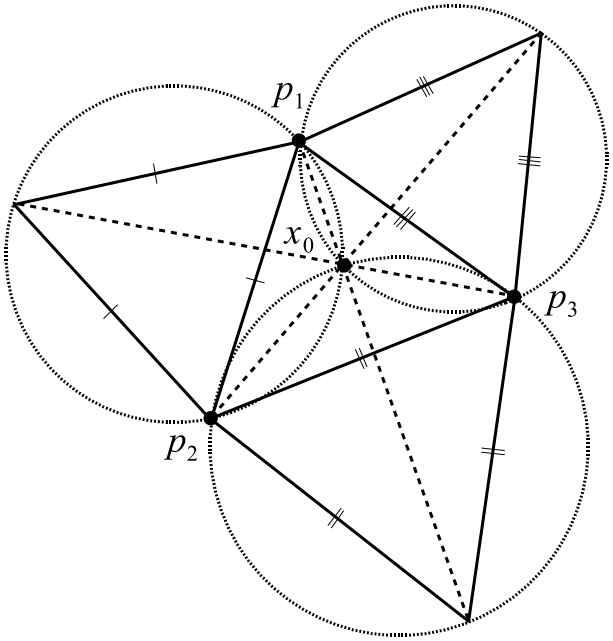

Figure 2.1: Torricelli's geometric solution to Fermat's original (unweighted) three-point problem.

shown in Figure 2.1 (we will derive this weighted construction in Section 2.4).

Fagnano discovered a solution for the four-point (unweighted) problem: if the convex hull of the four given points forms a convex quadrilateral, then x_0 is the intersection of the diagonals of that quadrilateral. Otherwise, x_0 coincides with the unique given point inside the convex hull of the four points.

Recently, Bajaj [3] discovered that if $n > 4$, no general construction of x_0 with compass and ruler exists. As a result, much of the research on this problem has focused on numerical techniques. The first and most famous iterative procedure for solving the FW problem was given by Andre Weiszfeld [86] in 1937. We discuss this algorithm in Section 2.6.

More recently, the FW problem has been studied in n-dimensional real normed spaces or *Minkowski spaces* (see, for example, [22], [31], [60]). We discuss this generalised problem in the next chapter.

2.3 Characterisation of Fermat-Weber points

The following theorem, which provides a characterisation of FW points in Euclidean n-space, is from [53]. It is noted in [53] that statements from the theorem were proved in [48], [49], [51], [86] and [87], and that its content was known to other authors as early as the 19th century.

Theorem 2.1. *Let $N = \{p_1, \ldots, p_k\}$ be a set of points in $\mathbb{R}^n$ with respective positive weights $w_1, \ldots, w_k$. Let $\mathbf{u}_i$ denote the unit vector from a point $x_0 \in \mathbb{R}^n$ to p_i, $i = 1, \ldots, k$.*

1. *If $x_0 \neq p_1, \ldots, p_k$, then x_0 is an FW point for N if and only if*

$$\sum_{i=1}^{k} w_i \mathbf{u}_i = \mathbf{0}. \tag{2.2}$$

2. *If $x_0 = p_j$ for some $j \in \{1, \ldots, k\}$ then x_0 is an FW point for N if and only if*

$$\left| \sum_{i=1, i \neq j}^{k} w_i \mathbf{u}_i \right| \leq w_j. \tag{2.3}$$

Proof. Refer to [53], pages 75-76. ∎

The characterisation in Theorem 2.1 has a natural interpretation, and can be demonstrated by a mechanical device (Figure 2.2) which, according to [85], was invented by Varignon to demonstrate the parallelogram of forces. In the figure, which depicts the three-point case, masses are attached to strings which are tied together in a knot at one end. The strings run over rollers which are fixed to the edge of a horizontal disc. When the masses are released, the knot moves to the FW point x_0 for given points at the roller positions, and weights proportional to the masses.

If one of the masses is large enough, x_0 will collapse onto the respective roller position. This corresponds to condition (2.3) which, throughout this work, we will refer to as the *collapse condition*. Otherwise, x_0 will settle at the location where the three forces induced by the masses are balanced. This corresponds to condition (2.2), which we will refer to as the *equilibrium condition*. In the next chapter, we generalise these conditions to characterise FW points in Minkowski spaces. Looking ahead, in Chapters 5 and 6, we show

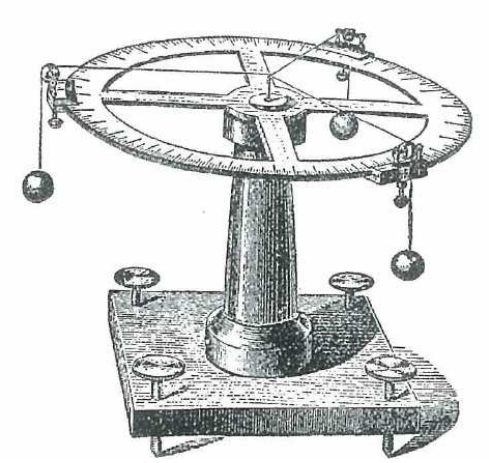

Figure 2.2: Mechanical device demonstrating the solution to the (weighted) three-point FW problem [85].

that the equilibrium condition is necessary for Steiner points in Gilbert arborescences to be locally minimal.

From Theorem 2.1 it is clear that, for noncollinear N, if $x_0 \neq p_1, \ldots, p_k$, then the FW point must lie in $\text{int}(\text{conv}(N))$, the interior of the convex hull of N, since otherwise the weighted unit vectors could not balance. Further to this, it was observed in [53] that, for each point $x \in \text{int}(\text{conv}(N)) \cup N$, there exists a set of weights such that x is an FW point for N.

Because $\mathbf{u}_1, \ldots, \mathbf{u}_k$ do not depend on the actual distances between $p_1, \ldots, p_k$ and x_0, we have the following corollary to Theorem 2.1.

Corollary 2.1. *If x_0 is an FW point for $p_1, \ldots, p_k$, then it is also an FW point for any points $p'_1, \ldots, p'_k$ lying on the rays from x_0 through $p_1, \ldots, p_k$ respectively.*

We conclude this section with some remarks about the case where the points in N are collinear. It is known [53] that, for noncollinear N, the FW point is unique. For collinear N, this is not always true. The following corollary to Theorem 2.1, which appears to be absent from the literature, characterises FW points for collinear N.

Corollary 2.2. *Let $N = \{p_1, \ldots, p_k\}$ be a set of collinear points in $\mathbb{R}^n$, ordered by increasing index, with respective positive weights $w_1, \ldots, w_k$.*

1. *If there exists some $j \in \{1, \ldots, k-1\}$ such that*

$$\sum_{i=1}^{j} w_i = \sum_{i=j+1}^{k} w_i, \tag{2.4}$$

   then all points on the line segment between p_j and p_{j+1}, including the endpoints, are FW points for N.

2. *Otherwise, the FW point coincides with the unique point p_j satisfying*

$$\left| \sum_{i=1}^{j-1} w_i - \sum_{i=j+1}^{k} w_i \right| < w_j. \tag{2.5}$$

Proof. Without loss of generality, assume that $p_1, \ldots, p_k$ lie on a horizontal line, and are ordered by increasing index from left to right. Let x_0 be a point on the line segment between p_j and p_{j+1} for some $j \in \{1, \ldots, k-1\}$. Then $\mathbf{u}_1 = \ldots = \mathbf{u}_j := -\mathbf{u}$ point to the left and $\mathbf{u}_{j+1} = \ldots = \mathbf{u}_k := \mathbf{u}$ to the right. If $x_0 \neq p_j, p_{j+1}$, then by Theorem 2.1, x_0 is an FW point if and only if $\mathbf{u}\left(\sum_{i=j+1}^{k} w_i - \sum_{i=1}^{j-1} w_i\right) = \mathbf{0}$, which reduces to (2.4). Now suppose $x_0 = p_j$ for some $j \in \{1, \ldots, k\}$. By Theorem 2.1, x_0 is an FW point if and only if $\left|\sum_{i=j+1}^{k} w_i \mathbf{u} - \sum_{i=1}^{j-1} w_i \mathbf{u}\right| \leq w_j$, which reduces to (2.5). If the equality in this expression holds, then assuming $\sum_{i=1}^{j-1} w_i < \sum_{i=j+1}^{k} w_i$, we have $\sum_{i=j+1}^{k} w_i - \sum_{i=1}^{j-1} w_i = w_j$, which rearranges to give (2.4). In this case every point on the line segment between p_j and p_{j+1} is an FW point, including the endpoints. ∎

2.4 Geometric solution to the three-point problem

We now discuss the special case of the FW problem where $k = 3$. This case, which has been widely studied in the literature (see, for example, [36], [37], [38], [47] and [79]), is interesting to study both as the smallest non-trivial instance of the FW problem, and because of its usefulness for analysing locally minimal solutions for the Gilbert arborescence problem studied in Chapter 5.

Suppose firstly that the given points $N = \{p_1, p_2, p_3\}$ are collinear. Corollary 2.2 can be used to show that the FW point x_0 for N is distinguished by four cases: (i) if $\max\{w_1, w_2\} \leq w_3 < w_1 + w_2$, then x_0 is the middle point of N; (ii) if $w_3 > w_1 + w_2$, then $x_0 = p_3$; (iii) if $w_3 = w_1 + w_2$ and p_3 is the middle point of N, then $x_0 = p_3$; (iv) if $w_3 = w_1 + w_2$ and p_3 is not the middle point of N, then x_0 lies anywhere on the closed segment between p_3 and the middle point.

Now suppose that p_1, p_2, p_3 are not collinear. Let α, β, γ denote the angles opposite the line segments p_1x_0, p_2x_0, p_3x_0 respectively (see Figure 2.3 (i)), and let $\alpha' = \pi - \alpha$, $\beta' = \pi - \beta$, $\gamma' = \pi - \gamma$. Let w_1, w_2, w_3 denote the weights associated with p_1, p_2, p_3, respectively, and let $\mathbf{u}_1, \mathbf{u}_2, \mathbf{u}_3$ be the unit vectors from x_0 to p_1, p_2, p_3 respectively.

By Theorem 2.1, if $x_0 \neq p_1, p_2, p_3$, then x_0 is an FW point for N if and only if $w_1\mathbf{u}_1 + w_2\mathbf{u}_2 + w_3\mathbf{u}_3 = \mathbf{0}$. If the three weighted unit vectors are placed from head to tail, a closed triangle is formed with edge lengths w_1, w_2, w_3, and internal angles α', β', γ' (Figure 2.3 (ii)). This is called the *weight triangle* [85]. Without loss of generality, assume that $w_3 \geq \max\{w_1, w_2\}$. If $w_3 > w_1 + w_2$, the weight triangle does not exist, and it is known [44] that in this case x_0 collapses onto p_3. If $w_3 = w_1 + w_2$, the weight triangle exists, but its three vertices are collinear. Again x_0 again collapses onto p_3 in this case. Thus we assume from this point on that $w_3 < w_1 + w_2$.

Using the weight triangle, the optimum angles between the three edges can be computed as functions of the three weights. Applying the cosine rule to the weight triangle, and using the identity $\cos(\pi - A) = -\cos A$, the following expressions, which appear frequently in the literature, can be derived:

$$\cos\alpha = \frac{w_1^2 - w_2^2 - w_3^2}{2w_2w_3}, \tag{2.6}$$

$$\cos\beta = \frac{w_2^2 - w_1^2 - w_3^2}{2w_1w_3}, \tag{2.7}$$

$$\cos\gamma = \frac{w_3^2 - w_1^2 - w_2^2}{2w_1w_2}. \tag{2.8}$$

Let $\angle p_2x_0p_3$, $\angle p_1x_0p_3$ and $\angle p_1x_0p_2$ denote the internal angles of the given triangle at p_1, p_2, p_3 respectively. It is known [44] that if $\alpha \leq \angle p_2x_0p_3$ or $\beta \leq \angle p_1x_0p_3$ or $\gamma \leq \angle p_1x_0p_2$, then x_0 will collapse onto p_1 or p_2 or p_3 respectively. Otherwise, (2.6), (2.7) and

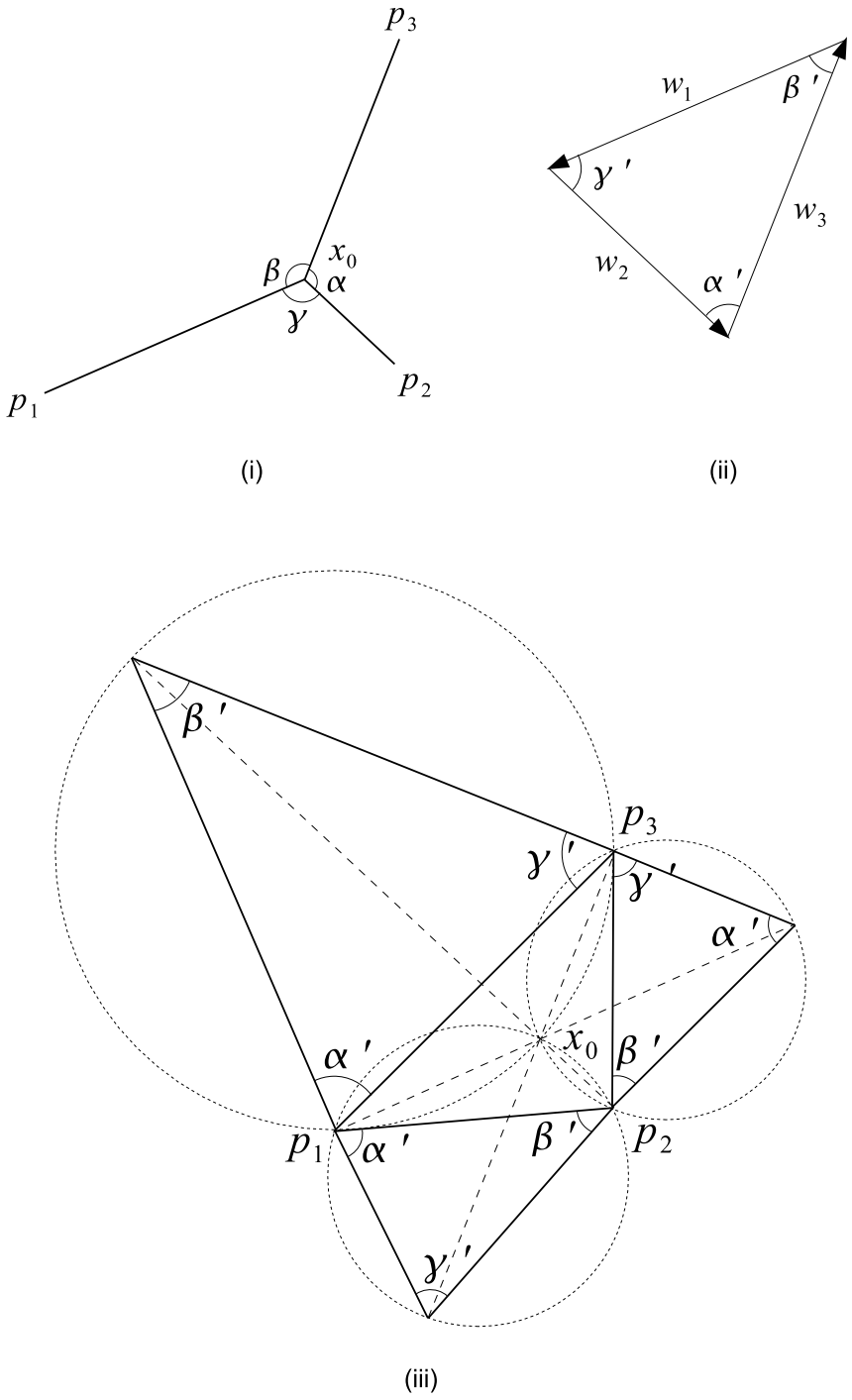

Figure 2.3: Three-point FW problem. (i) Given points and angles. (ii) Weight triangle. (iii) Generalised Torricelli construction.

(2.8) can be used to construct a geometric configuration for the three-point FW problem (Figure 2.3 (iii)), similar to the one shown previously in Figure 2.1 for the unweighted case.

According to [53], Engelbrecht proved in 1877 that if three directly similar triangles with inner angles α', β', γ' are erected externally on the sides of the given triangle $\triangle p_1 p_2 p_3$, such that α', β', γ' lie at p_1, p_2, p_3 respectively, then the three lines joining the outside vertices of the weight triangles to the opposite vertices of the given triangle intersect at the FW point x_0. The three lines, shown dashed in Figure 2.3 (iii), are called *generalised Simpson lines*, and the length of a Simpson line multiplied by the weight associated with the given point to which it is connected, equals the sum of the three weighted distances to the minimum point [53]. Moreover, the circumcircles of the erected triangles intersect at x_0. The resulting geometric construction, shown in Figure 5.7 (iii), is referred to in [53] as the *generalised Torricelli configuration.* When all the weights are equal, we obtain the special case where the weight triangle is equilateral, as was previously shown in Figure 2.1.

2.5 Exact solutions for special cases

Juel and Love [46] noted that certain instances of the FW problem can be solved with very little computational effort, if the weights satisfy certain conditions. For example, it is known that if one of the weights is greater than or equal to the sum of the other weights, then the FW point collapses onto the given point corresponding to that weight [53].

For the next example, suppose $N = \{p_1, p_2, p_3, p_4\}$ are points in $\mathbb{R}^2$ with corresponding weights $w_1 = w_2 = w_3 = w_4 = 1$. According to [24], Fagnano proved in 1775 that if the four points form the vertices of a convex quadrilateral, then x_0 is the intersection of the diagonals of that quadrilateral. Otherwise, x_0 coincides with the unique given point inside $\text{conv}(N)$.

In general, when the weights are not equal, the FW problem for $k = 4$ has no exact geometric construction [53]. However, the following trivial observation is worth noting. Let $N = \{p_1, p_2, p_3, p_4\}$ form the vertices of a convex quadrilateral with diagonals $p_1 p_3$

and p_2p_4. If $w_1 = w_3$ and $w_2 = w_4$, then $x_0 = p_1p_3 \cap p_2p_4$. This is seen by noting that pairs of weighted unit vectors are equal and opposite, thus satisfying the equilibrium condition. The following lemma, due to [46], generalises this observation to an even number of points in $\mathbb{R}^n$.

Lemma 2.1. *Let N be an even set of given points in $\mathbb{R}^n$. Suppose that the given points can be grouped into pairs such that the weights associated with the two points in a pair are equal, and when a straight line is drawn between the two points in each and every pair, this set of lines intersects at a single point x_0. Then x_0 is the unique FW point for N.*

Proof. Since the weighted unit vectors associated with p_i and p_{k+i} are equal and opposite, the equilibrium condition is satisfied, and therefore by Theorem 2.1, x_0 is an FW point for N. ∎

Some instances where Lemma 2.1 is applicable are shown in Figure 2.4 (i). Following on from Lemma 2.1, we now propose the following conjecture.

Conjecture 2.1. *Let $N = \{p_1, \ldots, p_{2k}\}$, $k \geq 2$, be given points at the vertices of a convex polygon, labelled in order of index around the perimeter of the polygon. Let $w_1, \ldots, w_{2k}$ denote their respective positive weights, and assume that $w_i = w_{k+i}$, $i = 1, \ldots, k$. Let D_i, $i = 1, \ldots, k$ denote the diagonal line through p_i and p_{k+i}, and let R be the union of all finite intersections of half-planes determined by $D_1, \ldots, D_k$. Then $x_0 \in \text{int}(R)$.*

An incomplete proof of the conjecture is as follows. Let x be a point in the region between D_j, D_{j+1}, $j \in \{1, \ldots, k\}$ and outside R. Note that x lies at the intersection of two ellipses for which the endpoints of D_j and D_{j+1} are the respective foci. It is believed that if x is perturbed by a small amount in some direction toward $D_j \cap D_{j+1}$, then for each $i \in \{1, \ldots, k\}$, the weighted sum $w_i\,(|p_i - x| + |p_{k+i} - x|)$ decreases, since x moves inside each ellipse associated with D_i, $i = 1, \ldots, k$. Hence the sum of weighted distances from x to $p_1, \ldots, p_{2k}$ would decrease.

An example demonstrating the conjecture is shown in Figure 2.4 (ii). Notice that, for a problem satisfying the assumptions of the conjecture, x_0 cannot coincide with a given point. It can also be seen from the conjecture that if $p_1, \ldots, p_{2k}$ form the vertices of a regular convex polygon with an even number of vertices (e.g. a hexagon, octagon,

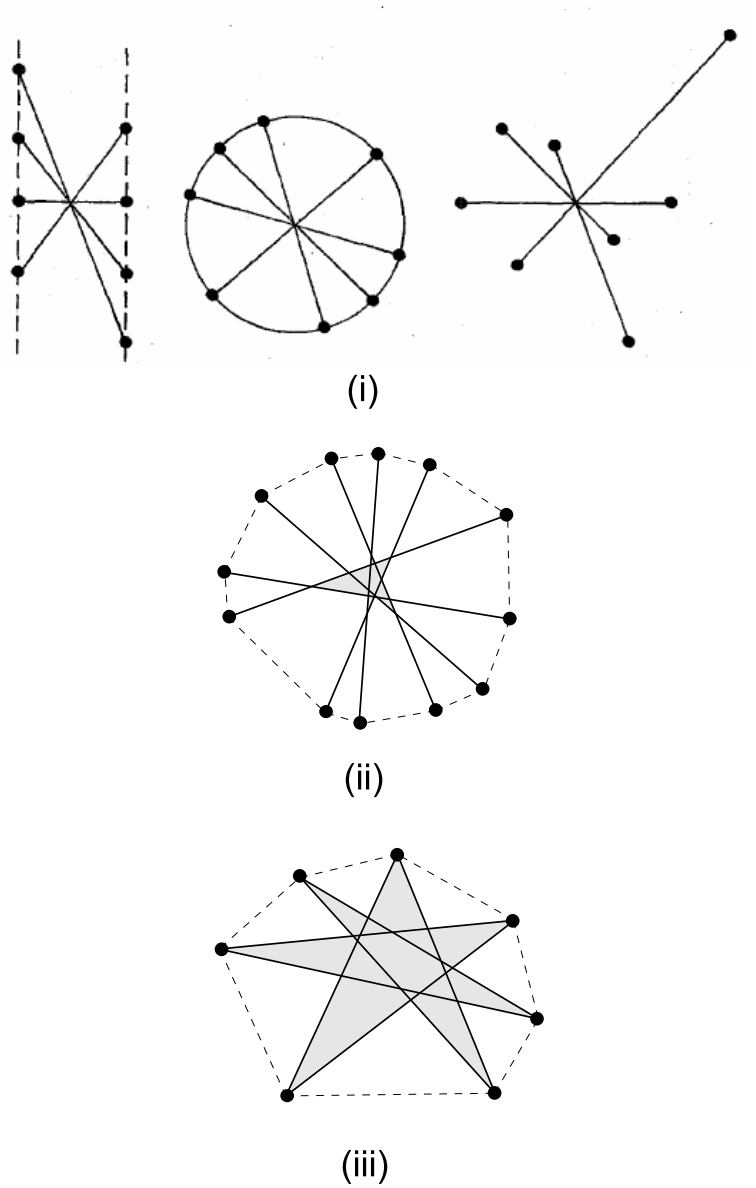

Figure 2.4: Special instances of the FW problem. (i) Three exactly obtainable solutions [46]. (ii)–(iii) Solution regions for even and odd sets of given points at the vertices of a convex polygon.

decagon, etc.), then R is the intersection of the k diagonals and the FW point corresponds to this intersection, as per Lemma 2.1. The following conjecture proposes a similar result for the case where the convex polygon has an odd number of vertices, and all the weights are equal.

Conjecture 2.2. *Let $N = \{p_1, \ldots, p_k\}$, $k \in \{3, 5, 7, \ldots\}$, be given points at the vertices of a convex polygon, labelled in order of index around the perimeter of the polygon. Let $w_1, \ldots, w_k$ denote their respective positive weights, and assume that $w_1 = \cdots = w_k$. Let D_{1i} and D_{2i}, $i = 1, \ldots, k$ denote the diagonal lines between p_i and its two opposite vertices, and let R be the union of all finite intersections of half-planes determined by all the diagonals. Then $x_0 \in \text{int}(R)$.*

An example demonstrating the conjecture is shown in Figure 2.4 (iii). Notice that, in contrast to the even case, for a problem satisfying the assumptions of the conjecture, x_0 can coincide with a given point when the number of vertices is odd.

2.6 Weiszfeld's algorithm

Although special instances of the FW problem can be solved with simple geometric constructions, in general for $k \geq 4$, the problem cannot be solved by exact methods [3]. Thus, significant research has been undertaken to develop numerical procedures for finding FW points. A famous iterative method for the FW problem (Algorithm 1) was posed in 1937 by Andre Weiszfeld [86]. This algorithm was independently discovered by Kuhn and Kuenne [52] in 1962. The first step of the algorithm checks whether x_0 coincides with a given point. If not, x_0 is determined iteratively.

The following example demonstrates the application of Weiszfeld's algorithm. Let $p_1 = (0, 1)$, $p_2 = (2, 0)$ and $p_3 = (2, 2)$ be given points in the plane with respective weights $w_1 = 1$, $w_2 = 1$ and $w_3 = 1.65$. By testing the collapse condition, it can be shown that $x_0 \neq p_1, p_2, p_3$. Selecting $\epsilon = 0.001$ and $x^{(0)} = (0.25, 1)$, the path of the iteration point converges to x_0, as shown in Figure 2.5.

Kuhn [50] proved that Weiszfeld's algorithm converges to the FW point, provided none of the iterates coincide with one of the given points. He concluded that whenever the k points are not collinear, Weiszfeld's algorithm converges to the unique FW

Algorithm 1 Weiszfeld's algorithm.

1. If there exists a point $p_j \in N$ such that
$$\left| \sum_{i=1, i\neq j}^{k} w_i \mathbf{u}_i \right| \leq w_j,$$
then p_j is an FW point; otherwise
2. Select an error estimate ϵ;
3. Select an initial point $x^{(0)} \in \text{int}(\text{conv}(N))$;
4. For $\kappa = 0, 1, \ldots$ do
$$x^{(\kappa+1)} := \frac{\sum_{p_i \in N} \frac{w_i p_i}{|p_i - x^{(\kappa)}|}}{\sum_{p_i \in N} \frac{w_i}{|p_i - x^{(\kappa)}|}};$$
5. Stop when $\left| x^{(\kappa)} - x^{(\kappa+1)} \right| \leq \epsilon$.

point except when the initial point is in a denumerable set. In 1989, Chandrasekaran and Tamir [23] demonstrated with counter-examples that these sets can be continuous rather than denumerable. Then in 1995, Brimberg [20] proved that Weiszfeld's algorithm converges to the unique optimal solution for all but a denumerable set of starting points if and only if the convex hull of the given points is of dimension n. Thus, when using Weiszfeld's algorithm, one must be careful that the iterate does not converge prematurely to a given point.

In the next section, we show how Weiszfeld's algorithm can be amended to suit a variation of the FW problem, where one of the terminals is not fixed, but rather is allowed to lie anywhere on a straight line. In Chapter 4, we show that an amended version of Weiszfeld's algorithm is not suitable for solving the FW problem in certain normed spaces.

2.7 The Fermat-Weber problem for a given set of points and a line

Consider the following variant of the FW problem: let $p_1, \ldots, p_{k-1}$ be given points in the Euclidean plane $\mathbb{R}^2$ with respective positive weights $w_1, \ldots, w_{k-1}$, and suppose that l is an infinitely long straight line in the same plane. Let p be a point on l with respective

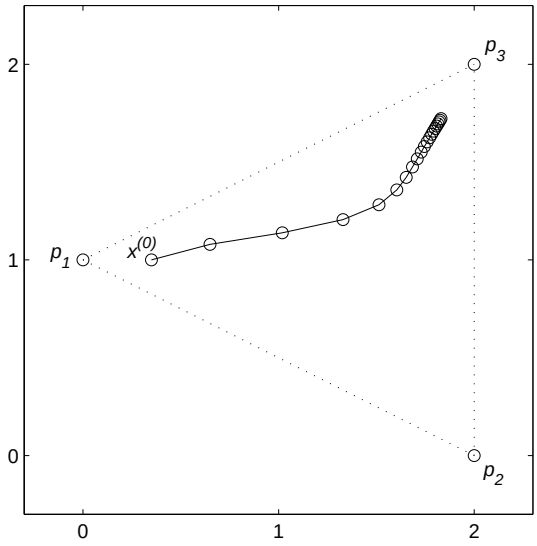

Figure 2.5: Iterations of Weiszfeld's algorithm for a three-point FW problem.

positive weight w_k. The amended problem is to find points x_0 and p_k that minimise the function

$$f(x,p) = \sum_{i=1}^{k-1} (w_i|p_i - x|) + w_k|p - x|, \quad x \in \mathbb{R}^2,\ p \in l. \tag{2.9}$$

The following example, which forms a subproblem of the case study presented in Chapter 9, demonstrates the application of this problem to mining. An underground mine consists of two parallel declines, one primary and the other secondary, accessing adjacent ore bodies with draw points at 40 m vertical intervals. Ore from the lower levels is trucked up both declines to a level, L1, from where it is transported to the base of a vertical hoisting shaft via a horizontal tunnel (Figure 2.6 (i)). Ore from the upper levels is trucked down both declines to another level, L3, from which it is transported via a horizontal tunnel to the top of an ore pass. It is dropped down the ore pass to L1 and transported to the shaft base. Ore from levels between L1 and L3 on the secondary decline is either trucked up to L3 or down to L1, whichever is closest. Ore from levels between L1 and L3 on the primary decline also has the option of being trucked to an intermediate level, L2,

which is between the top and bottom of the ore pass. It is transported to an intermediate tip point on the ore pass via a horizontal tunnel, dropped down the ore pass to L1, and transported to the shaft base. The arrangement is shown in Figure 2.6 (i) and (ii).

Let p_1, p_2 be points on the two respective declines at L1, p_3 the point on the main decline at L2, and p_4, p_5 points on the two respective declines at L3. Assuming L1, L2 and L3 are predetermined, then $p_1, \ldots, p_5$ are fixed points. Denote the plan location of the ore pass by x, and that of the shaft by p. While the ore pass is allowed to be positioned anywhere, the hoisting shaft must not be too close to the ore bodies. The boundary of this orebody standoff zone is modelled by the straight line l (Figure 2.6 (ii)). Clearly, the optimal position of p will be on l, rather than behind it, since in the latter case, $|p - x|$ can be reduced by moving p onto l. The system of tunnels can be modelled as a network T with a star topology, where x is the centre of the star, $p_1, \ldots, p_{k-1}$ are fixed, and p is free to slide along l.

Suppose that $t_1, \ldots, t_5$ tonnes of ore are to be transported from $p_1, \ldots, p_5$ respectively. Let d denote the cost per unit length of developing a tunnel, and h the cost per unit length per unit quantity of ore of haulage. Then the sum of development and haulage costs for the tunnel from p_i, $i = 1, \ldots, 5$, to x is $(d + ht_i)|p_i - x|$; thus the associated weight is $w_i := d + ht_i$. Similarly, the weight associated with the tunnel from x to p is $w_6 := d + h\sum_{i=1}^{5} t_i$, since that tunnel routes all the ore from the ore pass base to the shaft base.

The problem of minimising the development and haulage costs associated with the horizontal tunnels connecting the declines, ore pass and shaft, can be solved by projecting everything onto a horizontal plane. Then the problem reduces to positioning x and p so as to minimise (2.9). We can immediately state the following result.

Lemma 2.2. *If $x = x_0$ and $p = p_k$ minimise the cost function (2.9), then the line segment x_0p_k is perpendicular to l. Thus, the position of p is a function of the position of x.*

Proof. If x_0p_k is not perpendicular to l, then $|p_k - p_0|$ can be reduced by moving p_k along l until it does. ∎

By this lemma, we see that the unit vector, $\mathbf{u}_k$, associated with p_k, always points from x toward l in the direction perpendicular to l, irrespective of the position of x. As usual,

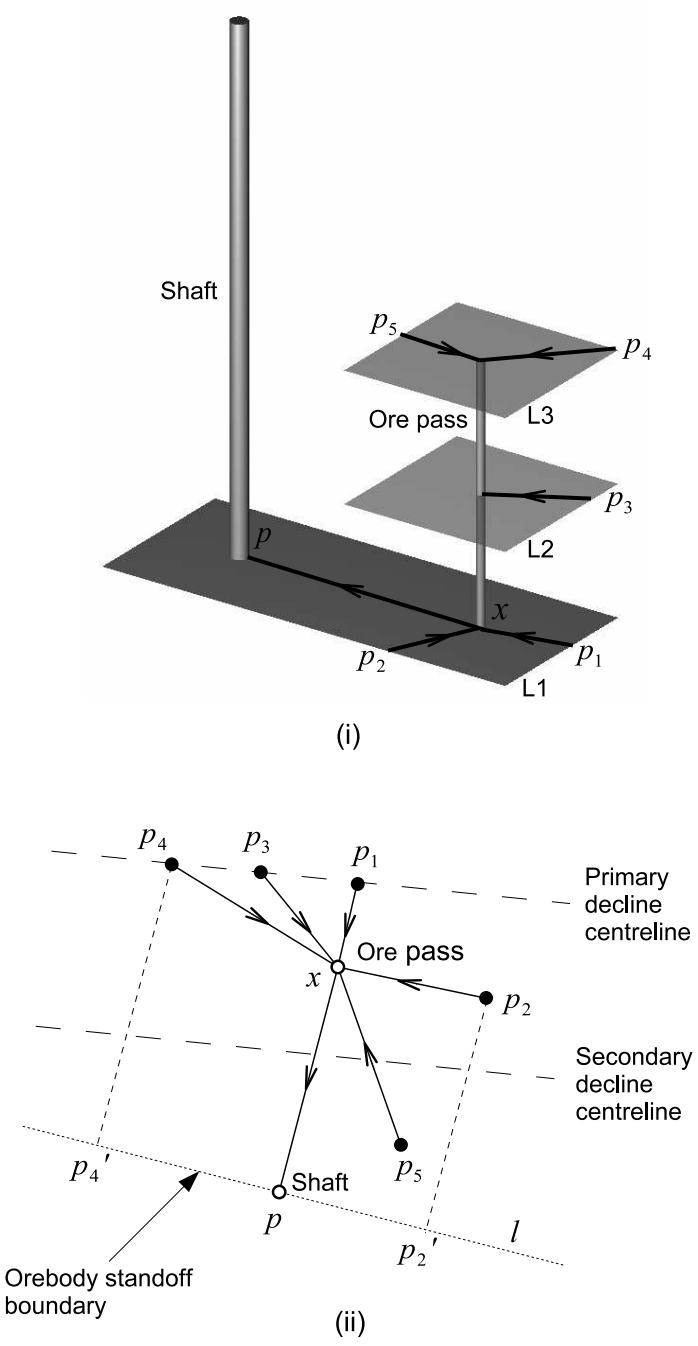

Figure 2.6: Amended FW problem applied to the Callie underground mine. (i) Perspective view. (ii) Plan view.

$\mathbf{u}_1, \ldots, \mathbf{u}_{k-1}$ are unit vectors from x to $p_1, \ldots, p_{k-1}$ respectively. Lemma 2.2 leads to the following simple corollary.

Corollary 2.3. *Let $p'_1, \ldots, p'_{k-1}$ be the respective orthogonal projections of $p_1, \ldots, p_{k-1}$ onto l. Then p_k lies on l between the two outermost elements of $\{p'_1, \ldots, p'_{k-1}\}$.*

In Figure 2.6, by the corollary, p_k must lie on l somewhere between p'_2 and p'_4. Using similar arguments, we see that the convex hull of $p_1, \ldots, p_k$ is the polygon with vertices $p_1, p_2, p'_2, p'_4, p_4, p_3$.

Now a modified Weiszfeld algorithm can be applied to this problem. If x does not coincide with $p_1, \ldots, p_{k-1}$ or l, select an initial point, $x^{(0)}$ in the convex hull described above, and let $p^{(0)}$ be the orthogonal projection of $x^{(0)}$ onto l. For $\kappa = 1, 2, \ldots$ compute

$$x^{(\kappa+1)} := \frac{\sum_{i=1}^{k-1} \left(\frac{w_i p_i}{|p_i - x^{(\kappa)}|} \right) + \frac{w_k p^{(\kappa)}}{|p^{(\kappa)} - x^{(\kappa)}|}}{\sum_{i=1}^{k-1} \left(\frac{w_i}{|p_i - x^{(\kappa)}|} \right) + \frac{w_k}{|p^{(\kappa)} - x^{(\kappa)}|}} \tag{2.10}$$

where $p^{(\kappa)}$ is the orthogonal projection of $x^{(\kappa)}$ onto l. The algorithm terminates when $\left| x^{(\kappa)} - x^{(\kappa+1)} \right| \leq \epsilon$, for some small $\epsilon > 0$.

Although we do not prove convergence of this amended algorithm here, we note that several numerical experiments have converged to the correct solution. As for the classical problem, the algorithm should be used with caution when an iteration lands on a given point.

We also note a complication with the initial step of the algorithm, where we are required to determine whether x collapses onto l, since the unit vectors can only be computed from a particular point on l. To overcome this difficulty, one might discretise l into a finite number of points and compute the weighted vectors to $p_1, \ldots, p_{k-1}$ at each point. If the collapse condition holds for any of these points, then x collapses onto l at that point.

Chapter 3

The Fermat-Weber Problem in Minkowski Spaces

In this chapter we investigate the Fermat-Weber problem in n-dimensional real normed spaces, or Minkowski spaces. Martini et al. [60] provided a minitheory of this problem for the case where all the weights equal one, and established a range of geometric results. Our main goal in this chapter is to generalise some of these results to the weighted case. We provide background relating to Minkowski spaces and functional analysis, including a method for constructing the dual ball for a given unit ball. We state a known geometric characterisation of Fermat-Weber points in normed spaces [31], the characterisation being in terms of weighted norming functionals associated with the given points. We then provide several properties of the set of solutions to the Fermat-Weber problem, and identify special instances of the problem that can be solved exactly with very little computational effort. The notions of double-clusters, ρ-concurrent ρ-segments, and cogeodesic sets are generalised to the weighted case, and corresponding theorems and proofs are provided. Finally, we generalise to the weighted case a geometric result originally posed in [22] for the three-point unweighted problem.

3.1 Introduction

HAVING studied the Fermat-Weber (FW) problem n-dimensional Euclidean space, we now consider the extension of this problem to n-dimensional real normed spaces, which are also called *Minkowski spaces*. The norm $\|\cdot\|$ associated with a Minkowski space provides a way of measuring distance. Euclidean space is itself an example of a normed space where the Euclidean norm $|\cdot|$ is used.

Let $N = \{p_1, \ldots, p_k\}$ be a set of given points in a Minkowski space with the norm $\|\cdot\|$, where the points have respective positive weights $w_1, \ldots, w_k$. The FW problem in

Minkowski spaces asks for a point x_0 minimising

$$f(x) = \sum_{i=1}^{k} w_i \|p_i - x\|. \tag{3.1}$$

The function is the same as (2.1) in Chapter 2, except that $\|\cdot\|$ is no longer restricted to the Euclidean norm $|\cdot|$. Geometric aspects of the unweighted version of the problem have been studied in [22], [24] and [60]. In the last reference, Martini et al. established a range of geometric results. Our main goal in this chapter is to generalise some of these results to the weighted case.

In Section 3.2, we provide necessary background relating to Minkowski spaces and functional analysis, including methods for constructing the dual ball for a given unit ball. In Section 3.3, we state a known geometric characterisation of FW points in normed spaces [31], the characterisation being in terms of weighted norming functionals associated with the given points. In Section 3.4, we then provide several properties of the set of solutions to the FW problem. In Section 3.5, we identify special instances of the problem that can be solved exactly with very little computational effort. The notions of double-clusters, ρ-concurrent ρ-segments and cogeodesic sets are generalised to the weighted case, and corresponding theorems and proofs are provided. Finally in Section 3.6, we generalise to the weighted case a geometric result originally posed in [22] for the unweighted three-point problem.

3.2 Background

The following facts about normed spaces are from [77] and [60]. Let X be an n-dimensional real linear space, and $x = (x_1, \ldots, x_n)$ a point in X. A *norm* on X is a mapping $\|\cdot\|$ from X into $\mathbb{R}^+$ satisfying the following conditions: $\|x\| \geq 0$ with equality if and only if $x = o$, where o is the origin; $\|\lambda x\| = |\lambda| \, \|x\|$, $\forall \lambda \in \mathbb{R}$; and $\|x + y\| \leq \|x\| + \|y\|$, the last condition being the *triangle inequality*. Informally, a norm provides a way of measuring the

lengths of vectors in X. A common norm is the ℓ_p norm

$$\|x\|_p = \left(\sum_{i=1}^{n} |x_i|^p \right)^{\frac{1}{p}}$$

where $p \geq 1$ is a real number. For $p = 2$ we have the Euclidean norm, denoted by $|\cdot|$, which we used in Chapter 2, and for $p = 1$ we have the rectilinear norm, also called the Manhattan, taxicab or ℓ_1 norm. A *Minkowski space*, also called a *normed space*, is a real linear space X, equipped with norm $\|\cdot\|$, in which the dimension n of X is finite.

3.2.1 The unit ball and dual ball

The *unit ball* in X is the set $B = \{x \in X : \|x\| \leq 1\}$. It is a centrally symmetric, closed and convex subset of X with origin o at its centre. A unit ball is called *smooth* if its boundary, $\mathrm{bd}(B)$, has no sharp (nondifferentiable) points, and *strictly convex* if $\mathrm{bd}(B)$ has no straight line segments. A *supporting hyperplane* of B is a hyperplane in X touching the boundary of B such that the interior of B lies on one side of the supporting hyperplane. An *exposed face* of B is the intersection of B with a supporting hyperplane.

The *dual space* of X, denoted by X^*, is the vector space of all linear functionals on X, a linear functional being a mapping from X into $\mathbb{R}^+$. If we identify X and X^* with the n-dimensional space $\mathbb{R}^n$, then the *dual ball* B^* is the polar body of B, that is

$$B^* = \{y : \langle x, y \rangle \leq 1, \quad \forall x \in B\} \tag{3.2}$$

where $\langle \cdot, \cdot \rangle$ is the dot product. Figures 3.1 and 3.2 show, in two and three dimensions respectively, the unit ball and and its dual ball for the Euclidean norm, the rectilinear norm, and two norms occurring in [62] and [32] respectively. In (i), B and B^* are smooth and strictly convex; in (ii) and (iii), B and B^* are neither smooth nor strictly convex; and in (iv), B is smooth but not strictly convex, while B^* is strictly convex but not smooth. We define $B(w)$ and $B^*(w)$ to be scaled copies of the unit ball and dual ball with radius $w > 0$.

While the following three lemmas are standard results of convexity, they have been

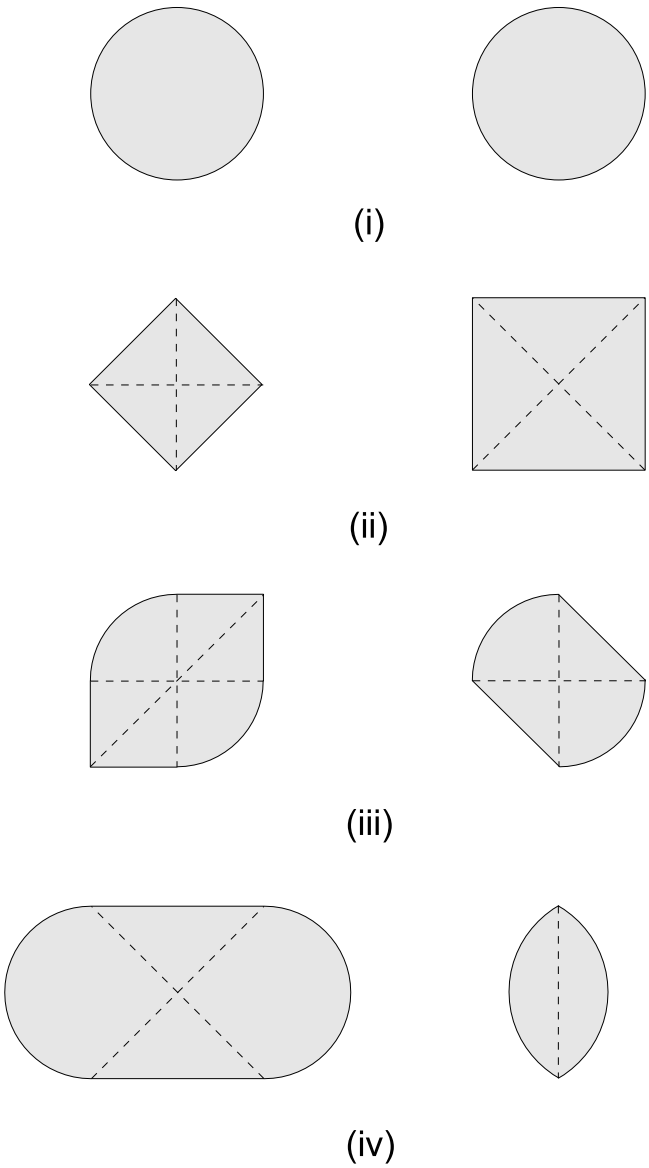

Figure 3.1: Unit ball (left) and dual ball (right) for norms in the plane. (i) Euclidean. (ii) Rectilinear. (iii)–(iv) Norms occurring in [62] and [32] respectively.

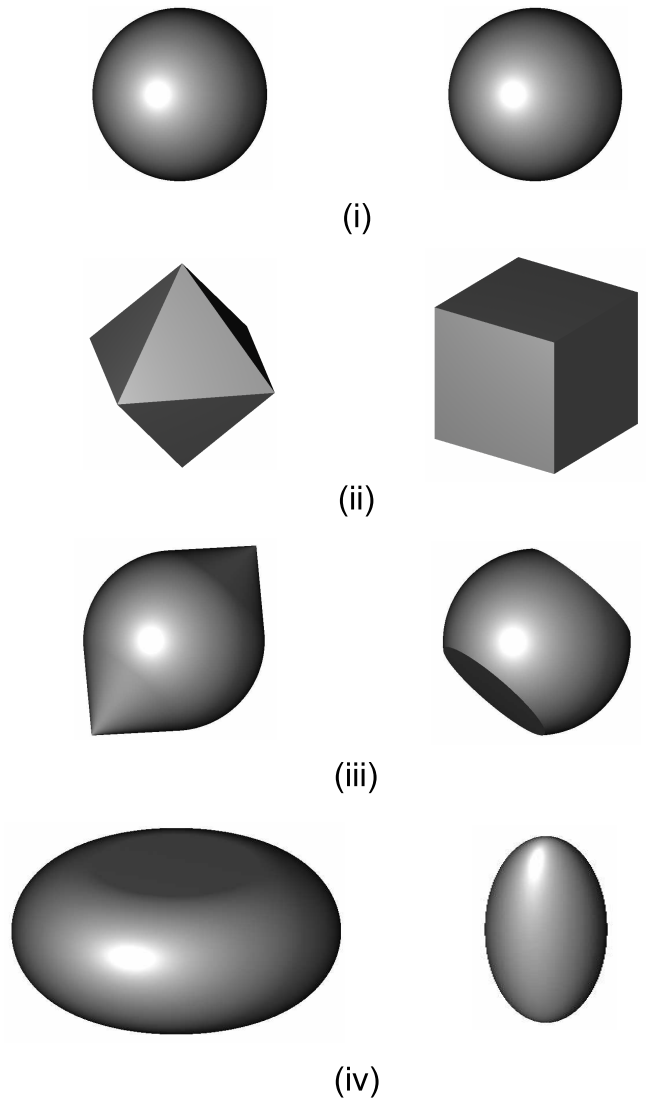

Figure 3.2: Unit ball (left) and dual ball (right) for norms in three-space. (i) Euclidean. (ii) Rectilinear. (iii)–(iv) Norms occurring in [62] and [32] respectively.

formulated and proved independently by the author. The first lemma provides a method for constructing B^* for a given B.

Lemma 3.1. *Let X be a Minkowski space with unit ball B. For a point $x \in X$, let $|x|$ denote the Euclidean distance from the origin o to x, $\vec{x}$ the ray with origin o passing through x, $W(x)$ the hyperplane that is orthogonal to $\vec{x}$ and intersects $\vec{x}$ at the point x' for which $|x'| = \frac{1}{|x|}$ and $S(x)$ the closed half-space defined by $W(x)$ which contains o. Then*

$$B^* = \bigcap_{\forall x \in \mathrm{bd}(B)} S(x)$$

where $\mathrm{bd}(B)$ denotes the boundary of B.

Proof. Let $y \in X$ and θ the angle between $\vec{x}$ and $\vec{y}$. By the orthogonal projection of y onto $\vec{x}$, we see that $|y| \cos\theta \leq \frac{1}{|x|}$ if and only if $y \in S(x)$, with equality if and only if $y \in W(x)$. Thus, $S(x) = \{y : \langle x, y \rangle \leq 1\}$, and from the definition of the dual ball (3.2), we have $B^* = \bigcap_{\forall x \in B} S(x)$. It is left to show that we need only consider $S(x)$ for points x on the boundary of B. Let $\tilde{x}$ be a point on $\vec{x}$ such that $|\tilde{x}| < |x|$. Then clearly $S(x) \subset S(\tilde{x})$, and consequently we can ignore points in the interior of B when computing B^* by this method. ∎

If B has straight line segments on its boundary, the construction of B^* by the method of Lemma 3.1 can be simplified by the following result.

Lemma 3.2. *Let X be a Minkowski space with unit ball B having a straight line segment l with endpoints e_1 and e_2 on its boundary. Then*

$$\bigcap_{\forall x \in l} S(x) \equiv S(e_1) \cap S(e_2)$$

and it follows that points in the interior of l need not be considered in the construction of B^* by the method proposed in Lemma 3.1.

Proof. Refer to Figure 3.3. Let x be a point on l, and let $\vec{x}$, x', $W(x)$ and $S(x)$ be as defined in Lemma 3.1. Let $l_\perp$ be the line passing through o which is orthogonal to l, and Δ the distance from o to the intersection of $l_\perp$ with the extension of l. It can be shown that the

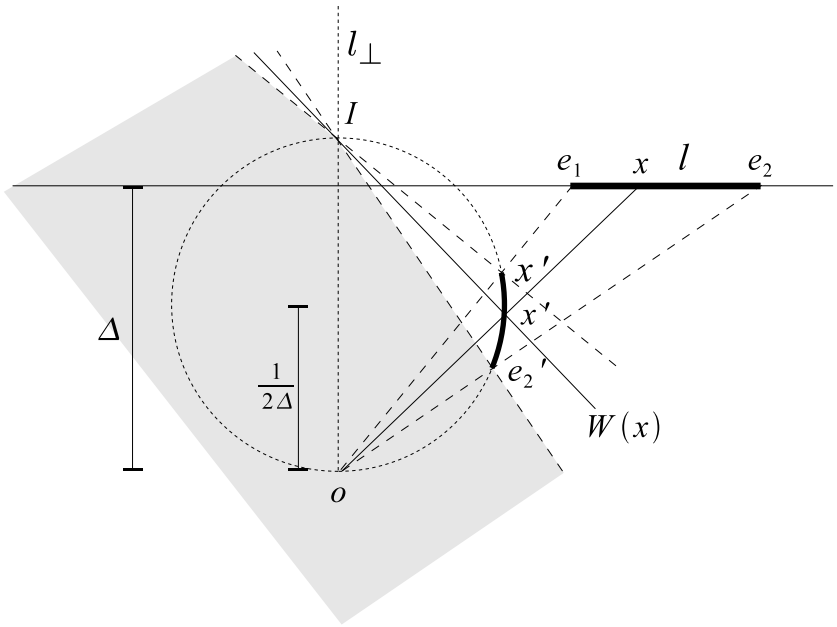

Figure 3.3: Straight line segment on the boundary of a unit ball.

set of x' for all points x on l forms the arc of a circle, the circle having radius $\frac{1}{2\Delta}$ and centre at a distance $\frac{1}{2\Delta}$ from o along $l_\perp$. Let I be the second point (other than o) where this circle intersects $l_\perp$. Then the chord oI bisects the circle, and the angle $\angle ox'I$ is 90° for all x' on the arc of the circle. Hence, all the hyperplanes $W(x),\ x \in l$ intersect at a common point I, which lies on $l_\perp$ at a distance $\frac{1}{\Delta}$ from o. From the figure it can be seen that $\bigcap_{x\in l} S(x)$ reduces to the intersection of $S(e_1)$ and $S(e_2)$, which completes the proof. ∎

From Lemma 3.2, we can see that it is relatively straightforward to construct the dual ball if the corresponding unit ball is polyhedral, since B^* is the intersection of a finite number of hyperplanes. For the rectilinear norm in Figure 3.1 (ii), we need only compute $S(x)$ for the four points at the corners of the diamond. Thus we obtain the square dual ball shown in the figure, which in fact corresponds to the ℓ_∞ norm in the plane given by $\|x\|_\infty = \max\{|x_1|, |x_2|\}$.

We demonstrate the application of the preceding results by constructing B^* for the unit balls shown in Figure 3.1 (iii) and (iv) respectively. In the case of (iii), the circle arcs

forming $\mathrm{bd}(B)$ in quadrants two and four correspond to equivalent boundary arcs for B^*, since B is the same as the Euclidean ball in these quadrants. For quadrants one and three, by Lemma 3.2 we need only compute $S(x)$ at the two corner points of B. It is easy to see that these half-planes are defined by lines $W(x)$ with slope -1, passing through $(1,0),(0,1)$ and $(-1,0),(0,-1)$, and it follows that the dual ball has the form shown in the figure.

Now consider the unit ball of Figure 3.1 (iv). By Lemma 3.2, we may disregard points in the interior of the two straight line segments. Using the construction method of Lemma 3.1, we compute $W(x)$ and $S(x)$ at points where lines making respective angles of $0, 15, 30, 45$ degrees with the horizontal, and passing through o, intersect $\mathrm{bd}(B)$. Then we obtain the approximate boundary of B^* shown dashed in the figure. This boundary becomes smoother as we increase the number of hyperplanes computed.

This last example demonstrates why a smooth but not strictly convex unit ball has a corresponding dual ball that is strictly convex but not smooth. In fact, by Lemma 3.2, we see that a straight line segment on $\mathrm{bd}(B)$ corresponds to a non-smooth point on $\mathrm{bd}(B^*)$, and a non-smooth point on $\mathrm{bd}(B)$ corresponds to a straight line segment on $\mathrm{bd}(B^*)$. Moreover, a smooth and strictly convex B has corresponding smooth and strictly convex B^*, while if B is neither smooth nor strictly convex, then B^* is also neither smooth nor strictly convex. It is also worth noting that the dual of the dual ball is the original unit ball.

We conclude our discussion of the unit ball and dual ball with an important geometric relationship between B and B^*.

Lemma 3.3. *Let X be a Minkowski space with unit ball B and dual ball B^*. For a point $x \in \mathrm{bd}(B)$, let $H(x)$ denote a supporting hyperplane of B at x, $\mathbf{u}(x)$ the outward unit normal vector of $H(x)$, $\delta(x)$ the distance from o to $H(x)$, $v(x)$ the point with position $\frac{\mathbf{u}(x)}{\delta(x)}$, and $V(x)$ the set of all $v(x)$ for x. Then*

$$\mathrm{bd}(B^*) = \bigcup_{x \in \mathrm{bd}(B)} V(x).$$

Proof. Refer to Figure 3.4 (ii). Let $x \in \mathrm{bd}(B)$, and let x' and $W(x)$ be as defined in Lemma 3.1. Let $\phi \in \{\mathrm{bd}(B^*) \cap W(X)\}$ (if x is a smooth boundary point, then this in-

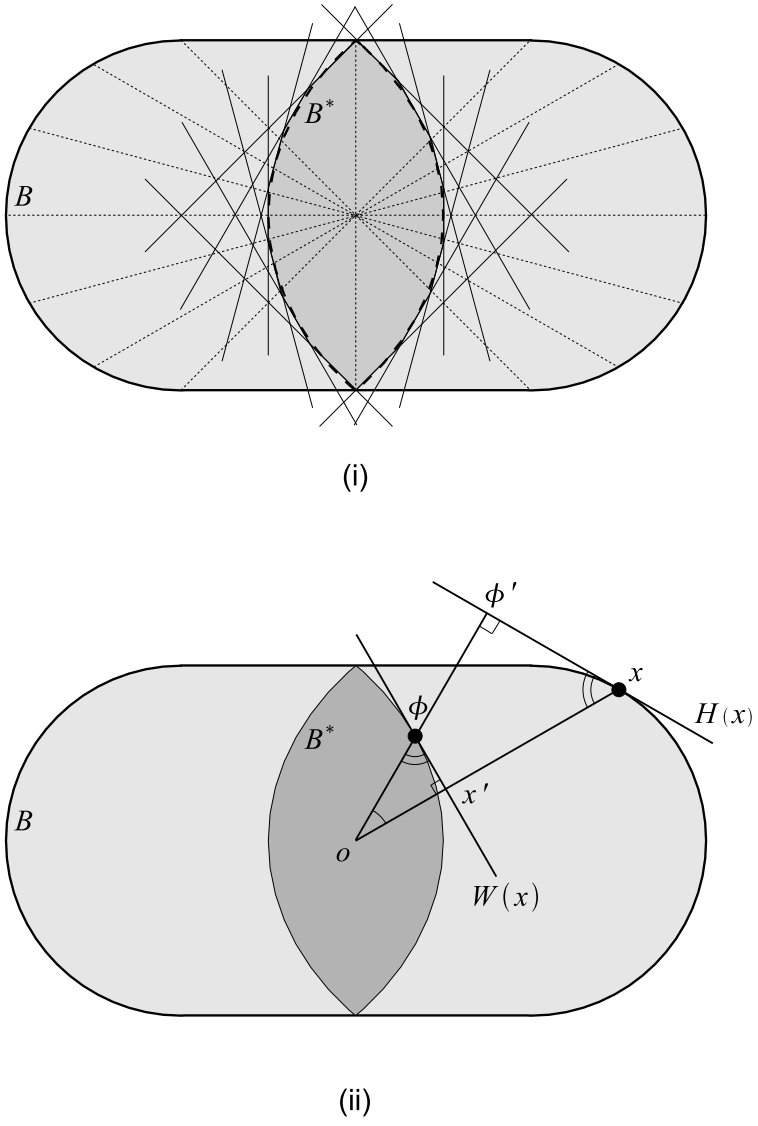

Figure 3.4: Unit ball and dual ball occurring in [32]. (i) Construction of the dual ball by Lemma 3.1. (ii) Relationship between corresponding points on the boundaries of the unit ball and dual ball.

tersection is a unique point), and let $\vec{\phi}$ denote the ray with origin o passing through ϕ. Let ϕ' be the intersection point of $\vec{\phi}$ with the supporting hyperplane $H(x)$ to B at x, for which the hyperplane is orthogonal to $\vec{\phi}$. Then $\triangle ox'\phi$ and $\triangle ox\phi'$ are similar triangles. Therefore, we have

$$\frac{|\phi|}{1/|x|} = \frac{|x|}{\delta(x)}$$

which gives $|\phi| = \frac{1}{\delta(x)}$, as required. ∎

The application of Lemma 3.3 to the dual ball of Figure 3.1 (iii) is demonstrated in Figure 3.5 (i). As shown in the figure, Lemma 3.3 provides an alternative approach for constructing B^* for a given B. Note that all the $v(x)$ for x on a straight line segment are equivalent; hence we need only compute one $v(x)$ for each x on a straight line segment when constructing B^* by this method.

3.2.2 Subdifferential calculus

The following facts about subdifferential calculus, which we use in the proof of a theorem in the next section, are taken from [73]. Let X be a Minkowski space with norm $\|\cdot\|$, unit ball B and dual ball B^*, and let X^* denote the dual space. A function, $f : X \to \mathbb{R}$, is *convex* if, for all $x, y \in X$ and $0 \leq \lambda \leq 1$,

$$f(\lambda x + (1-\lambda)y) \leq \lambda f(x) + (1-\lambda)f(y).$$

Convex functions on X are continuous on X. By the triangle inequality, every norm is a convex function, and it is well-known [65] that a sum of convex functions is itself a convex function. Thus $f(x) = \sum_{i=1}^{k} w_i \|p_i - x\|$ is convex, and is strictly convex if and only if B is strictly convex.

A *norming functional* of $x \in X$ is a $\phi \in X^*$ such that $\|\phi\| = 1$ and $\phi(x) = \|x\|$. The set of norming functionals of x is denoted by ∂x. By the Hahn-Banach separation theorem [65], each non-zero $x \in X$ has an associated norming functional. Each ∂x corresponds to an exposed face of B^*.

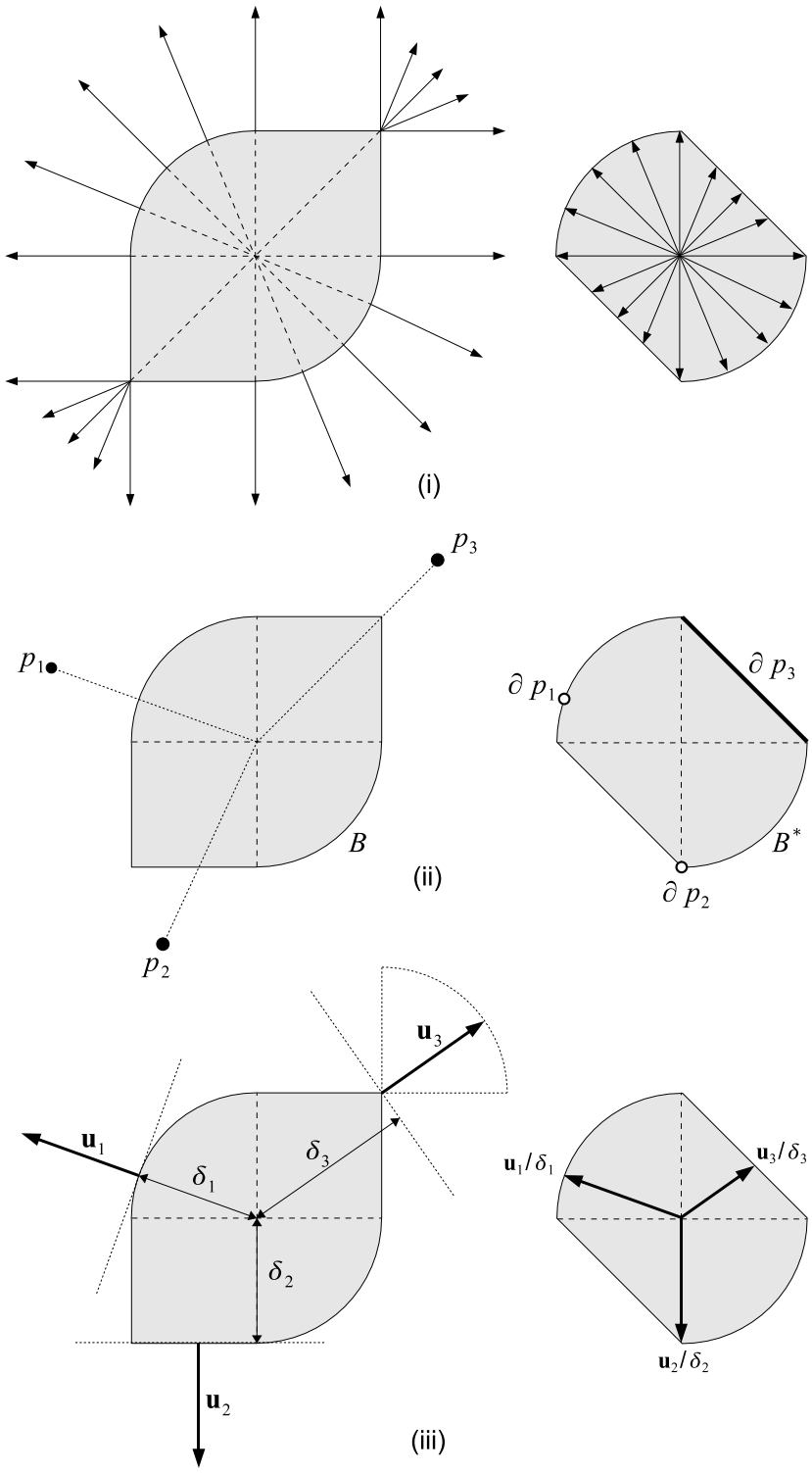

Figure 3.5: Unit ball and dual ball occurring in [62]. (i) Construction of the dual ball by Lemma 3.3. (ii) Norming functionals. (iii) Outward normal vectors.

A functional $\phi \in X^*$ is a *subgradient* of a convex function f at the point a if, for all $x \in X$,

$$f(x) - f(a) \geq \phi(x - a).$$

In particular, $o \in X^*$ is a subgradient of f at a if and only if f attains its minimum value at a. The *subdifferential* of f at a, denoted by $\partial f(a)$, is the set of all subgradients of f at a. The subdifferential of $f(x) = \sum_{i=1}^{k} \|p_i - x\|$ at any $x \in X$ is nonempty, compact and convex [65].

The *Minkowski sum* of two sets A and B in Euclidean space is the result of adding every element of A to every element of B, that is

$$A + B = \{a + b : a \in A,\ b \in B\}.$$

This defines a binary operation called *Minkowski addition*. Now we can state the following basic property of subdifferentials.

Lemma 3.4. *Let $p_1, \ldots, p_k$ be given points in a Minkowski space X with norm $\|\cdot\|$. Then for all $x \in X$,*

$$\partial \left(\sum_{i=1}^{k} w_i \|p_i - x\| \right) = \sum_{i=1}^{k} w_i \partial \|p_i - x\|$$

where the sum on the right is Minkowski addition.

Proof. Refer to [65], Theorem 23.8. ∎

We also have the following lemma.

Lemma 3.5. *Let x be a point in a Minkowski space X with norm $\|\cdot\|$. Then the subdifferential of the norm of x is given by*

$$\partial \|x\| = \begin{cases} B^*, & \text{if } x = o; \\ \partial x, & \text{if } x \neq o. \end{cases}$$

Proof. Refer to [65]. ∎

Using Lemma 3.3, for a given $x \in X$, we can compute $\partial \|x\| = \partial x$ as follows. Determine the unique point where the ray from o through x intersects $\mathrm{bd}(B)$. Compute the set of outward norming vectors $\mathbf{u}$ at this point, and their corresponding Euclidean distances

δ from o to their supporting hyperplanes. Then ∂x is the set of vectors $\frac{\mathbf{u}}{h}$, which corresponds to functionals on an exposed face of B^*. This is demonstrated in Figure 3.5 (ii) and (iii).

3.3 Characterisation of Fermat-Weber points

The following theorem, which provides a characterisation of FW points in Minkowski spaces is from [31]. It is a direct generalisation of Theorem 2.1. While reviewing this theorem, it might be useful to refer to the diagrams in Figure 3.5 (ii)–(iii).

Theorem 3.1. *Let $N = \{p_1, \ldots, p_k\}$ be a set of points in a Minkowski space X with norm $\|\cdot\|$ and unit ball B, where the points have respective positive weights $w_1, \ldots, w_k$. For a point $x_0 \in X$, let $\mathbf{u}_i$ denote the outward unit normal vector of the supporting hyperplane of $x_0 + B$ at the point where the ray from x_0 through $p_i \in N$ intersects the boundary of B, and δ_i the Euclidean distance from x_0 to this hyperplane.*

1. *If $x_0 \neq p_1, \ldots, p_k$, then the following statements are equivalent:*
   - *x_0 is an FW point for N.*
   - *Each $p_i - x_0$ has a norming functional ϕ_i such that*

$$\sum_{i=1}^{k} w_i \phi_i = o. \tag{3.3}$$

   - *Each $p_i - x_0$ has an outward normal unit vector $\mathbf{u}_i$ such that*

$$\sum_{i=1}^{k} \frac{w_i \mathbf{u}_i}{\delta_i} = \mathbf{0}. \tag{3.4}$$

2. *If $x_0 = x_j$ for some $j \in \{1, \ldots, k\}$, then the following statements are equivalent:*
   - *x_0 is an FW point for N.*
   - *Each $p_i - x_0$, $i \neq j$, has a norming functional ϕ_i such that*

$$\left\| \sum_{i=1, i\neq j}^{k} w_i \phi_i \right\| \leq w_j. \tag{3.5}$$

- *Each $p_i - x_0$, $i \neq j$, has an outward normal unit vector $\mathbf{u}_i$ such that*

$$\left\| \sum_{i=1, i\neq j}^{k} \frac{w_i \mathbf{u}_i}{\delta_i} \right\| \leq w_j. \tag{3.6}$$

Proof. (Adapted from [60].) The equivalence of a norming functional ϕ_i and an outward normal vector $\frac{w_i \mathbf{u}_i}{\delta_i}$ is established in Lemma 3.3. The point x_0 minimises the convex function $f(x) = \sum_{i=1}^{k} w_i \|p_i - x\|$ if and only if

$$\begin{aligned} o &\in \partial \left(\sum_{i=1}^{k} w_i \|p_i - x\| \right) && (3.7) \\ &= \sum_{i=1}^{k} w_i \partial \|p_i - x\| && (3.8) \\ &= \sum_{i=1}^{k} w_i \partial (p_i - x), && (3.9) \end{aligned}$$

where (3.8) is due to Lemma 3.4, and (3.9) is due to Lemma 3.5. This is equivalent to the conditions stated since, by Lemma 3.5, we have

$$\partial(p_i - x) = \begin{cases} \{\phi : \phi \text{ is a norming functional of } (p_i - x)\}, & \text{if } x \neq p_i; \\ \{\phi : \|\phi\| \leq 1\}, & \text{if } x = p_i. \end{cases}$$

∎

3.4 Properties of the Fermat-Weber locus

3.4.1 The Fermat-Weber locus

In Chapter 2, we noted that in Euclidean space, the solution to the FW problem is unique for all noncollinear N. This is not necessarily true in Minkowski spaces. Thus we require the following definition, which is due to [60].

Definition 3.1. *Let N be a set of given points in a Minkowski space X. Then the set of FW points for N is called the* FW locus *of N, and is denoted by* $\mathrm{fw}(N)$.

Now we can state the following lemma.

Theorem 3.2. *Let X be a Minkowski space with unit ball B. Then the FW locus is a unique point for all noncollinear sets N if and only if B is strictly convex.*

Proof. Refer to Theorem 3.3 of [60]. The proof is easily adapted to the weighted case. ∎

The following property of $\mathrm{fw}(N)$ can be stated immediately.

Lemma 3.6. *The FW locus of any finite set is always nonempty, compact and convex.*

Proof. Refer to [60]. The proof is easily adapted to the weighted case. ∎

For the case of a *Minkowski plane*, i.e. a Minkowski space of dimension two, we have the following result.

Lemma 3.7. *The FW locus of any finite set in a Minkowski plane is a point, a line segment or a convex polygon.*

Proof. Refer to [24]. ∎

3.4.2 Location of the Fermat-Weber locus relative to the convex hull

Let $\mathrm{conv}(\cdot)$ and $\mathrm{int}(\cdot)$ denote, respectively, the convex hull and interior of a set $(\cdot)$. Recall from Chapter 2 that, in Euclidean space, if x_0 is an FW point for a set N of noncollinear points, then $x_0 \in \mathrm{int}(\mathrm{conv}(N)) \cup N$. In Minkowski spaces this is not always true.

The relationship between $\mathrm{fw}(N)$ and $\mathrm{conv}(N)$ in a Minkowski *plane* can be examined by introducing the notion of a *balanced double cluster*, which generalises the notion of a double cluster proposed in [60] for the unweighted case. Recall that a proper exposed face of a unit ball B is an intersection of B with some supporting hyperplane.

Definition 3.2. *Let $N = \{p_1, \ldots, p_k, q_1, \ldots, q_l\}$ be a set of given points with respective positive weights in a Minkowski plane with unit ball B, and let $\widehat{p_i q_j}$ denote the vector from p_i to q_j. Then N forms a* double cluster *if, for all $i = 1, \ldots, k$ and $j = 1, \ldots, l$, $\widehat{p_i - q_j}$ pass through the same proper exposed face of $B + p_i$. A double cluster is said to be balanced when the sum of weights associated with $p_1, \ldots, p_k$ equals the sum of weights associated with $q_1, \ldots, q_l$.*

A double cluster is a special case of a balanced double cluster where $k = l$ and all the weights are equal to one. Unlike a double cluster, a balanced double cluster can have an odd number of points. The following result generalises Theorem 4.1 from [60] to the weighted case.

Theorem 3.3. *Let x_0 be an FW point for a set of noncollinear terminals N with respective positive weights in a Minkowski plane X such that $x_0 \notin \text{int}(\text{conv}(N)) \cup N$. Then N is a balanced double cluster.*

Proof. We adapt the proof provided in [60] to the weighted case. Since x_0 is an FW point for N, by Theorem 3.1, for each $p_i \in N$, there exist $\mathbf{u}_i$ and δ_i such that $\sum_{i=1}^{k} \frac{w_i \mathbf{u}_i}{\delta_i} = \mathbf{0}$. Since $x \notin \text{conv}(N)$, all the $\mathbf{u}_i$ must be contained in a closed half plane bounded by a line L through it. Since the sum of the $\frac{w_i \mathbf{u}_i}{\delta_i}$ is zero, all the $\mathbf{u}_i$ must lie on L and consequently the δ_i are equal. Hence N has two subsets, $p_1, \ldots, p_j$ and $p_{j+1}, \ldots, p_k$, such that the sum of weights associated with each subset are equal. ∎

We demonstrate the notion of a balanced double cluster by way of an example. Let X be a Minkowski plane with the unit ball B shown in Figure 3.6 (i). Let $N = \{p_1, p_2, p_3, p_4\}$, where $\{p_1 = (0,0),\ p_2 = (2,0)\}$, $p_3 = (2,3)$, $p_4 = (0,3)$ and the four points have respective weights $1, 4, 2, 3$. Then $\text{conv}(N)$ is the rectangle having p_1, p_2, p_3, p_4 as its vertices. It can be shown (refer to the next section) that $\text{fw}(N)$ is the parallelogram with vertices $\{(1.0, 0.6),\ (2.6, 1.5),\ (1.0, 2.4),\ (-0.6, 1.5)\}$ (the shaded region in Figure 3.6 (i)). Hence part of $\text{fw}(N)$ is outside $\text{conv}(N)$. Therefore, by Theorem 3.1, N must be a balanced double cluster. To show that this is the case, suppose B is centred on p_1. Then $\widehat{p_3 - p_1}$ and $\widehat{p_4 - p_1}$ pass through the straight line segment on the boundary of B. Similarly if B is centred on p_4, then $\widehat{p_1 - p_4}$ and $\widehat{p_2 - p_4}$ pass through the same segment. Since $w_1 + w_2 = w_3 + w_4$, we have that N is a balanced double cluster with sets $\{p_1, p_2\}$ and $\{p_3, p_4\}$.

3.5 Exact solutions for special cases

As for the Euclidean case, there are certain instances of the FW problem which can be solved with very little computational effort. One such instance is when the given points

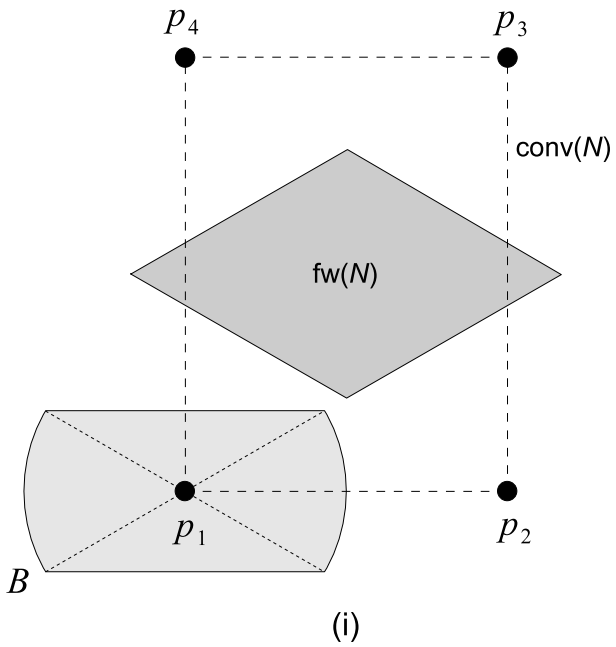

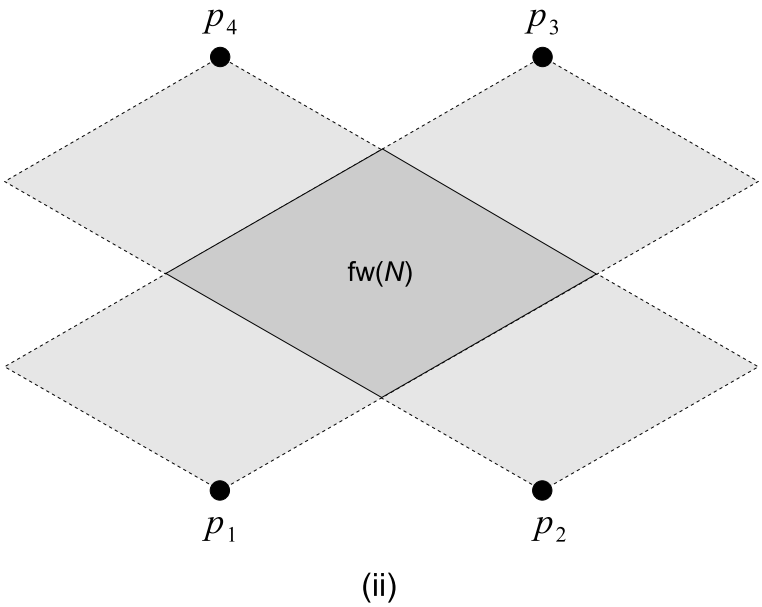

Figure 3.6: Special instances of the FW problem. (i) A balanced double cluster. (ii) Example of ρ-concurrent ρ-segments.

form ρ-concurrent ρ-segments, as described below.

3.5.1 Balanced ρ-concurrent ρ-segments

The definition of ρ-concurrent ρ-segments, due to [60], is provided below. We extend this definition to the weighted case.

Definition 3.3. *Let p_i, p_j be given points with respective positive weights w_i, w_j in a Minkowski space X with norm $\|\cdot\|$ giving rise to a metric $\rho(x,y) := \|x-y\|$. The* ρ-segment *between p_i and p_j, denoted by $[p_i, p_j]_\rho$ is*

$$[p_i, p_j]_\rho = \{x \in X : \|p_i - x\| + \|x - p_j\| = \|p_i - p_j\|\}.$$

The ρ-segment is said to be balanced *if $w_i = w_j$. Two ρ-segments are said to be* ρ-concurrent *if their intersection is nonempty. Three or more ρ-segments are said to be ρ-concurrent if every pair is ρ-concurrent.*

We now adapt Corollary 3.3 from [60] to the weighted case.

Lemma 3.8. *If given points $N = \{p_1, \ldots, p_{2k}\}$ can be matched up to form k balanced ρ-segments $[p_i, p_{k+i}]_\rho$, $i = 1, \ldots, k$ that are ρ-concurrent, then*

$$\mathrm{fw}(N) = \bigcap_{i=1}^{k} [p_i, p_{k+i}]_\rho.$$

Proof. Consider a point $x \in \bigcap_{i=1}^{k} [p_i, p_{k+i}]_\rho$. Since $x \in [p_j, p_{k+j}]_\rho$ for each ρ-segment $[p_j, p_{k+j}]_\rho$, $i = 1, \ldots, k$, there exist norming functionals such that $w_j\phi_j + w_{k+j}\phi_{k+j} = o$ and, by Theorem 3.1, x is an FW point for N. ∎

To demonstrate this concept, consider the set of given points and the unit ball of the previous example, illustrated in Figure 3.6 (i). It can be shown (see [60], Proposition 3.3) that the ρ-segment $[p_1, p_3]_\rho$ is the parallelogram shown in Figure 3.6 (ii), while the ρ-segment $[p_2, p_4]_\rho$ is constructed in the same way. By Lemma 3.8, if $w_1 = w_3$ and $w_2 = w_4$, then $\mathrm{fw}(\mathcal{P})$ is the intersection of the two ρ-segments (the shaded region in Figure 3.6 (ii)).

Suppose now that we increase one of the weights, say w_1 by an arbitrarily small amount. Then, the weighted functionals are no longer balanced. It can be shown that the FW point degenerates to the unique point at the base of the dark shaded region.

3.5.2 Collinear and cogeodesic sets

In Euclidean space, a finite set of distinct points $N = \{p_1, \ldots, p_k\}$ is *collinear* if all the p_i lie on the same straight Euclidean line. The following definition extends the concept of collinear points to Minkowski spaces.

Definition 3.4. *A set of points, $N = \{p_1, \ldots, p_k\}$, in a Minkowski space with norm $\|\cdot\|$ is ρ-collinear if all the $p_i \in N$, $i = 1, \ldots, k$ lie on the same Euclidean metric line.*

A further extension of collinear points to Minkowski spaces was posed in [60].

Definition 3.5. *A set of points $N = \{p_1, \ldots, p_k\}$, in a Minkowski space with norm $\|\cdot\|$ is ρ-cogeodesic if all the p_i lie on a single geodesic in X between two of the points in N.*

Note that in [60], a ρ-cogeodesic set is called a ρ-collinear set. In this work, we reserve the term ρ-collinear for points lying on a Euclidean straight line (Definition 3.4).

Examples of ρ-collinear and ρ-cogeodesic sets for the rectilinear norm in the plane are shown in Figure 3.7 (i) and (ii) respectively. Every ρ-collinear set is ρ-cogeodesic, but not all ρ-cogeodesic sets are ρ-collinear. Also, every ρ-cogeodesic set forms a double cluster, but not every double cluster is a ρ-cogeodesic set. The solution to the FW problem for unweighted ρ-cogeodesic sets in Minkowski spaces is given by Corollaries 3.5 and 3.6 of [60]. Here we generalise to the weighted case. The following result solves the FW problem.

Lemma 3.9. *Suppose $N = \{p_1, \ldots, p_k\}$ is a ρ-cogeodesic set of points, and each point $p_i \in N$ has an associated positive weight w_i. Then one of the following conditions holds for some j: $\mathrm{fw}(N) = [p_j, p_{j+1}]_\rho$ if and only if $\sum_{i=1}^{j} w_i = \sum_{i=j+1}^{k} w_i$; or $\mathrm{fw}(N) = p_j$ if and only if $\left|\sum_{i=1}^{j-1} w_i - \sum_{i=j+1}^{k} w_i\right| < w_j$.*

Proof. For any $p_j \in N$, the rays from p_j through p_i for $i < j$ all pass through the same exposed face of $p_j + B$, and the rays from p_j through p_i for $i > j$ all pass through the opposite exposed face of $p_j + B$. Let L be any line through p_j that is orthogonal to these two

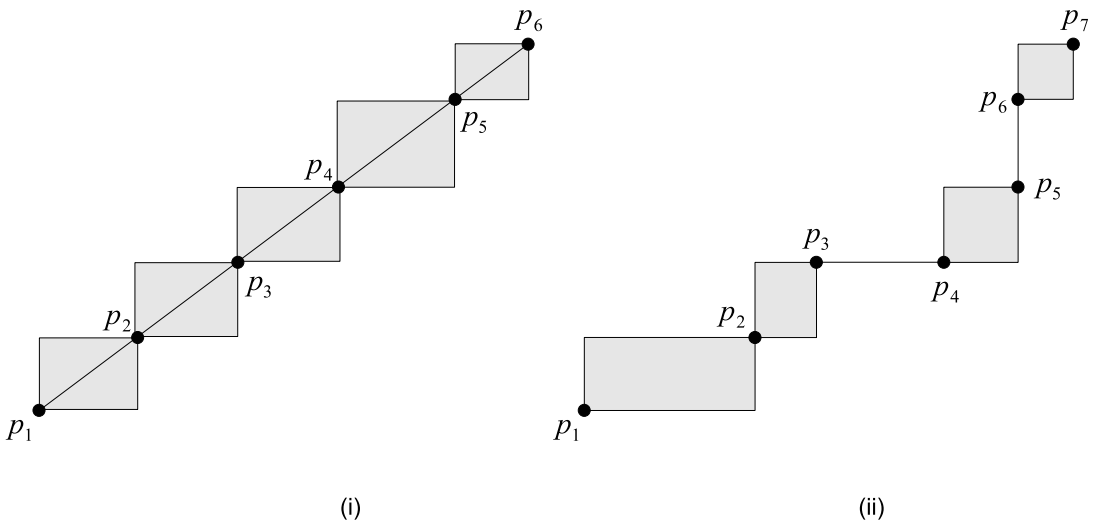

Figure 3.7: Colinear and cogeodesic sets in the rectilinear norm in the plane. (i) Set of six ρ-collinear points. (ii) Set of seven ρ-cogeodesic points.

exposed faces (note that L does not necessarily correspond to the metric line containing the given points). Suppose that a point x lies on the line segment between p_j and p_{j+1}, $j = 1, \ldots, k-1$. The optimality condition for x is $\sum_{i=1}^{k}(w_i/\delta_i)\mathbf{u}_i = \mathbf{0}$. Since the points in N are ρ-cogeodesic, there exist unit vectors $\mathbf{u}_i$ associated with each p_i that are all parallel to L, with the $\mathbf{u}_i$, $i = 1, \ldots, j$ being in the opposite direction to the $\mathbf{u}_i$ $i = j+1, \ldots, k$. It is also clear that all δ_i, $i = 1, \ldots, k$ are equal. If x is optimal, then the above equation reduces to $\left(\sum_{i=1}^{j} w_i - \sum_{i=j+1}^{k} w_i\right) = \mathbf{0} \Rightarrow \sum_{i=1}^{j} w_i = \sum_{i=j+1}^{k} w_i$. Now suppose p_j is an FW point. The optimality condition is $\left|\sum_{i=1, i\neq j}^{k}(w_i/\delta_i)\mathbf{u}_i\right| \leq w_j$. Since the points in N are ρ-cogeodesic, there exist unit vectors associated with each p_i, $i \neq j$ that all lie on L, with the $\mathbf{u}_i$, $i = 1, \ldots, j-1$ being in the opposite direction to the $\mathbf{u}_i$, $i = j+1, \ldots, k$. If x is optimal, then the above equation reduces to $\left|\sum_{i=1}^{j-1} w_i - \sum_{i=j+1}^{k} w_i\right| \leq w_j$. Similar reasoning can be used to show that in each case the reverse implication is true. ∎

The following simple corollary is observed from Theorem 3.9.

Corollary 3.1. *For any ρ-cogeodesic set of points in a Minkowski space, $|\mathrm{fw}(N) \bigcap N| \in \{1, 2\}$.*

3.6 Geometric property of the solution to the three-point problem

In this section we study the FW problem in two-dimensional Minkowski spaces for the case where there are three given points. This case is interesting to study both as the smallest nontrivial case of the FW problem, and because of its application to finding locally minimal solutions to the Gilbert arborescence problem in Minkowski spaces studied in Chapter 6, since many Steiner points in Gilbert arborescences have degree three. The following is a twofold generalisation of Theorem 4 in [22]. The theorem was originally posed for the unweighted problem where the given points are at the vertices of an n-dimensional simplex in Minkowski spaces with smooth and strictly convex unit balls. We provide the generalised result for the two-dimensional case. The theorem is illustrated in Figure 3.8, in which the unit ball shown is that of the gradient metric, discussed in more detail in the following chapter.

Theorem 3.4. *Let $N = \{p_1, p_2, p_3\}$ be a given set of non-cogeodesic points not forming a balanced double cluster in a Minkowski space X with norm $\|\cdot\|$ and unit ball B, and let w_1, w_2, w_3 be the respective weights. Let x be a variable point in X. Let H_1, H_2, H_3 be supporting lines of $x + B$ at the points where the rays from x through p_i intersect the boundary of $x + B$, and let D be the triangle formed by these supporting lines. Let a_i be the vertex of D opposite H_i, with corresponding weight, w_i (see Figure 3.8). Then x_0 is an FW point for N if and only if there exists a choice of supporting lines H_1, H_2, H_3 for x_0 such that x_0 is the centre-of-gravity of the weights of the vertices of D, that is*

$$x_0 = \frac{w_1 a_1 + w_2 a_2 + w_3 a_3}{w_1 + w_2 + w_3}.$$

Proof. We adapt the proof from [22] to the weighted case. Refer to Figure 3.8. Let $\mathbf{u}_i$ be an outward unit normal vector to H_i, and δ_i the Euclidean distance from x to H_i. Let $\mathbf{b}_i$ be the vector form x to a_i. Then, for $i \neq j$, we have

$$(\mathbf{b}_i \cdot \mathbf{u}_j) = \delta_j. \tag{3.10}$$

The optimality condition for x is $\sum_{i=1}^{3}(w_i/\delta_i)\mathbf{u}_i = \mathbf{0}$. Hence, for any $j \in \{1,2,3\}$, we have

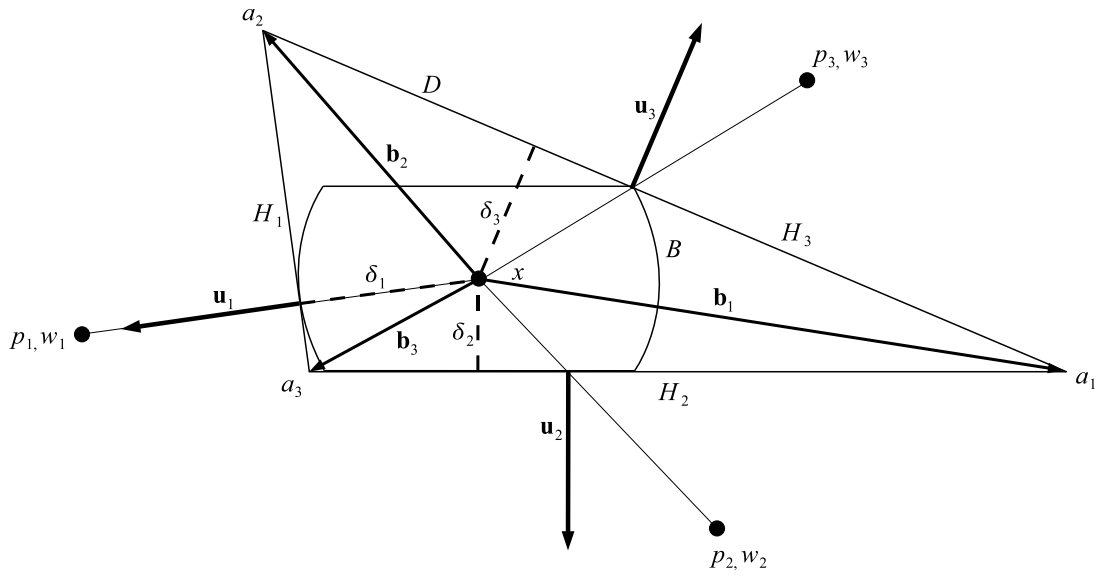

Figure 3.8: Geometric property of the solution to the three-point FW problem.

$\mathbf{b}_j \cdot \sum_{i=1}^{3}(w_i/\delta_i)\mathbf{u}_i = \mathbf{0}$ and therefore $\sum_{i=1}^{3}(w_i/\delta_i)(\mathbf{b}_j \cdot \mathbf{u}_i) = \mathbf{0}$. From (3.10), for $i \neq j$, we can replace the $(\mathbf{b}_j \cdot \mathbf{u}_i)$ with δ_i, giving $\sum_{i\neq j,\, i=1}^{3} w_i + (w_j/\delta_j)(\mathbf{b}_j \cdot \mathbf{u}_j) = \mathbf{0}$, where the second term is for the case where $i = j$. Again from (3.10), for $i \neq j$, we can multiply the w_i terms by $(\mathbf{b}_i \cdot \mathbf{u}_j)/\delta_j = 1$, giving $\sum_{i\neq j,\, i=1}^{3}(w_i/\delta_j)(\mathbf{b}_i \cdot \mathbf{u}_j) + (w_j/\delta_j)(\mathbf{b}_j \cdot \mathbf{u}_j) = \mathbf{0}$. All the terms can be combined to form $\sum_{i=1}^{3}(w_i/\delta_j)(\mathbf{b}_i \cdot \mathbf{u}_j) = \mathbf{0}$. Rearranging gives $\sum_{i=1}^{3} w_i\mathbf{b}_i \cdot (\mathbf{u}_j/\delta_j) = \mathbf{0}$, which implies that $\sum_{i=1}^{3} w_i\mathbf{b}_i = \mathbf{0}$. So x is optimal when $\sum_{i=1}^{3} w_i\mathbf{b}_i = \mathbf{0}$, which can be rewritten $\sum_{i=1}^{3} w_i \cdot \widehat{a_i - x} = \mathbf{0}$, where $\widehat{a_i - x}$ denotes the vector from x to a_i. Solving for x gives $x = \left(\sum_{i=1}^{3} w_i a_i\right) / \left(\sum_{i=1}^{3} w_i\right)$. ∎

Note that if N is a balanced double cluster, then the rays from x through p_i, $i = 1,2,3$ all pass through the same pair of opposite exposed faces of B. Hence, H_1, H_2, H_3 are all parallel, and do not form a triangle.

Chapter 4

The Gradient-Constrained Fermat-Weber Problem

In this chapter we introduce the gradient-constrained Fermat-Weber (FW) problem, an instance of the FW problem in Minkowski spaces where distance is measured by a special metric, called the gradient metric [13]. Under this metric, the distance between two points is the minimum length of a piecewise smooth curve connecting the points such that the absolute value of the instantaneous gradient at each differentiable point on the curve is no more than a given upper bound $m > 0$. Such curves can be used to model tunnels in underground mines, where m is the maximum grade at which haulage vehicles can operate. We concentrate on two- and three-dimensional spaces, which are natural contexts for underground mining problems.

We begin by outlining the gradient metric, deriving its unit ball and dual ball in two and three dimensions, and demonstrating how to compute the set of norming functionals associated with a point in gradient-constrained space. We then present an iterative scheme for solving the gradient-constrained FW problem numerically, and prove convergence for the two- and three-dimensional cases. Finally, we demonstrate the application of the problem to the optimal design of underground mines by using it to solve a simplified version of the case study presented in Chapter 9.

4.1 Introduction

SO far in this work we have studied, in Chapters 2 and 3 respectively, the n-dimensional Fermat-Weber (FW) problem in Euclidean space and in real finite-dimensional normed spaces, or Minkowski spaces. We have discussed how an FW point x_0 in Euclidean space has a characterisation with a natural physical interpretation; namely, if x_0 does not coincide with a given point, then it is located such that the weighted unit vectors from x_0 to the given points are balanced. We showed that this characterisation

generalises to Minkowski spaces, where the orientations and lengths of the vectors associated with the given points correspond to norming functionals, and are determined by the geometry of the unit ball and the dual ball of the space. We have presented a wide range of geometric properties of the FW problem in Euclidean and Minkowski spaces, discussed special instances where the problems can be solved exactly with very little computational effort, and stated a known algorithm for solving the Euclidean problem numerically.

In this chapter we introduce the *gradient-constrained FW problem*, an instance of the FW problem in Minkowski spaces where distance is measured by a special metric, called the *gradient metric* [13]. Under this metric, the distance between two points is the minimum length of a piecewise smooth curve connecting the points such that the absolute value of the instantaneous gradient at each differentiable point on the curve is no more than a given upper bound $m > 0$. Such curves can be used to model tunnels in underground mines, where m is the maximum grade at which haulage vehicles can operate. While many of the results in this chapter generalise to higher dimensions, we concentrate on two- and three-dimensional spaces, which are natural contexts for underground mining problems.

We begin in Section 4.2 by presenting background from [13] on the gradient metric. Using results from Section 3.2 in Chapter 3, we derive the unit ball B_g and dual ball B_g^* in two and three dimensions. For a point x in gradient-constrained space, we demonstrate how to compute its associated set of norming functionals ∂x and their analogous vectors. We show that ∂x is a unique point on the boundary of B^* unless x lies on a straight line through the origin such that the absolute value of the gradient of the line is exactly m, in which case ∂x is a line segment on the boundary of B^*, in two and three dimensions.

In Section 4.3, we propose an iterative scheme for solving the gradient-constrained FW problem numerically, based on a modification of the subgradient method [69] for nondifferentiable convex functions. The algorithm incorporates exact directional minimisation instead of predetermined step sizes, and provides an alternative search direction when the iterative point is in some neighborhood of a nondifferentiable region. In Section 4.4, we provide convergence results for the two- and three-dimensional cases.

Finally in Section 4.5, we demonstrate the application of the gradient-constrained FW problem to the optimal design of underground mines, by using it to solve a simplified version of the case study presented in Chapter 9. The simplified problem, which ignores some of the constraints dealt with in the detailed study, involves determining the optimum location of the base of a vertical hoisting shaft in the Callie underground mine.

4.2 The gradient constraint

The following account of the gradient constraint, gradient-constrained networks and the gradient metric, is taken primarily from [13].

4.2.1 The gradient metric

Let $p = (x_p, y_p, z_p)$ and $q = (x_q, y_q, z_q)$ be points in Euclidean three-space, where the z-axis is vertical. Let pq denote a minimum-length piecewise smooth curve connecting p and q. We define the *gradient* of pq, denoted by $g(pq)$, to be the absolute value of the slope of the Euclidean straight line segment connecting p and q, that is

$$g(pq) = \frac{|z_q - z_p|}{\sqrt{(x_q - x_p)^2 + (y_q - y_p)^2}}.$$

Let $m > 0$ be a maximum allowable gradient. Under the *gradient constraint*, the absolute value of the instantaneous gradient at each differentiable point on pq must not exceed m. A curve satisfying this condition is called *gradient-constrained*. If $g(pq) \leq m$, then pq is a Euclidean straight line segment connecting p and q, and is called *straight*. On the other hand, if $g(pq) > m$, then pq cannot be represented by a straight line segment without violating the gradient constraint. It can, however, be represented by a zigzag line connecting p and q, each segment of the zigzag having gradient m. Such a curve is called *bent*. It is easily seen that such zigzag lines are geodesics under the gradient constraint. In general, there are many other ways of embedding a bent edge, for example, by a helical arc. In the mining context such embeddings can overcome the haulage vehicle navigability problems associated with zigzag lines.

The distance between two points p and q in gradient-constrained space can be measured with respect to the positions of p and q in a special metric, called the *gradient metric*. Define the *vertical metric* of the distance between p and q to be $|q-p|_v = c|z_q - z_p|$, where c is a given constant. Then the gradient metric can be defined in terms of the Euclidean metric $|\cdot|$ and the vertical metric $|\cdot|_v$. For a given m, the distance between p and q in the gradient metric is defined to be

$$|q-p|_g = \begin{cases} |q-p| = \sqrt{(x_q-x_p)^2+(y_q-y_p)^2+(z_q-z_p)^2}, & \text{if } g(pq) \le m; \\ |q-p|_v = \sqrt{1+m^{-2}}|z_q - z_p|, & \text{if } g(pq) \ge m. \end{cases}$$

It is easily checked that this defines a metric. Note that $|q-p| \le |q-p|_g$, and that the gradient metric is convex, although it is not strictly convex.

A curve pq is defined to be an *f-edge*, *m-edge* or *b-edge* if the gradient of pq is less than, equal to, or greater than m, respectively. The *label* of an f-edge, m-edge or b-edge is 'f' (meaning flat), 'm' (meaning maximum), or 'b' (meaning bent), respectively. The label of pq can be thought of as indicating which metric is 'active' for that edge, with an 'm' label indicating that both metrics hold simultaneously. Throughout this work we let α denote the acute angle between an m-edge and a horizontal plane; thus $m = \tan\alpha$. Also note that $\sqrt{1+m^{-2}} = \frac{1}{\sin\alpha}$. Further identities relating m and α are provided in Appendix B.

Let $N = \{p_1, \ldots, p_k\}$ be given points in three-dimensional space with respective positive weights $w_1, \ldots, w_k$, and let m be a maximum gradient satisfying $0 < m \le 1$. The *gradient-constrained FW problem* asks for a point x_0 minimising

$$f(x) = \sum_{i=1}^{k} w_i |p_i - x|_g$$

where $|\cdot|_g$ is the gradient metric. As per Chapter 3, x_0 is called an *FW point*, and the set of all FW points for a given N, denoted by $\mathrm{fw}(N)$, is called the *FW locus*.

It should be noted that the study of the gradient-constrained Fermat-Weber problem was initiated by Hyam Rubinstein in an unpublished research note [66]. Some early work on the problem was presented at the 18th National Conference of the Australian Society for Operations Research [14].

4.2.2 The unit ball and dual ball

For the remainder of this section, most of the material presented is new to the literature on gradient-constrained networks.

It is easily checked that $\mathbb{R}^3$ equipped with $|\cdot|$ is an example of a Minkowski space. Therefore, we can apply the principles of Chapter 3 to the gradient-constrained FW problem. The unit ball B_g and dual ball B_g^* in three-dimensional gradient-constrained space are shown in Figure 4.1, for the case where $m = \frac{1}{\sqrt{3}}$.

The unit ball is constructed by noting that points $x \in B_g$ for which $g(ox) \leq m$ correspond to points in the Euclidean unit ball, which is a sphere in $\mathbb{R}^3$. Points $x \in B_g$ for which $g(ox) > m$ have $|ox|_g = \sqrt{1+m^{-2}}|z|$, where z is the vertical component of x. Since this distance does not depend on horizontal components, points on a horizontal plane have the same distance from o. Thus, the top and bottom flat faces correspond to the set of points x for which $z = \frac{1}{\sqrt{1+m^{-2}}}$. Note that a diagonal line passing through o and connecting opposite non-smooth points on the boundary of B_g has gradient m.

The dual ball is constructed as per Lemmas 3.1 and 3.2 in Chapter 3, by constructing hyperplanes for each point on the boundary of B_g, excluding points on straight line segments. Thus B_g^* is the union of B_g and right circular cones whose bases coincide with the flat faces of B_g, such that a line from the base perimeter to the cone vertex has gradient $\frac{1}{m}$.

Note that the unit ball is neither smooth nor strictly convex, and the same is true for the dual ball. The lack of strict convexity implies that the FW locus is not a unique point for all given point sets. The lack of smoothness implies that the set of norming functionals of an arbitrary point x is not unique for all x.

4.2.3 Norming functionals

Recall from Chapter 3 that the set of norming functionals ∂x of a point x corresponds to an exposed face of the dual ball, and that a norming functional is equivalent to a vector $\frac{\mathbf{u}}{\delta}$, where $\mathbf{u}$ is an outward unit vector normal to the hyperplane supporting B_g at the point where the ray from o through x intersects B_g, and δ is the distance from x to this

hyperplane.

For a given point set $N = \{p_1, \ldots, p_k\}$, we can characterise the $\mathbf{u}_i$ and δ_i for the gradient metric according to the gradient of the Euclidean straight line segment connecting x and p_i. For each point $p_i \in N$, it is sufficient to consider only the vertical plane containing o and p_i. Refer to Figure 4.2. Suppose op_1 is an f-edge. Then $\mathbf{u}_1$ points directly from o to p_1 and $\delta_1 = 1$. Now suppose op_2 is a b-edge. Then $\mathbf{u}_2$ points vertically up or down, if p_2 is above or below o respectively, and $\delta_2 = 1/\sqrt{1+m^{-2}}$. Now let op_3 be an m-edge. Then there is a continuum of possible supporting hyperplanes at the non-smooth point on the boundary of B_g. The resulting normal unit vectors all lie in a vertical plane and have all possible directions between an m-edge and a vertical edge. If, in a vertical plane, a given $\mathbf{u}_3$ forms an angle ψ with the m-edge, then the corresponding $\delta_3 = \cos\psi$. Note that the set of all possible $\mathbf{u}_3/\delta_3$ associated with an m-edge forms a right-angled triangle corresponding to a subset of B^*.

4.2.4 The dual norm in the gradient-constrained dual space

The dual norm is defined as

$$\|\phi\|^* = \max\{\phi(x) : \|x\| = 1\}. \tag{4.1}$$

Given the coordinates of a functional in the gradient-constrained dual space, we can compute $\|\phi\|^*$ by consideration of the dual ball, as per the following lemma.

Lemma 4.1. *Let $\phi = (\phi_1, \phi_2, \phi_3)$ be a functional in the three-dimensional gradient-constrained dual space. If $m > 0$ is a maximum allowable gradient, then the dual norm of ϕ is*

$$|\phi|_g^* = \begin{cases} \sqrt{\phi_1^2 + \phi_2^2 + \phi_3^2}, & \text{if } g(\phi) \le m; \\ \sqrt{\phi_1^2 + \phi_2^2}\cos\alpha + |\phi_3|\sin\alpha, & \text{if } g(\phi) \ge m. \end{cases} \tag{4.2}$$

where $g(\phi)$ is the gradient of the Euclidean straight line connecting o and ϕ, and $\alpha = \tan^{-1} m$.

Proof. Consider the dual ball B^* in the gradient-constrained dual space. If $g(\phi) \le m$, then clearly the dual norm of ϕ in the gradient metric is the same as the Euclidean norm.

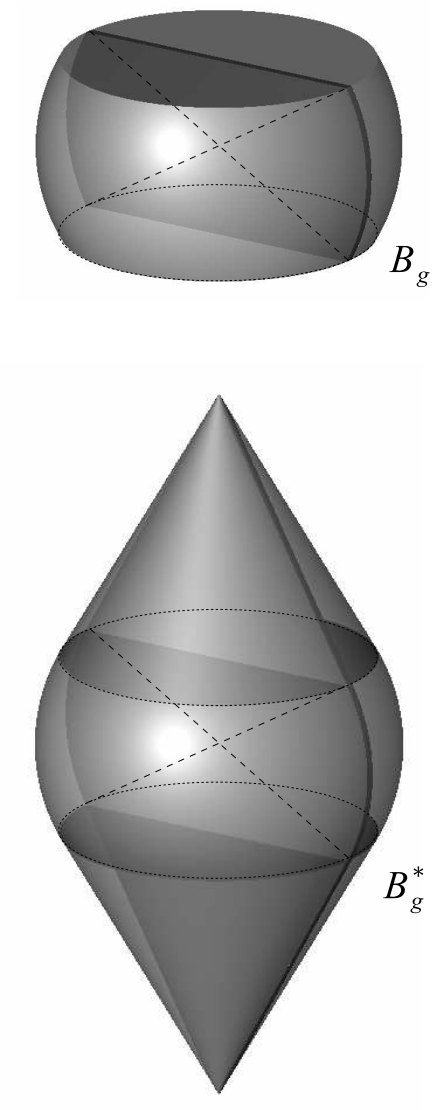

Figure 4.1: Unit ball and dual ball in three-dimensional gradient-constrained space.

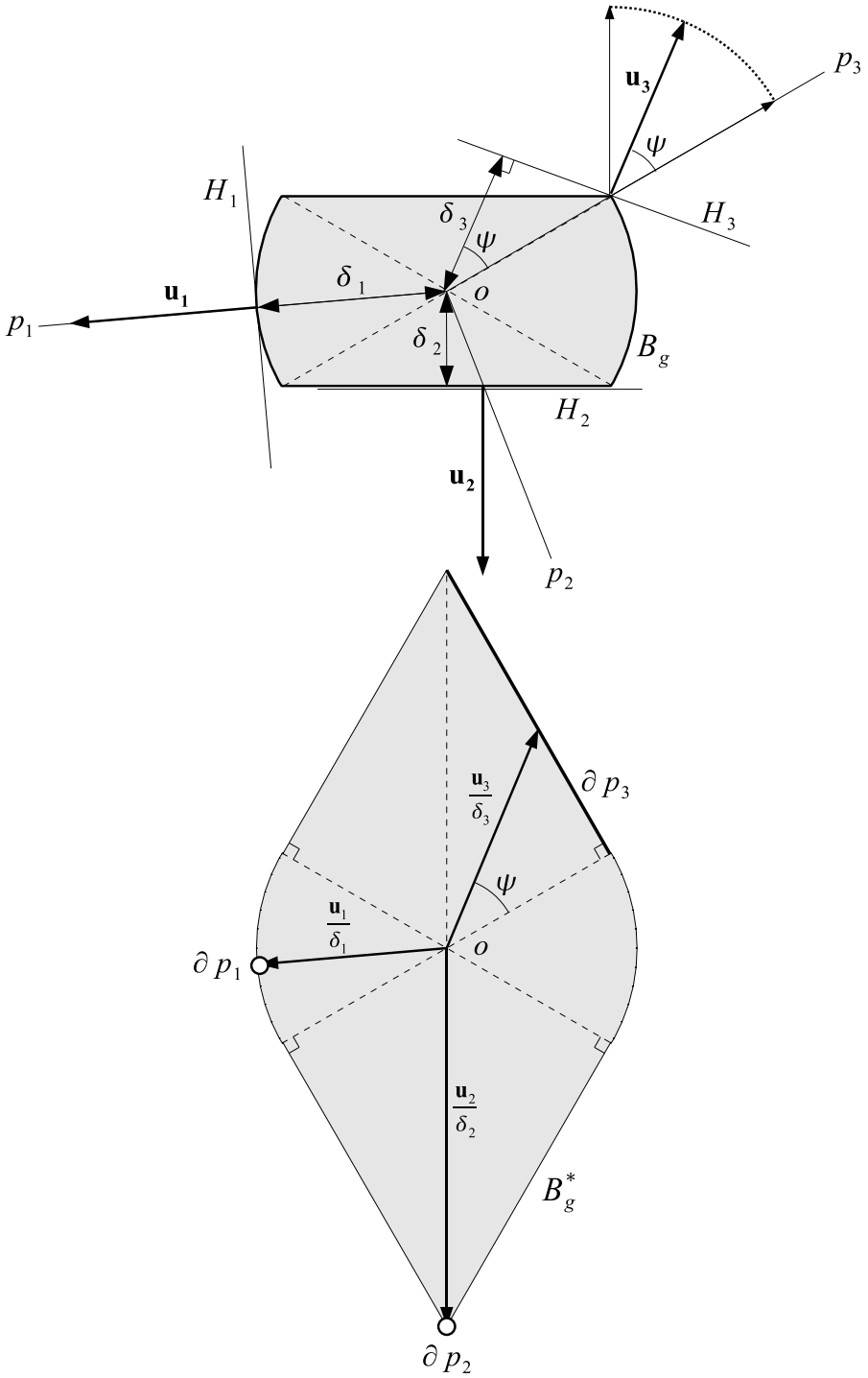

Figure 4.2: Norming functionals and outward normal vectors for f-, m- and b-edges.

Now suppose that $g(\phi) > m$ (Figure 4.3). Imagine we construct a scaled copy of the dual ball with radius $|\phi|_g^*$ centred on the origin o. Then ϕ lies on the boundary of $B^*(|\phi|_g^*)$. Moreover, since $g(\phi) > m$, it must lie on a straight segment of the dual ball. The dual norm of ϕ in the gradient metric is the projection of ϕ onto the m-edge in the same vertical plane (Cross-section A-A in Figure 4.3). From the figure, it is easily seen that this projection has Euclidean length $\sqrt{\phi_1^2 + \phi_2^2}\cos\alpha + |\phi_3|\sin\alpha$. ∎

4.2.5 Planar versus three-dimensional problems

We briefly comment on the difference between two- and three-dimensional versions of the gradient-constrained FW problem. Suppose $N = \{p_1, \ldots, p_k\}$ are given points lying on an inclined plane $\mathcal{P}$ passing through o and making an angle of θ with a horizontal plane. By taking the intersection of the three-dimensional unit ball B_g and $\mathcal{P}$, we obtain a new unit ball B_g' lying on $\mathcal{P}$. Now there are two cases: (1) if $\theta < \alpha$, then B_g' is the Euclidean ball in $\mathbb{R}^2$ (see Figure 4.4 (i)), and the problem can be solved using Weiszfeld's algorithm as per Chapter 2. However, if $\theta \geq \alpha$, then B_g' looks similar to B_g in a vertical plane for $m = \tan\theta$. We cannot simply solve the problem assuming this unit ball though, because the unit vectors associated with m- and b-edges do not necessarily lie on $\mathcal{P}$ (see Figure 4.4 (ii)). Therefore, unless $\mathcal{P}$ is a vertical plane, this latter case must be treated as a genuine three-dimensional problem.

4.3 A descent algorithm

In Euclidean space, the FW problem can be solved using the Weiszfeld algorithm [86] stated in Chapter 2, Section 2.6. However, numerical tests have shown that this method does not lend itself well to the gradient-constrained problem. In this section, we propose a new iterative scheme for finding a point x_0 minimising

$$f(x) = \sum_{i=1}^{k} |p_i - x|_g.$$

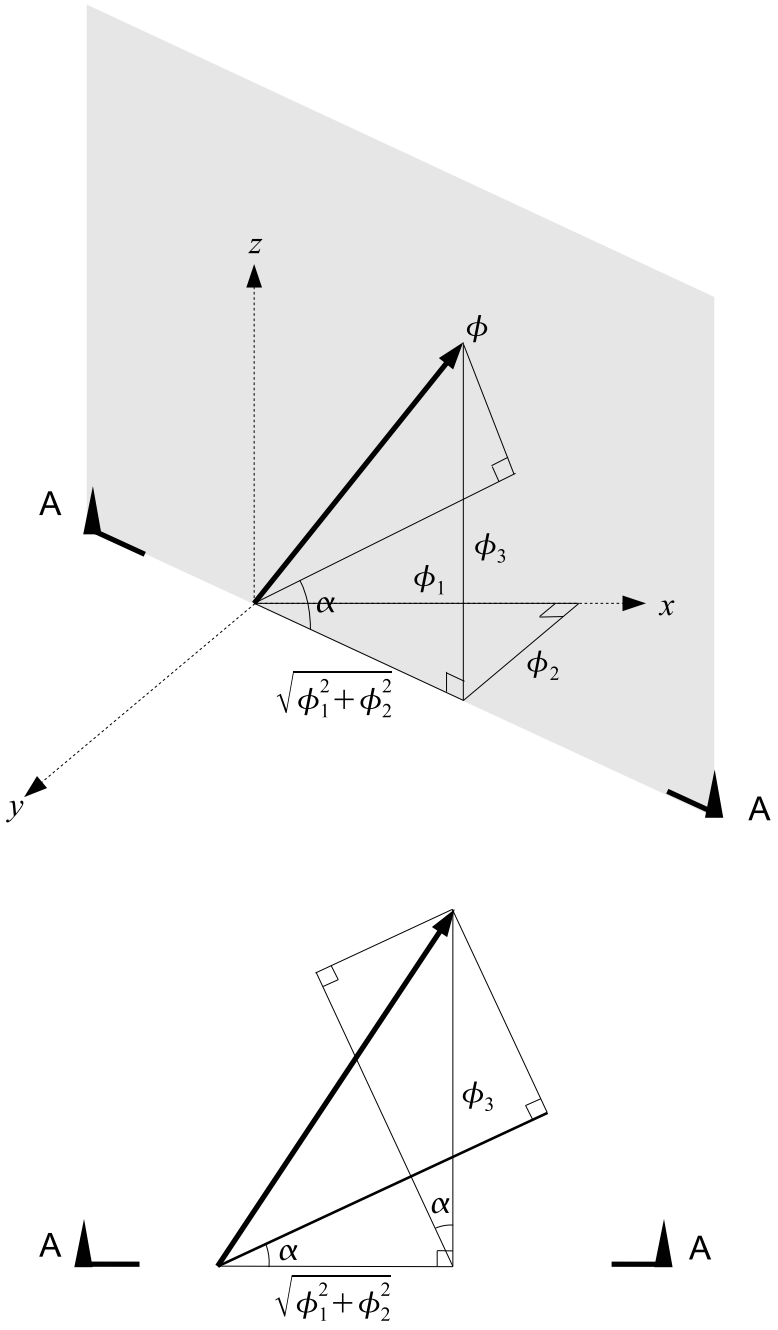

Figure 4.3: Length of a vector in the gradient-constrained dual space.

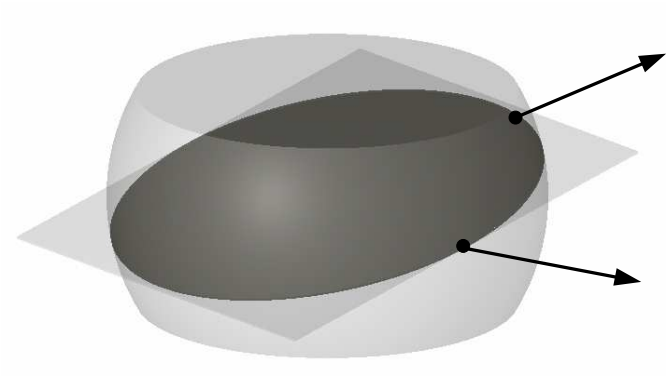

(i)

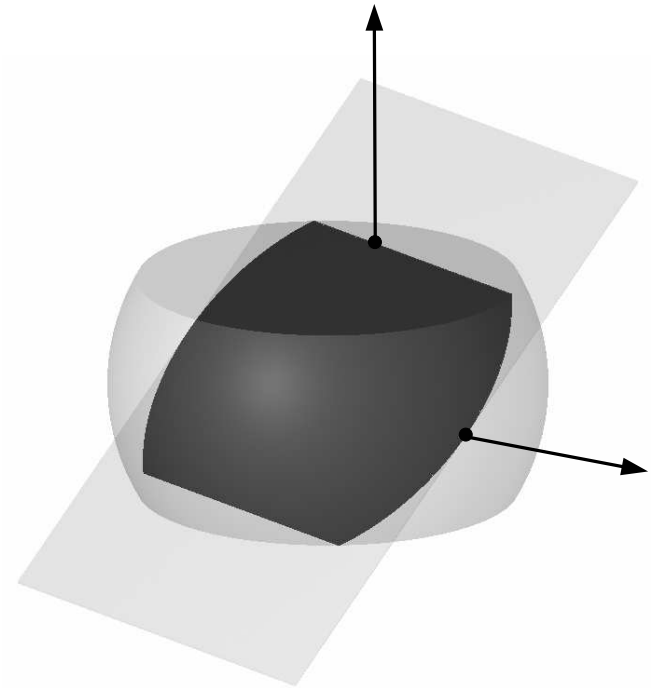

(ii)

Figure 4.4: The gradient-constrained FW problem in a plane. The gradient of the plane is (i) less than, and (ii) greater than or equal to the maximum.

Recall from Lemmas 3.4 and 3.5 in Chapter 3 that the subdifferential of $f(x)$ is given by

$$\partial f(x) = \sum_{i=1}^{k} w_i \partial(p_i - x)$$

where $\partial(p_i - x)$ is the set of norming functionals of $p_i - x$. If $p_i x$ is an f-edge, $\partial(p_i - x)$ can be treated as a vector $\mathbf{v}_i$ from x to p_i with length w_i, while if $p_i x$ is a b-edge, $\partial(p_i - x)$ can be treated as a vector $\mathbf{v}_i$ pointing from x vertically up or down, if p_i is above or below x respectively, with length $w_i\sqrt{1+m^{-2}}$. If $p_i x$ is an m-edge, $\mathbf{v}_i$ is continuum of vectors lying in the vertical plane containing x and p_i, the vectors having all possible directions between the m-edge and a vertical edge. By selecting any vector from this continuum, we can compute a subgradient of f. Thus a simple gradient descent procedure [5] seems suitable for solving the gradient-constrained FW problem, as a subgradient is easily computed as the sum of vectors associated with the given points. However, problems can arise due to the fact that $f(x)$ is not everywhere differentiable.

Let S denote the set of points x in $\mathbb{R}^3$ for which $p_j x$ is an m-edge for any $p_j \in N$. Then f is differentiable everywhere except in the set S, since the vector associated with an m-edge, and consequently the gradient, is not unique. The problem for nondifferentiable convex functions can be solved by the *subgradient method* [69], [6], which minimises $f(x)$ using the iteration

$$x^{(\kappa+1)} = x^{(\kappa)} + s_\kappa \mathbf{v}^{(\kappa)} \tag{4.3}$$

where $x^{(\kappa)}$ is the κ^{th} iterate, $\mathbf{v}^{(\kappa)}$ is *any* subgradient of f at $x^{(\kappa)}$ and s_κ is the κ^{th} step size. For guaranteed convergence, the step sizes, s_κ, $i = 1, 2, \ldots$, must satisfy certain rules, otherwise the iteration may convergence to a nonstationary point. For constant step size, $s_\kappa = \Delta$, the subgradient method is guaranteed to converge to within some range of the optimal value [69]. For diminishing step sizes satisfying $\lim_{\kappa\to\infty} s_\kappa = 0$, $\sum_{\kappa=1}^{\infty} = \infty$, the algorithm is guaranteed to converge to the optimal value. The convergence proof is based on the Euclidean distance to the optimal set decreasing at each iteration. Note that the subgradient method is not a descent method; the function can, and often does, increase over consecutive iterations.

In some circumstances, use of the subgradient method is problematic. Convergence

can be extremely slow due to the gradient being almost perpendicular to the direction towards the minimum. This problem is demonstrated by the following example.

We are given three points in a vertical plane; $p_1 = [0\ 1]$, $p_2 = [2\ 0]$ and $p_3 = [2\ 2]$. The three points have respective weights $w_1 = 1$, $w_2 = 1$ and $w_3 = 1.94$. The maximum allowable gradient is $m = 1$. Let $x_0 \in \mathrm{fw}(N)$. The exact solution, which can in this case be determined exactly by simple calculus, is $x_0 = [1.9\ 1.9]$. Starting at $x^{(0)} = [0.1\ 1]$ and using an initial step size $s_0 = 0.345$ we execute the subgradient method where step sizes diminish at each iterate κ according to $s_\kappa = s_0/\sqrt{\kappa}$. The iterative path, shown in Figure 4.5, shows that convergence is very slow due to extreme oscillation about the line through p_3 with gradient m. At each iteration, the gradient is almost perpendicular to the direction towards the minimum. In fact, after 50,000 iterations, $x^{(\kappa)}$ is still noticeably distant from x_0. If s_κ is chosen to minimise $f(x^{(\kappa)} + s_\kappa \mathbf{v}^{(\kappa)})$ (i.e. an exact line search is adopted), then $x^{(\kappa)}$ converges to the nonstationary point [1.3385 1.3385] after one iteration, due to the optimum step size diminishing to zero too early.

A notable extension of the subgradient method involves the concept of space dilation [69]. The method aims to reduce at subsequent iterations the components of the gradient that are parallel to the latest gradient, by applying a linear nonorthogonal space transformation. The space is dilated in the direction of the gradient (the SDG algorithms) or alternatively in the direction of the difference of two successive gradients (the *r*-algorithms). Numerical tests have shown that convergence can be significantly accelerated, but the oscillation problem demonstrated in the example is not completely eradicated. Moreover the method needs to store the space dilation matrix and update it at every iteration, leading to significant computational effort.

We propose a new method that overcomes these problems by exploiting the fact that f is differentiable everywhere except in the set S. The idea is to use exact directional minimisation at each iteration, and to consider a second search direction when $x^{(\kappa)}$ converges to a point in some neighborhood of S. Let ϵ be small and positive. Define S_ϵ to be the set of points x for which the Euclidean distance between x and S is at most ϵ. Suppose at the κ^{th} iteration we have arrived at a point, $x^{(\kappa)}$, such that $x^{(\kappa)} \in S_\epsilon$. If exact directional minimisation results in a step size that is very small, then $x^{(\kappa)}$ may have converged to a

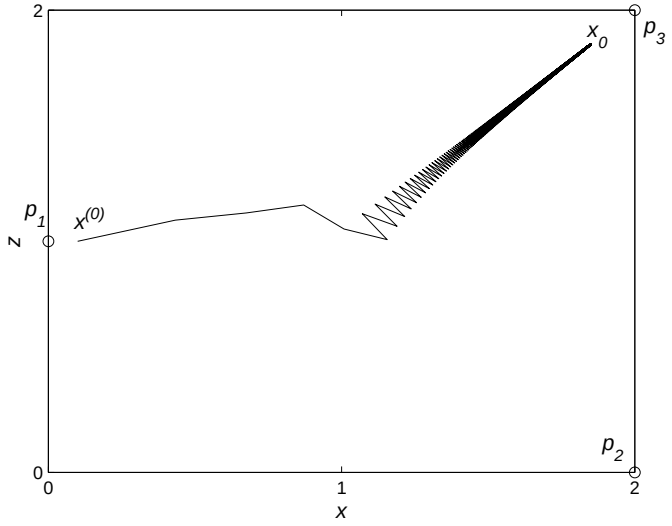

Figure 4.5: Iterations of the subgradient method with diminishing step sizes for a three-point gradient-constrained FW problem.

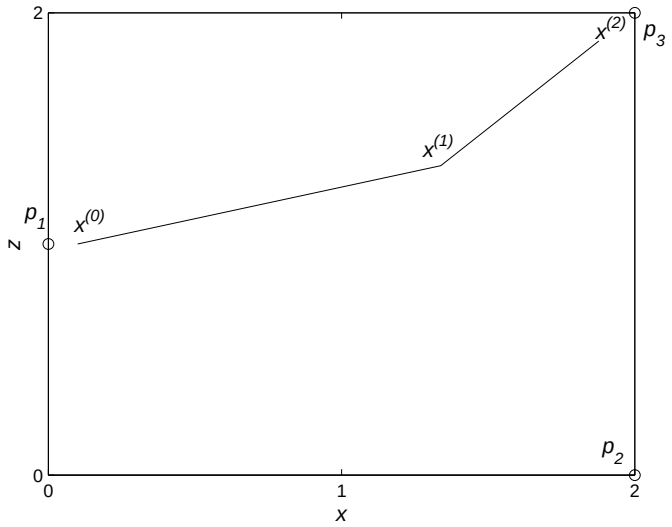

Figure 4.6: Iterations of a new descent method for a three-point gradient-constrained FW problem.

nonstationary point. If so, we hope to be able to 'escape' from this nonstationary point by searching in the direction of an m-edge close to $x^{(\kappa)}$. We denote such a direction by $\mathbf{v}_g$. The notion of searching in an m-edge direction was first employed in an algorithm for finding gradient-constrained minimum Steiner trees [10]. This was implemented into the UNO software product (refer to Chapter 1). The procedure for the gradient-constrained FW problem is outlined in Algorithm 2.

Algorithm 2 Algorithm for solving the gradient-constrained Fermat-Weber problem

Let η be small and positive, and let $\text{conv}(N)$ denote the convex hull of N.
given a starting point $x^{(0)} \in \text{conv}(N)$
repeat
1. $\mathbf{v} := \sum_{i=1}^{k} (w_i/h_i)\mathbf{u}_i$
2. *Line search.* Choose step size, s, via exact line search
3. **if** $s > \eta$
Update. $x := x + s\mathbf{v}$
Return to 1.
else
if $x \in S_\epsilon$
(a) compute $\mathbf{v}_g$ (vector in m-edge direction)
(b) *Line search.* Choose step size, s_g, via exact line search
(c) **if** $s_g > \eta$
Update $x := x + s_g\mathbf{v}_g$
Return to 1.
else stop.
else stop.

Applying Algorithm 2 to the previous example results in the sequence converging to the exact solution in two iterations, $\{(0.1, 1), (1.3385, 1.3385), (1.9, 1.9)\}$ (Figure 4.6). It is believed that Algorithm 1 is applicable to the FW problem in general Minkowski spaces. This will be investigated in future research.

4.4 Convergence analysis

One of the main differences between Algorithm 2 and the subgradient method is that Algorithm 2 employs an exact line search in a gradient direction at each iteration. The sole problem with exact directional minimisation is that it may cause convergence to a nonstationary point, due to the discontinuity of the gradient at that point. To obtain a

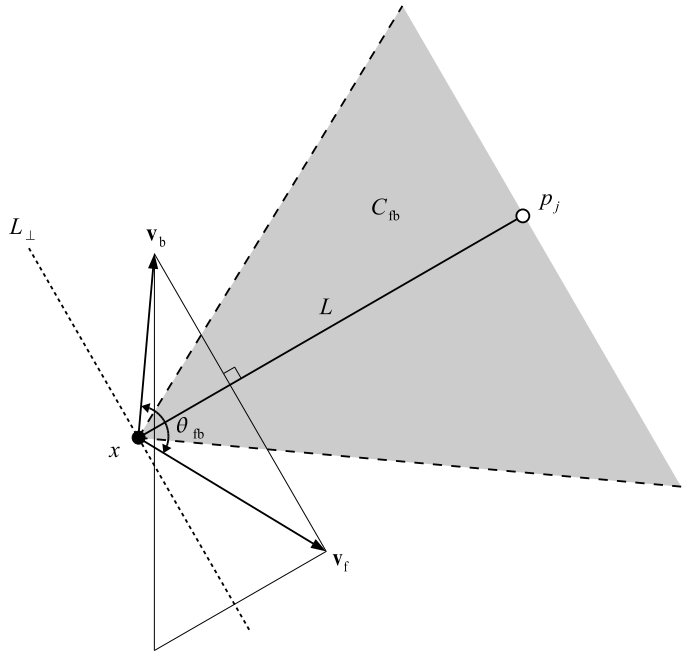

Figure 4.7: Gradient-constrained FW problem in a vertical plane. Descent directions at a point on an m-edge containing an FW point.

convergence proof for Algorithm 1, we must show that whenever the iteration converges to a nonstationary point, it can escape by stepping in the direction of an m-edge passing through a terminal and the nonstationary point. In other words, we must show that stepping in the m-edge direction gives a finite reduction in the cost function.

We begin by analysing the two-dimensional case where N lies in a vertical plane. Refer to Figure 4.7. Let L be a line with absolute gradient m passing through a terminal $p_j \in N$. Let x be a second point in the vertical plane that is arbitrarily close to L, so that $g(p_j x) \approx m$, and let $L_\perp$ be the line passing through x that is perpendicular to L.

Define $\mathbf{v}_\mathrm{f}$ to be the resultant of all the vectors associated with the points in N, assuming that $p_j x$ is an f-edge. Similarly define $\mathbf{v}_\mathrm{b}$ to be the resultant assuming that $p_j x$ is a b-edge. Theoretically, if $p_j x$ has gradient exactly equal to m, then the subdifferential of f at x is the set of all directions between these two vectors. We now state the following simple lemma.

Lemma 4.2. *The two vectors, $\mathbf{v}_\mathrm{f}$ and $\mathbf{v}_\mathrm{b}$, lie on the same side of (but not on) $L_\perp$.*

Proof. From the convergence proof for the subgradient method [69], moving by a predetermined amount in either direction $\mathbf{v}_\mathrm{f}$ or $\mathbf{v}_\mathrm{b}$ must move $x^{(\kappa)}$ closer to a minimum. Therefore, the angle between $\mathbf{v}_\mathrm{f}$ and $\mathbf{v}_\mathrm{b}$ cannot be 180°, and hence the vectors cannot both lie on $L_\perp$. Without loss of generality, assume that one of the vectors, say $\mathbf{v}_\mathrm{b}$, lies on the same side of $L_\perp$ as p_j, as in Figure 4.7. We can obtain $\mathbf{v}_\mathrm{f}$ by subtracting the vertical vector, $\mathbf{u}_j/\delta_j$, associated with p_jx (assuming it is a b-edge so that $\delta_j = 1/\sqrt{1+m^{-2}}$) from $\mathbf{v}_\mathrm{b}$, and adding the vector, $\mathbf{u}_j/\delta_j$, with absolute gradient m pointing from x to p_j (the vector associated with p_jx assuming it is an f-edge so that $\delta_j = 1$). We know that the triangle, T, formed by this process (shown in Figure 4.7) is right-angled (this triangle corresponds to a subset of the dual ball B_g^* for the gradient metric). Therefore the line connecting the tips of $\mathbf{v}_\mathrm{f}$ and $\mathbf{v}_\mathrm{b}$ is necessarily parallel to $L_\perp$. Hence the two vectors will always lie on the same side of $L_\perp$. ∎

Note that the above proof also works if $\mathbf{v}_\mathrm{b}$ lies on the opposite side of $L_\perp$ from p_j. For smooth convex functions, a search direction is a descent direction (meaning the cost function decreases by stepping in that direction) if and only if it makes an acute angle with the gradient, i.e. the angle is less than 90°. Hence, for smooth convex functions, the set of descent directions forms an unbounded half-plane.

If x has an incident m-edge, the descent direction must make an acute angle with all the vectors in the continuum bounded by $\mathbf{v}_\mathrm{f}$ and $\mathbf{v}_\mathrm{b}$. Define $\mathcal{C}_\mathrm{fb}$ to be the pointed cone with apex x and boundary defined by rays that are perpendicular to, and on the same side of $L_\perp$ as $\mathbf{v}_\mathrm{f}$ and $\mathbf{v}_\mathrm{b}$. Let int denote the interior of a set. It is easily shown that all rays in $\mathrm{int}(\mathcal{C}_\mathrm{fb})$ make acute angles with every vector in the continuum of directions bounded by $\mathbf{v}_\mathrm{f}$ and $\mathbf{v}_\mathrm{b}$, and hence $\mathrm{int}(\mathcal{C}_\mathrm{fb})$ is the set of all descent directions. We now state the following lemma and corollary.

Lemma 4.3. *Refer to Figure 4.7. Let θ_fb be the angle between the two vectors $\mathbf{v}_\mathrm{f}$ and $\mathbf{v}_\mathrm{b}$. Then x converges to a nonstationary point if and only if $\theta_\mathrm{fb} \geq 90^\circ$ at that point.*

Proof. It is easily seen from the construction of $\mathcal{C}_\mathrm{fb}$ that if $\theta_\mathrm{fb} = 90^\circ$, then the two vectors lie on the boundary of $\mathcal{C}_\mathrm{fb}$ and are therefore not descent directions. If $\theta_\mathrm{fb} > 90^\circ$ then

the cone bounded by one of the vectors, say $\mathbf{v}_b$, and its perpendicular, will not contain the other vector $\mathbf{v}_f$. If x has converged to a nonstationary point, then the two vectors $\mathbf{v}_f$ and $\mathbf{v}_b$ at x must both lie outside $\text{int}(\mathcal{C}_{fb})$, since otherwise stepping in either of the two directions would result in a finite reduction in the cost function, and x would not have actually converged. Since $\mathbf{v}_f$ and $\mathbf{v}_b$ are outside $\mathcal{C}_{fb}$ if and only if $\theta_{fb} \geq 90°$, the theorem is proved. ∎

Corollary 4.1. *If x converges to a nonstationary point, then* $\text{int}(\mathcal{C}_{fb})$ *always contains L.*

Proof. From Lemma 4.3, if x converges to a nonstationary point, then $\theta_{fb} \geq 90°$. Also from Lemma 4.2 both vectors, $\mathbf{v}_f$ and $\mathbf{v}_b$, are on the same side of $L_\perp$. As a result, both vectors necessarily lie on opposite sides of L, and consequently so too do their perpendiculars. Hence L is always inside $\text{int}(\mathcal{C}_{fb})$. ∎

It follows from the corollary that if x converges to a nonstationary point on L, then L will always be contained in $\mathcal{C}_{fb}$, and x can always escape from the nonstationary point by stepping in the direction of L.

We now turn our attention to the more difficult three-dimensional case. Like the two-dimensional case, we have two vectors $\mathbf{v}_f$ and $\mathbf{v}_b$ associated with p_j, but they do not necessarily lie in the same vertical plane as x and p_j. Moreover, the set of descent directions will be a wedge, which we denote by W_{fb} (Figure 4.8).

We can analyse this case by considering the vertical plane containing x and p_j. The arrangement is similar to Figure 4.7 except that now the vectors $\mathbf{v}_f$ and $\mathbf{v}_b$ may have components orthogonal to the vertical plane though x and p_j.

The direction along the line where the two planes defining W_{fb} intersect is perpendicular to both vectors $\mathbf{v}_f$ and $\mathbf{v}_b$, and hence it can be computed by their vector cross-product $\mathbf{v}_f \times \mathbf{v}_b$. By consideration of this cross-product, the following lemma is evident.

Lemma 4.4. *The orthogonal projection of the vector cross-product $\mathbf{v}_f \times \mathbf{v}_b$ onto the vertical plane containing x and p_j lies on L.*

Proof. Let $\mathbf{v}_f = [x_f,\ y_f,\ z_f]$ and $\mathbf{v}_b = [x_b,\ y_b,\ z_b]$, where z is vertical and x is in the horizontal direction of the plane containing x and p_j. The vector cross-product is given by $\mathbf{v}_f \times \mathbf{v}_b = [y_f z_b - y_b z_f,\quad -(x_f z_b - x_b z_f),\quad x_f y_b - x_b y_f]$. From Figure 4.7, the triangle

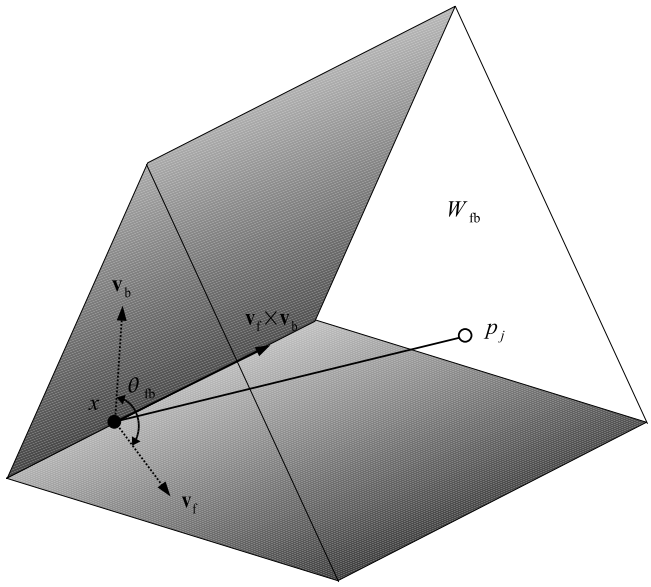

Figure 4.8: Gradient-constrained FW problem in three-space. Descent directions at a point on an m-edge containing an FW point.

T is contained in a vertical plane that is parallel to the vertical plane through x and p_j, and so the y components of the two vectors $\mathbf{v}_{\text{f}}$ and $\mathbf{v}_{\text{b}}$ are equal. Letting $y_{\text{f}} = y_{\text{b}} = y_{\text{fb}}$ we have $\mathbf{v}_{\text{f}} \times \mathbf{v}_{\text{b}} = y_{\text{fb}}\,[z_{\text{b}} - z_{\text{f}}, \quad -(x_{\text{f}} z_{\text{b}} - x_{\text{b}} z_{\text{f}})/y_{\text{fb}}, \quad x_{\text{f}} - x_{\text{b}}]$. It is easily seen that $(x_{\text{f}} - x_{\text{b}})/(z_{\text{b}} - z_{\text{f}}) = m$, and hence the lemma is proved. ∎

Using similar arguments as for the two-dimensional case, it follows that if x converges to a nonstationary point on L, then L will always be contained in W_{fb}, and x can always escape from the nonstationary point by stepping in the direction of L.

4.5 A simplified case study

In this section we demonstrate the importance of the gradient-constrained FW problem to underground mining by applying it to a simplified version of the case study presented in Chapter 9. The case study, which was introduced in Chapter 2, Section 2.7, involves determining the cost-optimal position for a vertical hoisting shaft in the Callie underground mine. The mine includes parallel declines accessing an orebody which plunges

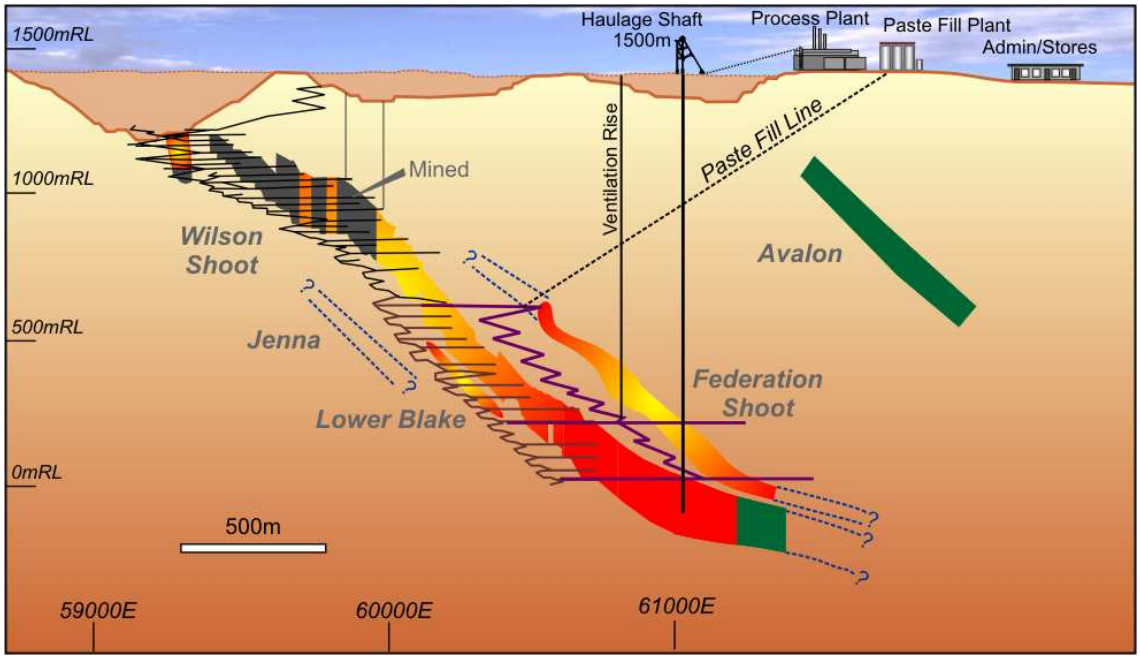

Figure 4.9: Conceptual long section of the Callie underground mine.

at 45 degrees to the horizontal, and roughly lies in a vertical plane (Figure 4.9). The reduced level (RL) at the surface is roughly 1400 m, and by 2011 the orebody will have been mined to an approximate depth of 1100 m (390 m RL) below the surface.

The primary decline, called the *Callie decline*, is to be mined from 340 m RL down to -660 m RL, with draw points on the decline at 40 m vertical increments (26 points in total). The secondary decline, called the *Wilson drill decline* (WDD), is to be mined from 390 m RL down to 70 m RL, also with draw points at 40 m vertical intervals (nine points in total). To account for uncertainty in production forecasting, three haulage schedules have been proposed. These are *base*, *probable* and *best*, having low, average and high rates respectively. Haul point levels and tonnages are summarised in Tables 4.1 and 4.2 for Callie and WDD respectively.

The Callie Decline and WDD have respective gradients 1:8 and 1:7 or, alternatively, 1:7 and 1:6. The shaft development cost is \$25,000/m, \$50,000/m or \$75,000/m. The ore pass development cost is \$1210/m. Haulage up and down a decline is \$0.75/(t.km) and

Level	Base	Probable	Best
340	59,253	59,253	59,253
300	296,746	500,000	700,000
260	194,808	500,000	700,000
220	298,691	750,000	700,000
180	200,000	750,000	1,050,000
140	551,408	1,000,000	1,050,000
100	736,412	1,125,000	1,400,000
60	418,845	1,125,000	1,575,000
20	500,000	1,000,000	1,225,000
-20	500,000	1,375,000	1,575,000
-60	600,000	1,125,000	1,225,000
-100	800,000	1,375,000	1,400,000
-140	600,000	1,125,000	1,575,000
-180	600,000	1,125,000	1,225,000
-220	700,000	875,000	1,575,000
-260	500,000	875,000	1,225,000
-300	400,000	875,000	1,400,000
-340	500,000	875,000	1,575,000
-380	300,000	625,000	1,225,000
-420	200,000	750,000	1,225,000
-460	300,000	250,000	1,125,000
-500	100,000	-	1,050,000
-540	-	-	1,225,000
-580	-	-	875,000
-620	-	-	1,050,000
-660	-	-	350,000

Table 4.1: Callie Decline draw point levels and tonnages.

Level	Base	Probable	Best
390	110,000	150,000	150,000
350	230,000	325,000	325,000
310	240,000	500,000	500,000
270	230,000	500,000	500,000
230	230,000	500,000	500,000
190	240,000	350,000	500,000
150	120,000	175,000	500,000
110	-	-	350,000
70	-	-	175,000

Table 4.2: Wilson Drill Decline draw point levels and tonnages.

\$0.85/(t.km) respectively or, alternatively, \$1.05/(t.km) and \$1.20/(t.km) respectively.

An alternative to trucking ore down the ramp from a given level is to tip the ore down an ore pass, a near-vertical tunnel, to a horizontal main haulage drive at the same level as the base of the shaft. The pass services all levels above a specified level.

In Chapter 2, we discussed how to optimise the network of tunnels interconnecting the declines, ore pass and shaft, using a variation of the FW problem in the Euclidean plane where one of the given points (representing the shaft) is allowed to exist anywhere on a straight line in the plane. The costs associated with these elements can be considered to be 'horizontal'.

In this chapter, we optimise the three principal 'vertical' cost components of the mine — shaft development, decline haulage and ore pass development — by placing the shaft base at an optimum level. The techniques of Chapter 2 can then be used to find an optimum horizontal network interconnecting the declines, ore pass and shaft. In Chapter 9, we refine our approach so as to minimise the horizontal and vertical cost components simultaneously, resulting in a globally-optimal solution.

4.5.1 Solution procedure

We model the mine as a weighted network and treat the shaft base as an FW point. The collective set of 35 access points on the two declines is treated as a set of given points.

We begin by placing the shaft base at an initial level $z^{(0)}$. This could be the median level or, alternatively, the level closest to the centre of gravity (with respect to tonnages) of the draw points. The shaft can be thought of as a b-edge extending from $z^{(0)}$ up to a point on the surface. However, since the length of the shaft is Euclidean, it is not subjected to the gradient constraint. Thus, we assign to the shaft an upwards vertical vector $\mathbf{v}_s$ with length 25,000, 50,000 or 75,000, depending on the case considered.

Consider a draw point p_i with tonnage t_i at a level z_i which is above $z^{(0)}$. Material is trucked from p_i down to $z^{(0)}$ along a gradient-constrained path at a haulage cost rate of h_d. Hence, we assign to p_i an upwards vertical vector $\mathbf{v}_i$, with length $\sqrt{1+m_C^{-2}}h_d t_i(z_i - z^{(0)})$ if p_i is on the Callie decline whose gradient is m_C, or $\sqrt{1+m_W^{-2}}h_d t_i(z_i - z^{(0)})$ if p_i is on the Wilson decline whose gradient is m_W. Similarly, if p_i is at a level z_i below $z^{(0)}$,

then we assign it a downwards vertical vector with length $\sqrt{1+m_C^{-2}}h_u t_i(z_i - z^{(0)})$ or $\sqrt{1+m_W^{-2}}h_u t_i(z_i - z^{(0)})$ if p_i is on Callie or WDD respectively, and h_u is the cost rate of upwards haulage.

When an ore pass is modelled, it is assigned an upwards vertical vector having length $d_{op} = 1210$. However, for all levels above the specified lowest level from which ore is transported to the top of the ore pass, the cost of haulage does is independent of the position of the shaft base. Thus it can be treated as a fixed cost, and consequently these levels are assigned a zero vector.

Taking the sum of vectors associated with the 35 access points, the shaft and the ore pass (if applicable), we obtain a resultant vertical vector. If the vector points upward, then we select $z^{(1)}$ to be the level immediately above $z^{(0)}$; otherwise, it is the level immediately below $z^{(0)}$. We repeat the process until the iterate $z^{(\kappa)}$ oscillates between two levels. Which of these two levels is the optimal solution, denoted by z^*, is determined by computing the costs at each level, and selecting the one with the lower cost.

4.5.2 Results and analysis

Results are summarised in Table 4.3. In the tests, we have assumed for the base, probable and best cases that the top of ore pass is at levels 300, 220 and 180 respectively, and the ore pass facilitates ore from levels above and including 220, 140 and 100 respectively. The total cost C includes shaft development, decline haulage, ore pass development and, if applicable, ore pass fitout ($1M fixed). From the table, we make the following brief observations. A detailed discussion is provided in Chapter 9.

- The shaft development cost has the greatest impact on the optimal position of the shaft base. Increasing the cost from $25,000/m to $75,000/m causes the base to move up by three to six levels.
- The decline gradients and haulage costs have a relatively small impact on the optimal position of the shaft base. Changing parameters causes the shaft base to move one level at most.
- For the $25,000/m shaft development, including an ore pass causes the shaft base to move down by two to three levels. In all cases where the shaft development

is \$25,000/m, it is more economical to include an ore pass (the \$50,000/m and \$75,000/m cases are considered in Chapter 9).

- Over all the cases considered, the shaft base ranges from -140 m RL to 390 m RL, spanning a vertical distance of 530 m.

In Chapter 9, we provide a thorough treatment of the case study, where the vertical and horizontal components of the mine are optimised simultaneously, and additional constraints are imposed to account for orebody standoff requirements, faults and surface geology boundaries. The ore pass is included for the \$50,000/m and \$75,000/m shaft development cost scenarios, and the impact of including a second tipping point between the top and bottom of the ore pass is investigated. The top level of the ore pass and lowest level hauling to the top of the ore pass (or to the second tipping point) are included as variables in the optimisation.

						No ore pass		Ore pass	
Case	d_s	h_u	h_d	m_C	m_W	z^*	C	z^*	C
Base	\$25,000	\$0.75	\$1.05	1:8	1:7	140	\$47.6M	60	\$46.5M
Base	\$25,000	\$0.75	\$1.05	1:7	1:6	140	\$45.6M	100	\$45.0M
Base	\$25,000	\$0.85	\$1.20	1:8	1:7	140	\$49.8M	60	\$48.1M
Base	\$25,000	\$0.85	\$1.20	1:7	1:6	140	\$47.6M	60	\$46.5M
Base	\$50,000	\$0.75	\$1.05	1:8	1:7	270	\$77.6M	-	-
Base	\$50,000	\$0.75	\$1.05	1:7	1:6	310	\$74.8M	-	-
Base	\$50,000	\$0.85	\$1.20	1:8	1:7	230	\$80.3M	-	-
Base	\$50,000	\$0.85	\$1.20	1:7	1:6	270	\$77.4M	-	-
Base	\$75,000	\$0.75	\$1.05	1:8	1:7	390	\$104M	-	-
Base	\$75,000	\$0.75	\$1.05	1:7	1:6	390	\$100M	-	-
Base	\$75,000	\$0.85	\$1.20	1:8	1:7	390	\$107M	-	-
Base	\$75,000	\$0.85	\$1.20	1:7	1:6	390	\$103M	-	-
Probable	\$25,000	\$0.75	\$1.05	1:8	1:7	100	\$60.2M	20	\$56.9M
Probable	\$25,000	\$0.75	\$1.05	1:7	1:6	100	\$56.7M	20	\$54.3M
Probable	\$25,000	\$0.85	\$1.20	1:8	1:7	60	\$63.9M	20	\$59.7M
Probable	\$25,000	\$0.85	\$1.20	1:7	1:6	100	\$60.0M	20	\$56.8M
Probable	\$50,000	\$0.75	\$1.05	1:8	1:7	140	\$92.3M	-	-
Probable	\$50,000	\$0.75	\$1.05	1:7	1:6	180	\$88.5M	-	-
Probable	\$50,000	\$0.85	\$1.20	1:8	1:7	140	\$96.2M	-	-
Probable	\$50,000	\$0.85	\$1.20	1:7	1:6	140	\$92.1M	-	-
Probable	\$75,000	\$0.75	\$1.05	1:8	1:7	220	\$123M	-	-
Probable	\$75,000	\$0.75	\$1.05	1:7	1:6	230	\$118M	-	-
Probable	\$75,000	\$0.85	\$1.20	1:8	1:7	180	\$127M	-	-
Probable	\$75,000	\$0.85	\$1.20	1:7	1:6	220	\$123M	-	-
Best	\$25,000	\$0.75	\$1.05	1:8	1:7	-20	\$89.5M	-140	\$74.0M
Best	\$25,000	\$0.75	\$1.05	1:7	1:6	-20	\$82.8M	-140	\$69.7M
Best	\$25,000	\$0.85	\$1.20	1:8	1:7	-20	\$96.9M	-140	\$78.6M
Best	\$25,000	\$0.85	\$1.20	1:7	1:6	-20	\$89.2M	-140	\$74.9M
Best	\$50,000	\$0.75	\$1.05	1:8	1:7	60	\$124M	-	-
Best	\$50,000	\$0.75	\$1.05	1:7	1:6	60	\$117M	-	-
Best	\$50,000	\$0.85	\$1.20	1:8	1:7	20	\$132M	-	-
Best	\$50,000	\$0.85	\$1.20	1:7	1:6	60	\$124M	-	-
Best	\$75,000	\$0.75	\$1.05	1:8	1:7	100	\$157M	-	-
Best	\$75,000	\$0.75	\$1.05	1:7	1:6	100	\$150M	-	-
Best	\$75,000	\$0.85	\$1.20	1:8	1:7	60	\$165M	-	-
Best	\$75,000	\$0.85	\$1.20	1:7	1:6	100	\$157M	-	-

Table 4.3: Simplified case study results.

Part II

The Gilbert Arborescence Problem

Introduction to Part II

PART II of this thesis is devoted to the *Gilbert arborescence problem*, which asks for a minimum-cost flow-dependent network interconnecting given sources and a unique sink. We begin Chapter 5 by studying the problem in the classical environment for Gilbert networks, Euclidean space. Euclidean networks provide valuable insights into gradient-constrained networks, and have applications to drainage [56] and gas pipeline [4] networks.

In Chapter 6, we study the Gilbert arborescence problem in Minkowski spaces. Our main goal is to provide a geometric characterisation of vertices in minimum Gilbert arborescences in Minkowski spaces, generalising a result for Steiner minimum trees in Minkowski spaces [73].

In Chapters 7 and 8, we study gradient-constrained minimum Gilbert arborescences in a vertical plane and in three dimensions respectively, assuming a linear cost function $w(t) = d + ht$, where d and h are strictly positive, and $m \leq 1$. We investigate geometric properties of gradient-constrained minimum Gilbert arborescences, and use these properties to provide a classification of Steiner points, extending work done in [17] and [13].

Chapter 5

Minimum Gilbert Arborescences in Euclidean Space

We introduce the Gilbert arborescence problem, *which is a special case of the Gilbert network problem [34] where the k terminals consist of $k-1$ sources and a unique sink, and flow is routed from the sources to the sink via directed paths. This problem has applications to drainage [56], gas pipeline [4] and underground mining [8] networks. We present some useful properties of minimum Gilbert arborescences (MGAs), and provide a characterisation of the local structure of their Steiner points, generalising a known result for unweighted networks. We use this characterisation to investigate the maximum degree of Steiner points in MGAs. We then briefly discuss how some known algorithms can be applied to the problem. In particular, we look at a generalised Melzak algorithm which provides exact solutions, and an angle-splitting heuristic for obtaining approximate solutions. Finally, we investigate the Gilbert arborescence problem in Euclidean 3-space.*

5.1 Introduction

THE *Euclidean Steiner problem* (ESP) asks for a shortest network spanning a given set of points, called *terminals*, in the Euclidean plane. It differs from the minimum spanning tree problem in that additional points, called *Steiner points*, are permitted to create a spanning network that is shorter than would otherwise be possible.

Gilbert [34] proposed a generalisation of the ESP whereby non-negative *flows* are assigned between each pair of terminals. The cost of an edge is its length multiplied by a non-negative *weight*. The weight is determined by a given function of the total flow being routed through that edge, where the function satisfies a number of conditions. The *Gilbert network problem* (GNP) asks for a minimum-cost network spanning a given set of

terminals with given flow demands and a given cost function.

A special case of the GNP is when the k terminals consist of $k-1$ sources and a unique sink (or, equivalently, $k-1$ sinks and a unique source), and all flows not between a source and the sink are zero. This problem has applications to drainage [56], gas pipeline [4], and underground mining [8] networks.

As we will show, the resulting minimum network has a tree topology, and provides a directed path from each source to the sink (or from the source to each sink). Such a network is called an *arborescence*, and we refer to this special case of the GNP as the *Gilbert arborescence problem* (GAP). Traditionally, the term 'arborescence' has been used to describe a rooted tree providing directed paths from the root (source) to $k-1$ sinks. Here we are interested in the case where the flow directions are reversed, i.e. flow is from $k-1$ sources to a unique sink. Since the two problems are clearly equivalent, we will continue to use the term 'arborescence' for the latter case. A *minimum Gilbert arborescence* (MGA) is a (global) minimum-cost arborescence for a given set of terminals and flows, and a given cost function.

In this chapter we investigate geometric properties of MGAs, and discuss how some known algorithms can be used to solve the problem exactly and approximately. In Section 5.2, we give some background on the ESP and the GNP. Then in Section 5.3, we provide some useful properties of MGAs. In Section 5.4, we present a characterisation of MGAs, generalising a known result for unweighted networks. The characterisation is in terms of weighted unit vectors from a Steiner point to its adjacent vertices. We use this characterisation in Sections 5.5 and 5.6 to investigate the maximum degree of Steiner points in MGAs in the Euclidean plane, and in Euclidean three-space respectively.

In Section 5.7, we examine properties of angles between edges incident with a degree-three Steiner point in an MGA. Finally, in Section 5.8, we briefly discuss how some known algorithms can be applied to the problem. In particular, we look at a generalised Melzak algorithm which provides exact solutions, and a heuristic which returns approximate solutions.

5.2 Background

It is useful to begin by discussing some aspects of the ESP, since the ESP is a special case of the GNP. The following material on the ESP is generally taken from [42]. Let T be a network interconnecting a set $N = \{p_1, \ldots, p_k\}$ of points, called *terminals*, lying in a Euclidean plane. A vertex in T which is not a terminal is called a *Steiner point*. Let $G(T)$ denote the *topology* of T, i.e. $G(T)$ represents the graph structure of T but not the embedding of the Steiner points. Then $G(T)$ for a shortest network T is necessarily a tree, since if a cycle exists, the length of T can be reduced by deleting an edge in the cycle. A network with a tree topology is called a *tree*, its links are called *edges*, and its nodes are called *vertices*. An edge connecting two vertices a, b in T is denoted by ab, and its (Euclidean) length by $|ab|$.

The *shrinking* of an edge in T is the operation of deleting an edge and collapsing its two endpoints to a single point. The *splitting* of a vertex is the operation of disconnecting two edges av, bv from a vertex v and connecting a, b, v to a newly created Steiner point. A *degeneracy* of a topology $G(T)$ is another topology that can be obtained by shrinking edges of $G(T)$. Though the positions of terminals are fixed, Steiner points can be subjected to small movements provided the resulting network is still connected. Such movements are called *perturbations*, and are useful for examining whether the length of a network is minimal.

A *Steiner tree* (ST) is a tree whose length cannot be shortened by a small perturbation of its Steiner points, even when splitting is allowed. By convexity, an ST is a minimum-length tree for its given topology. A *Steiner minimum tree* (SMT) is a shortest tree among all STs. It is well-known that every Steiner point in an ST has degree three, and the three incident edges at a Steiner point make angles of 120° with each other.

Given a set N of terminals, the *Steiner problem* (or *Steiner tree problem*) asks for an SMT spanning the terminals. This problem was introduced in 1934 by Járnik and Kössler [45], and interest in the problem began to spread following publication of the famous 1941 book, *What is Mathematics?* by Courant and Robbins [26].

Gilbert, who studied Steiner trees in [35], proposed the following generalisation of the ESP [34]. Let T be an undirected network interconnecting a set $N = \{p_1, \ldots, p_k\}$ of

k terminals in the Euclidean plane. For each pair $p_i, p_j,\ i \neq j$ of terminals, a bilateral non-negative *flow* $t_{ij} = t_{ji}$ is assigned between the pair of terminals. The cost of an edge e in T is $w(t_e)l_e$, where l_e is the Euclidean length of e, t_e is the sum of flows being routed through e, and $w(\cdot)$ is a cost function satisfying

$$w(t) \geq 0 \quad \text{and} \quad w(t) > 0 \text{ if } t > 0 \qquad (\text{non} - \text{negative}) \tag{5.1}$$

$$w(t_1 + t_2) \geq w(t_1) \quad \text{for all } t_2 > 0 \qquad (\text{nondecreasing}) \tag{5.2}$$

$$w(t_1 + t_2) \leq w(t_1) + w(t_2) \quad \text{for any } t_1, t_2 > 0 \qquad (\text{triangular}) \tag{5.3}$$

In [27], condition (5.3), which we call the *triangular condition*, was incorrectly interpreted as concavity of the cost function. In [75] it was shown that this is not correct, as demonstrated by the following counterexample from N. C. Wormald. Let the cost function be

$$w(t) = \begin{cases} \sqrt{t}, & \text{if } 0 \leq t \leq 1; \\ 1 + \frac{1}{4}(t-1)^2, & \text{if } 1 \leq t \leq 3; \\ 2, & \text{if } t \geq 3. \end{cases}$$

This function satisfies (5.1), (5.2) and (5.3), but it is not concave.

The total cost of T is the sum of all edge costs, i.e.

$$C(T) = \sum_{e \in E} w(t_e) l_e$$

where E is the set of all edges in T. A network satisfying the above conditions is called a *Gilbert network*. For a given edge e in T, $w(t_e)$ is called the *weight* of e, and is also denoted simply by w_e.

A Gilbert network T is a *minimum Gilbert network* (MGN), if T has the minimum cost of all Gilbert networks spanning the same point set N, with the same flow demands t_{ij} and the same cost function $w(\cdot)$. The *Gilbert network problem* (GNP) is to find an MGN for a given terminal set N, flows t_{ij} and cost function $w(\cdot)$. Since its inception in [34], various aspects of the GNP have been studied, although the emphasis has been on discovering geometric properties of MGNs (see [27], [75], [78]).

As for the ESP, additional vertices are permitted to create a weighted network whose cost is less than would otherwise be possible, and these additional points are still called *Steiner points*. A Steiner point s in T is called *locally minimal* if a perturbation of s does not reduce the cost of T. A Gilbert network is called *locally minimal* if no perturbation of the Steiner points reduces the cost of T.

One can also study a directed version of the GNP, where flows t_{ij} are defined for every ordered pair (i, j) (see [42], page 80). Each Steiner point in the network satisfies Kirchhoff's conservation of flow rule (i.e. the net incoming and outgoing flows at the Steiner point are equal). A special case of this model is when the k terminals $N = \{p_1, \ldots, p_k\}$ consist of $k-1$ *sources*, $p_1, \ldots, p_{k-1}$, and a unique *sink* p_k. Then t_{ij} is zero except when i is a source and j is the sink. To simplify notation, we let t_i denote the flow between a source p_i and the sink p_k. We refer to the problem with this flow structure as the *Gilbert arborescence problem* (GAP), and an MGN with this flow structure is called a *minimum Gilbert arborescence* (MGA).

Traditionally, the term 'arborescence' has been used to describe a rooted tree providing directed paths from the root (source) to $k-1$ sinks. Here we are interested in the case where the flow directions are reversed, i.e. flow is from $k-1$ sources to a unique sink. It is clear, however, that the resulting weights for the two problems are equivalent, hence we will continue to use the term 'arborescence' for the latter case. Moreover, if we take the sum of these two cases, and rescale the flows (dividing flows in each direction by two), then again the weights for the total flow on each edge are the same as in the previous two cases. This justifies our claim that the GAP can be treated as a special case of the GNP. It will be convenient, however, to think of arborescences as networks with a unique sink.

We point out that there is a problem similar to the GAP in the literature, called the *grade of service Steiner minimum tree (GOSST) problem* [88], which we do not discuss here.

5.3 Fundamental properties of minimum Gilbert arborescences

We now establish some fundamental properties of MGAs.

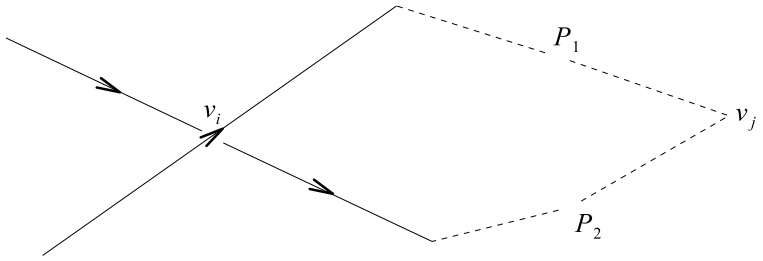

Figure 5.1: Cycles and crossing edges in a Gilbert arborescence.

5.3.1 Cycles and crossing edges

In contrast to SMTs, an MGN is not necessarily a tree, i.e. it may contain cycles. Moreover, edges in an MGN can cross each other in such a way that the bilateral flows do not change direction. In the following lemma, we show that neither of these phenomena can occur in an MGA.

Lemma 5.1. *An MGA has a tree topology, i.e. it contains no cycles or crossing edges.*

Proof. Suppose that v_i and v_j are vertices in an MGA T, such that there exist two paths P_1, P_2 routing respective flows t_1 and t_2 from v_i to v_j, where the two paths have no shared edges (Figure 5.1). Thus T has a cycle T', in the sense that the underlying undirected network has a cycle. Let E_1 and E_2 denote the sets of edges used by the two respective flow paths. Then

$$C(T') = \sum_{e \in E_1} w(t_e) l_e + \sum_{e \in E_2} w(t_e) l_e.$$

where t_e is the total flow through edge e, and l_e is the length of e. Without loss of generality, suppose that $\sum_{e \in E_1} l_e \leq \sum_{e \in E_2} l_e$, i.e. the total length of P_1 is no greater than the total length of P_2. Now suppose we route all flow exiting v_i through P_1. Then for the new subtree T'', we have

$$C(T'') = \sum_{e \in E_1} w(t_e + t_2) l_e + \sum_{e \in E_2} w(t_e - t_2) l_e$$

$$
\begin{aligned}
&\leq \sum_{e\in E_1}(w(t_e)+w(t_2))l_e + \sum_{e\in E_2}(w(t_e)-w(t_2))l_e \qquad (5.4)\\
&= \sum_{e\in E_1} w(t_e)l_e + \sum_{e\in E_1} w(t_2)l_e + \sum_{e\in E_2} w(t_e)l_e - \sum_{e\in E_2} w(t_2))l_e\\
&\leq \sum_{e\in E_1} w(t_e)l_e + \sum_{e\in E_2} w(t_e)l_e\\
&= C(T')
\end{aligned}
$$

where (5.4) results from the triangular condition (5.3). The cost of T'' is further reduced by deleting the first edge on P_2, which now facilitates zero flow. Thus T'' is not a cycle, and $C(T'') < C(T')$.

If T contains a crossing edge, a Steiner point can be created at the point where the two edges cross without affecting the network. But then T contains a cycle, and the cost of T can be reduced by the above procedure. ∎

Note that Lemma 5.1 does not hold for a general MGN. This is because in an MGN bilateral flows are assigned between pairs of terminals. Hence the paths P_1 and P_2 may both be justified if there are large flows assigned between v (assuming v is a terminal) and additional terminals on P_1 and P_2.

5.3.2 Minimum degree of Steiner points

The *degree* of a Steiner point s is the number of edges incident with s. The following lemma places a lower bound on the degree of Steiner points in MGAs.

Lemma 5.2. *Let T be an MGA and let s be a Steiner point in T. Then the degree of s is at least three.*

Proof. Suppose s is a degree-one Steiner point (Figure 5.2 (i)). Since s is neither a source nor a sink, no flow be routed through s. Thus s can be deleted along with its incident edge to reduce the cost of the network.

Now suppose s is a degree-two Steiner point with adjacent vertices p_1, p_2 (Figure 5.2 (i)). Assume that flow is routed from p_1 to p_2 via s. The weights on p_1s and sp_2 must be the same since, by the law of conservation of flow, flow entering s is the same as flow

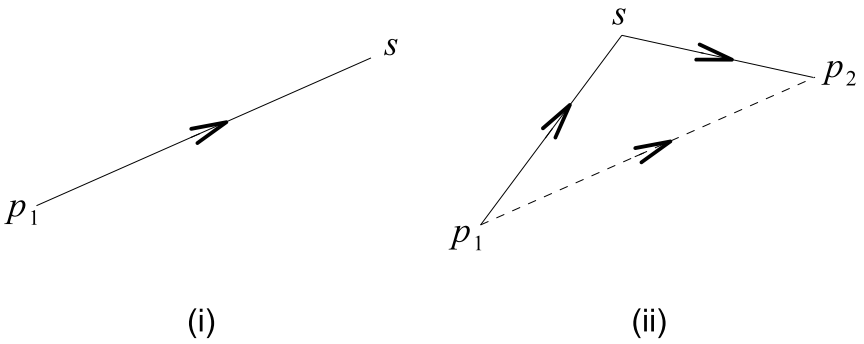

Figure 5.2: Minimum degree of Steiner points. (i) Degree-one Steiner point. (ii) Degree-two Steiner point.

exiting s. Therefore the cost of the network can be reduced by deleting s and its two incident edges and constructing a single edge between p_1 and p_2. ∎

5.3.3 Properties of weights

Let s be a degree-k Steiner point in a minimum Gilbert arborescence T. The subtree of T composed of s, its incident edges and neighbouring vertices has a *star* topology. We say that s has incident *source edges* $p_1s, \ldots, p_{k-1}s$ directed into s, and an incident *sink edge* sp_k directed away from s. Denote the weight on edge $sp_i,\ i = 1, \ldots, k$ by w_i.

Given a cost function $w(\cdot)$ satisfying the conditions for Gilbert networks, the weights on the edges are computed as follows:

$$w_i = w(t_i),\ i = 1, \ldots, k-1, \tag{5.5}$$

$$w_k = w\left(\sum_{i=1}^{k-1} t_i\right). \tag{5.6}$$

Since $w(\cdot)$ is a nondecreasing function, it follows that the weight on the sink edge is strictly greater than any of the weights on the source edges, i.e.

$$w_k > w_i,\ i = 1, \ldots, k-1. \tag{5.7}$$

Moreover, if we assume that the cost function is of the form $w(t) = d + ht$, where $d > 0$ and $h \geq 0$, the weight on the sink edge is strictly less than the sum of the weights on the source edges, i.e.

$$w_k \quad < \quad \sum_{i=1}^{k-1} w_i. \tag{5.8}$$

For the case where $w(t) = ht,\ h > 0$, we have $w_k = \sum_{i=1}^{k-1} w_i$, i.e. the weight on the sink edge is equal to the sum of the weights on the source edges. In such a case it is easy to see that the subtree is minimal when s collapses onto p_k, i.e. all flows are routed via straight edges from the sources to the sink.

5.3.4 Linear cost function

The linear cost function $w(t) = d + ht$, where d, h are non-negative constants, is of particular interest, because it provides a realistic basis for modelling development and haulage costs in underground mines. In this case the weights on the edges localised around a degree-k Steiner point are

$$w_i \quad = \quad d + ht_i,\ i = 1, \ldots, k-1 \tag{5.9}$$

$$w_k \quad = \quad d + h \sum_{i=1}^{k-1} t_i. \tag{5.10}$$

For any $d > 0$, if we set $h = 0$, then the MGA reduces to the (unweighted) SMT. On the other hand, if $h > 0$ and $d = 0$, then the weighted SMT consists of a star configuration connecting each source directly to the sink. In this work we assume that the values of d and h are strictly positive, and hence the MGAs obtained usually lie somewhere between these two extremes.

A useful intuitive result is that increasing the weight w_e on an edge e while keeping the other weights fixed tends to cause the network to distort so as to reduce the length of e. Moreover, increasing some $t_j,\ j \in \{1, \ldots, k-1\}$ tends to cause the path between p_j and the sink p_k to shorten. Assuming the other $t_i,\ i \in \{1, \ldots, k-1\},\ i \neq j$ are fixed at finite values, then as $t_j \to \infty$, the path between p_j and p_k approaches a straight line.

5.3.5 Collinear terminals

Suppose $N = \{p_1, \ldots, p_k\}$ is a set of terminals lying on a Euclidean straight line, where $p_1, \ldots, p_{k-1}$ are sources with respective positive flows $t_1, \ldots, t_{k-1}$, and p_k is the sink. Then the minimum Gilbert arborescence for N is trivial; it simply consists of an edge between each pair of adjacent terminals, and the edges are directed towards p_k. From this point on, we will assume that the terminals in N are not collinear.

5.4 Characterisation of Steiner points

Recall from Chapter 2 that an FW point x_0 for a given set of points $N = \{p_1, \ldots, p_k\}$ in Euclidean space can be characterised in terms of the weighted unit vectors from x_0 to the points in N (Theorem 2.1). That is, if x_0 does not coincide with a point in N, then x_0 is an FW point for N if and only if

$$\sum_{i=1}^{k} w_i \mathbf{u}_i = 0, \tag{5.11}$$

where $\mathbf{u}_i$ is the unit vector from x_0 to p_i and $w_i > 0$ is the weight assigned to p_i. Otherwise, if x_0 does coincide with a point $p_j \in N$, then $x_0 = p_j$ is an FW point for N if and only if

$$\left| \sum_{i=1, i \neq j}^{k} w_i \mathbf{u}_i \right| \leq w_j, \tag{5.12}$$

where $\mathbf{u}_i$ is the unit vector from p_j to p_i.

We are interested in this characterisation because the FW problem is the local version of the Gilbert arborescence problem. That is, each Steiner point in a Gilbert arborescence T is an FW point with respect to its adjacent vertices in T. Therefore, if s is a Steiner point in T, then the weighted unit vectors from s to its adjacent vertices must sum to zero. Moreover, if (5.11) holds for some x_0 not equal to any p_i, then (5.12) will automatically not hold, since the FW point is unique (assuming that the p_i are noncollinear).

Although condition (5.11) is necessary for s to be a Steiner point in T, in general it is not sufficient. It ensures that s is locally minimal with respect to its adjacent vertices, but does not guarantee that the star T is of lesser cost compared to any other minimal graph

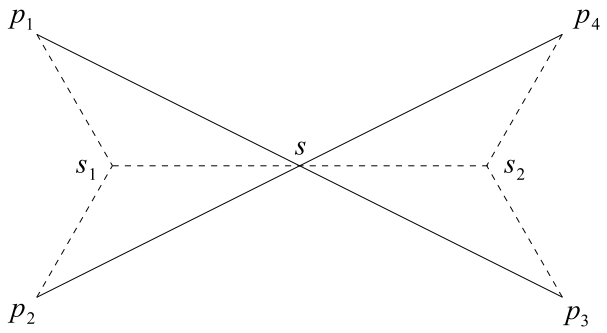

Figure 5.3: Splitting a degree-four Steiner point.

with a different topology.

Take for example the unweighted problem shown in Figure 5.3, i.e. all the weights are equal to one. A Steiner point s has adjacent vertices p_1, p_2, p_3, p_4 lying at the corners of a rectangle two units long by one unit wide. If s lies at the intersection of the two diagonals p_1p_3 and p_2p_4, then clearly the unit vectors from s to p_1, p_2, p_2, p_4 sum to zero, since the two vectors on a diagonal are equal and opposite. The length of the resulting subtree is $2\sqrt{5} \approx 4.47$.

If we replace s with two Steiner points s_1 and s_2, and position the new points such that all meeting edges make angles of 120° with each other, then the length of the new subtree (shown dashed in Figure 5.3) is $2 + \sqrt{3} \approx 3.73$, which is shorter than the previously computed subtree.

Lawlor and Morgan [54] gave necessary and sufficient conditions for a tree with a star topology to be an SMT in Euclidean space. Here we generalise this result to the GAP.

Theorem 5.1. *Let $N = \{p_1, \ldots, p_k\}$ be a set of terminals in Euclidean space, where $p_1, \ldots, p_{k-1}$ are sources with respective positive flows $t_1, \ldots, t_{k-1}$, and p_k is the sink. Let T be an arborescence with a star topology joining an additional point $s \notin N$ to each p_i, $i \in \{1, \ldots, k\}$, so that flows are routed from the sources to the sink via s. Let $w(\cdot)$ be a cost function satisfying the conditions for Gilbert networks, so that the weight on p_is, $i = 1, \ldots, k-1$ is $w_i = w(t_i)$ and the weight on sp_k is $w_k = w\left(\sum_{i=1}^{k-1} t_i\right)$. Let $\mathbf{u}_i$ denote the unit vector from s to p_i. Then T is an MGA on N if*

and only if

$$\sum_{i=1}^{k} w_i \mathbf{u}_i = \mathbf{0}, \tag{5.13}$$

and, for each $I \subseteq \{1, \ldots, k\}$,

$$\left| \sum_{i \in I} w_i \mathbf{u}_i \right| \leq w_I, \tag{5.14}$$

where w_I *is computed as follows: If* $k \notin I$, *then* $w_I = w\left(\sum_{i \in I} t_i\right)$; *otherwise, if* $k \in I$, *then* $w_I = w\left(\sum_{i \in I'} t_i\right)$, *where* $I' = \{1, \ldots, k\} \backslash I$.

Proof. ($\Rightarrow$) Assume that T is an MGA on N for the given flows and the given cost function. Then s is a Fermat-Weber point for N and, since $s \notin N$, condition (5.13) must be satisfied.

Now consider an arbitrary set $I \subseteq \{1, \ldots, k-1\}$, i.e. I does not contain k. Let $N' = \{p_i : i \in I\} \cup s$. Construct an arborescence T' connecting a new point s' with each point in N', where $\{p_i : i \in I\}$ are sources with flows t_i, and s is the sink. Thus the weight on $p_i s'$, $i \in I$, is $w(t_i)$, and the weight on $s's$ is $w\left(\sum_{i \in I} t_i\right)$. Since T is an MGA by assumption, s' must collapse onto s, otherwise the cost of T could be reduced by replacing $\{p_i s : i \in I\}$ with T', leaving the remaining parts of T unchanged. This implies that condition (5.14) must be satisfied for any $I \subseteq \{1, \ldots, k-1\}$.

Now suppose that $k \in I$. Defining N' as in the previous paragraph, we again construct an arborescence connecting s' with each point in N', but now the sources are $\{p_i : i \in I,\ i \neq k\}$ and s, while the sink is p_k. The weight on $p_i s'$, $i \in I$, $i \neq k$ is $w(t_i)$, the weight on $s' p_k$ is $w\left(\sum_{i=1}^{k} t_i\right)$, and the weight on ss' is $w\left(\sum_{i \in I'} t_i\right)$. Since T is an MGA by assumption, s' collapses onto s, and therefore condition (5.14) must be satisfied for any $I \subseteq \{1, \ldots, k-1\} \cup k$.

($\Leftarrow$) Suppose that conditions (5.13) and (5.14) are satisfied. Condition (5.13) implies that T is locally minimal for its (star) topology. Thus a perturbation of s will increase the cost of T. Now suppose we split s into s_1 and s_2, such that s_1 is connected to $\{p_i : i \in I\} \cup s_2$ and s_2 is connected to $\{p_i : i \in I'\} \cup s_1$. By condition (5.14), any perturbation of s_1 or s_2 will increase the cost of T. Thus T is an MGA on N, which completes the proof. ∎

5.5 Maximum degree of Steiner points in the plane

A major difference between Euclidean Steiner trees and Gilbert networks is that the degree of a Steiner point in a Euclidean Steiner tree is always three, whereas the degree of a Steiner point in an MGN can be arbitrarily large [27]. In this section we show that, for MGAs in the Euclidean plane with a linear cost function, the degree of all Steiner points is three. For the remainder of this section we will assume a linear cost function $w(t) = d + ht$, where d and h are positive constants.

We begin by looking at the four-terminal case. Let $N = \{p_1, p_2, p_3, p_4\}$ be a set of terminals in the Euclidean plane, where p_1, p_2, p_3 are sources with respective positive flows t_1, t_2, t_3, and p_4 is the sink. Let T be the star joining an additional point $s \notin N$ to each $p_i,\ i = 1, \ldots, 4$, so that flow is from the sources to the sink via s (Figure 5.4 (i)).

Since we are assuming a linear cost function $w(t) = d + ht$, the weights w_i on edges $p_i s,\ i = 1, 2, 3$, are given by $w_i = d + ht_i$, while the weight on sp_4 is $w_4 = d + h(t_1 + t_2 + t_3)$.

Let $\mathbf{u}_i,\ i = 1, \ldots, 4$, denote the unit vectors from s to p_i, and let $\mathbf{v}_i = w_i \mathbf{u}_i$ denote the weighted unit vectors. By Theorem 5.1, T is an MGN on N for the given flows and the given cost function if and only if the following conditions are all satisfied:

$$\mathbf{v}_1 + \mathbf{v}_2 + \mathbf{v}_3 + \mathbf{v}_4 = \mathbf{0} \tag{5.15}$$

$$|\mathbf{v}_1 + \mathbf{v}_2| \leq d + h(t_1 + t_2) \tag{5.16}$$

$$|\mathbf{v}_1 + \mathbf{v}_3| \leq d + h(t_1 + t_3) \tag{5.17}$$

$$|\mathbf{v}_2 + \mathbf{v}_3| \leq d + h(t_2 + t_3) \tag{5.18}$$

(Note that we have ignored trivial cases where $|I| = 1, 3, 4$. It is easy to see that such trivial inequalities are always satisfied if (5.15) is satisfied.) Denote $|\mathbf{v}_1 + \mathbf{v}_2|$, $|\mathbf{v}_1 + \mathbf{v}_3|$ and $|\mathbf{v}_2 + \mathbf{v}_3|$ by D_{12}, D_{13} and D_{23}, respectively. Adding pairs of equations (5.16), (5.17) and (5.18) together, we have

$$D_{12} + D_{13} \leq d + h(t_1 + t_2) + d + h(t_1 + t_3) = w_1 + w_4 \tag{5.19}$$

$$D_{12} + D_{23} \leq d + h(t_1 + t_2) + d + h(t_2 + t_3) = w_2 + w_4 \tag{5.20}$$

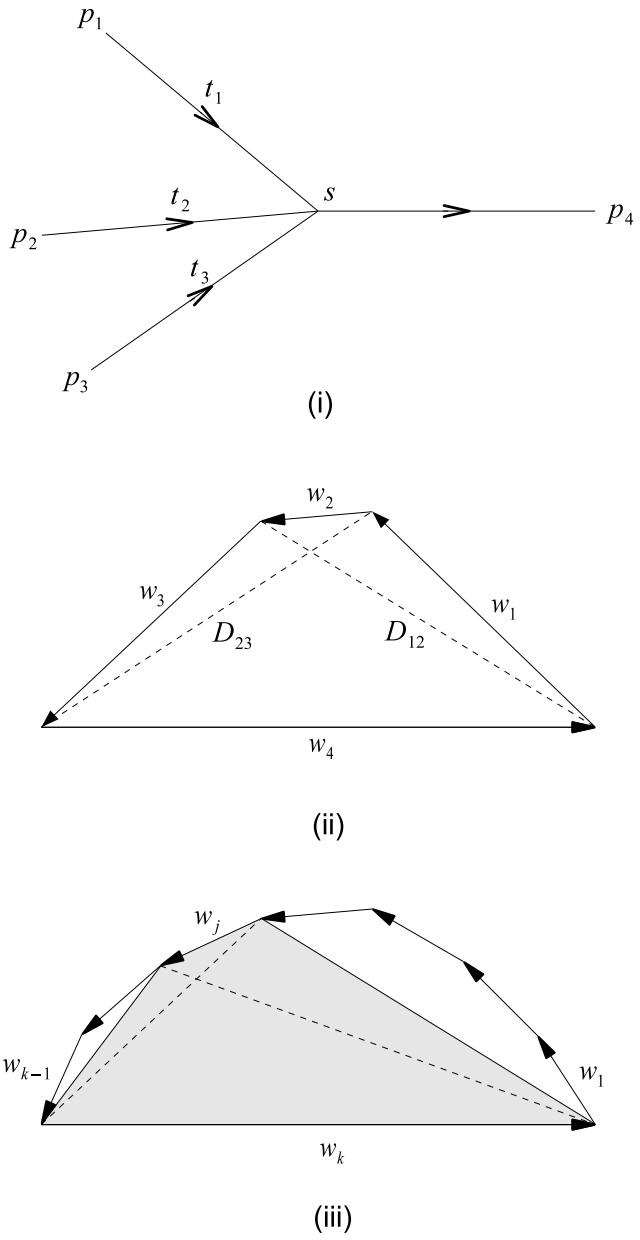

Figure 5.4: Degree-four Steiner point in a Gilbert arborescence in the Euclidean plane. (i) Gilbert arborescence. (ii)–(iii) Convex quadrilateral (polygon) with edges corresponding to weighted unit vectors.

$$D_{23} + D_{13} \quad \leq \quad d + h(t_2 + t_3) + d + h(t_1 + t_3) = w_3 + w_4. \tag{5.21}$$

Thus, to prove that a degree-four Steiner point cannot exist in an MGA in the Euclidean plane (assuming a linear cost function), we need only show that condition (5.15) implies that at least one of (5.19), (5.20), (5.21) is always broken. This idea is the basis for the proof of the following lemma.

Lemma 5.3. *Let T be an MGA in the Euclidean plane, and let s be a Steiner point in T. Then the degree of s is not four.*

Proof. Assume that (5.15) is satisfied. Therefore, if the vectors $\mathbf{v}_1, \mathbf{v}_2, \mathbf{v}_3, \mathbf{v}_4$ are positioned 'head to tail' in order of index, they form a convex quadrilateral with sides of length w_1, w_2, w_3, w_4 (Figure 5.4 (ii)). From the triangle inequality, we have

$$D_{12} + D_{23} \quad > \quad w_2 + w_4,$$

which contradicts condition (5.20). Thus s cannot have degree four. ∎

The previous lemma can be extended to Steiner points with arbitrary degree. Suppose s is a degree-k Steiner point in T with adjacent edges $sp_1, \ldots, sp_k$ having respective positive weights $w_1, \ldots, w_k$. Again, assume that the edges are arranged in order of index around s. If s is a Steiner point, then $\sum_{i=1}^{k} \mathbf{v}_i = 0$, and if the vectors are positioned head to tail in order of index, the result is a convex polygon whose sides have lengths corresponding to the edge weights (Figure 5.4 (iii)).

We now choose an arbitrary side of the polygon corresponding to some weight w_j, $j \neq k$, so that the sides corresponding to w_j and w_k form the opposite sides of a convex quadrilateral (shown shaded in Figure 5.4 (iii)). Applying the triangle inequality to the polygon, we have

$$\left| \sum_{i=1}^{j} \mathbf{v}_i \right| + \left| \sum_{i=j}^{k-1} \mathbf{v}_i \right| > w_j + w_k \tag{5.22}$$

But from Theorem 5.1, for s to be a Steiner point, we require

$$\left| \sum_{i=1}^{j} \mathbf{v}_i \right| + \left| \sum_{i=j}^{k-1} \mathbf{v}_i \right| \quad \leq \quad w\left(\sum_{i=1}^{j} t_i \right) + w\left(\sum_{i=j}^{k-1} t_i \right)$$

$$\begin{aligned} &= w\left(t_j + \sum_{i=1}^{k-1} t_i\right) \\ &< w_j + w_k \end{aligned}$$

which contradicts (5.22). This leads to the following theorem.

Theorem 5.2. *Let T be an MGA in the Euclidean plane with a linear cost function, and let s be a Steiner point in T. Then s has degree three.*

5.6 Maximum degree of Steiner points in three-space

In this section we consider MGAs in Euclidean three-space. Starting with the four-terminal problem, the situation is as shown in Figure 5.4 (i), except that the edges are no longer confined to the plane. We now state the following conjecture.

Conjecture 5.1. *Let T be an MGA with a linear cost function in Euclidean three-space, and let s be a Steiner point in T. Then s has degree three.*

The following discussion provides a partially-complete proof of the conjecture. Suppose we position the vectors $\mathbf{v}_1$, $\mathbf{v}_2$ and $\mathbf{v}_3$ emanating from the same point. We can consider the three vectors to define the sides of a parallelepiped with edge lengths w_1, w_2, w_3 (Figure 5.5 (i)). Then D_{12}, D_{23}, D_{13} are the lengths of the three *face diagonals* of the parallelepiped (shown fine dashed in Figure 5.5 (i)).

We will refer to the diagonal from the tail of the three vectors to the opposite corner of the parallelepiped as the *main diagonal* (the dashed line in Figure 5.5 (i)). Assume that condition (5.15) is satisfied, i.e. the vectors are in equilibrium. Then it is easy to see that the length of the main diagonal must be w_4.

For the three given positive weights w_1, w_2, w_3, we can also define a corresponding *cuboid*, which is a rectangular parallelepiped (or rectangular prism), i.e. a parallelepiped in which all angles are right angles (Figure 5.5 (ii)). For a cuboid, we have

$$D_{12} = \sqrt{w_1^2 + w_2^2} \tag{5.23}$$

$$D_{23} = \sqrt{w_2^2 + w_3^2} \tag{5.24}$$

$$D_{13} = \sqrt{w_1^2 + w_3^2} \tag{5.25}$$
$$w_4 = \sqrt{w_1^2 + w_2^2 + w_3^2}. \tag{5.26}$$

The following lemma regarding cuboids is useful.

Lemma 5.4. *For $w_1, w_2, w_3 > 0$, we have*

$$\sqrt{w_1^2 + w_2^2} + \sqrt{w_1^2 + w_3^2} > w_1 + \sqrt{w_1^2 + w_2^2 + w_3^2} \tag{5.27}$$
$$\sqrt{w_1^2 + w_2^2} + \sqrt{w_2^2 + w_3^2} > w_2 + \sqrt{w_1^2 + w_2^2 + w_3^2} \tag{5.28}$$
$$\sqrt{w_1^2 + w_3^2} + \sqrt{w_2^2 + w_3^2} > w_3 + \sqrt{w_1^2 + w_2^2 + w_3^2}. \tag{5.29}$$

Proof. First observe that, for any positive numbers A, B, C, if $A > C$, we have

$$\sqrt{A} + \sqrt{B + C} > \sqrt{A + B} + \sqrt{C}.$$

Now, set $A = w_1^2 + w_2^2$, $B = w_3^2$ and $C = w_1^2$. Since $A > C$, condition (5.27) follows. The other two conditions are proved similarly. ∎

The parallelepiped corresponding to the original vectors $\mathbf{v}_1, \mathbf{v}_2, \mathbf{v}_3$ can be obtained from the cuboid with edge lengths w_1, w_2, w_3, by applying an *edge-length-preserving distortion* until the required parallelepiped is obtained. An edge-length-preserving distortion can be considered to have three components, where the vector defining each component lies in the plane of one of the orthogonal faces of the rectangular parallelepiped. Each component is applied separately to one corner of the corresponding face, and the opposite corner is fixed. The effect is to distort the corresponding face, leaving the shapes of the other faces unchanged. Examples of the three perturbation components are shown in Figure 5.6 (i)–(iii) respectively.

Suppose that the lengths of all three face diagonals increase under the perturbation or that two face diagonals decrease and one increases under. Since the length of any of the face diagonals increases faster than the length of the main diagonal, the sum of the lengths of any pair of face diagonals increases faster than the length of the main diagonal. Now suppose that two of the face diagonals increase, and the other decreases. Then the

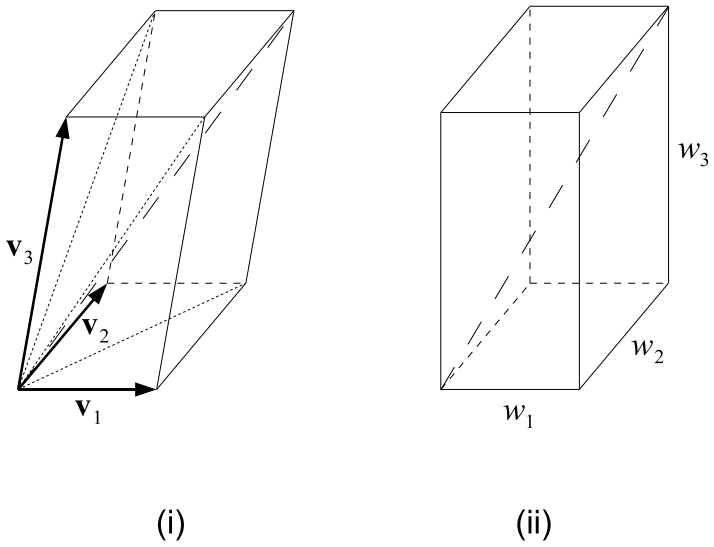

Figure 5.5: Degree-four Steiner point in a Gilbert arborescence in Euclidean three-space. (i) Parallelepiped with edges corresponding to weighted unit vectors. (ii) Cuboid with edge lengths corresponding to source weights.

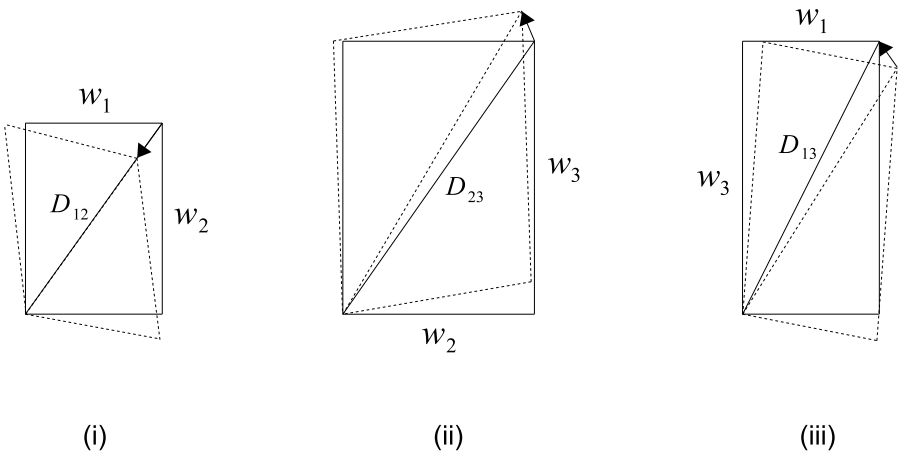

Figure 5.6: Cuboid subjected to an edge-length-preserving distortion with three orthogonal components (i)–(iii).

sum of the two increasing face diagonals increases faster than the main diagonal.

Assume that the lengths of all three face diagonals do not increase under the perturbation. We now require the *variational argument*, which is discussed in detail in Chapter 7 Section 7.2.3 and briefly described here. Let $\dot{D}$ denote the directional derivative of the length of D. If one end b of D is perturbed while the other a end remains fixed, such that b moves to b', then $\dot{D} = -\cos(\angle abb')$ (see [67]). Thus, under the assumption that all three face diagonals do not increase under a perturbation of the cuboid, we have $-1 \leq \dot{D}_{12} \leq 0$, $-1 \leq \dot{D}_{23} \leq 0$, and $-1 \leq \dot{D}_{13} \leq 0$. Without loss of generality, assume that

$$\dot{D}_{12} \leq \dot{D}_{23} \leq \dot{D}_{13}. \tag{5.30}$$

Noting that for a cuboid we have

$$\frac{D_{12}}{w_4} + \frac{D_{23}}{w_4} + \frac{D_{13}}{w_4} > 2, \tag{5.31}$$

the directional derivative of the length of the main diagonal, denoted by $\dot{w}_4$, is given by

$$\begin{aligned}
\dot{w}_4 &= \frac{D_{12}}{w_4}\dot{D}_{12} + \frac{D_{23}}{w_4}\dot{D}_{23} + \frac{D_{13}}{w_4}\dot{D}_{13} \\
&\leq \left(\frac{D_{12}}{w_4} + \frac{D_{23}}{w_4}\right)\dot{D}_{23} + \frac{D_{13}}{w_4}\dot{D}_{13} && (5.32) \\
&< \left(2 - \frac{D_{13}}{w_4}\right)\dot{D}_{23} + \frac{D_{13}}{w_4}\dot{D}_{13} && (5.33) \\
&= 2\dot{D}_{23} - \frac{D_{13}}{w_4}\dot{D}_{23} + \frac{D_{13}}{w_4}\dot{D}_{13} \\
&= 2\dot{D}_{23} + \frac{D_{13}}{w_4}\left(\dot{D}_{13} - \dot{D}_{23}\right) \\
&< 2\dot{D}_{23} + \left(\dot{D}_{13} - \dot{D}_{23}\right) && (5.34) \\
&= \dot{D}_{23} + \dot{D}_{13}
\end{aligned}$$

where (5.32) follows from (5.30), (5.33) follows from (5.31), and (5.34) follows from the fact that $\frac{D_{13}}{w_4} < 1$. Therefore, under an edge-length-preserving distortion of a cuboid with edge lengths w_1, w_2, w_3, under which the lengths of at least two of the diagonals decrease, the length of the main diagonal decreases more quickly than the sum of the lengths of at

least one pair of face diagonals.

We have shown in Theorem 5.2 that, if we continue to distort the parallelepiped until it is completely flat (i.e. it lies in a plane), then the sum of the lengths of at least one pair of diagonals exceeds $w_i + w_4$, where w_i is the weight common to both diagonals. To complete the proof of the conjecture, we need to show that the length of the main diagonal decreases more quickly than the sum of the lengths of a pair of face diagonals for perturbations of all parallelepipeds between the cuboid and the flattened quadrilateral. The result could then be generalised to higher-degree Steiner points using a similar argument to the one used in the proof on Theorem 5.2.

5.7 Angles between edges incident to a Steiner point

We have shown that, assuming a linear cost function, the degree of all Steiner points in MGAs in the Euclidean plane is three, and there is strong evidence to suggest that this is so for MGAs in three-space. Hence it is useful to analyse the optimum angles between edges incident to a degree-three Steiner point. Such knowledge can be useful for developing techniques for solving the Gilbert arborescence problem.

Let $N = \{p_1, p_2, p_3\}$ be a set of terminals in the Euclidean plane, where p_1, p_2 are sources with respective positive flows t_1, t_2, and p_3 is the sink (Figure 5.7 (i)). Let T be the star connecting a variable point s to each terminal in N. Let α, β, γ denote the angles opposite sp_1, sp_2, sp_3 respectively. Hence α and β are angles between a source edge and the sink edge, and γ is the angle between the two source edges. Let $\alpha' = \pi - \alpha$, $\beta' = \pi - \beta, \gamma' = \pi - \gamma$. Define $w(\cdot)$ to be a cost function satisfying (5.1), (5.2) and (5.3), so that the weights on sp_1, sp_2, sp_3 are $w_1 = w(t_1), w_2 = w(t_2), w_3 = w(t_1 + t_2)$, respectively.

Let $\mathbf{u}_1, \mathbf{u}_2, \mathbf{u}_3$ be the unit vectors from s to p_1, p_2, p_3, respectively, and let $\mathbf{v}_i = w_i \mathbf{u}_i$, $i = 1, 2, 3$. Assuming s does not optimally coincide with a terminal, then by Theorem 2.1 in Chapter 2, s is an FW point for N (and hence, by Theorem 5.1, T is a MGA for N for the three-point case), if and only if $\mathbf{v}_1 + \mathbf{v}_2 + \mathbf{v}_3 = \mathbf{0}$. This vector sum forms a triangle, called the *weight triangle* (Figure 5.7 (ii)), with edge lengths w_1, w_2, w_3, and internal angles α', β', γ'. From the weight triangle, we can compute the optimum angles between the

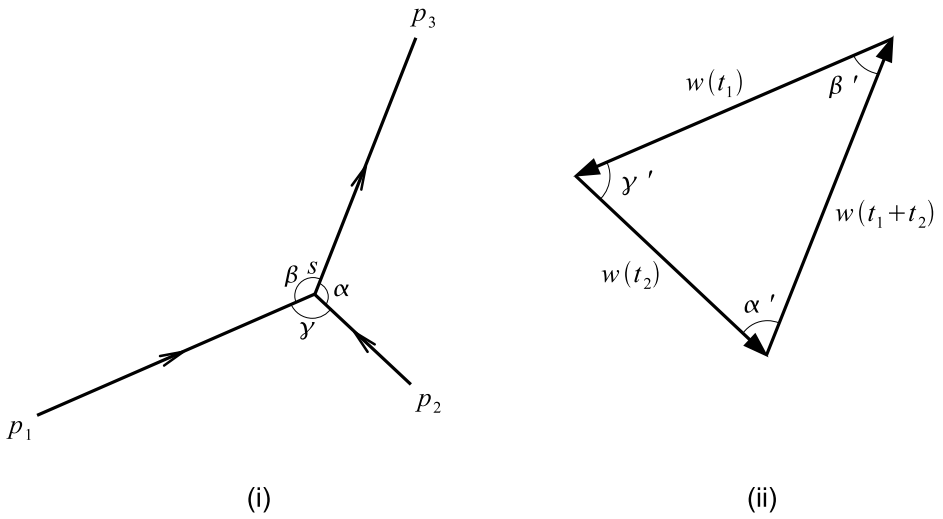

Figure 5.7: Three-terminal Gilbert arborescence problem. (i) Terminals and angles. (ii) Weight triangle.

three edges as functions of the three weights. Applying the cosine rule to the weight triangle, and using the identity $\cos(\pi - A) = -\cos A$, we have

$$\cos\alpha = \frac{w^2(t_1) - w^2(t_2) - w^2(t_1+t_2)}{2w(t_2)w(t_1+t_2)}, \tag{5.35}$$

$$\cos\beta = \frac{w^2(t_2) - w^2(t_1) - w^2(t_1+t_2)}{2w(t_1)w(t_1+t_2)}, \tag{5.36}$$

$$\cos\gamma = \frac{w^2(t_1+t_2) - w^2(t_1) - w^2(t_2)}{2w(t_1)w(t_2)}. \tag{5.37}$$

From these expressions we can find upper and lower bounds for the angle γ between two source edges incident with a degree-three Steiner point and the angle α (or β) between a source and a sink edge incident with a degree-three Steiner point.

From (5.35), it is clear that $\cos\alpha < 0$, since $w^2(t_1) - w^2(t_1+t_2) < 0$. Thus $\alpha > \frac{\pi}{2}$ and, similarly, $\beta > \frac{\pi}{2}$. To examine the maximum angle between a source and a sink edge, consider Equation (5.35). To maximise α, we need to minimise $\cos\alpha$. To do this, note that,

from condition (5.3), as $t_1, t_2 \to \infty$, we have $w(t_1 + t_2) \to w(t_1) + w(t_2)$. Then we have

$$\begin{aligned} \cos\alpha &\to \frac{w^2(t_1) - w^2(t_2) - (w(t_1) + w(t_2))^2}{2w(t_2)(w(t_1) + w(t_2))} \\ &= \frac{-2w^2(t_2) - 2w(t_1)w(t_2)}{2w(t_1)w(t_2) + 2w^2(t_2)} \\ &= -1. \end{aligned}$$

Therefore $\alpha \to \pi$. To examine the maximum angle between two source edges, again assume that $\frac{t_1}{t_2}$ is large. Then $w(t_1 + t_2) \approx w(t_1)$. From (5.37), we have

$$\begin{aligned} \cos\gamma &\approx -\frac{1}{2}\frac{w(t_2)}{w(t_1)} \\ &\geq -\frac{1}{2}. \end{aligned}$$

Thus $\gamma \approx \frac{2\pi}{3}$. For the minimum angle between two source edges, let $t_1, t_2 \to \infty$. Then $w(t_1 + t_2) \to w(t_1) + w(t_2)$, and we have

$$\begin{aligned} \cos\gamma &\to \frac{(w(t_1) + w(t_2))^2 - w^2(t_1) - w^2(t_2)}{2w(t_1)w(t_2)} \\ &= \frac{2w(t_1)w(t_2)}{2w(t_1)w(t_2)} \\ &= 1. \end{aligned}$$

Therefore $\gamma \to 0$. The upper and lower bounds are summarised in the following lemma.

Lemma 5.5. *Let s be a degree-three Steiner point in an MGA. Then:*

- *The angle between a source edge and a sink edge is strictly greater than $\frac{\pi}{2}$, and strictly less than π.*
- *The angle between two source edges is strictly greater than zero, and strictly less than $\frac{2\pi}{3}$.*

The following known result provides a condition which guarantees that the angle between any two adjacent edges incident with a Steiner point is greater than $\frac{\pi}{2}$.

Lemma 5.6. *[78] If the cost function satisfies the condition*

$$w^2(t_1) + w^2(t_2) > w^2(t_1 + t_2), \quad \forall t_1, t_2 > 0, \tag{5.38}$$

then the angle between any two adjacent edges incident with a Steiner point is greater than $\frac{\pi}{2}$.

Proof. From (5.37), if (5.38) is satisfied, then $\cos\gamma < 0$, which implies that $\gamma > \frac{\pi}{2}$. ∎

Thus, if this condition holds, the minimum angle between two source edges is increased from zero to $\pi/2$. We can also make the following observation about the optimal angles α, β, γ.

Lemma 5.7. *The angle* γ *between the two source edges is always less than or equal to the angle between a source edge and a sink edge.*

Proof. Applying the sine rule to the weight triangle, we have:

$$\frac{w(t_1 + t_2)}{w(t_1)} = \frac{\sin\gamma'}{\sin\alpha'} \geq 1 \tag{5.39}$$

Thus $\sin\gamma' \geq \sin\alpha'$, which implies that $\sin\gamma \geq \sin\alpha$, and therefore $\gamma \leq \alpha$. ∎

5.7.1 Critical and absorbing angles

When the points in N lie in a Euclidean plane, necessary conditions for a vertex to be a Steiner point in an MGA can be stated in terms of so-called *critical* and *absorbing angles*. Critical and absorbing angles were posed in [72] and [71] for SMTs in Minkowski planes.

An angle $\angle p_1 s p_2$ between two edges $p_1 s$ and $p_2 s$ is *critical* if there exists a point $p_3 \neq s$ such that s is an FW point for the set $N = \{p_1, p_2, p_3\}$, where the given points have respective positive weights w_1, w_2, w_3. Critical angles are a direct generalisation of Euclidean 120° angles in SMTs. The angle $\angle p_1 s p_2$ is *absorbing* if s is an FW point for $N = \{p_1, p_2, s\}$.

In the following lemma we generalise the definitions of critical and absorbing angles provided in [72] to the weighted case.

Lemma 5.8. *Let* $\angle p_1 s p_2$ *be an angle between two edges* $p_1 s$ *and* $p_2 s$ *with respective positive weights* w_1 *and* w_2. *Let* $w_3 > 0$ *be an additional given weight. Denote the unit vectors from* s *to* p_i, $i = 1, 2$ *by* $\mathbf{u}_i$. *Then*

1. $\angle p_1 s p_2$ *is a critical angle if and only if* $|w_1\mathbf{u}_1 + w_2\mathbf{u}_2| = w_3$ *if and only if*

$$\cos\angle p_1 s p_2 = \frac{w_3^2 - w_1^2 - w_2^2}{2w_1 w_2}.$$

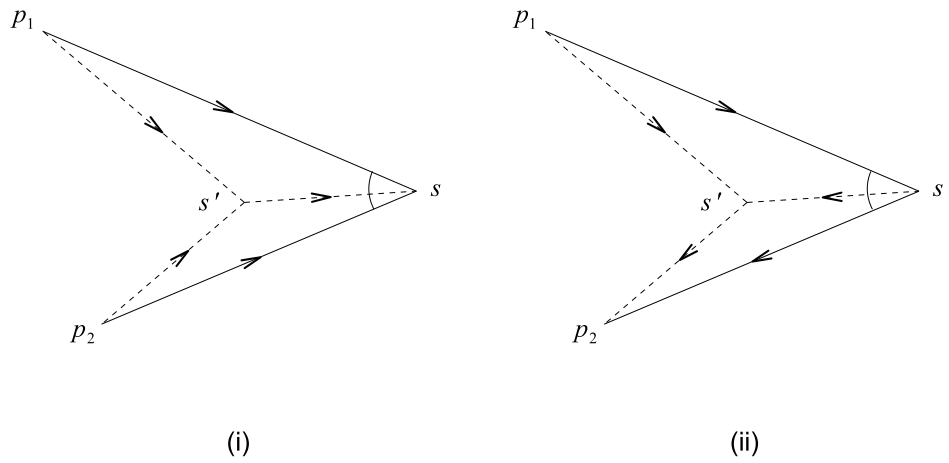

Figure 5.8: Absorbing angles. (i) Source edges. (ii) Source and sink edges.

2. *$\angle p_1 s p_2$ is an absorbing angle if and only if $|w_1\mathbf{u}_1 + w_2\mathbf{u}_2| \leq w_3$ if and only if*

$$\cos\angle p_1 s p_2 \leq \frac{w_3^2 - w_1^2 - w_2^2}{2w_1 w_2}.$$

Proof. Follows directly from the proof in [72] and identities (5.35), (5.36) and (5.37). ∎

Thus a critical angle is also an absorbing angle, but an absorbing angle is, in general, not a critical angle. It was noted in [72] that all angles between edges incident with a Steiner point in an SMT are absorbing.

If an angle $\angle p_1 s p_2$ is not absorbing, then clearly the cost of the arborescence can be reduced by splitting s into s and s'. This is shown in Figure 5.8 where (i) $p_1 s, p_2 s$ are source edges and (ii) $p_1 s$ is a source edge and $s p_2$ is a sink edge.

We now state necessary conditions for a vertex to be a Steiner point in an MGA in the Euclidean plane.

Theorem 5.3. *Let $N = \{p_1, \ldots, p_k\}$ be a set of terminals in the Euclidean plane, where $p_1, \ldots, p_{k-1}$ are sources with respective positive flows $t_1, \ldots, t_{k-1}$, and p_k is the sink. Let T be an arborescence with a star topology joining an additional point $s \notin N$ to each p_i, $i \in \{1, \ldots, k\}$, so that flows are routed from the sources to the sink via s. Let $w(\cdot)$ be a cost function satisfying the*

conditions for Gilbert networks, so that the weight on an edge e with total flow t_e is $w(t_e)$. Let $\mathbf{u}_i$ denote the unit vector from s to p_i. If T is an MGA on N, then

1. *The sum of the weighted unit vectors from s to each p_i $i \in \{1, \ldots, k\}$ is zero; and*
2. *All angles in the star configuration are absorbing.*

Proof. Follows from Theorem 5.1. ∎

5.8 Exact and approximate algorithms

To conclude this chapter, we briefly discuss two known algorithms which can be adopted to provide exact or approximate solutions to the Gilbert arborescence problem. We begin by looking at a generalisation of the well-known *Melzak algorithm* for (unweighted) Euclidean Steiner trees in the plane; an algorithm which provides exact solutions but is computationally inefficient for large numbers of terminals. We then discuss a heuristic proposed by Thomas and Weng [75], and suggest some possible improvements to this procedure.

5.8.1 The Melzak algorithm

The *Melzak algorithm* [61] was the first finite algorithm for finding (unweighted) Euclidean Steiner trees in the plane. This and other algorithms for the ESP are also discussed in [40], [41] and [43].

The Melzak algorithm finds a (locally) minimal tree for every topology on N, and selects the shortest one as an SMT. The algorithm consists of a *merging stage* and a *reconstruction stage*. At each step of the merging stage, two arbitrary siblings a and b adjacent to a Steiner point s are replaced by a new point, called an e-*point*. Points a and b and their edges to s are deleted, and s is then treated as a terminal. The merging stage ends when only two terminals remain.

The reconstruction stage starts by connecting the two remaining terminals by a straight line, called a *Simpson line*. At each step of the reconstruction stage, an edge connected to an e-point is replaced by a Steiner point and its three edges, where the Steiner point lies

at the intersection of the Simpson line and the circle circumscribing the three points associated with the e-point.

In 1967, Gilbert [34] identified that a generalisation of Melzak's algorithm can be used for finding minimum Gilbert networks, provided every Steiner point in the Gilbert network has degree three. It uses the same geometric construction procedure except the angles in the triangles are altered to account for edge weights. This generalised Melzak algorithm is discussed in a working paper [12]. We now apply the main result of this to the Gilbert arborescence problem.

Theorem 5.4. *A minimal Gilbert arborescence T for a given topology can be constructed in $O(2^n)$ time by using a Melzak-type algorithm, where n is the number of terminals.*

Once the minimal Gilbert arborescence has been found for every topology on N, global optimisation techniques, such as simulated annealing, can be used to find an optimal or suboptimal solution.

As noted in [24], the Melzak algorithm cannot be extended to higher-dimensional spaces. The reason is that for two given points, there is an infinite number of e-points. Since all known exact methods for finding SMTs use the Melzak algorithm as a subroutine, or determine the e-point directly, these methods cannot be applied in higher dimensions. Hence, other tools are required for solving the Gilbert arborescence problem in higher dimensions.

5.8.2 Angle-splitting heuristic

The ESP is known to be NP-hard, and since the ESP is a special case of the Gilbert network problem, we immediately conclude that the Gilbert network problem is also NP-hard. Moreover, since the Gilbert arborescence problem is a special case of the Gilbert network problem, it too is NP-hard. As a result, it is important to derive effective heuristics for constructing good approximate solutions in linear time.

There exists a number of heuristics in the literature on minimum Gilbert networks. Here we discuss one such heuristic, and suggest some possible improvements when applying the heuristic to the special case of the Gilbert arborescence problem.

Thomas and Weng [75] proposed three heuristics for constructing minimum Gilbert networks. The one we are interested in is the so-called *angle-splitting heuristic*. It starts with the complete network, i.e. the network having edges between every pair of terminals. At each iteration, a new tree is constructed by splitting an angle not satisfying a required angle condition. It terminates when all angles in the network satisfy the angle condition.

During the process, if a degree-two Steiner point occurs as a result of edge splitting, the Steiner point is deleted, its incident edges are deleted, and a single edge is installed between the two remaining vertices.

To apply the angle-splitting heuristic to the Gilbert arborescence problem, the algorithm can be refined by implementing a number of changes to suit the characteristics of arborescences.

First, rather than starting with the complete graph on N, we instead have as our initial network the set of edges $p_i p_k$, $i = 1, \ldots, k-1$ connecting each source p_i with the sink p_k (we can call this a *complete arborescence*). This seems logical since the flow between two arbitrary sources is zero, and hence the cost of the complete network is greater than that of the complete arborescence.

One aspect of the angle-splitting heuristic that is not made clear in [75] is the order in which angles are split. Since an order is not stated, it is assumed that an angle is chosen somewhat arbitrarily. One idea to potentially improve the algorithm is to check every angle at each iteration, and split the angle that is furthest from satisfying the angle condition. Moreover, multiple angles in different subtrees could be split simultaneously to improve efficiency.

Another idea is to start with the star topology obtained by solving the FW problem for N, rather than starting with the complete arborescence. These ideas may be further explored in future work.

Chapter 6

Minimum Gilbert Arborescences in Minkowski Spaces

We study the Gilbert arborescence problem in Minkowski spaces. We provide a geometric characterisation of Steiner points and terminals in minimum Gilbert arborescences in Minkowski spaces, generalising a result for Steiner minimum trees [73].

6.1 Introduction

IN the previous chapter, we introduced the *Gilbert arborescence problem* (GAP) in Euclidean space, a special case of the Gilbert network problem [34] where the k terminals consist of $k-1$ sources and a unique sink. For a given set N of terminals, a given set of flows $t_1, \ldots, t_{k-1}$ and a given cost function $w(\cdot)$ satisfying conditions (5.1), (5.2) and (5.3), we defined a *minimum Gilbert arborescence* (MGA) to be a network having the minimum cost among all networks spanning N, with the same flows and the same cost function. In this chapter, we extend our study of MGAs from the Euclidean setting to *Minkowski spaces*, which are finite-dimensional real normed spaces.

Although Euclidean Steiner trees have been widely studied since their inception in 1934 [45], the study of Steiner trees in Minkowski spaces is relatively new. Hanan [39] initiated the study of Steiner trees in rectilinear space. In 1967, Cockayne [25] initiated the study of the Steiner problem in Minkowski planes (two-dimensional Minkowski spaces) and obtained some results for three-terminal SMTs. Du et al. [29] investigated further properties of SMTs in Minkowski planes. They showed that if the unit disk is differentiable and strictly convex, then every full SMT consists of three sets of parallel segments.

Alfaro et al. [1] showed that for Steiner trees in Minkowski planes, Steiner points have degree three if the norm is smooth, and degree three or four if the norm is not smooth.

Du and Hwang [30] studied Steiner trees in Minkowski spaces where the unit ball is a n-dimensional symmetric polytope with $2n$ extreme points. They proved that there always exists an SMT such that the coordinates of the Steiner points are taken from the set of coordinates of the terminals. Brazil and Zachariasen [19] studied Steiner trees in Minkowski planes where the unit ball is a polygon, providing a linear-time algorithm for computing an SMT for a given full Steiner topology.

Lawlor and Morgan [54] derived upper bounds for the degrees of Steiner points in SMTs in Minkowski spaces, with emphasis on the ℓ_p norm. They showed that the degree of Steiner points in smooth n-dimensional Minkowski spaces is at least three, and no greater than $n+1$. Swanepoel [70] strengthened this result by showing that the upper bound also holds for terminals. He then studied the local structure of vertices in SMTs in arbitrary Minkowski planes, providing a geometric characterisation of all Steiner points and terminals in terms of the so-called *absorbing angles* [72]. This characterisation provides necessary and sufficient conditions for a set of edges emanating from a point to be in the neighbourhood of a vertex in an SMT. In a later paper [73], Swanepoel extended this work by providing necessary and sufficient conditions for certain star configurations in n-dimensional Minkowski spaces to be SMTs. It is this last paper which forms a basis for the material in this chapter.

Recall that in Chapter 3 we studied a similar but simpler problem, called the *Fermat-Weber problem*, which asks for a point, called a *Fermat-Weber point*, minimising the sum of weighted distances to k given points in a Minkowski space. Many of the results for Fermat-Weber points are applicable to Steiner points in MGAs, since a Steiner point is a Fermat-Weber point with respect to its adjacent vertices. However, as noted in the previous chapter, the added complexity for MGAs stems from the fact that the cost of a Gilbert arborescence can often be reduced by *splitting* Steiner points to produce a network with a new topology.

Although the literature on Steiner trees in Minkowski spaces is growing steadily, it appears to contain very little, if anything, relating to Gilbert networks. Here we extend

some of the work done on Steiner minimum trees (SMTs) in Minkowski spaces to MGAs in Minkowski spaces. We are particularly interested in generalising a geometric characterisation of vertices in SMTs [73] to MGAs. This characterisation will be useful in Chapters 7 and 8, where we study gradient-constrained MGAs in a vertical plane and in three dimensions. Moreover, the generalisation of these results to the Gilbert network problem in Minkowski spaces seems to be straightforward, and such a problem has a potentially vast range of applications.

In Section 6.2, we provide necessary background relating to Minkowski spaces, functional analysis and subdifferential calculus. In Section 6.3 we generalise an important operation called *reduced Minkowski addition* [73] so that it is applicable to the Gilbert arborescence problem. In Section 6.4, we present the geometric characterisation of terminals and Steiner points in MGAs in Minkowski spaces and demonstrate their application by examples.

6.2 Background

6.2.1 Minkowski spaces and the unit ball

For the necessary background relating to Minkowski spaces, we refer the reader to Section 3.2, in particular, Lemmas 3.1, 3.2 and 3.3 in Section 3.2.1, which provide results relating to the dual and unit ball.

6.2.2 Subdifferential calculus

Section 3.2.2 contains the necessary background relating to subdifferential calculus and convex analysis. In particular, Lemmas 3.4 and 3.5 are very important, and are used in the proof of the main theorem in this chapter. Definitions are required for the *Minkowski sum* of two sets, and *Minkowski addition*.

The following additional results about subdifferential calculus, which are required for the proof of the main theorems in this chapter, were collected from various sources and summarised in [73]. Here we simply restate the results, without proof (for details,

refer to [73] and its source references).

Lemma 6.1. [89] *Let $f_i : X_i \to \mathbb{R}$, $i = 1, \ldots, k$ be convex, and define $f : X_1 \times \cdots \times X_k \to \mathbb{R}$ by $f(x_1, \ldots, x_k) = \sum_{i=1}^{k} f_i(x_i)$. Then the subdifferential of the convex function f at $(a_1, \ldots, a_k)$ is the Cartesian product*

$$\partial f(a_1, \ldots, a_k) = \prod_{i=1}^{k} \partial f_i(a_i).$$

The next lemma is as follows.

Lemma 6.2. [73] *Let X be a Minkowski space with norm $\|\cdot\|$ and corresponding dual space X^*. For any $x, y \in X$, we have*

$$\partial \|x - y\| = \{(\phi, -\phi) : \phi \in \partial(x - y) \subseteq X^* \times X^*\}.$$

By Lemma 6.2, if e is an edge in a Gilbert arborescence in a Minkowski space X such that its endpoints are Steiner points, then the subdifferential of the length of e corresponds to two opposite exposed faces of the dual ball B^*.

6.3 Generalised theory for flow-dependent networks

In this section we generalise some concepts presented in [73] so that they are applicable to the Gilbert arborescence problem in Minkowski spaces. These concepts are required in the proof of the main theorems.

Parenthesisations and abstract Steiner trees

Consider a finite nonempty family $\Sigma = \{A_i : i \in I\}$ of operands, where $I \subseteq \{1, \ldots, k\}$ is called the *support* of Σ, and each A_i is a closed convex subset of B^*. A *parenthesisation* of Σ, denoted by $\langle \Sigma \rangle$, is a parenthesisation, in the usual sense, of some ordering

$$A_{j(1)} \boxplus \cdots \boxplus A_{j(|I|)}$$

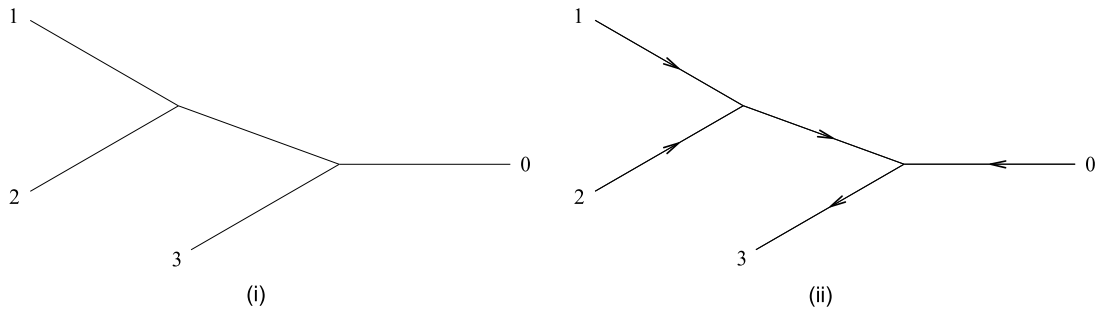

Figure 6.1: Examples of rooted abstract trees for a set of three elements. (i) Rooted abstract Steiner tree. (ii) Rooted abstract Gilbert arborescence.

of Σ, where $j : [|I|] \to I$ is some bijection. For example, suppose $\Sigma = \{A_1, A_2, A_3\}$. Then

$$\begin{aligned} \langle\Sigma\rangle_1 &= A_1 \boxplus (A_2 \boxplus A_3) \\ \langle\Sigma\rangle_2 &= A_2 \boxplus (A_1 \boxplus A_3) \\ \langle\Sigma\rangle_3 &= A_3 \boxplus (A_1 \boxplus A_2) \end{aligned}$$

are all parenthesisations of Σ. Two parenthesisations are *equivalent* if they can be transformed into each other using the commutative law on any subexpression. For example, $A_1 \boxplus (A_2 \boxplus A_3)$ is equivalent to $(A_3 \boxplus A_2) \boxplus A_1$.

The collection of equivalence classes of parenthesisations of a set Σ with support I corresponds bijectively with the collection of abstract trees with $|I| + 1$ leaves labelled by the elements of $\{0\} \cup I$, and with $|I| - 1$ internal vertices of degree three. Such a tree is called a *rooted abstract Steiner tree* on I. The node 0 is the root of the tree, node i corresponds to A_i for each $i \in I$, and each internal vertex corresponds to an instance of $\boxplus$ in the parenthesisation corresponding to the tree. The rooted abstract Steiner tree associated with $\langle\Sigma\rangle$ is denoted by $T_0\langle\Sigma\rangle$. For example, a rooted abstract Steiner tree corresponding to the parenthesisation $(A_1 \boxplus A_2) \boxplus A_3$ is shown in Figure 6.1 (i). An *abstract Steiner tree* on I is a tree with set of leaves I, and with $|I| - 2$ internal vertices of degree 3.

It is easy to see that two parenthesisations are equivalent if and only if their associated

rooted abstract Steiner trees are equal. The number of equivalence classes of parenthesisations with support $\{1,\ldots,k\}$, denoted by a_k, is the product of the first $k-1$ odd numbers, i.e.

$$a_k = \prod_{i=1}^{k-1}(2i-1).$$

For example, $a_3 = 3$, $a_4 = 15$, etc.

We define a *rooted abstract Gilbert arborescence* on I (still denoted by $T_0\langle\Sigma\rangle$) to be a rooted abstract Steiner tree whose edges are directed from $|I|$ sources to a designated sink, where $|I|$ denotes the number of elements in the support set I. For example, a rooted abstract Gilbert arborescence corresponding to the parenthesisation $(A_1 \boxplus A_2) \boxplus A_3$, where node 3 is the sink, is shown in Figure 6.1 (ii). Note that the sink need not coincide with the root.

Weighted reduced Minkowski addition

Recall from Chapter 3 that the *Minkowski sum* of two sets A and B in Euclidean space is given by

$$A + B = \{a + b : a \in A, b \in B\}.$$

The *reduced Minkowski sum* of two closed, convex subsets C and D of the dual ball B^* is defined by [73]

$$A \boxplus B = \{a + b : a \in A, b \in B, \|a+b\|^* \leq 1\},$$

i.e. $A \boxplus B$ is the intersection of the usual Minkowski sum with the dual ball.

We now introduce a generalisation of reduced Minkowski addition. Let $B^*(w)$ denote a scaled copy of the dual ball B^* with radius w, i.e. $B^*(w) = \{\phi \in X^* : \|\phi\|^* \leq w\}$. Let $p_i s$ and $p_j s$ be two source edges in a Gilbert arborescence. Suppose that the two edges route flows t_i and t_j from p_i and p_j to s, so that the weights on the two edges are $w(t_i)$ and $w(t_j)$ respectively, where $w(\cdot)$ is a cost function satisfying the conditions for Gilbert networks. Let $A_i = w_i\partial(p_i - s)$ and $A_j = w_j\partial(p_j - s)$. We define the *weighted reduced Minkowski addition* $A_i \boxplus A_j$ associated with two source edges as the usual Minkowski sum $A_i + A_j$ intersected by $B^*(w(t_i + t_j))$.

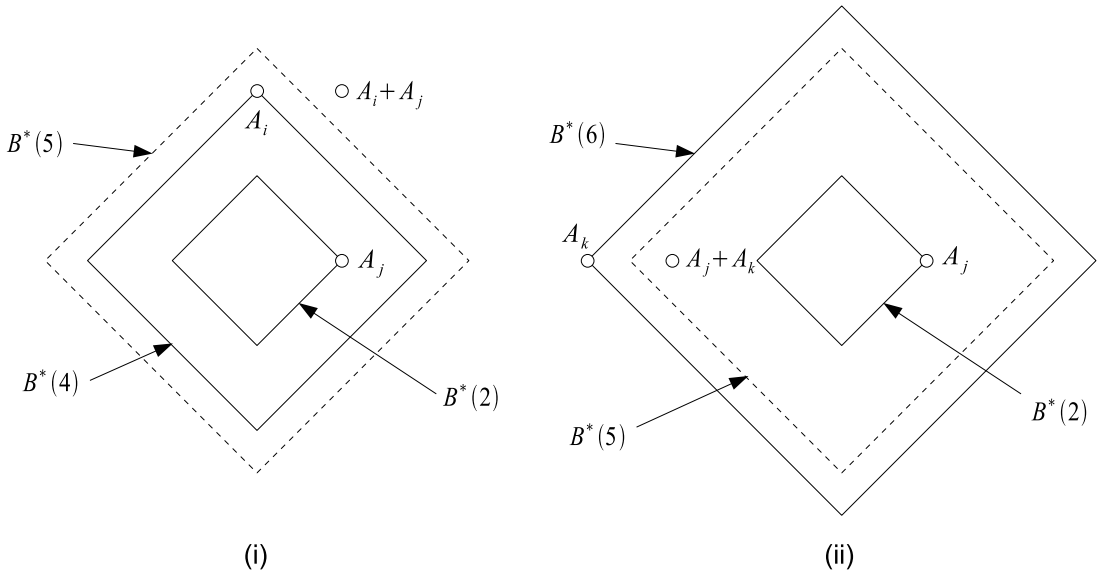

Figure 6.2: Weighted Minkowski addition of (i) source edges and (ii) source and sink edges.

Now suppose that sp_j is a source edge and sp_k is a sink edge, where the flow routed through sp_j is t_j, and all the other flow exiting s not from p_j is denoted by $\tilde{t}$. Thus the weights on sp_j and sp_k are $w(t_j)$ and $w(t_j + \tilde{t})$ respectively. If $A_j = w_j \partial(p_j - s)$ and $A_k = w_k \partial(p_k - s)$, then the weighted reduced Minkowski addition $A_j \boxplus A_k$ associated with a source edge and a sink edge is the intersection of the usual Minkowski sum $A_j + A_k$ with $B^*(w(\tilde{t}))$.

We demonstrate the concept of weighted reduced Minkowski addition by an example. Suppose X is the plane equipped with the ℓ_∞ norm. Then the dual ball B^* is the same as the unit ball B for the rectilinear norm. Let the cost function be given by $w(t) = 1 + t$. Suppose sp_i, sp_j are source edges with respective positive flows $t_i = 3$ and $t_j = 1$. Then the weights on the two edges are $w_i = 4$ and $w_j = 2$, and $B^*(w(t_i + t_j)) = B^*(5)$. Let A_i and A_j be points on the boundaries of $B^*(4)$ and $B^*(2)$, as shown in Figure 6.2 (i). Then $A_i + A_j$ is outside $B^*(w(t_i + t_j))$, and hence $A_i \boxplus A_j = \emptyset$.

Now suppose that $p_j s$ is a source edge routing flow $t_j = 1$ and sp_k is a sink edge routing flow $t_k = 5$. Then the flow exiting s not from p_j is $\tilde{t} = 4$. The weights are

therefore $w_j = 2$, $w_k = 6$ and $w(\tilde{t}) = 5$. Let A_j and A_k be points on the boundaries of $B^*(2)$ and $B^*(6)$, as shown in Figure 6.2 (ii). Then $A_j + A_k$ is inside $B^*(w(\tilde{t}))$, and hence $A_j \boxplus A_k = A_j + A_k$.

6.4 Characterisation of terminals

A characterisation of vertices (Steiner points and terminals) in Steiner trees in n-dimensional Minkowski spaces was given in [73]. The characterisation is in terms of reduced Minkowski addition defined on sets of subdifferentials associated with the terminals.

In this section we generalise the characterisation to Steiner points and terminals in MGAs in Minkowski spaces. The proofs for the main results follow closely with the proofs provided in [73]. We begin with the characterisation of terminals.

Theorem 6.1. *Let $N = \{p_0, \ldots, p_k\}$ be a set of terminals in a Minkowski space X, where $p_0, \ldots, p_{k-1}$ are sources with respective positive flows $t_0, \ldots, t_{k-1}$, and p_k is the sink. Let T be an arborescence with a star topology joining p_0 to each p_i, $i \in \{1, \ldots, k\}$. Let $w(\cdot)$ be a cost function satisfying the conditions for Gilbert networks. Then T is an MGA on N for the given flows and cost function if and only if $\langle\Sigma\rangle \neq \emptyset$ for each parenthesisation $\langle\Sigma\rangle$ of $\Sigma = \{w_i \partial(p_i - p_0) : i \in \{1, \ldots, k\}\}$.*

Proof. (Adapted from [73]) ($\Rightarrow$) Consider any parenthesisation $\langle\Sigma\rangle$ of Σ and its corresponding rooted abstract Gilbert arborescence $T_0\langle\Sigma\rangle$. Turn this tree into a Gilbert arborescence in X by associating leaf i with p_i for each $i \in \{0, \ldots, k\}$, and associating each of the $k-1$ internal vertices with a Steiner point $s_i \in X$, $i \in \{1, \ldots, k-1\}$. In doing this we have constructed an arborescence with a full topology spanning the terminals in X, where the topology is determined by the parenthesisation being considered, the Steiner points are free to move, and flows are directed from the sources to the sink. The Steiner points s_i in $T_0\langle\Sigma\rangle(s_1, \ldots, s_{k-1})$ may in fact coincide, resulting in the arborescence having a degenerate topology.

Denote this arborescence in X by $T_0\langle\Sigma\rangle(s_1,\ldots,s_{k-1})$. Its cost is given by

$$C(s_1,\ldots,s_{k-1}) = \sum_{e\in E(T_0\langle\Sigma\rangle)} w_e\rho_e(s_1,\ldots,s_{k-1}),$$

where $E(T_0\langle\Sigma\rangle)$ is the set of edges in $T_0\langle\Sigma\rangle$, $w_e = w(t_e)$ is the weight on edge e which is a function of the total flow t_e routed through e, and $\rho_e(s_1,\ldots,s_{k-1}) = \|a-b\|$, where a and b are the two endpoints of e. Thus $C : X\times\cdots\times X \to \mathbb{R}$ is a convex function since it is a sum of convex functions.

Since $T_0\langle\Sigma\rangle(p_0,\ldots,p_0)$ is an arborescence with a star topology joining p_0 to all p_i, $i\in\{1,\ldots,k\}$, which is an MGA by assumption, C attains its minimum at $(p_0,\ldots,p_0)$. Thus

$$o \in \partial C(p_0,\ldots,p_0) = \sum_{e\in E(T_0\langle\Sigma\rangle)} w_e\partial\rho_e(p_0,\ldots,p_0)$$

by Lemma 3.4 in Chapter 3. By Lemmas 6.1, 3.5 (Chapter 3) and 6.2, if $e = s_is_j$ (i.e. both endpoints of e are Steiner points), then

$$\partial\rho_e(p_0,\ldots,p_0) = \{(o,\ldots,o,\phi,o,\ldots,o,-\phi,o,\ldots,o) : \phi\in B^*\}$$

while if $e = p_is_j$ (i.e. one endpoint of e is a terminal and the other is a Steiner point), then

$$\partial\rho_e(p_0,\ldots,p_0) = \{(o,\ldots,o,\phi,o,\ldots,o) : \phi\in\partial(p_i-p_0)\}.$$

By considering each coordinate $i\in\{1,\ldots,k-1\}$ of ∂C (each coordinate corresponding to a Steiner point in $T_0\langle\Sigma\rangle(s_1,\ldots,s_{k-1})$), we obtain a weighted functional $w_e\phi_e\in X^*$ for each edge $e\in E(T_0\langle\Sigma\rangle)$ such that

$$w_e\phi_e \in \begin{cases} B^*(w_e), & \text{if } e = s_is_j \text{ or } e = p_0s_i; \\ w_e\partial(p_i-p_0), & \text{if } e = p_is_j,\ i\neq 0, \end{cases}$$

and for each Steiner point s_i,

$$w_e\phi_e = w_f\phi_f + w_g\phi_g,$$

where e is the incoming edge and f,g are the two outgoing edges of s_i, when the tree is di-

rected away from the root p_0 (these directions may be different to the flow directions). By induction on the definition of $T_0\langle\Sigma\rangle$ (which is equivalent to induction on subexpressions of $\langle\Sigma\rangle$), we obtain $w_e\phi_e \in \langle\Sigma\rangle$, where $e = p_0 s_i$ is the root edge. This gives $\langle\Sigma\rangle \neq \emptyset$.

($\Leftarrow$) Consider any Gilbert arborescence in X spanning $N = \{p_0, \ldots, p_k\}$. By splitting Steiner points if necessary, we obtain a tree with leaves $\{p_0, \ldots, p_k\}$ and with $k-1$ Steiner points s_i of degree three, some of them possibly coinciding with each other or with the p_i. This tree is the rooted abstract Gilbert arborescence of some parenthesisation $\langle\Sigma\rangle$ of Σ. As in the ($\Rightarrow$) argument, we obtain $\langle\Sigma\rangle \neq \emptyset$ which implies that $o \in \partial C(p_0, \ldots, p_0)$, i.e. C attains its minimum at $(p_0, \ldots, p_0)$, which occurs when the tree is $T_0\langle\Sigma\rangle(p_0, \ldots, p_0)$, an arborescence with a star topology joining p_0 to the other p_i. ∎

6.4.1 An example

We demonstrate the application of Theorem 6.1 by the following example. Let X be a Euclidean (x, z)-plane, where x is horizontal and z is vertical, equipped with the gradient-constrained norm introduced in Chapter 4, i.e.

$$|op|_g = \begin{cases} \sqrt{x_p^2 + z_p^2}, & \text{if } g(op) \leq m; \\ \sqrt{1 + m^{-2}}|z_p|, & \text{if } g(op) \geq m \end{cases}$$

where o is the origin, $p = (x_p, z_p)$ is a point in X, $m > 0$ is a constant and $g(op)$ denotes the absolute value of the gradient of the straight line segment between o and p. Setting $m = \frac{1}{\sqrt{3}}$, the unit ball and dual ball are as shown in Figure 4.2 in Chapter 4.

Let $N = \{p_0, p_1, p_2, p_3\}$ be a set of terminals in the plane, where p_0, p_1, p_2 are sources with respective positive flows $t_0 = 1, t_1 = 1, t_2 = 2$, and p_3 is the sink. Let T denote the arborescence connecting p_0 to each p_i, $i = 1, 2, 3$. Assuming a linear cost function $w(t) = 1 + t$, the weights on $p_1 s, p_2 s, s p_3$ are $w_1 = 2$, $w_2 = 3$ and $w_3 = 5$ respectively. Let $p_0 = (0, 0)$ $p_1 = (-1, 0)$, $p_2 = (\frac{\sqrt{3}}{2}, -\frac{1}{2})$, $p_3 = (\frac{\sqrt{3}}{2}, \frac{1}{2})$ (Figure 6.3 (i)). Thus $p_2 p_0$ and $p_0 p_3$ have absolute gradient m and $p_1 p_0$ has absolute gradient less than m.

Let $\Sigma = \{A_1, A_2, A_3\}$, where $A_i = w_i \partial(p_i - s)$, $i = 1, 2, 3$. Then the A_i are as shown

in Figure 6.4 (i). The three parenthesisations for Σ are shown shaded in Figure 6.4 (i)–(iii) respectively. Since all three parenthesisations are not empty, we conclude that T is an MGA for $N = \{p_0, p_1, p_2, p_3\}$ for the given flows and the given cost function.

6.5 Characterisation of Steiner points

We now generalise the characterisation for Steiner points in MGAs in Minkowski spaces.

Theorem 6.2. *Let $N = \{p_1, \dots, p_k\}$ be a set of terminals in a Minkowski space X, where $p_1, \dots, p_{k-1}$ are sources with respective positive flows $t_1, \dots, t_{k-1}$, and p_k is the sink. Let T be an arborescence with a star topology joining an additional point s to each p_i, $i \in \{1, \dots, k\}$. Let $w(\cdot)$ be a cost function satisfying the conditions for Gilbert networks. Then T is an MGA on N for the given flows and the given cost function if and only if $o \in \langle\Sigma\rangle$ for each parenthesisation $\langle\Sigma\rangle$ of $\Sigma = \{w_i \partial(p_i - s) : i \in \{1, \dots, k\}\}$.*

Proof. ($\Rightarrow$) Consider any parenthesisation $\langle\Sigma\rangle$ of Σ. Turn its associated rooted abstract Gilbert arborescence $T_0\langle\Sigma\rangle$ into an abstract Gilbert arborescence $T\langle\Sigma\rangle$ by deleting the root 0 and its incident edge, and replacing the remaining degree-two Steiner point and its incident edges with a single edge spanning the two endpoints opposite the degree-two Steiner point.

Denote the (new) edge into which the root was contracted by $\bar{e}$, and give it both directions, denoting the two directed edges by e^+ and e^-. Give all other edges of $T\langle\Sigma\rangle$ a single direction away from $\bar{e}$ (these directions may differ from the flow directions).

Turn $T\langle\Sigma\rangle$ into a Gilbert arborescence in X as follows. Associate leaf i with p_i for each $i \in \{1, \dots, k\}$, and associate each of the $k-2$ internal vertices with a variable point s_i, $i \in \{1, \dots, k-2\}$. Denote this Gilbert arborescence by $T\langle\Sigma\rangle(s_1, \dots, s_{k-2})$, and its cost by $C(s_1, \dots, s_{k-2})$.

Note that the Steiner points s_i in $T\langle\Sigma\rangle(s_1, \dots, s_{k-2})$ may coincide, and then the tree is a degeneracy of $T\langle\Sigma\rangle$. Since $T\langle\Sigma\rangle(s, \dots, s)$ is the star joining s to all p_i, $i \in \{1, \dots, k\}$, which is an SMT by assumption, C attains its minimum at $(s, \dots, s)$. Calculating the subdifferential coordinatewise, we obtain a weighted functional $w_{\vec{e}}\phi_{\vec{e}} \in X^*$ for each directed edge of $E(T\langle\Sigma\rangle)$ such that

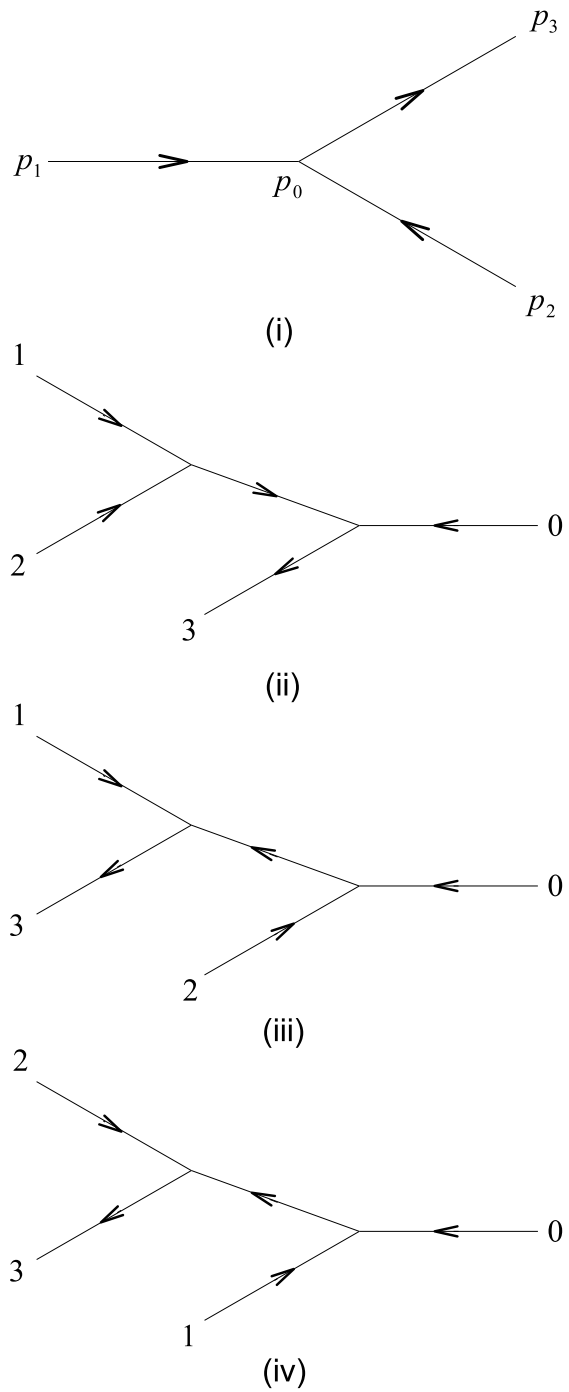

Figure 6.3: Characterisation of terminals. (i) Gilbert arborescence with a degree-three terminal. (ii)–(iv) Rooted abstract Gilbert arborescences.

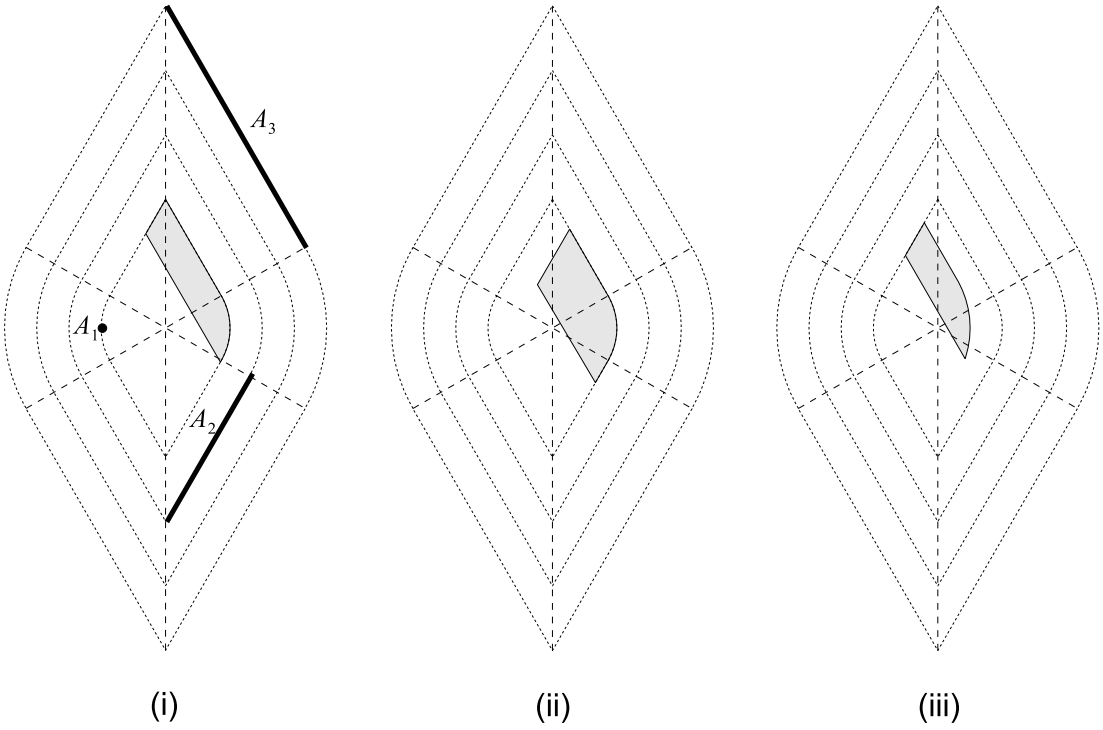

Figure 6.4: Parenthesisations (shaded) for a Gilbert arborescence with a degree-three terminal.

$$w_{\vec{e}}\phi_{\vec{e}} \in \begin{cases} B^*(w_{\vec{e}}), & \text{if } \vec{e} \text{ is incident with two Steiner points,} \\ w_{\vec{e}}\partial(p_i - s), & \text{if } \vec{e} \text{ is incident with } p_i, \end{cases}$$

$$\phi_{e^+} = -\phi_{e^-},$$

and for each Steiner point s_i, we have $w_{\vec{e}}\phi_{\vec{e}} = w_{\vec{f}}\phi_{\vec{f}} + w_{\vec{g}}\phi_{\vec{g}}$, where $\vec{e}$ is the incoming edge and $\vec{f}, \vec{g}$ are the two outgoing edges of s_i, with the convention that we ignore the outgoing e^+ or e^- if s_i is incident with $\bar{e}$.

Write $\langle \Sigma \rangle = \langle \Sigma^+ \rangle \boxplus \langle \Sigma^- \rangle$, where $e^\pm$ points to the subtree associated with $\langle \Sigma^\pm \rangle$. Let $I^\pm$ be the support of $\langle \Sigma^\pm \rangle$, and for each $i \in \{1, \ldots, k\}$ let $\phi_i = \phi_{\vec{e}}$, where $\vec{e}$ is incident with s_i. By induction on subexpressions we obtain $w_{e^\pm}\phi_{e^\pm} = \sum_{i \in I^\pm} w_i \phi_i \in \langle \Sigma^\pm \rangle$. From

$\phi_{e^+} = -\phi_{e^-}$ it follows that $o \in \langle\Sigma\rangle$.

($\Leftarrow$) Similar to the corresponding direction in the proof of Theorem 6.1. ∎

6.5.1 An example

We demonstrate the application of Theorem 6.2 by the following example. Suppose we are given the same problem provided in Section 6.4.1, except that the terminal p_0 is replaced by a Steiner point s, and the source flows are $t_1 = 1, t_2 = 2, t_3 = 3$. Let T denote the arborescence connecting s to each p_i, $i = 1,2,3$. Assuming a linear cost function $w(t) = 1 + t$, the weights on p_1s, p_2s, sp_3 are $w_1 = 2$, $w_2 = 3$ and $w_3 = 4$ respectively.

Let $\Sigma = \{A_1, A_2, A_3\}$, where $A_i = w_i\partial(p_i - s)$, $i = 1,2,3$. Then the A_i are as shown in Figure 6.5 (i). The three parenthesisations for Σ are shown shaded in Figure 6.5 (i), (ii) and (iii). Since all three parenthesisations contain o, we conclude that T is an MGA on $N = \{p_1, p_2, p_3\}$ for the given flows and the given cost function.

Theorems 6.1 and 6.2 can be used to determine whether an arborescence with a star topology is an MGA for given sets of terminals and flows, and a given cost function. Here we derive additional results as corollaries to the main theorems. These results are particularly useful for quickly identifying when a given arborescence is not an MGA.

Corollary 6.1. *Let T be an MGA with a star topology connecting a Steiner point s with a given set of terminals N. Then*

$$o \in \sum_{i=1}^{k} w_i\partial(p_i - s). \tag{6.1}$$

where the sum on the right is Minkowski addition.

Proof. Since T is an MGA on N, we have $o \in \langle\Sigma\rangle$ for all parenthesisations of $\Sigma = \{w_i\partial(p_i - s) : i \in \{1,\ldots,k\}\}$. Since $\langle\Sigma\rangle \subseteq \sum_{i=1}^{k} w_i\partial(p_i - s)$, the result is proved. Alternatively, the corollary can be proved by noting that (6.1) is a necessary and sufficient condition for s to be a Fermat-Weber point for N, and a Steiner point is a Fermat-Weber point with respect to its adjacent vertices. ∎

Thus if condition (6.1) is not satisfied, we can immediately conclude that T is not an MGA on N for the given flows and given cost function. We now state a second corollary.

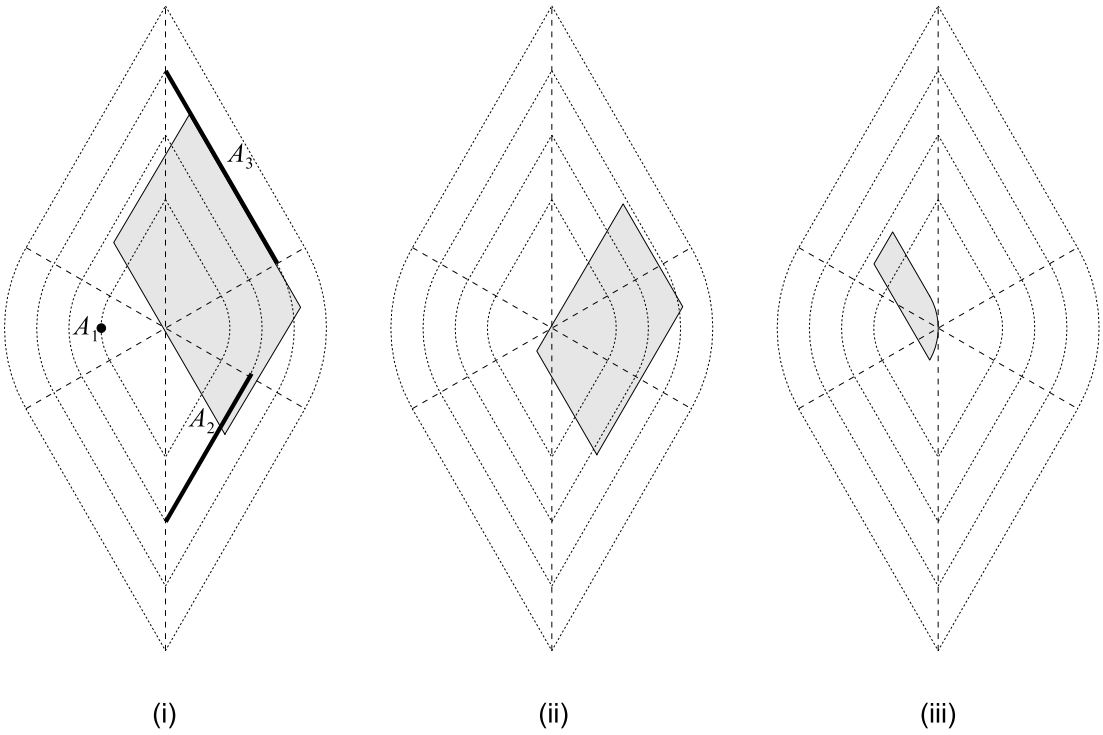

Figure 6.5: Parenthesisations (shaded) for a Gilbert arborescence with a degree-three Steiner point.

Corollary 6.2. *Let T be an MGA with a star topology connecting a Steiner point s with a given set of k terminals N. Then for each $I \subseteq \{1, \ldots, k\}$, we have*

$$\sum_{i \in I} w_i \partial(p_i - s) \cap B^*(w_I) \neq \emptyset,$$

where w_I is computed as follows: If $k \notin I$, then $w_I = w\left(\sum_{i \in I} t_i\right)$; otherwise, if $k \in I$, then $w_I = w\left(\sum_{i \in I'} t_i\right)$, where $I' = \{1, \ldots, k\} \backslash I$.

Proof. The proof follows directly from Theorems 6.1 and 6.2. ∎

Chapter 7

Gradient-Constrained Gilbert Arborescences in a Vertical Plane

We study gradient-constrained minimum Gilbert arborescences (MGAs) in a vertical plane, assuming a linear cost function $w(t) = d + ht$, where d and h are strictly positive, and the maximum gradient satisfies $m \leq 1$. We establish a range of fundamental properties of gradient-constrained MGAs in a vertical plane. In particular, we show that a Steiner point in a gradient-constrained MGA in a vertical plane has degree three or four. We provide a classification of degree-three and four Steiner points, extending results in [17] for gradient-constrained Steiner minimum trees in a vertical plane. The classification of a Steiner point is in terms of the labels *of its incident edges, where a label indicates whether the absolute value of the gradient of the Euclidean straight line connecting the endpoints of an edge is less than, equal to or greater than m. We show that there are seven feasibly optimal labellings for degree-three Steiner points, and three feasibly optimal labellings for degree-four Steiner points. We conclude with a discussion of hulls in a gradient-constrained vertical plane.*

7.1 Introduction

HAVING studied the Gilbert arborescence problem in the Euclidean setting in Chapter 5, and its generalisation to n-dimensional Minkowski spaces in Chapter 6, we are now ready to introduce the *gradient-constrained Gilbert arborescence problem*.

As was initially discussed in Chapter 1, an application of the Gilbert arborescence problem is to the underground mining industry. Suppose we are given a set $N = \{p_1, \ldots, p_k\}$ of points, called *terminals*, in Euclidean space. The points p_i, $i = 1, \ldots, k-1$ represent fixed underground locations, called *draw points*, from which t_i tonnes of ore is to be extracted. The remaining point, p_k, called the *breakout point*, is a fixed point at the surface to which all mined material is transported.

An underground mine is required to provide access to the draw points and to allow excavated ore to be transported to the surface. While underground mines may include different types of infrastructure components (such as a vertical hoisting shaft, ore passes, etc.), in this chapter we focus on mines comprised entirely of tunnels. The set of interconnected tunnels can be modelled as a Gilbert arborescence T, where draw points correspond to sources whose associated tonnages correspond to flows, the breakout point corresponds to the sink, tunnels correspond to edges, and the junctions not in N at which three or more tunnels intersect correspond to Steiner points.

There are two principal costs associated with a tunnel over the life of the mine. The first is the *development cost* associated with building the tunnel. The second is the *haulage cost* associated with transporting mined material across the tunnel. The total cost of an edge, e, can be formulated as $C(e) = w(t_e)l_e$ where $w(\cdot)$ is a cost function satisfying the conditions for Gilbert networks, l_e is the length of e and t_e is the quantity of ore to be hauled along e over the life of the mine. A simple but sufficiently realistic cost function used regularly in mining applications is the linear function

$$w(t) = d + ht \tag{7.1}$$

where d is the cost per unit length of developing a tunnel and h is the cost per unit length of hauling a unit quantity of ore through the tunnel. Typical values for these constants are $d = \$3000/\text{m}$ and $h = \$0.75/(\text{t.km})$. In this chapter we will consider only the linear cost function (7.1). Furthermore, we will assume that the constants d and h, and the tonnages $t_i,\ i = 1, \ldots, k-1$, are strictly positive.

Because of navigability requirements of haulage trucks, a tunnel cannot be very steep. A typical maximum grade at which haulage trucks can operate is 1:7. A network is called *gradient-constrained* if the absolute value of the instantaneous gradient at any differentiable point on the edges in the network is no more than a given value, $m > 0$. In this work we assume that $m \leq 1$. This condition is easily satisfied in real mining networks.

Fundamental properties of gradient-constrained Steiner minimum trees (SMTs) were studied for the case where the terminals lie in a vertical plane [17], and in three dimensions [13]. These properties have played a valuable role in improving the efficiency of

a heuristic algorithm for solving the gradient-constrained Steiner tree problem. The algorithm has been implemented into the UNO software product (refer to Chapter 1), which has been successfully applied to several industry case studies [10]. The fundamental properties of gradient-constrained MGAs have, up until now, not been investigated. The goal of this and the following chapter is to establish the fundamental properties for gradient-constrained MGAs in two and three dimensions respectively.

We begin by considering a two-dimensional version of the gradient-constrained Gilbert arborescence problem where the terminals lie in a vertical plane $\mathcal{P}$. This planar problem is of interest not only as a specific case of the three-dimensional problem but also because of its application to underground mining in its own right. For example, it is not unusual for an orebody (and its draw points) to lie approximately in a vertical plane. In such a case, the mining network servicing the orebody can realistically be modelled by the vertical plane problem.

In Section 7.2, we restate background from Chapter 4 relating to the gradient metric, in the context of the Gilbert arborescence problem. Then, in Section 7.3, we establish a range of fundamental properties of gradient-constrained MGAs in a vertical plane. In particular, we show that the degree of a Steiner point in a gradient-constrained MGA in a vertical plane is either three or four.

A classification of degree-three and degree-four Steiner points in gradient-constrained MGAs in a vertical plane is presented in Sections 7.4 and 7.5 respectively. The classification of a Steiner point is in terms of the *labels* of its incident edges, where a label indicates whether the absolute value of the gradient of the Euclidean straight line connecting the endpoints of an edge is less than, equal to, or greater than m. We show that there are seven feasibly optimal labellings for degree-three Steiner points, and three feasibly optimal labellings for degree-four Steiner points. We conclude in Section 7.6 with a discussion of hulls in a gradient-constrained vertical plane.

7.2 Background

In this section we provide background and notation required in this chapter.

7.2.1 The gradient metric

Although we have already introduced the gradient metric in Chapter 4, we restate its background here in the context of the Gilbert arborescence problem. The following account is taken primarily from [13].

A network T is called *gradient-constrained* if the absolute value of the instantaneous gradient at any differentiable point on the edges in T is no more than a given positive constant m. Let $p = (x_p, z_p)$ and $q = (x_q, z_q)$ be two points in a vertical plane $\mathcal{P}$, and assume that the z-axis is vertical. Denote the Euclidean straight line segment connecting p and q by pq. We define the *gradient*, g, of pq to be the absolute value of the gradient of pq, that is

$$g(pq) = \left| \frac{z_q - z_p}{x_q - x_p} \right|.$$

Suppose pq is an edge in a gradient-constrained network T embedded in a vertical Euclidean plane $\mathcal{P}$. If $g(pq) \leq m$, then pq is a straight line segment connecting p and q, and is called a *straight edge*. If $g(pq) > m$, then pq cannot be represented as a straight line without violating the gradient constraint. It can, however, be represented by a zigzag line joining p and q, with each segment of the zigzag having gradient equal to m. Such edges are called *bent edges*, and are geodesics (shortest paths) under the gradient metric. It is not difficult to show that the union of all geodesics between p and q forms a parallelogram whose sides have gradient m (Figure 7.1). One can select any zigzag contained in this parallelogram, provided each segment of the zigzag has gradient m. An example is shown in the figure. The points where the zigzag changes direction are called *corner points*. If r_1, r_2 are the corner points for the two geodesics on the boundary of the parallelogram, then the geodesics pr_1q and pr_2q can be interchanged by the process of *flipping*.

The length of an edge pq in a gradient-constrained network can be measured in a special metric, called the *gradient metric*. Define the *vertical metric* of pq to be $|pq|_v = c|z_p - z_q|$ where c is a given constant. Then the gradient metric can be defined in terms of the Euclidean and vertical metrics as

$$|pq|_g = \begin{cases} |pq| = \sqrt{(x_q - x_p)^2 + (z_q - z_p)^2}, & \text{if } g(pq) \leq m; \\ |pq|_v = \sqrt{1 + m^{-2}}|z_q - z_p|, & \text{if } g(pq) \geq m. \end{cases}$$

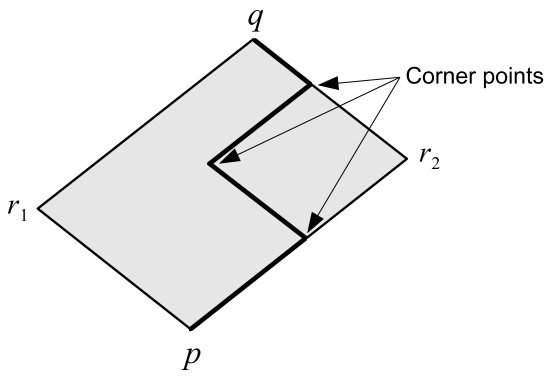

Figure 7.1: Parallelogram formed by the union of gradient-constrained geodesics between the endpoints of a line with gradient greater than the maximum.

Note that $|pq| \leq |pq|_g$, and the gradient metric is convex although it is not strictly convex. We define pq to be an *f-edge*, *m-edge* or *b-edge* if $g(pq) < m$, $g(pq) = m$ or $g(pq) > m$, respectively. The *label* of an f-edge, m-edge or b-edge is 'f' (meaning flat), 'm' (meaning maximum) or 'b' (meaning bent), respectively. The label of an edge can be viewed as an indication of which metric is 'active' for that edge, with an 'm' label indicating that both metrics hold simultaneously.

7.2.2 Edge vectors

Euclidean space equipped with the norm associated with the gradient metric is an example of a Minkowski space (see Chapter 6). In a gradient-constrained vertical plane, the unit ball B_g and dual ball B_g^* are as shown in Figure 7.2 (i)–(ii). Note that the diagonal lines (shown dashed) have gradient m, and that the shapes of the unit ball and dual ball depend on the value of m.

Recall from Chapter 3 that the set of norming functionals $\partial(p - s)$ associated with an edge ps with fixed p and variable s corresponds to an exposed face of the dual ball. Also, a norming functional is equivalent to a vector $\frac{\mathbf{u}}{\delta}$, where $\mathbf{u}$ is an outward unit vector normal to the hyperplane supporting $s + B_g$ at the point where the ray from s through p intersects B_g, and δ is the distance from s to this hyperplane. We will refer to these vectors

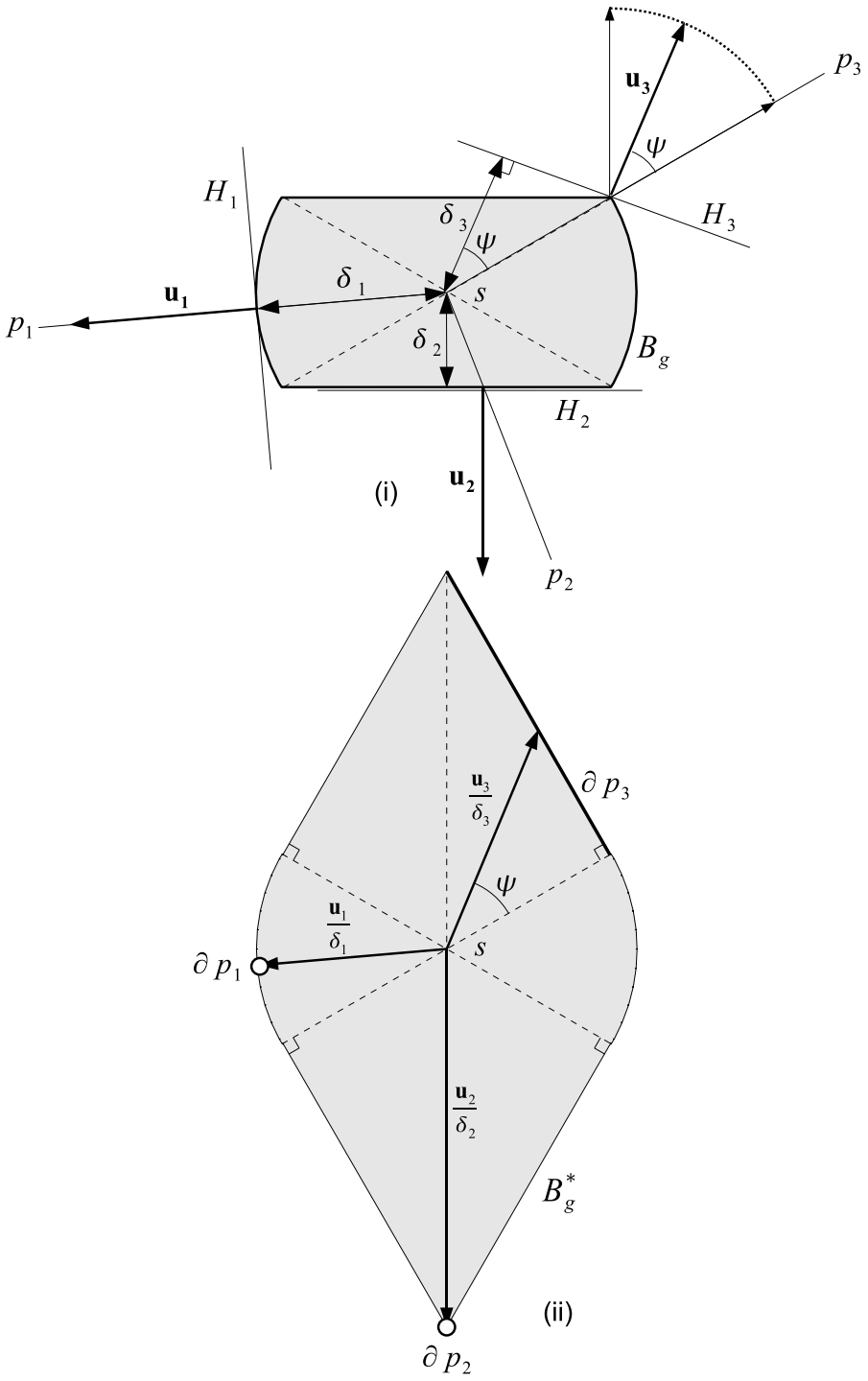

Figure 7.2: Edge vectors and outward normal vectors for f-, m- and b-edges in the gradient metric. (i) The unit ball. (ii) The dual ball.

as *edge vectors*.

In the gradient metric, we can characterise vectors for edges connecting a fixed point and a Steiner point by the following lemma (refer to Figure 7.2).

Lemma 7.1. *Let ps be an edge with an associated weight w in a gradient-constrained MGA connecting a terminal p and a Steiner point s. Then an edge vector $\mathbf{v}$ corresponding to an element of $w\partial|p-s|_g = w\partial(p-s)$ is computed as follows:*

- *If sp is an f-edge, $\mathbf{v}$ points from s to p and has length w.*
- *If sp is a b-edge, then $\mathbf{v}$ points vertically up or down, if p is above or below s respectively, and has length $w\sqrt{1+m^{-2}}$.*
- *If sp is an m-edge, then any $\mathbf{v}$ can be selected from the continuum of vectors having all possible directions between an m-edge and a vertical edge. The length of $\mathbf{v}$ is given by $w/\cos\psi$, where ψ is the angle that $\mathbf{v}$ makes with the m-edge.*

Note that the set of all possible $\mathbf{v}$ associated with an m-edge all point to one of the straight line segments on the boundary of B^*, and forms a right-angled triangle.

7.2.3 The variational argument

The *variational argument* is a powerful tool that is widely applicable in the study of Euclidean Steiner trees [67] and gradient-constrained SMTs [13]. The following definition of the variational argument applied to gradient-constrained networks is taken from [13].

Lemma 7.2. *For a minimum-cost arborescence T, the directional derivative of the cost of T, denoted by $\dot{T}$, is greater than or equal to zero when its Steiner points are perturbed in any direction.*

The following lemma provides a method for computing the variation of f-, m- and b-edges (refer to Figure 7.3) under an arbitrarily small movement, called a *perturbation*, of an endpoint.

Lemma 7.3. *Suppose $e = ps$ is an edge in T with weight w, and let s be a Steiner point which is perturbed to s' in direction $\mathbf{r}$. Let $\dot{e}_{\mathbf{r}}$ (or simply $\dot{e}$ if $\mathbf{r}$ is known) denote the directional derivative of the length of e.*

- *If e is an f-edge, then $\dot{e}_{\mathbf{r}} = -w\cos(\angle pss')$.*

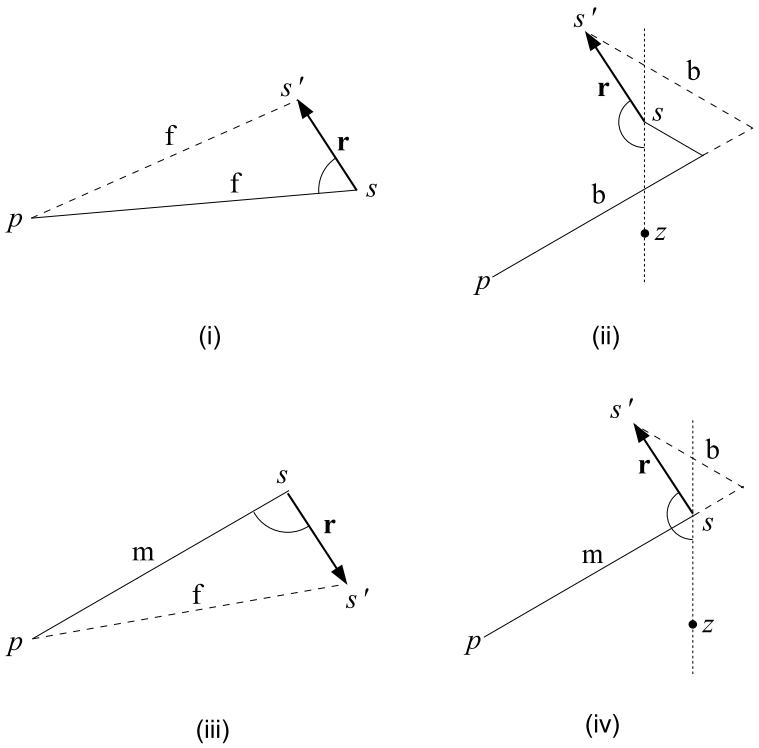

Figure 7.3: Variational argument applied to (i) an f-edge, (ii) a b-edge, (iii) an m-edge which becomes an f-edge and (iv) an m-edge which becomes a b-edge.

- *If e is a b-edge, then $\dot{e}_{\mathbf{r}} = -w\sqrt{1+m^{-2}}\cos(\angle zss')$, where z is a point on the vertical line through s such that $\angle psz \leq \frac{\pi}{2}$.*
- *If e is an m-edge, then $\dot{e}_{\mathbf{r}}$ is equal to either $-w\cos(\angle ass')$ or $-w\sqrt{1+m^{-2}}\cos(\angle zss')$, depending on whether $g(ps') \leq m$ or $g(ps') > m$.*

7.3 Fundamental properties of gradient-constrained MGAs in a vertical plane

In this section, we conduct a rigorous study of the fundamental properties of gradient-constrained MGAs in a vertical plane, with emphasis on the local structure at Steiner points. The main tools used are the variational argument (Lemma 7.2), and the properties of edge vectors (Lemma 7.1). We begin with a known [13] basic property of optimal

Steiner points, which follows from the equilibrium of edge vectors.

Lemma 7.4. *If a Steiner point s is optimal with respect to its adjacent points $p_1, \ldots, p_k$, then s is also optimal with respect to any points $p'_1, \ldots, p'_k$ lying on the rays from s through $p_1, \ldots, p_k$ respectively.*

Since an optimal Steiner point s in a gradient-constrained MGA is necessarily a Fermat-Weber point with respect to its adjacent points $p_1, \ldots, p_k$, we have the following result, which follows from Theorem 3.1 in Chapter 3.

Lemma 7.5. *Let T be a gradient-constrained MGA and let s be a Steiner point in T with incident edges $p_1s, \ldots, p_{k-1}s, sp_k$ having respective weights $w_1, \ldots, w_k$. If s is locally minimal with respect to its adjacent vertices, then there exist edge vectors $\mathbf{v}_1, \ldots, \mathbf{v}_k$, computed by Lemma 7.1, for which*

$$\sum_{i=1}^{k} \mathbf{v}_i = \mathbf{0} \tag{7.2}$$

which we again refer to as the *equilibrium condition*. Note that the equilibrium condition is necessary but not sufficient for s to be locally minimal with respect to its adjacent vertices. This is in contrast to Fermat-Weber points in the gradient-constrained problem, for which the equilibrium condition is both necessary and sufficient.

We now show that, for terminals lying in a vertical plane $\mathcal{P}$, there must be a gradient-constrained MGA spanning N on $\mathcal{P}$. It has been shown in [17] that, for the gradient-constrained Steiner tree problem, if all the terminals lie in a vertical plane $\mathcal{P}$, then there exists a gradient-constrained SMT in $\mathcal{P}$. We now show that this result also applies to gradient-constrained MGAs in a vertical plane.

Lemma 7.6. *If N is a set of points lying in a vertical plane $\mathcal{P}$, then there exists a gradient-constrained MGA for N lying in $\mathcal{P}$.*

Proof. (Adapted from [17].) Refer to Figure 7.4. Suppose T is a gradient-constrained MGA for N, with T not lying in $\mathcal{P}$. Let $p_1 = (x_1, y_1, z_1)$ and $p_2 = (x_2, y_2, z_2)$ be the endpoints of an edge of T. Let T' be the (orthogonal) projection of T on $\mathcal{P}$, and let $p'_1 = (x'_1, y'_1, z'_1)$ and $p'_2 = (x'_2, y'_2, z'_2)$ be the images of p_1 and p_2 under this projection. Note

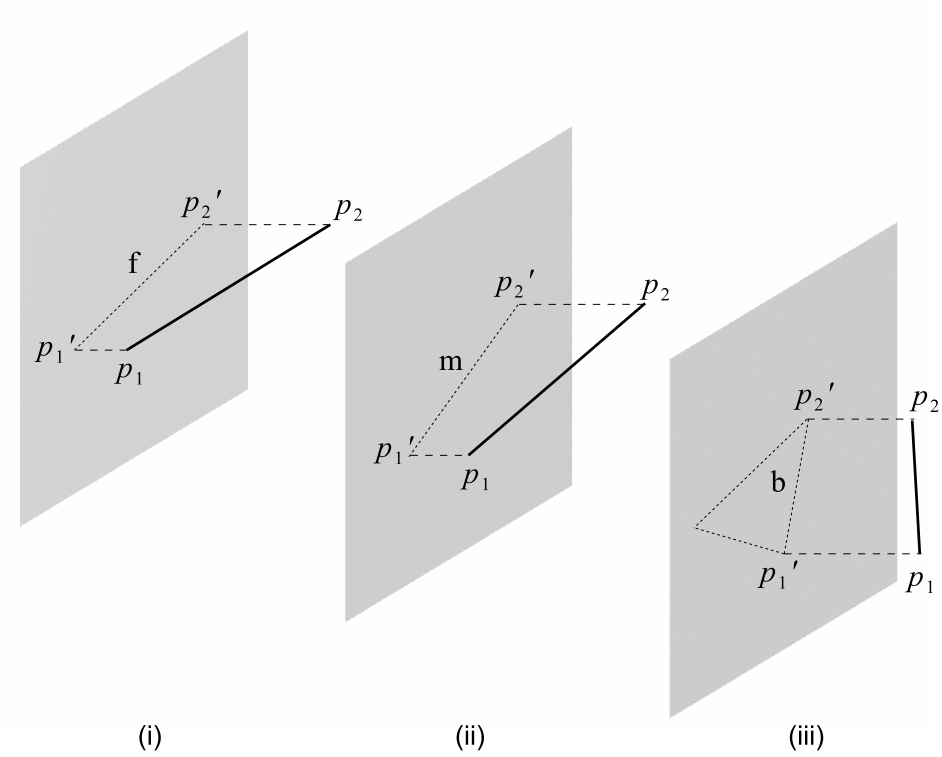

Figure 7.4: Projections of edges onto a vertical plane, where the projected edge is (i) an f-edge, (ii) an m-edge and (iii) a b-edge.

that $z_1' = z_1$ and $z_2' = z_2$, since $\mathcal{P}$ is a vertical plane. We now transform T' into a gradient-constrained tree as follows. For each edge $p_1'p_2'$ leave it unchanged if $g(p_1'p_2') \leq m$ or replace it by a bent edge on $\mathcal{P}$ with the same endpoints if $g(p_1'p_2') > m$. In the former case $w|p_1'p_2'| \leq w|p_1p_2|$ since the component of $p_1'p_2'$ orthogonal to $\mathcal{P}$ is zero and the other two components are unchanged. In the latter case $w|p_1'p_2'| = w|p_1p_2|$ because $z_1' = z_1$ and $z_2' = z_2$. Hence the cost of T' is not greater than the cost of T, and T' is also a weighted gradient-constrained MGA for N. ∎

Hence, for the remainder of this section, we will assume that T lies on $\mathcal{P}$.

For the next result, we require the following definition.

Definition 7.1. *Let T be a gradient-constrained MGA in a vertical plane and let s be a Steiner point in T. Then the horizontal and vertical lines passing through s are denoted by $\mathcal{H}_s$ and $\mathcal{V}_s$*

respectively.

Two edges incident with s are said to lie on the same side of $\mathcal{H}_s$ if they lie in the same closed half-plane determined by $\mathcal{H}_s$; i.e. this includes the possibility that one or both edges lie on $\mathcal{H}_s$. Two edges are said to be on different sides of $\mathcal{H}_s$ only if their interiors lie in different open half-spaces (determined by $\mathcal{H}_s$). Clearly, if T is an MGA in a vertical plane, a Steiner point s in T can have at most two incident m-edges on the same side of $\mathcal{H}_s$. The following lemma provides a result for m- and b-edges on the same side of $\mathcal{H}_s$.

Lemma 7.7. *Let T be a gradient-constrained MGA in a vertical plane and let s be a Steiner point in T. If s has an incident b-edge, then there are no other m- or b-edges on the side of $\mathcal{H}_s$ containing the b-edge.*

Proof. Let p_1s be a b-edge and let p_2s be an m- or b-edge such that the two edges lie on the same side of $\mathcal{H}_s$. Let $\mathcal{G}_i$, $i = 1, 2$ denote the union of geodesics between p_i and s under the gradient metric. Then $\mathcal{G}_1$ is a parallelogram in $\mathcal{P}$ whose edges have gradient m. If s has two incident b-edges or an incident m-edge and an incident b-edge (Figure 7.5 (i)–(ii)), then the cost of T can be reduced by creating a new Steiner point s' at the point in $\mathcal{G}_1 \cap \mathcal{G}_s$ with the lowest z-coordinate. In both cases the total length of the network is decreased, while the total flow component remains fixed, since the paths from sources to the sink are geodesics under the gradient metric. ∎

In the following lemma, we examine feasible orientations for f-edges relative to the sink edge.

Lemma 7.8. *Let T be a gradient-constrained MGA in a vertical plane and let s be a Steiner point in T with incident sink edge sp_k. If sp_k is labelled 'f' or 'm', then s has no incident f-edges on the side of $\mathcal{V}_s$ containing sp_k except, possibly, for sp_k itself. If sp_k is a b-edge, then s has no incident f-edges.*

Proof. Refer to Figure 7.6, in which s has an incident f-edge sp_1 on the same side of $\mathcal{V}_s$ as sp_k, where sp_k is an f-, m- and b-edge in (i), (iii) and (v) respectively. Suppose we create a new Steiner point s_1 at the same position as s such that s_1 is connected to p_1, s, p_k while s is connected to s_1 (initially, ss_1 has zero length).

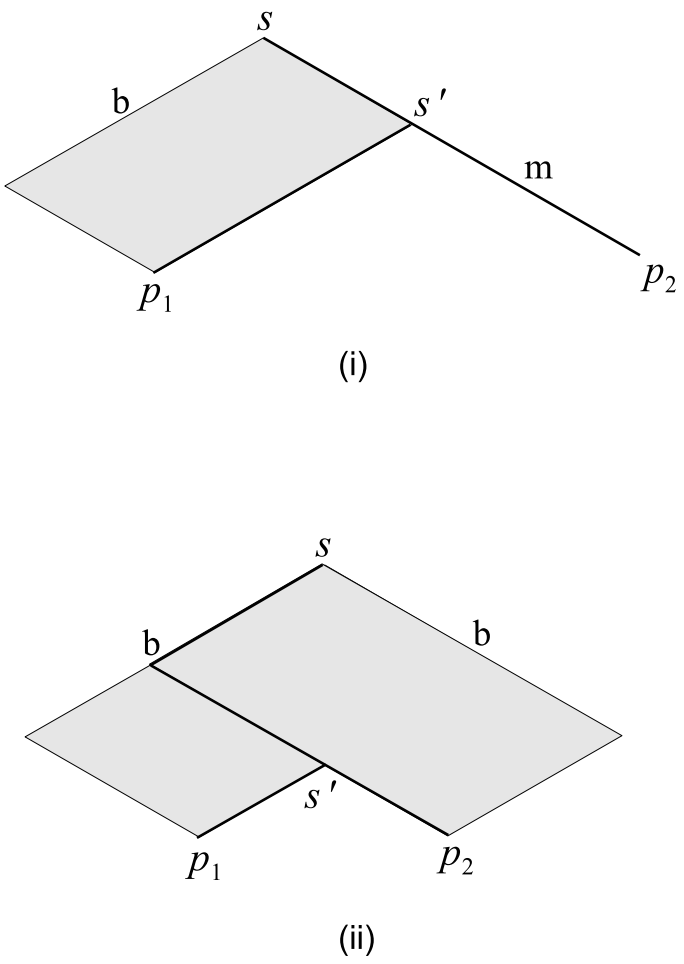

Figure 7.5: Steiner point with incident m- and b-edges. (i) m- and b-edges on the same side of the horizontal plane through the Steiner point (ii) Two b-edges on the same side of the horizontal plane through the Steiner point.

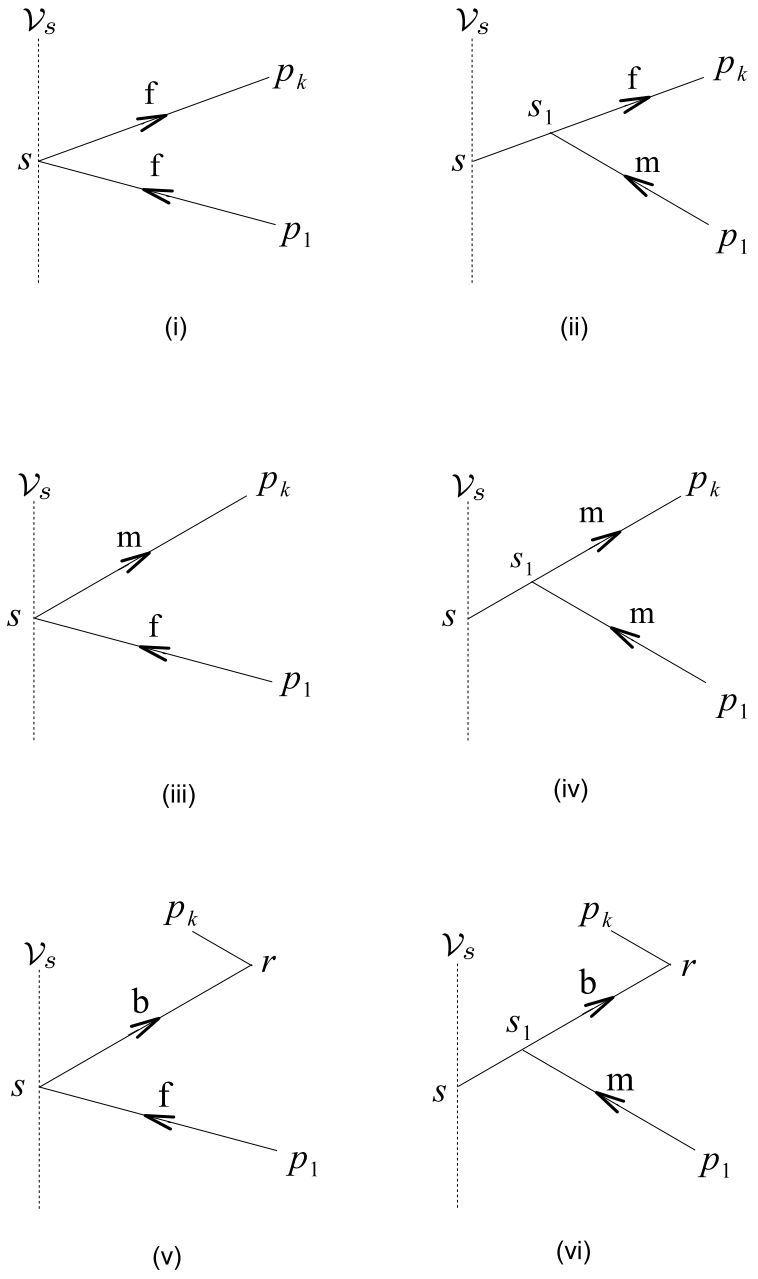

Figure 7.6: Steiner point with an incident f-edge on the same side of the vertical line through the Steiner point as the sink edge, where the sink edge is (i)–(ii) an f-edge, (iii)–(iv) an m-edge and (v)–(vi) a b-edge.

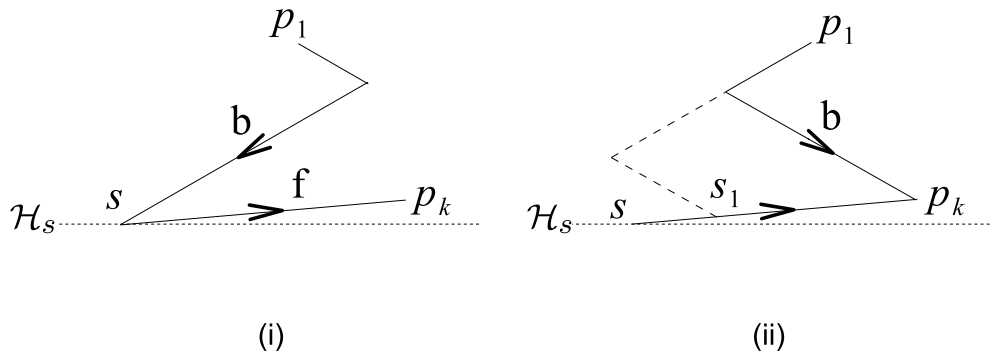

Figure 7.7: Steiner point with an incident b-edge on the same side of the horizontal line through the Steiner point as the sink edge, which is an f-edge.

Suppose sp_k is labelled 'f' or 'm'. If we perturb s_1 from s toward p_k (Figure 7.6 (ii), (iv)) then, under the assumption that $m \leq 1$, the cost of p_1s_1 decreases, and the total cost of the other edges remains fixed. This perturbation can continue until either sp_1 has label 'm' or s_1 collapses onto p_k (whichever occurs first).

Now suppose sp_k is a b-edge. If we perturb s_1 from s toward the corner point r (Figure 7.6 (vi)), then the cost of p_1s_1 decreases, and the total cost of the other edges remains fixed. This perturbation can continue until either sp_1 has label 'm' or s_1 collapses onto r (which ever occurs first). If s has an incident f-edge on the other side of $\mathcal{V}_s$, then the above argument can be applied by flipping the b-edge so that its corner point is on the opposite side of the line connecting s and p_k. Therefore if sp_k is a b-edge, then s has no incident f-edges. ∎

In the following lemma we examine feasible orientations for b-edges relative to the sink edge.

Lemma 7.9. *Let T be a gradient-constrained MGA and let s be a Steiner point in T with sink edge sp_k. Then there are no b-edges on the side of $\mathcal{H}_s$ containing sp_k except, possibly, for sp_k itself.*

Proof. Let sp_1 be a b-edge. If sp_k is an m-edge or a b-edge, then sp_1 cannot lie on the same side of $\mathcal{H}_s$ as sp_k by Lemma 7.7. Now suppose sp_k is an f-edge (Figure 7.7 (i)). Then the argument is similar to the argument posed in Lemma 7.8. Suppose we create a new

Steiner point s_1 at the same position as s such that s_1 is connected to p_1, s, p_k while s is connected to s_1 (initially, ss_1 has zero length). If we perturb s_1 from s toward p_k (Figure 7.7 (ii)), then under the assumption that $m \leq 1$, the cost of $p_1 s_1$ decreases while the total cost of the other edges remains fixed. This perturbation can continue until either sp_1 has label 'm' or s_1 collapses onto p_k (which ever occurs first). This argument is still valid if sp_k is perfectly flat (in this case only the flow component of $p_1 s_1$ decreases under the move. ∎

Suppose $\mathcal{P}$ is partitioned into quadrants by $\mathcal{H}_s$ and $\mathcal{V}_s$. Then we have the following result.

Lemma 7.10. *Let T be a gradient-constrained MGA in a vertical plane and let s be a Steiner point in T with incident sink edge sp_k. If $\mathcal{P}$ is partitioned into quadrants by $\mathcal{H}_s$ and $\mathcal{V}_s$, then sp_k is the sole edge incident to s in the quadrant containing sp_k. Moreover, if sp_k is an f-edge that is horizontal, then it is the sole edge on its side of $\mathcal{V}_s$.*

Proof. Let $\mathcal{Q}_k$ denote the quadrant containing sp_k. Suppose sp_k is labelled 'm' or 'b'. It is obvious that there can be no other m- or b-edges incident to s in $\mathcal{Q}_k$, and by Lemma 7.8, $\mathcal{Q}_k$ contains no f-edges incident to s. Now suppose that sp_k is an f-edge. Again by Lemma 7.8, there are no other f-edges incident to s in $\mathcal{Q}_k$. Let sp_k be an m- or b-edge in $\mathcal{Q}_k$. By a similar variational argument to that in the proof of Lemma 7.8, it can be shown that the cost of T can be reduced by connecting p_j, p_k and s to a new Steiner point, s', and perturbing s' from s toward p_k until $s'p_j$ has gradient m or $s' = p_k$ (whichever occurs first). If sp_k is horizontal, then the variation described above applies to edges above and below sp_k, and therefore sp_k must be the only edge on its side of $\mathcal{V}_s$. ∎

The following theorem, which establishes the unique local structure at a Steiner point whose incident sink edge is a b-edge, follows directly from Lemma 7.8.

Theorem 7.1. *Let T be a gradient-constrained MGA in a vertical plane and let s be a Steiner point in T with incident sink edge sp_k. If sp_k is a b-edge, then the degree of s is three, and the two source edges are m-edges on the opposite side of $\mathcal{H}_s$ to sp_k.*

Proof. By Lemma 7.8, s has no incident f-edges. By Lemma 7.7, there cannot be any other m- or b-edges on the same side of $\mathcal{H}_s$ as the sink; hence sp_k is the sole edge on its side of $\mathcal{H}_s$. Suppose s has an incident source b-edge on the opposite side of $\mathcal{H}_s$ to sp_k. Since there

cannot be any other m- or b-edges on the same side of $\mathcal{H}_s$ (Lemma 7.7), the degree of s must be two, contradicting Lemma 5.2 in Chapter 5 (which easily generalises to gradient-constrained networks). All that is left is to have m-edges on the opposite side of $\mathcal{H}_s$ to sp_k. Since the degree of s is at least three, s must have two incident source m-edges. ∎

The following theorem establishes fundamental properties of the local structure at Steiner points in gradient-constrained MGAs in a vertical plane when the incident sink edge is either an f-edge or an m-edge.

Theorem 7.2. *Let T be a gradient-constrained MGA in a vertical plane and let s be a Steiner point in T with incident sink edge sp_k, where sp_k is not a b-edge. Let L denote the infinite line passing through s, p_k and let H^+, H^- denote the two open half-planes into which L divides the vertical plane, such that H^+ is the upper half-plane if and only if the slope of L is positive. Then:*

1. *The Steiner point has at most one incident edge in H^+, and this edge is either an f-edge or an m-edge on the opposite side of $\mathcal{V}_s$ to sp_k.*
2. *If sp_k is an f-edge, s has no incident edges on L and either one or two incident edges in L^-. In the latter case, one of the two edges must be an m-edge on the same side of $\mathcal{V}_s$ as sp_k, and the other must be either an f-edge or an m-edge on the opposite side of $\mathcal{V}_s$.*
3. *If sp_k is an m-edge, s has at most one incident edge on L, which is necessarily an m-edge, at most one incident edge in L^-, which is necessarily an m-edge on the same side of $\mathcal{V}_s$ as sp_k, and at most one incident edge in L^+, which is either an f-edge or an m-edge.*

Proof. Consider the subtree T in Figure 7.8 (i) in which p_1, p_2 are sources with respective flows t_1, t_2 and p_k is the sink, and the points are connected to a Steiner point s such that the three edges are in H^+ (which lies above L since L is positively-sloped). Suppose the sink edge sp_k is an f-edge and p_1s, p_2s are source edges labelled 'f' and 'm' respectively. Let the angles between p_1s, p_2s and p_2s, sp_k be denoted by γ and β respectively, and observe that $\beta + \gamma < \pi$.

Suppose we create a new Steiner point s_1 at the same position as s such that s_1 is connected to p_1, s, and s is connected to s_1, p_2, p_k (initially, ss_1 has zero length). If we perturb s_1 from s toward p_2 (Figure 7.8 (ii)), the variation in the cost of T, denoted by $\dot{T}_1$, is

$$\dot{T}_1 = -(d + ht_1)\cos\gamma + ht_1.$$

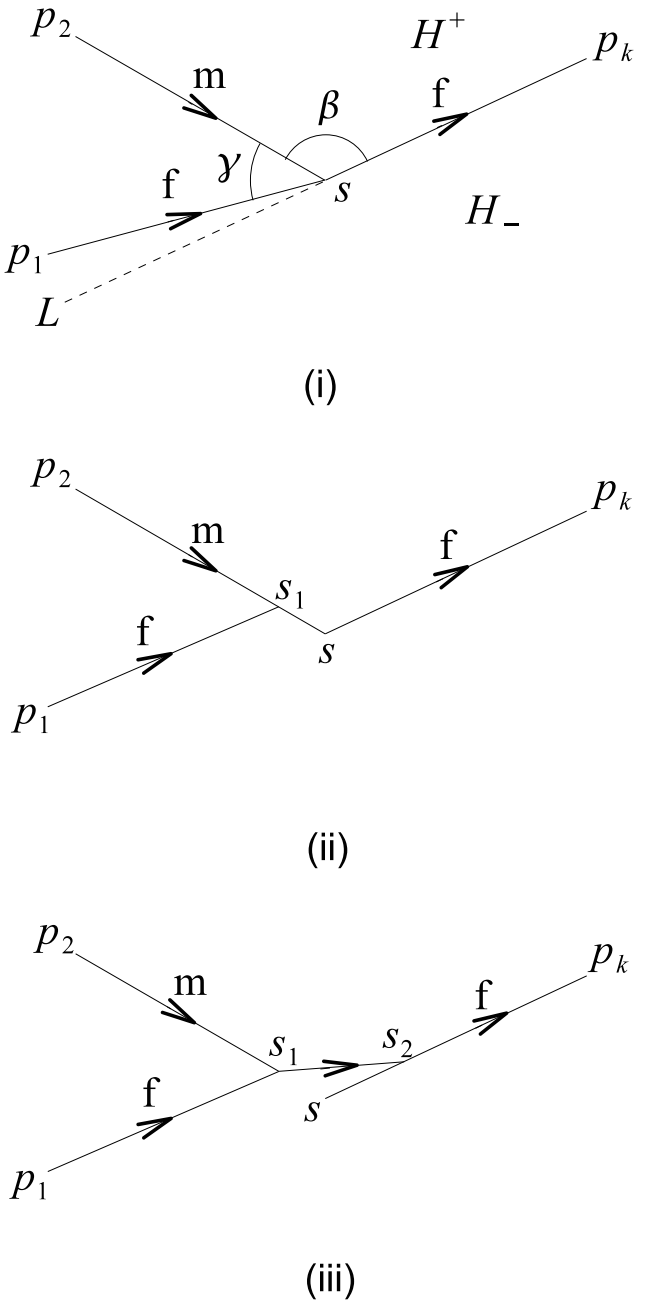

Figure 7.8: Network with f- and m-edges in an open half-plane bounded by the line through the sink edge. (i) Subtree. (ii)–(iii) Perturbations of two newly created Steiner points.

Now suppose we create a third Steiner point s_2 at the same location as s, such that s_2 is connected to s, p_k and s_1 is connected to p_1, p_2, s_2 (initially, ss_2 has zero length). If we perturb s_2 from s toward p_k (Figure 7.8 (iii)), the variation in the cost of T, denoted by $\dot{T}_2$, is

$$\dot{T}_2 = -(d + ht_1 + ht_2)\cos\beta - (ht_1 + ht_2).$$

Note that the costs of any other edges connected to s are unaffected by the above variations, since the flow path from s to p_k does not change. The total variation, denoted by T, is

$$\dot{T} \;=\; -(\cos\beta + \cos\gamma)(d + ht_1) - (1 + \cos\beta)ht_2.$$

It is easily checked that $\cos\beta + \cos\gamma \geq 0$ for all β, γ satisfying $\beta + \gamma \leq \pi$. Therefore $\dot{T} < 0$ and, by the variational argument (Lemma 7.2), T is not of minimum cost. The above argument is still valid if p_2s is an f-edge, and if sp_k is an m-edge. The argument also demonstrates when there cannot be a source f-edge on L in the case where sp_k is an f-edge. The proof of the first statement is completed by noted that there are no f-edges on the side of $\mathcal{V}_s$ containing sp_k (Lemma 7.8), and there are no b-edges on the side of $\mathcal{H}_s$ containing sp_k (Lemma 7.9).

Now consider H^-. Note that the above variation is still valid for p_1s, p_2s in H^-, if the two edges have labels (f,f), (f,b) or (f,m) provided the m-edge is on the opposite side of $\mathcal{V}_s$ to sp_k. If it is on the same side of $\mathcal{V}_s$ as sp_k, then there is no incident b-edge in H^- (Lemma 7.7), and at most one additional edge, with label 'f' or 'm' in H^-. ∎

From Theorem 7.2, we can deduce the following results.

Corollary 7.1. *Let T be a gradient-constrained MGA in a vertical plane and let s be a Steiner point in T. Then s has at most one incident b-edge.*

Proof. If the sink edge sp_k is a b-edge then s has degree three and the other two edges are m-edges (Lemma 7.1). Otherwise, there are no b-edges on the side of $\mathcal{H}_s$ containing sp_k (Lemma 7.9), and it follows from Theorem 7.2 that s has at most one incident edge on the opposite side of $\mathcal{H}_s$ to sp_k. ∎

Proof. This is easily seen from Theorem 7.2. ∎

A second corollary to Theorem 7.2 is as follows.

Corollary 7.2. *Let T be a gradient-constrained MGA in a vertical plane and let s be a Steiner point in T whose incident sink edge is an m-edge. Then s has at most one incident f-edge.*

Proof. This is easily seen from Theorem 7.2. ∎

The preceding results lead up to the following theorem.

Theorem 7.3. *Let T be a gradient-constrained MGA in a vertical plane and let s be a Steiner point in T. Then the degree of s is either three or four.*

Proof. If the sink edge sp_k is a b-edge, then the degree of s is three by Theorem 7.1. If sp_k is an f-edge, then s has at most one incident edge on L, at most one incident edge in L^+, and at most two incident edges in L^- (Theorem 7.2), totalling four edges. If sp_k is an m-edge, then s has at most one incident edge in L^-, at most one incident edge in L^+, and either one or two incident edges on L (Theorem 7.2), again totalling four edges. ∎

Having determined that the degree of a Steiner point in a gradient-constrained MGA in a vertical plane is either three or four, we now study specific properties of degree-three and four Steiner points.

7.4 A classification of degree-three Steiner points

Let T be a gradient-constrained MGA in a vertical plane, and let s be a degree-three Steiner point in T, with incident edges p_1s, p_2s, sp_3, where p_1s, p_2s are source edges with positive flows t_1, t_2, and sp_3 is the sink edge. Assuming a linear cost function, p_1s, p_2s, sp_3 have respective weights $w_1 = d + ht_1$, $w_2 = d + ht_2$ and $w_3 = d + h(t_1 + t_2)$.

Let g_1, g_2, g_3 denote the respective *labels* of p_1s, p_2s, sp_3. Then we say the *labelling* of s is $(g_ig_jg_k)$, where $i, j, k \in \{1, 2, 3\}$. In [13], a $'/'$ sign was used to distinguish between edges lying above and below the horizontal plane $\mathcal{H}_s$ through a Steiner point s in a gradient-constrained SMT. For example, if p_1s, p_2s are two incident edges lying on one side of $\mathcal{H}_s$, and the third edge p_3s lies on the other, then the labelling of s was denoted by (g_1g_2/g_3).

The situation is more complex for gradient-constrained MGAs, and distinguishing between edges above and below $\mathcal{H}_s$ becomes less useful. Hence in this work, we will drop the $'/'$ sign in the labelling. Moreover, we adopt the notation that the edge labels are stated in order of increasing gradient, i.e. 'f' followed by 'm' followed by 'b'.

Since each $g_i \in \{f, m, b\}$, there are 10 possible labellings of s to examine:

(fff)	(ffm)	(ffb)
(fmm)	(fmb)	(fbb)
(mmm)	(mmb)	(mbb)
(bbb)		

A labelling that can occur in a gradient-constrained MGA is called *feasibly optimal*. Our aim in this section is to determine which of the 10 labellings above are feasibly optimal. Note that for gradient-constrained SMTs in a vertical plane, only three of these labellings are feasibly optimal [17]. They are (fmm), (mmm) and (mmb). As we will show, additional labellings are possible for gradient-constrained MGAs. We begin by eliminating three labellings that are not feasibly optimal.

Lemma 7.11. *Let T be a gradient-constrained MGA in a vertical plane and let s be a Steiner point in T. Then the labelling of s is not (fbb), (mbb) or (bbb).*

Proof. By Corollary 7.1, s has at most one incident b-edge. ∎

Before examining the remaining labellings, we state a lemma which follows from Theorem 6.2 in Chapter 6.

Lemma 7.12. *Let T be a gradient-constrained MGA and let s be a degree-three Steiner point in T. Then s is locally minimal with respect to its adjacent vertices if and only if there exist edge vectors $\mathbf{v}_1, \mathbf{v}_2, \mathbf{v}_3$ (Lemma 7.1) associated with the three incident edges for which*

$$\mathbf{v}_1 + \mathbf{v}_2 + \mathbf{v}_3 = \mathbf{0}.$$

Hence, the equilibrium condition is necessary and sufficient for s to be locally minimal,

because splitting is not an issue for degree-three Steiner points. The following remark is also useful in this section.

Remark: For given positive weights w_1, w_2, w_3 satisfying $\max\{w_1, w_2\} < w_3 < w_1 + w_2$, there exist flows t_1, t_2 and positive constants d and h such that $w_1 = d + ht_1$, $w_2 = d + ht_2$ and $w_3 = d + h(t_1 + t_2)$.

Proof. (By construction.) Suppose we are given positive weights w_1, w_2, w_3. Let $d := w_1 + w_2 - w_3$, which is strictly positive since $w_3 < w_1 + w_2$, and let h be any positive constant. Now let

$$\begin{aligned} t_1 &:= \frac{w_1 - d}{h} = \frac{w_1 - (w_1 + w_2 - w_3)}{h} = \frac{w_3 - w_2}{h} \\ t_2 &:= \frac{w_2 - d}{h} = \frac{w_2 - (w_1 + w_2 - w_3)}{h} = \frac{w_3 - w_1}{h}. \end{aligned}$$

It follows from $w_3 > \max\{w_1, w_2\}$ that $t_1, t_2 > 0$, which completes the proof. ∎

This remark is useful in that it allows us to forget about flows and undertake analysis using only positive weights satisfying the above condition on w_3, which corresponds to the weight on the sink edge. We now examine the labelling (fff).

Lemma 7.13. *Let T be a gradient-constrained MGA in a vertical plane and let s be a Steiner point in T. Then the labelling (fff) is feasibly optimal.*

Proof. If all three edges have label 'f', then the problem reduces to the Euclidean problem studied in Chapter 5. From the analysis of the optimum angles between edges incident with a degree-three Steiner point in an MGA in the Euclidean plane (refer Section 5.7), the angle between two source edges can be arbitrarily small, while the angle between a source edge and a sink edge can become arbitrarily close to π. If, for example, the sink edge is horizontal, it is easy to see that the labelling (fff) is feasibly optimal for arbitrarily small m. ∎

It is worth noting that the sink edge must be on the opposite side of $\mathcal{V}_s$ to the two source edges by Lemma 7.8. We now examine the labellings (ffm) and (ffb).

Lemma 7.14. *Let T be a gradient-constrained MGA in a vertical plane and let s be a Steiner point in T. Then the labellings (ffm) and (ffb) are feasibly optimal provided the sink edge is an*

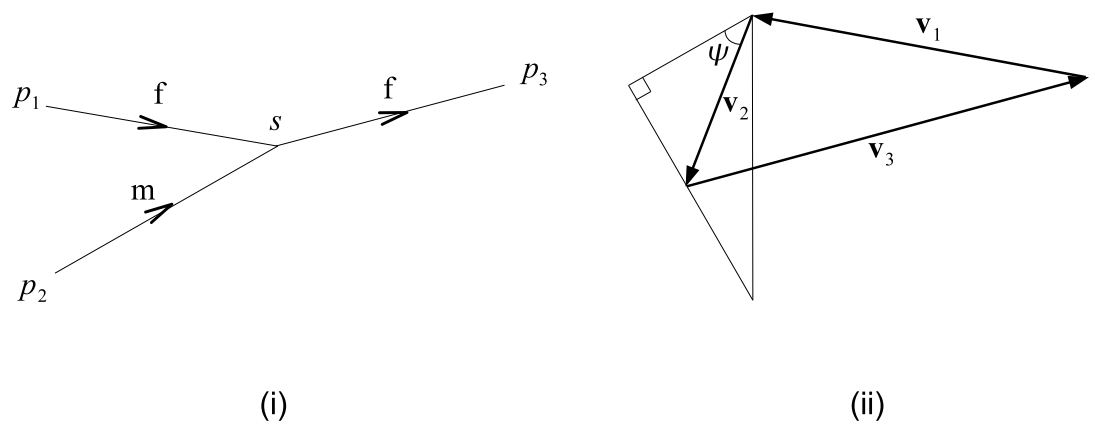

Figure 7.9: Weight triangle for a Steiner point with labelling (ffm).

f-edge.

Proof. By Corollary 7.2, the sink edge cannot have label 'm', since s has two incident f-edges, and by Theorem 7.1, the sink edge cannot have label 'b'. Hence the sink must be one of the f-edges, and by Lemma 7.8, the two f-edges must then be on opposite sides of $\mathcal{V}_s$. Consider the labelling (ffm), and assume that p_1s, p_2s, sp_3 have labels 'f', 'm' and 'f' respectively (Figure 7.9 (i)). Let $\mathbf{v}_1, \mathbf{v}_2, \mathbf{v}_3$ be corresponding edge vectors, such that $\mathbf{v}_2$ makes an angle of ψ with p_2s. If the equilibrium condition is satisfied, then $\mathbf{v}_1 + \mathbf{v}_2 + \mathbf{v}_3$ form the edges of a triangle (Figure 7.9 (ii)). Clearly there exist weights such that this triangle exists; thus (ffm) is feasibly optimal by Lemma 7.12. Since (ffb) is a special case of the above where $\psi = \frac{\pi}{2} - \alpha$ (recall that $\alpha = \tan^{-1}(m)$), the labelling (ffb) is also feasibly optimal. ∎

We now examine the labelling (fmm). For Steiner points in gradient-constrained SMTs in a vertical plane, (fmm) is feasibly optimal provided the two m-edges are on one side of $\mathcal{V}_s$, and the f-edge is on the other. For the weighted case, it is not immediately obvious whether this labelling is feasibly optimal, since the three flow-induced edge weights are never exactly equal, and it is conceivable that variations in edge weights could force the Steiner point labelling to change. In the following lemma, we show that this is not the

case.

Lemma 7.15. *Let T be a gradient-constrained MGA in a vertical plane and let s be a Steiner point in T. Then the labelling (fmm) is feasibly optimal in two cases:*

- *The two m-edges are on one side of $\mathcal{V}_s$ and the f-edge is on the other, in which case any of the edges can feasibly be the sink edge.*
- *The two m-edges are collinear, in which case one of the m-edges must be the sink edge.*

Proof. If the two m-edges lie on one side of $\mathcal{H}_s$, then it is easily observed that the equilibrium condition cannot be satisfied.

Now consider the case where the two m-edges are not collinear. Assume initially that $w_1 = w_2 = w_3$. Let the edges be arranged as per Figure 7.10 (i). Let $A_i = \partial(p_i - s),\ i = 1,2,3$. Thus A_1 corresponds to a unique vector $\mathbf{v}_1$ from s to p_1 with length one, while A_2 and A_3 correspond to sets of vectors from s to the straight segments on the boundary of B^*. It can be shown that the Minkowski sum (see Chapter 3, Section 3.2.2) $A_2 + A_3$ forms a parallelogram with sides having gradient $1/m$ (see the shaded region in Figure 7.10 (ii)). It follows from the equilibrium condition that s is locally minimal if and only if the Minkowski sum $A_1 + A_2 + A_3$ contains the origin o. This is satisfied when $\mathbf{v}_1$ is directed from a point in the parallelogram to o. It is easily seen that this is true when the weights are equal, and that small changes in the weights do not affect the equilibrium of the vectors. From this we can also see that the largest weight can be on any of the three edges. Thus (fmm) for this configuration is feasibly optimal.

Now assume that sp_2, sp_3 are collinear m-edges with p_2 located at the bottom-left of the line connecting p_2, p_3, with p_3 at the top-right (Figure 7.10 (iii)). Assume that the weights can take on any values, and let $A_i = w_i\partial(p_i - s),\ i = 1,2,3$. This time the Minkowski sum $A_2 + A_3$ results in a straight line segment with gradient $1/m$ (Figure 7.10 (iv)). To satisfy the equilibrium condition, the f-edge vector must be directed from a point on this line back to the origin. Clearly this is possible, and thus (fmm) for this configuration is feasibly optimal. ∎

We now examine the labelling (fmb).

Lemma 7.16. *Let T be a gradient-constrained MGA in a vertical plane and let s be a Steiner*

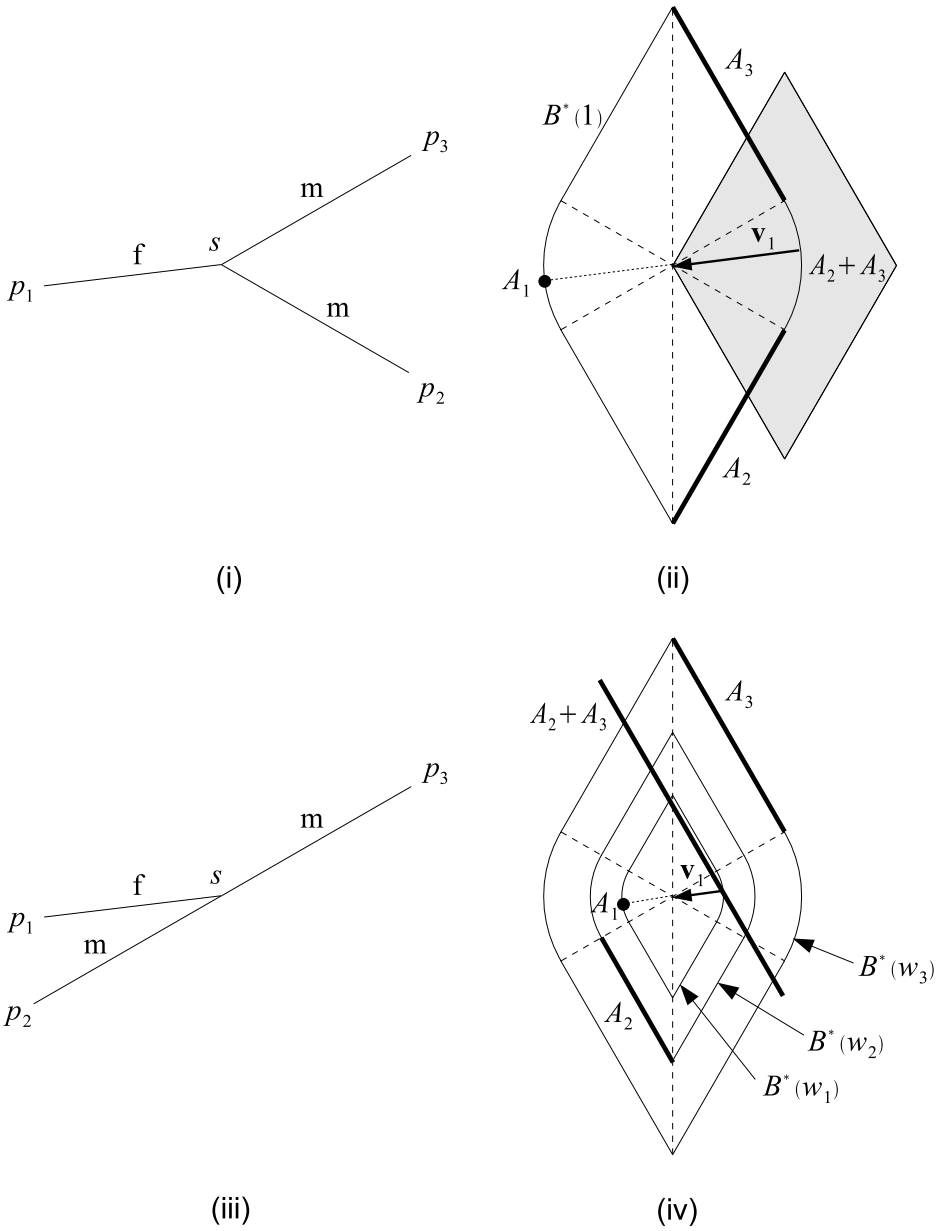

Figure 7.10: Steiner points with labelling (fmm) and corresponding Minkowski sums. (i)–(ii) Noncollinear m-edges. (iii)–(iv) Collinear m-edges.

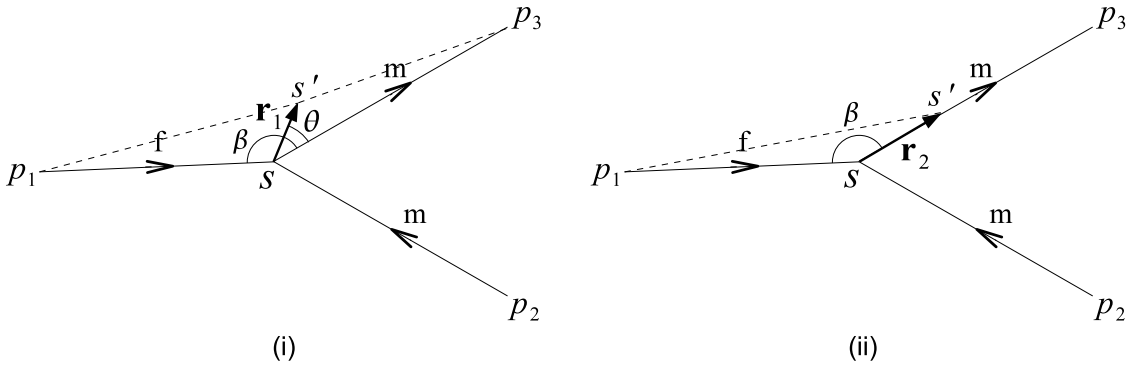

Figure 7.11: Steiner point with labelling (fmm). (i) Perturbation off an m-edge. (ii) Perturbation along an m-edge.

point in T. Then the labelling (fmb) is feasibly optimal provided the sink edge is an m-edge.

Proof. Consider the network in Figure 7.11, in which s has labelling (fmm). Suppose we perturb s in direction $\mathbf{r}_1$, as shown in Figure 7.11 (i). Using Lemma 7.2, it can be shown that the variation $\dot{T}$ is minimised for $\theta = 0$ when

$$\frac{w_1}{w_2} \leq \frac{1}{m \sin \beta}.$$

The implication is that the Steiner point will never move off the line sp_3 provided w_2 is sufficiently large. Now consider the perturbation $\mathbf{r}_2$ in Figure 7.11 (ii). It can be shown that the variation is strictly less than zero when

$$w_3 > w_2 - w_1 \cos \beta.$$

Hence, if the two conditions above are satisfied, and provided w_3 is not too large, a new Steiner point s' is optimally located on the m-edge between s and p_3, and has labelling (fmb). ∎

We now examine the labellings (mmm) and (mmb), both of which are feasibly optimal in gradient-constrained SMTs in a vertical plane.

Lemma 7.17. *Let T be a gradient-constrained MGA in a vertical plane and let s be a Steiner*

point in T. Then the labellings (mmm) and (mmb) are feasibly optimal.

Proof. Refer to Figure 7.12 (i)–(ii), in which the three edges have weights equal to one. Let $A_i = \partial(p_i - s),\ i = 1,2,3$. The Minkowski sum $A_1 + A_2 + A_3$ forms a parallelogram whose edges have gradient $1/m$. Since the origin is an element of this parallelogram, it follows that the equilibrium condition is satisfied, and s is locally minimal. It is easily seen that small changes in the weights do not affect the equilibrium of the vectors, and so the largest weight can be on any of the three edges. Moreover, it is clear that the largest weight can be on any of the m-edges. Hence (mmm) is feasibly optimal. The proof for (mmb) is similar to the proof for (mmm), except that A_3 is now a vertical vector (Figure 7.12 (iii)–(iv)). ∎

We now state the main result of this section.

Theorem 7.4. *Let T be a gradient-constrained MGA in a vertical plane and let s be a degree-three Steiner point in T. Then s has seven feasibly optimal labellings: (fff), (ffm), (ffb), (fmm), (fmb), (mmm) and (mmb).*

The labelling (ffm) has two feasibly optimal geometries and hence there are eight possible configurations for s, as shown in Figure 7.13. In the figure, edges which can feasibly be sink edges are indicated by arrows.

It is worth noting that, of the eight possible geometries for degree-three Steiner points in gradient-constrained MGAs in a vertical plane, the three configurations (iv), (vii) and (viii) are the only labellings in which any edge can feasibly be the sink edge. Also note that these are the only three feasibly optimal labellings for Steiner points in gradient-constrained SMTs in a vertical plane.

7.5 A classification of degree-four Steiner points

Suppose s is a degree-four Steiner point in a gradient-constrained MGA T in a vertical plane with four edges p_1s, p_2s, p_3s, sp_4, where p_1s, p_2s, p_3s are source edges with respective positive flows t_1, t_2, t_3 and sp_4 is the sink edge. Let g_1, g_2, g_3, g_4 be the respective labels of these edges. Then the labelling of s is denoted by $(g_1g_2g_3g_4)$. Our aim in this

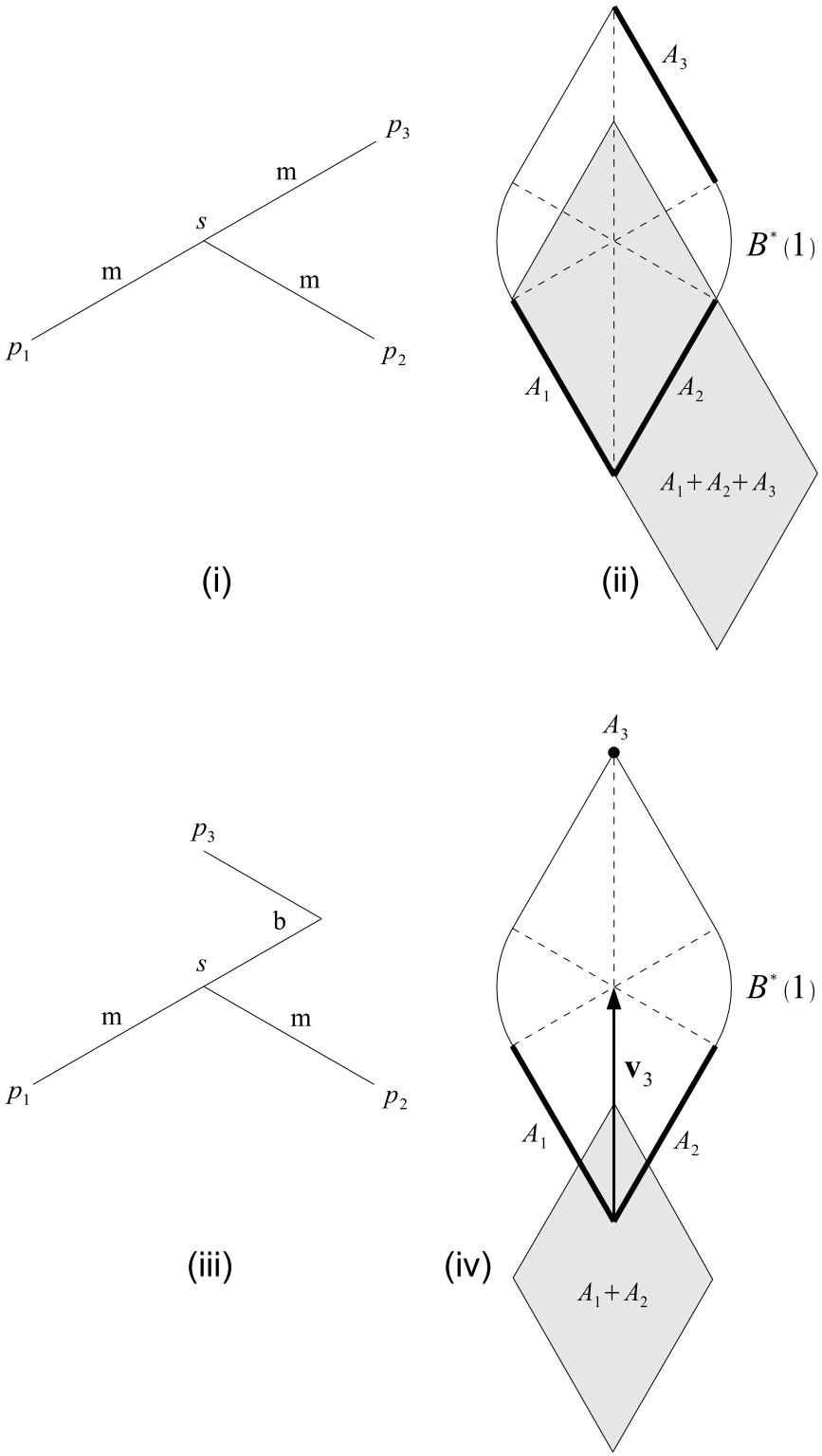

Figure 7.12: Steiner points with labellings (mmm) and (mmb) and unweighted Minkowski sums. (i)–(ii) Labelling (mmm). (iii)–(iv) Labelling (mmb).

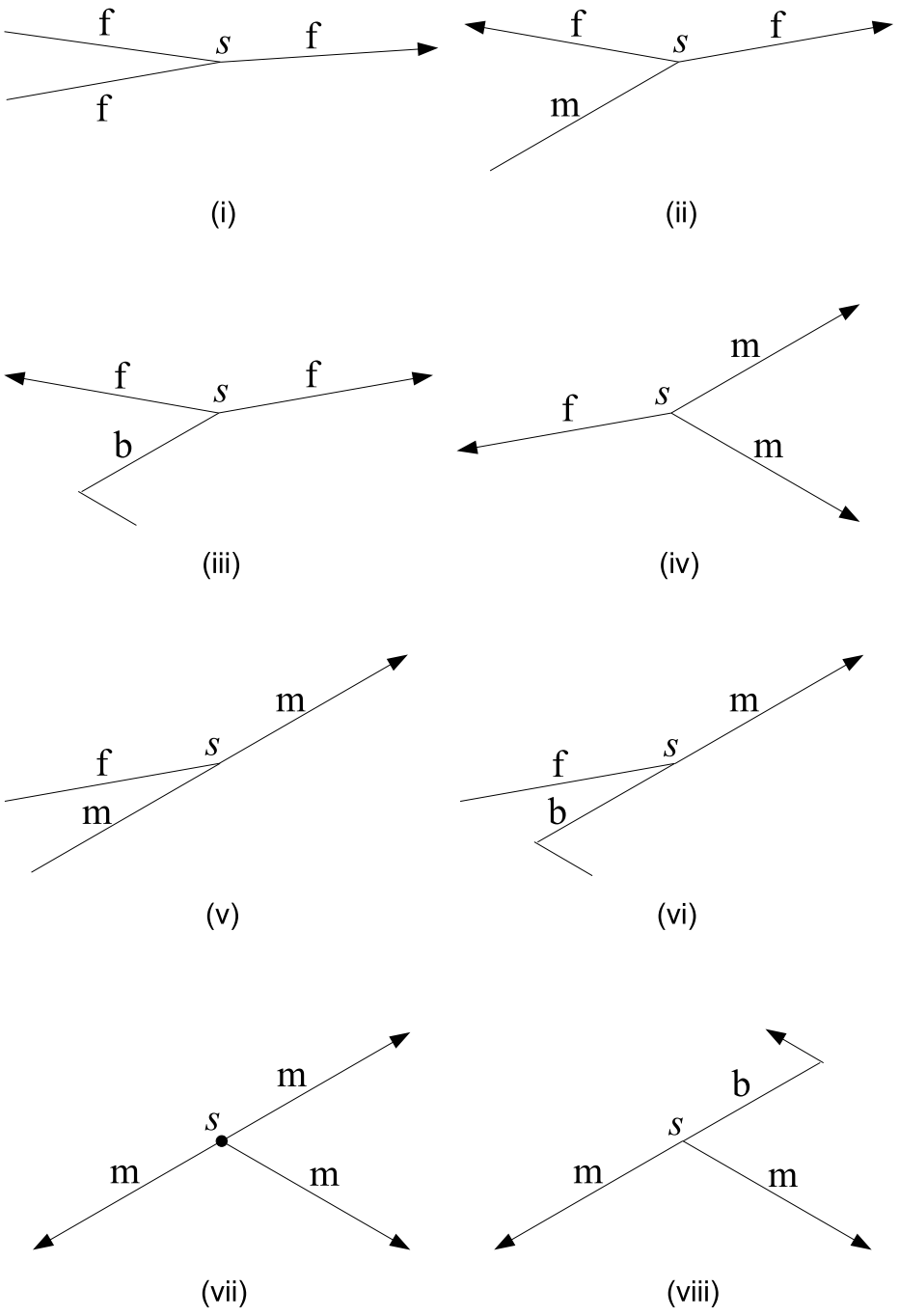

Figure 7.13: Feasibly optimal labellings for degree-three Steiner points.

section is to determine the set of feasibly optimal labellings of s. There are 15 potential labellings to examine:

(ffff)	(fffm)	(fffb)
(ffmm)	(ffmb)	(ffbb)
(fmmm)	(fmmb)	(fmbb)
(fbbb)	(mmmm)	(mmmb)
(mmbb)	(mbbb)	(bbbb)

For gradient-constrained SMTs in a vertical plane, only one of these labellings is feasibly optimal [17]; namely, (mmmm), which forms a *cross* (therefore, a gradient-constrained vertical plane is an example of an *X-plane* discussed in [72]). As we will show, additional labellings are possible for gradient-constrained MGAs in a vertical plane. We begin by eliminating six labellings that are not feasibly optimal.

Lemma 7.18. *Let T be a gradient-constrained MGA in a vertical plane and let s be a Steiner point in T. Then the labelling of s is not (ffbb), (fmbb), (fbbb), (mmbb), (mbbb) or (bbbb).*

Proof. By Corollary 7.1, s has at most one incident b-edge. ∎

We now eliminate the labelling (mmmb).

Lemma 7.19. *Let T be a gradient-constrained MGA in a vertical plane and let s be a Steiner point in T. Then the labelling of s is not (mmmb).*

Proof. By Lemma 7.7, s cannot have two incident edges with labels 'm' and 'b' on the same side of $\mathcal{H}_s$. ∎

We now eliminate the labelling (ffff).

Lemma 7.20. *Let T be a gradient-constrained MGA in a vertical plane and let s be a Steiner point in T. Then the labelling of s is not (ffff).*

Proof. By Theorem 5.2 in Chapter 5, a Steiner point whose incident edges all have label 'f' has degree at most three. ∎

We now show that the labellings (fffb), (ffmb) and (fmmb) are not possible in gradient-constrained MGAs in a vertical plane.

Lemma 7.21. *Let T be a gradient-constrained MGA in a vertical plane and let s be a Steiner point in T. Then the labelling of s is not (fffb), (ffmb) or (fmmb).*

Proof. Consider the labellings (fffb) and (ffmb). By Corollary 7.2 and Theorem 7.1, the sink edge cannot be an m-edge or a b-edge. Remaining f-edges must be on the opposite side of $\mathcal{V}_s$ to sp_4 (Lemma 7.8) and, in the case of (fffb), the b-edge must be on the opposite side of $\mathcal{H}_s$ to the sink edge (Lemma 7.9). But now there is either an f-edge and a b-edge in H^-, or two f-edges (or an f-edge and an m-edge) in H^+, which is not possible by Theorem 7.2.

Now consider the labelling (fmmb). By Lemma 7.7, the two m-edges must be on the opposite side of $\mathcal{H}_s$ to the b-edge which, by Theorem 7.1, cannot be the sink edge. It follows that the f-edge cannot be the sink edge, since it necessarily shares a quadrant with either an m-edge or a b-edge, which is not possible by Lemma 7.10. Therefore, sp_4 must be an m-edge. But now there is either an f-edge and a b-edge in H^-, or an f-edge and an m-edge in H^+, which is not possible by Theorem 7.2. ∎

We now state the main result of this section.

Theorem 7.5. *Let T be a gradient-constrained MGA in a vertical plane and let s be a degree-four Steiner point in T. Then s has three feasibly optimal labellings: (ffmm), (fmmm) and (mmmm).*

Proof. Steiner points with these labellings were obtained by a Matlab program which generates random arborescences with degree-four Steiner points, and tests whether these are MGAs by checking whether the necessary and sufficient conditions of Theorem 6.2 in Chapter 6 are satisfied. The optimal networks generated by this program were double-checked using the UNO software product. ∎

Feasible configurations for degree-four Steiner points are shown in Figure 7.14. In the figure, edges which can feasibly be sink edges are indicated by arrows. Whether or not the labelling (fffm) is feasibly optimal remains open to question, although we can say that if the labelling is feasible, then one of the f-edges is the sink edge sp_4, the m-edge is on the same side of $\mathcal{V}_s$ as sp_4 (and on the opposite side of $\mathcal{H}_s$ to sp_4) and the two remaining f-edges are on the opposite side of $\mathcal{V}_s$ to sp_4.

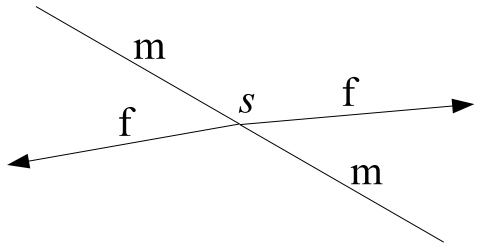

(i)

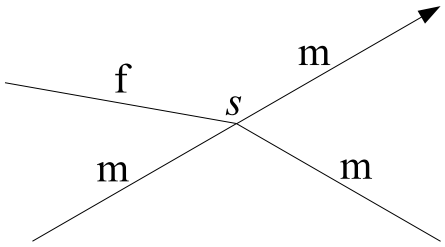

(ii)

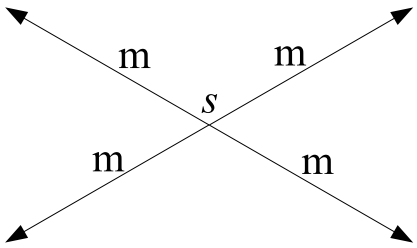

(ii)

Figure 7.14: Feasibly optimal labellings for degree-four Steiner points. Edges which can feasibly be sink edges are indicated by arrows.

We now provide a brief discussion of the labelling (ffmm). Ignoring trivial cases, there are five ways in which the four edges can be arranged around s (Figure 7.15). The arrangement in (i) is feasibly optimal by Theorem 7.5, provided one of the f-edges is the sink edge. All four edges must be in their own quadrants, and the edges must be arranged so as to avoid an f-edge and an m-edge lying in H^+.

Now consider cases (ii)–(iii). By Lemma 7.8, one of the m-edges must be the sink in both cases. But now there are two edges in H^+, which is not possible by Theorem 7.2. In case (iv), the sole f-edge on its side of $\mathcal{H}_s$ must be the sink edge by Lemma 7.8, but now there is an f-edge and an m-edge in H^- or H^+, which is not possible by Theorem 7.2. Whether the structure shown in (v) is feasibly optimal remains open to question.

We conclude this section with a brief discussion of the labelling (fmmm), beginning with the following definition.

Definition 7.2. *Let T be a gradient-constrained MGA and let s be a Steiner point in T. Then the labelling of s is said to be* unstable *if an arbitrarily small change in one of the edge weights causes the labelling to change.*

We can now state the following result about the labelling (fmmm).

Lemma 7.22. *Let T be a gradient-constrained MGA in a vertical plane and let s be a Steiner point in T. Then the labelling (fmmm) is unstable.*

Proof. Refer to Figure 7.16. Perturbing s in direction $\mathbf{r}_1$, then the variation is greater than or equal to zero when

$$t_1 \leq \frac{d}{h}\frac{\cos\gamma}{1-\cos\gamma}.$$

Perturbing s in direction $\mathbf{r}_2$, then the variation is greater than or equal to zero when

$$t_1 \geq \frac{d}{h}\frac{\cos\gamma}{1-\cos\gamma}.$$

Therefore, for the variation to be greater than or equal to zero, it must be exactly zero, and this can only occur when

$$t_1 = \frac{d}{h}\frac{\cos\gamma}{1-\cos\gamma}.$$

An arbitrarily small change in t_1 will cause the labelling of s to change. ∎

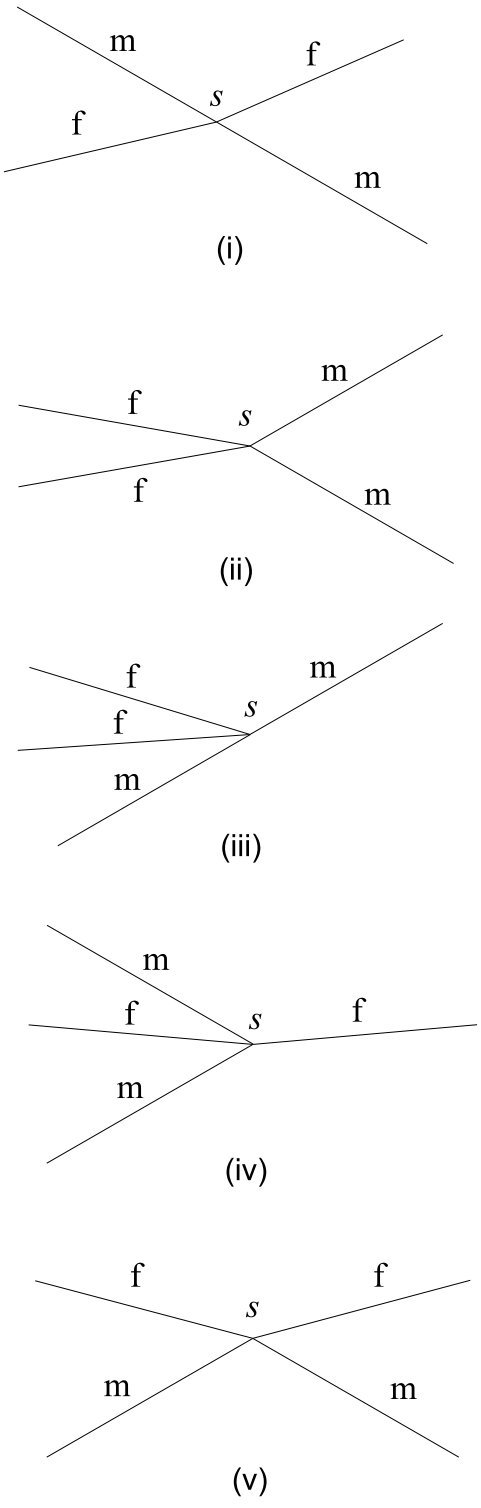

Figure 7.15: (i)–(v) Possible configurations for a Steiner point with labelling (ffmm).

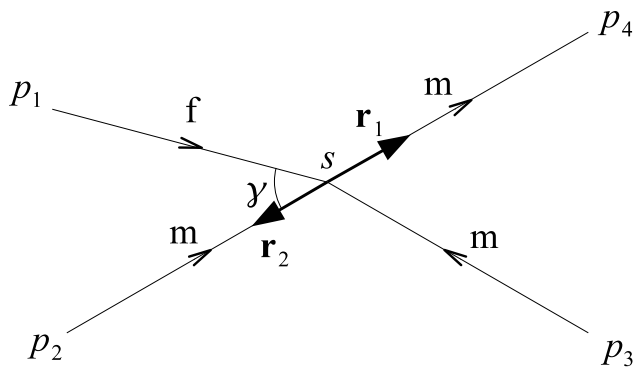

Figure 7.16: Steiner point with labelling (fmmm).

Finally, we note that the question of whether the sink edge can be the f-edge is still open. Numerical tests indicate, however, that the f-edge cannot be the sink edge for a Steiner point with the labelling (fmmm).

7.6 Hulls in a gradient-constrained plane

We conclude this chapter by investigating the regions in which Steiner points can optimally exist. We begin with some definitions of hulls. The (Euclidean) *convex hull* of a set of terminals N, denoted by $\text{conv}(N)$, is the minimal set for which N is in $\text{conv}(N)$ and, if p and q are two points in $\text{conv}(N)$, then all points on the Euclidean line segment joining p and q are in $\text{conv}(N)$. The hull of N in the gradient-constrained metric, denoted by $\text{hull}_g(N)$, was defined in [13] to be the minimal set such that N is in $\text{hull}_g(N)$ and, if p and q are two points in $\text{hull}_g(N)$, then all points on all *shortest paths* joining p and q are in $\text{hull}_g(N)$. It was shown in [13] that, if T is an SMT on N, then all Steiner points of T lie in $\text{hull}_g(N)$. In fact, this result can be strengthened in the vertical plane case. We define the *reduced hull* of N in the gradient metric as follows.

Definition 7.3. *Let $\mathcal{V}_p$ denote the vertical line through a point, p, in a vertical plane $\mathcal{P}$. Let N be a set of terminals in $\mathcal{P}$, and let* $\text{int}(\text{conv}(N))$ *denote the interior of the (Euclidean) convex hull*

of N. Then the reduced hull *of N in the gradient metric is*

$$\text{hull}'_g(N) \quad := \quad \{p \in \text{int}(\text{conv}(N)) : \exists p_i, p_j \in N \text{ such that } g(pp_i) \leq m \text{ and } g(pp_j) \leq m\},$$

where p_i and p_j are on opposite sides of $\mathcal{V}_p$.

In other words, $\text{hull}'_g(N)$ is the interior of the convex hull of N excluding points p with the property that Euclidean line segments connecting p and all terminals lying on one side (or both sides) of $\mathcal{V}_p$ have gradients strictly greater than m. For example, suppose p and q are adjacent points on the boundary of $\text{conv}(N)$, such that $g(pq) > m$ (Figure 7.17 (i)). If prq is a zigzag geodesic between p and q, such that r 'points toward' $\text{conv}(N)$, and there are no additional terminals in the interior of the triangle $\triangle prq$, then $\text{hull}'_g(N)$ does not include the interior of $\triangle prq$, but it does include segments pr and rq.

Now suppose there exist additional terminals in the interior of $\triangle prq$ (Figure 7.17 (ii)). Then $\text{hull}'_g(N)$ does not include the region to the right of the dashed line shown in the figure. In the following lemma, we show that all Steiner points in an MGA in $\mathcal{P}$ must lie in $\text{hull}'_g(N)$.

Lemma 7.23. *Let T be a gradient-constrained MGA in a vertical plane, and let s be a Steiner point in T. Then $s \in \text{hull}'_g(N)$.*

Proof. Suppose that $s \notin \text{hull}'_g(N)$. Let $N' \subseteq N$ be the subset of terminals lying on one side of $\mathcal{V}_s$, and assume that $g(sp_i) > m \ \ \forall p_i \in N'$. Then all edges incident with s on one side of $\mathcal{V}_s$ are b-edges, unless there exist other Steiner points on that side. If other Steiner points exist, there must be at least one Steiner point s' such that there are no Steiner points on one side of $\mathcal{V}_{s'}$. It is easily seen that all the vectors lie in a closed half plane on one side of $\mathcal{V}_s$, and thus the equilibrium condition cannot be satisfied. Hence s' is not a Steiner point, which completes the proof. ∎

We illustrate these ideas using two examples. In the first example, $N = \{p_1, p_2, p_3, p_4\}$ form the corners of a rectangle, as shown in Figure 7.18 (i). Then $\text{conv}(N)$ is the closed rectangle with vertices at p_1, p_2, p_3, p_4, $\text{hull}_g(N)$ is the closed convex body with vertices $p_1, r'_1, p_2, p_3, r'_2, p_4$ and $\text{hull}'_g(N)$ is the union of the interior of the non-convex body with vertices $p_1, r_1, p_2, p_3, r_2, p_4$ and the m-edge boundary segments $p_1r_1, r_1p_2, p_3r_2, r_2p_4$.

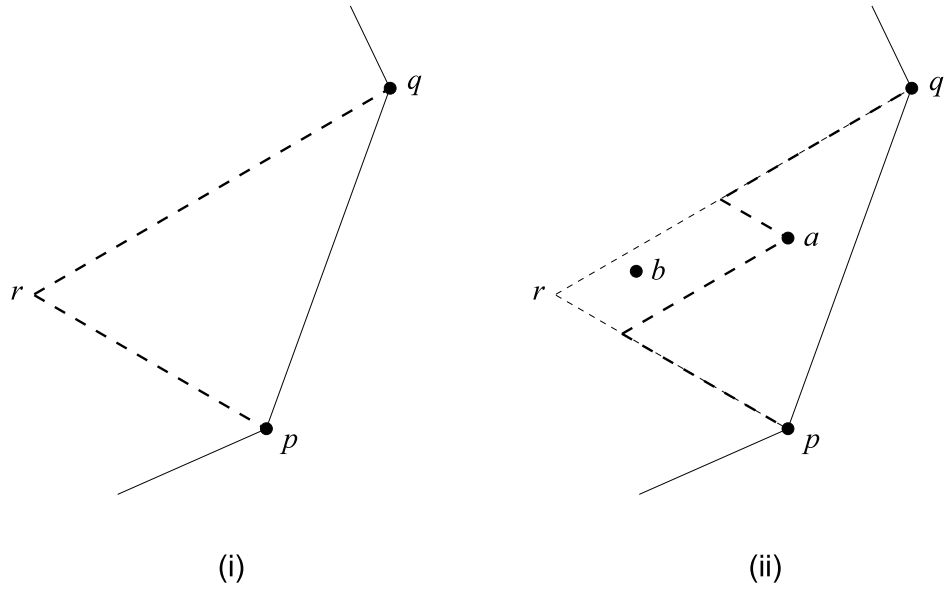

Figure 7.17: Reduced hull of terminals in a gradient-constrained vertical plane.

In the second example (Figure 7.18 (ii)), $\mathrm{conv}(N)$ is the closed rectangle with vertices p_1, p_2, p_3, p_4, $\mathrm{hull}_g(N)$ is the closed convex body with vertices $p_1, r'_1, p_2, p_3, r'_2, p_4$ and $\mathrm{hull}'_g(N)$ is the union of the interiors of the two disjoint triangles with respective vertices $p_1 s_2 p_4$ and $p_2 p_3 s_1$, and the m-edge segments $p_1 s_2, s_2 p_4, p_2 s_1, s_1 p_3$.

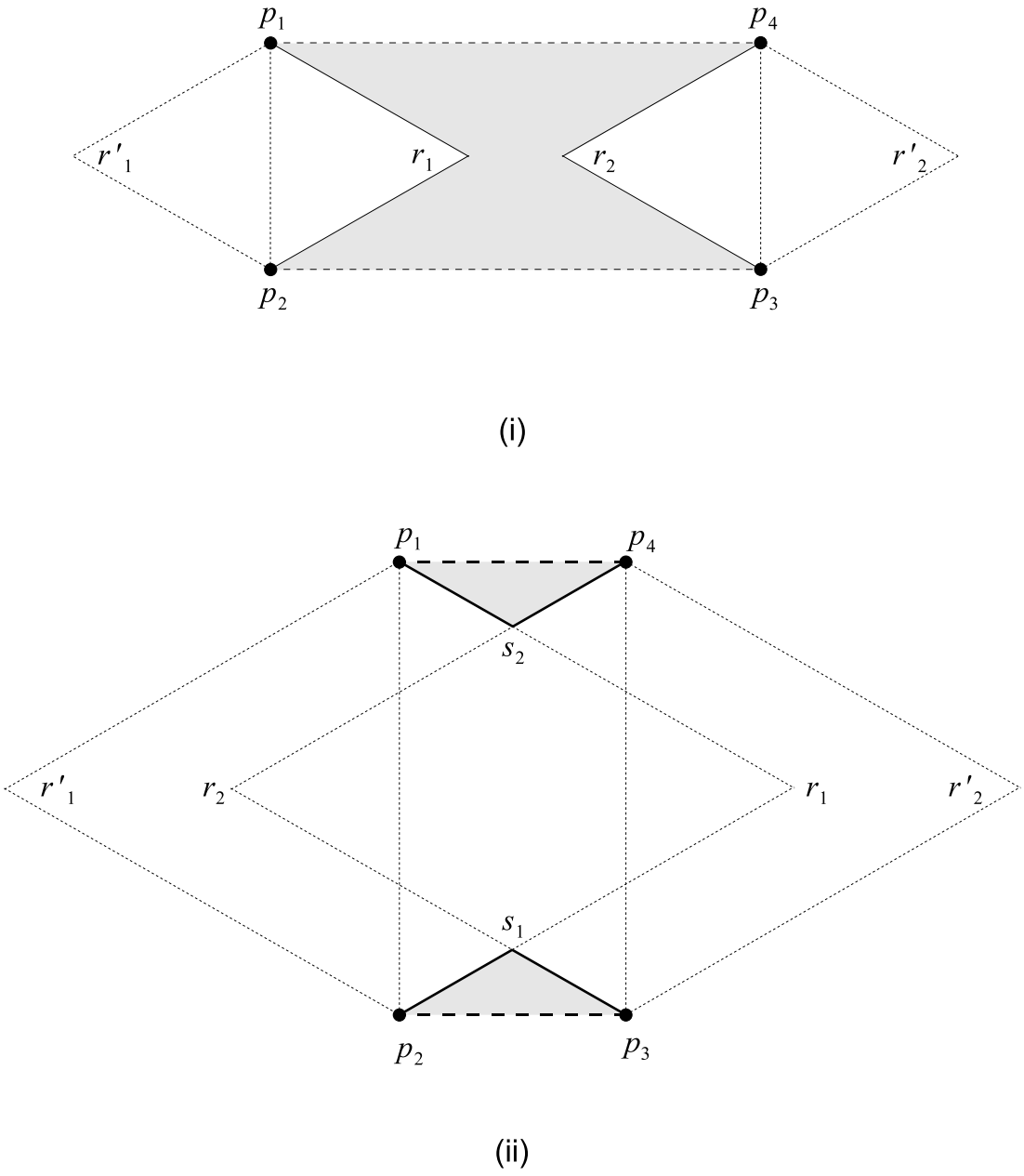

Figure 7.18: (i)–(ii) Reduced hull of terminals at the vertices of two rectangles in a vertical plane.

Chapter 8

Gradient-Constrained Gilbert Arborescences in Three Dimensions

We study gradient-constrained minimum Gilbert arborescences (MGAs) in three dimensions, assuming a linear cost function $w(t) = d + ht$, where d and h are strictly positive, and the maximum gradient satisfies $m \leq 1$. We establish a range of fundamental properties of gradient-constrained MGAs in three dimensions. We provide a classification of degree-three and four Steiner points, extending results in [13] for gradient-constrained Steiner minimum trees in three dimensions. The classification of a Steiner point is in terms of the labels *of its incident edges, where a label indicates whether the absolute value of the gradient of the Euclidean straight line connecting the endpoints of an edge is less than, equal to, or greater than m. We show that there are seven feasibly optimal labellings for degree-three Steiner points, and four feasibly optimal labellings for degree-four Steiner points. We then show that there is no upper bound on the degree of a Steiner point in a gradient-constrained MGA in three dimensions. We conclude with a discussion of hulls in gradient-constrained three-space.*

8.1 Introduction

IN the previous chapter we introduced the gradient-constrained Gilbert arborescence problem, and investigated gradient-constrained minimum Gilbert arborescences (MGAs) lying in a vertical plane. While the vertical plane problem is potentially applicable for underground mines accessing ore bodies that roughly lie in a vertical plane, most mining networks are three-dimensional. Properties of gradient-constrained Steiner minimum trees (SMTs) were studied in [13]. The goal of this chapter is to establish these fundamental properties for gradient-constrained MGAs in three dimensions.

In Section 8.2, we restate selected aspects from Chapters 4 and 7 relating to the gradient metric, in the context of the Gilbert arborescence problem in three dimensions. Then,

in Section 8.3, we establish a range of fundamental properties of gradient-constrained MGAs in three-space.

A classification of degree-three and degree-four Steiner points in gradient-constrained MGAs in three-space is presented in Sections 8.4 and 8.5 respectively. The classification of a Steiner point is in terms of the *labels* of its incident edges, where a label indicates whether the absolute value of the gradient of the Euclidean straight line connecting the endpoints of an edge is less than, equal to, or greater than m. We show that there are seven feasibly optimal labellings for degree-three Steiner points, and four feasibly optimal labellings for degree-four Steiner points. In Section 8.6, we show that there is no upper bound on the degree of a Steiner point in a gradient-constrained MGA in three dimensions. We conclude in Section 8.7 with a discussion of hulls in a gradient-constrained three-space.

8.2 Background

In this section we provide background and notation required in this chapter.

8.2.1 The gradient metric

Background relating to the gradient metric was provided in Chapters 4 and 7. Here we restate relevant material in the context of three-dimensional gradient-constrained networks. This material is primarily from [13].

Let $p = (x_p, y_p, z_p)$ and $q = (x_q, y_q, z_q)$ be two points in $\mathbb{R}^3$, and assume that the z-axis is vertical. Denote the Euclidean straight line segment between p and q by pq. We define the *gradient*, g, of pq to be the absolute value of the Euclidean straight line segment between p and q, i.e.

$$g(pq) = \frac{|z_q - z_p|}{\sqrt{(x_q - x_p)^2 + (y_q - y_p)^2}}.$$

Recall that an edge, pq, is a *bent edge* if $g(pq) > m$. In vertically-planar networks, a bent edge is represented by a zigzag line joining p and q, where each segment of the zigzag has gradient m. It is easily seen that such zigzag lines are geodesics under the gradient

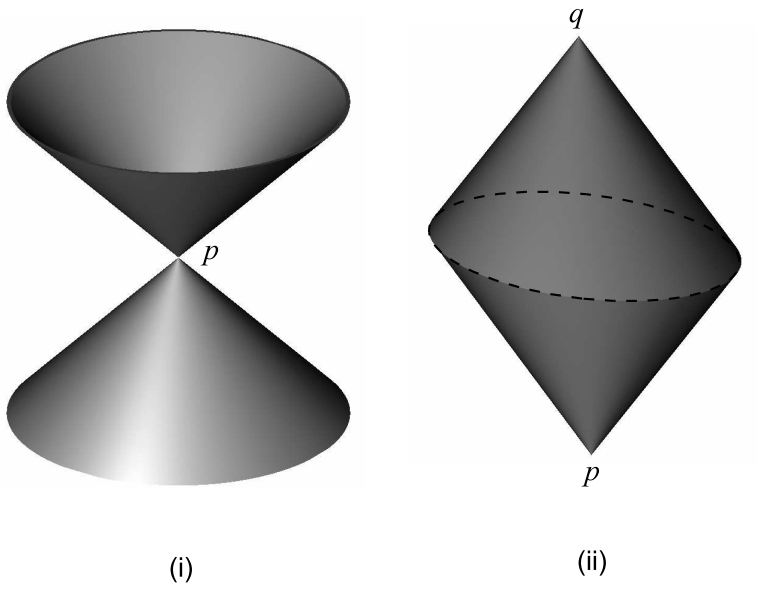

Figure 8.1: Cones generated by rotating a line with maximum gradient about a vertical line. (i) An m-cone cone. (ii) Intersection of two m-cones.

constraint. In three dimensions there are many other ways of embedding a bent edge, for example by a helical arc.

Let $\mathcal{C}_p$ denote the right circular cone generated by taking a line through p with gradient m and rotating it 360° about the vertical line through p (Figure 8.1 (i)). We will refer to these cones as *m-cones*. Assuming $g(pq) > m$ and $z_q > z_p$, the boundary of the union of all shortest paths between p and q is the intersection of $\mathcal{C}_p$ and $\mathcal{C}_q$ between horizontal planes $\mathcal{H}_p$ and $\mathcal{H}_q$ through p and q respectively (Figure 8.1 (ii)). Thus any b-edge can exist within this region, provided each differentiable point on the edge has instantaneous gradient m.

In three dimensions, the gradient metric is defined as

$$|pq|_g = \begin{cases} |pq| = \sqrt{(x_q - x_p)^2 + (y_q - y_p)^2 + (z_q - z_p)^2}, & \text{if } g(pq) \leq m; \\ |pq|_v = \sqrt{1 + m^{-2}}|z_q - z_p|, & \text{if } g(pq) \geq m. \end{cases} \tag{8.1}$$

In gradient-constrained three-space, the unit ball B_g and its dual B_g^* are as shown in Fig-

ures 8.2 and 8.3 respectively, for $m = 0.14, 0.58, 1$.

In three-space, edge vectors corresponding to norming functionals are computed in exactly the same manner as for the vertical plane problem, i.e. by Lemma 7.1. Note that in three-space, the set of m-edge vectors is still a line segment on the boundary of B^* (rather than, say, a face of B^*, as one might expect as we move from two to three dimensions), and these vectors all lie in the vertical plane containing the edge.

8.3 Fundamental properties of gradient-constrained MGAs in three-space

In this section, we conduct a rigorous study of the fundamental properties of gradient-constrained MGAs in a vertical plane, with emphasis on the local structure at Steiner points. The main tools used here, introduced in Chapter 7, are the variational argument (Lemma 7.2), and the properties of edge vectors (Lemma 7.1).

Recall from Chapter 7 that $\mathcal{H}_s$ and $\mathcal{V}_s$ denoted the horizontal and vertical lines passing through a Steiner point s. The following definition generalises these lines to planes in three-space.

Definition 8.1. *Let T be a gradient-constrained MGA in three-space and let s be a Steiner point in T with incident sink edge sp_k. Then $\mathcal{H}_s$ denotes the horizontal* plane *passing through s, while $\mathcal{V}_s$ denotes the unique vertical plane that is orthogonal to the projection of sp_k onto $\mathcal{H}_s$.*

The planes $\mathcal{H}_s$ and $\mathcal{V}_s$ are orthogonal, and partition three-space into quadrants, as shown in Figure 8.4.

We now generalise Lemma 7.7 in Chapter 7 to the three-dimensional case.

Lemma 8.1. *Let T be a gradient-constrained MGA in three-space and let s be a Steiner point in T. If s has an incident b-edge, then it has no other incident b or m-edges on the side of $\mathcal{H}_s$ containing the b-edge.*

Proof. Refer to the proof of Lemma 7.7. The main difference in three-space is that sets of geodesics are now intersections of up-cones and down-cones (Figure 8.1 (ii)) rather than a parallelogram. The proof is demonstrated in Figure 8.5. ∎

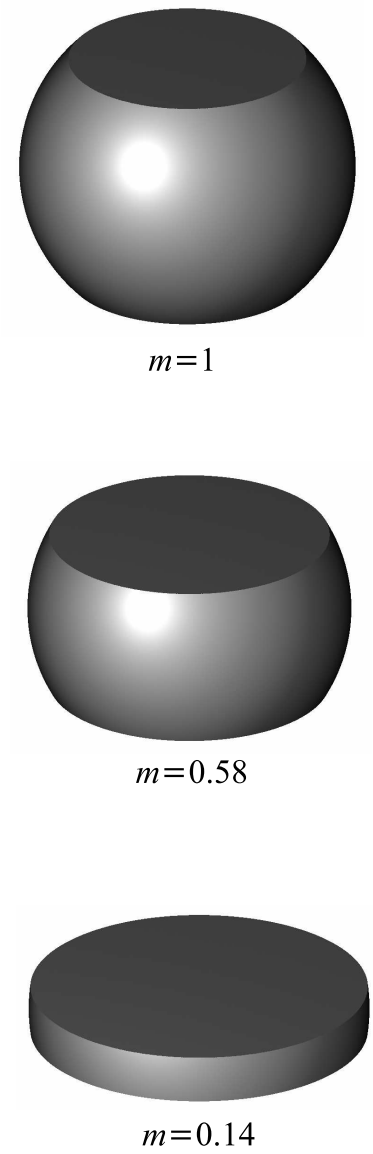

Figure 8.2: Unit ball in gradient-constrained three-space for selected maximum gradients.

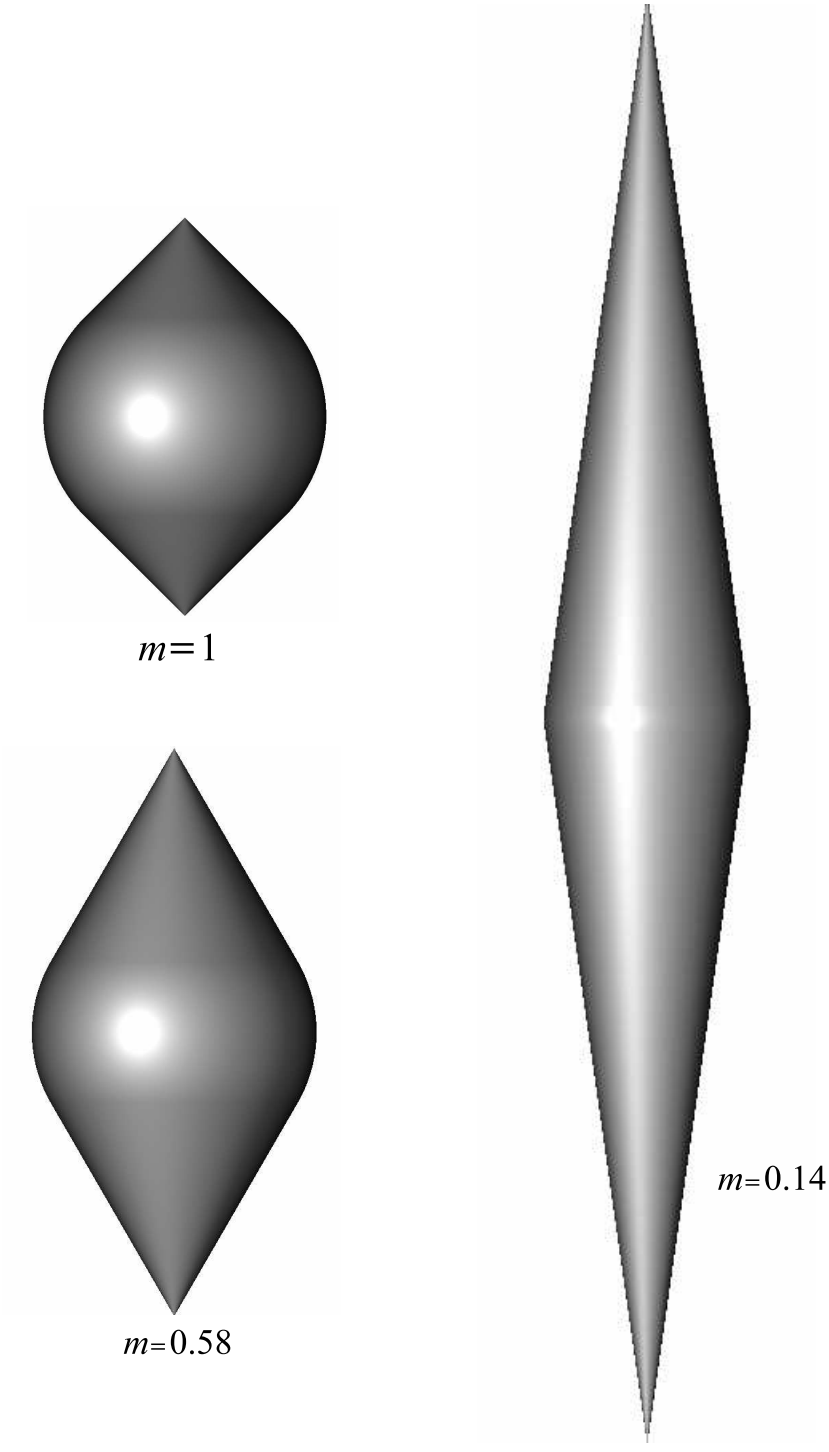

Figure 8.3: Dual ball in gradient-constrained three-space for selected maximum gradients.

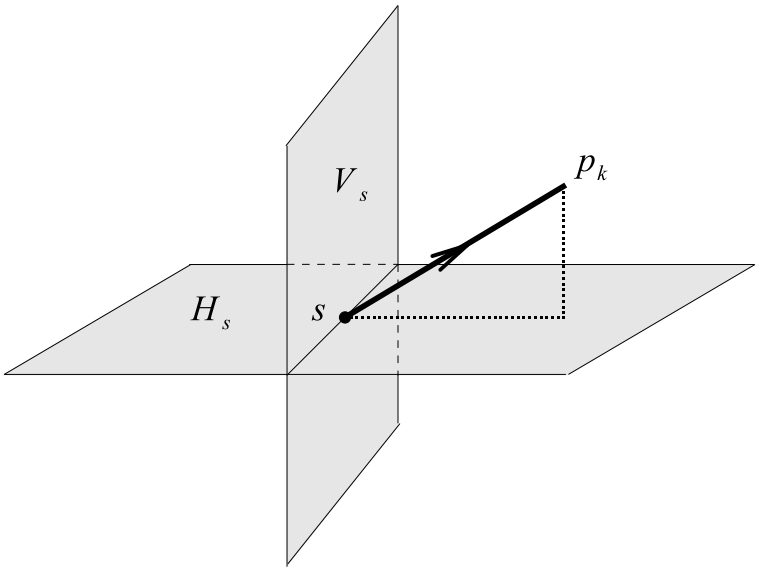

Figure 8.4: Partitioning of three-space into quadrants.

Lemma 8.2. *Let T be a gradient-constrained MGA in three-space and let s be a Steiner point in T with incident sink edge sp_k. If sp_k is labelled 'f' or 'm', then s has no incident f-edges on the side of $\mathcal{V}_s$ containing sp_k except, possibly, for sp_k itself. If sp_k is a b-edge, then s has no incident f-edges.*

Proof. Refer to the proof of Lemma 7.8. ∎

The following lemma generalises Lemma 7.9 to three-space.

Lemma 8.3. *Let T be a gradient-constrained MGA and let s be a Steiner point in T with sink edge sp_k. Then there are no b-edges on the side of $\mathcal{H}_s$ containing sp_k except, possibly, for sp_k itself.*

Proof. Refer to the proof for Lemma 7.9, and note that in three-space, a b-edge with two zigzags can be constructed in the vertical plane containing the f-edge, such that the corner point of the zigzag points towards the f-edge. ∎

The next result generalises Lemma 7.10 to three-space.

Lemma 8.4. *Let T be a gradient-constrained MGA in three-space and let s be a Steiner point in T with incident sink edge sp_k. If three-space is partitioned into quadrants by $\mathcal{H}_s$ and $\mathcal{V}_s$, then sp_k*

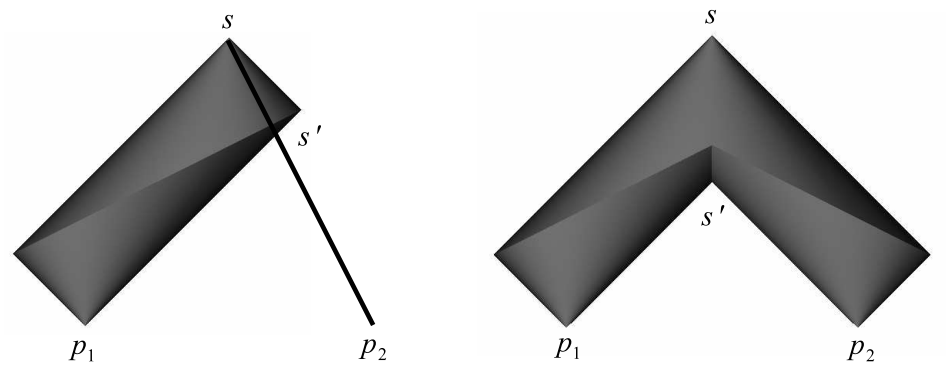

Figure 8.5: Steiner point with (i) incident m- and b-edges, and (ii) incident b-edges on the same side of the horizontal plane through the Steiner point.

is the sole edge incident to s in the quadrant containing sp_k. Moreover, if sp_k is an f-edge that is horizontal, then it is the sole edge on its side of $\mathcal{V}_s$.

Proof. Refer to the proof for Lemma 7.10. ∎

8.4 A classification of degree-three Steiner points

In [13] it was shown that there are five feasibly optimal labellings for degree-three Steiner points in gradient-constrained SMTs in $\mathbb{R}^3$. They are (fff), (ffm), (fmm), (mmm) and (mmb). Additional labellings are possible for gradient-constrained MGAs in three-space.

By Theorem 8.1, the labellings (fff), (ffm), (ffb), (fmm), (fmb), (mmm) and (mmb) are feasibly optimal for gradient-constrained MGAs in a vertical plane. Since the vertical plane case is a special case of the three-dimensional case, these seven labellings are also feasibly optimal in gradient-constrained MGAs in three-space. The remaining labellings are (fbb), (mbb) and (bbb). Labellings (mbb) and (bbb) are not feasibly optimal by Lemma 8.1, since two edges with respective labels m,b or b,b cannot co-exist on the same side of $\mathcal{H}_s$. The labelling (fbb) is not feasibly optimal by noting that there is no horizontal vector component to counterbalance that of the f-edge vector (since the two b-edge vectors are vertical). Hence the equilibrium condition cannot be satisfied. Therefore we

have the following theorem.

Theorem 8.1. *Let T be a gradient-constrained MGA in three-space and let s be a degree-three Steiner point in T. Then s has seven feasibly optimal labellings: (fff), (ffm), (ffb), (fmm), (fmb), (mmm) and (mmb).*

Steiner points with these labellings are shown in Figure 8.6, where the m-cones associated with the Steiner point are included to distinguish between f-, m- and b-edges in three-space. We note that in three-space, for the labellings (fff), (ffm), (fmm), (mmm) and (mmb), any of the three edges can potentially be the sink edge. However, for the labellings (ffb) and (fmb), the sink edge must be labelled 'f' and 'm' respectively.

8.5 A classification of degree-four Steiner points

We now discuss degree-four Steiner points in MGAs in three-space. In [13] it was shown that the labelling (mmmm) is the only feasibly optimal labelling for degree-four Steiner points in gradient-constrained SMTs in three-space. For this labelling, two of the m-edges must lie above $\mathcal{H}_s$, and the other two below. Moreover, the four edges incident to s are *bi-vertically coplanar*, meaning the two m-edges above $\mathcal{H}_s$ lie in the same vertical plane, and the two m-edges below $\mathcal{H}_s$ lie in the same vertical plane (Figure 8.7). When the two planes align to form a single vertical plane, then the four m-edges form a *cross*, a structure that is feasibly optimal for gradient-constrained MGAs in a vertical plane (refer to Chapter 7 for details).

As we will demonstrate, additional labellings are possible for degree-four Steiner points in gradient-constrained MGAs in three-space. In Chapter 5 we conjectured that all Steiner points in Euclidean MGAs in three-space have degree three. If this is true, the labelling (ffff) is not feasibly optimal. We now examine the remaining labellings, starting with (ffbb).

Lemma 8.5. *Let T be a gradient-constrained MGA in three-space and let s be a Steiner point in T. Then the labelling of s is not (ffbb).*

Proof. By Lemma 8.2, the sink edge cannot be a b-edge, since s has incident f-edges.

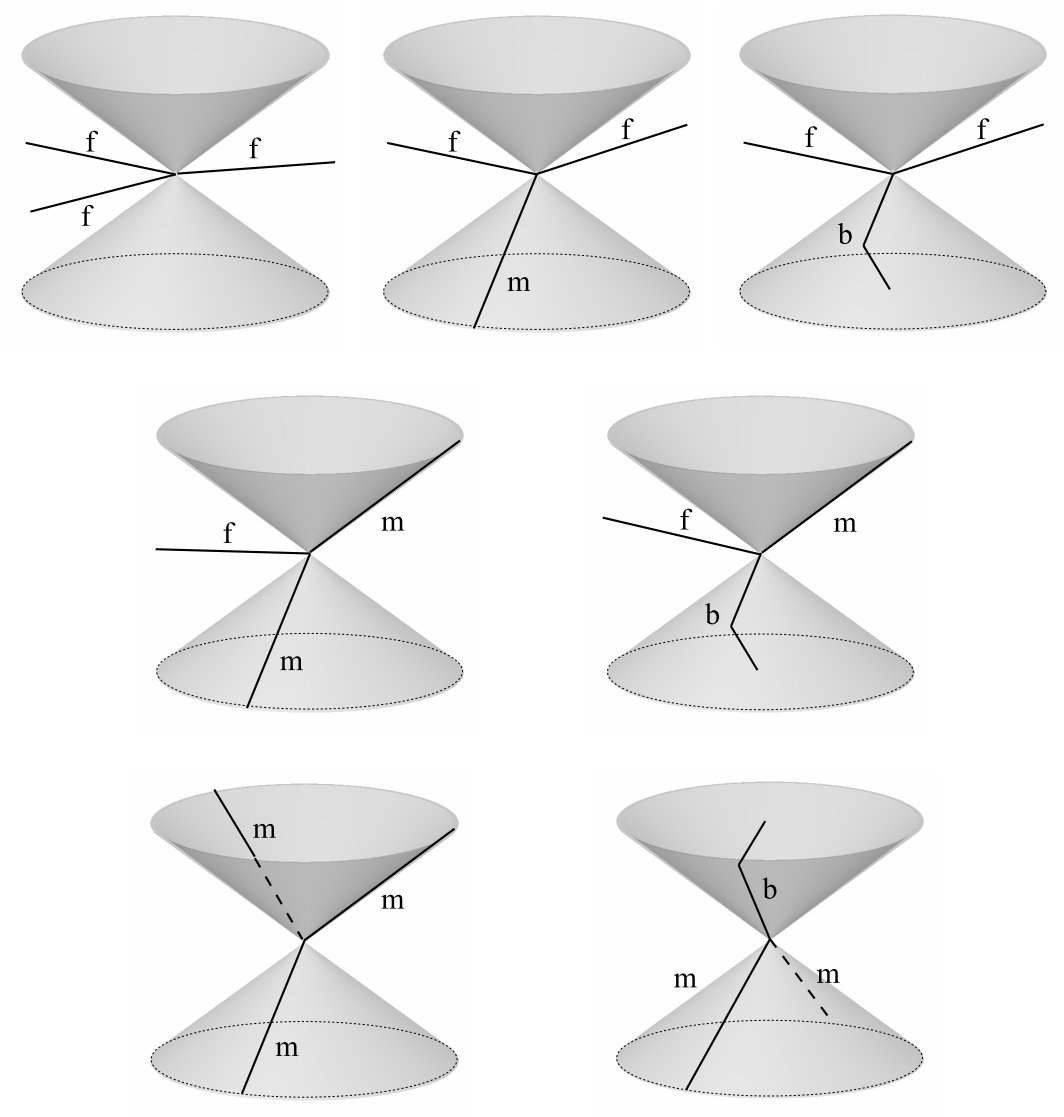

Figure 8.6: Feasibly optimal labellings for degree-three Steiner points in three-space.

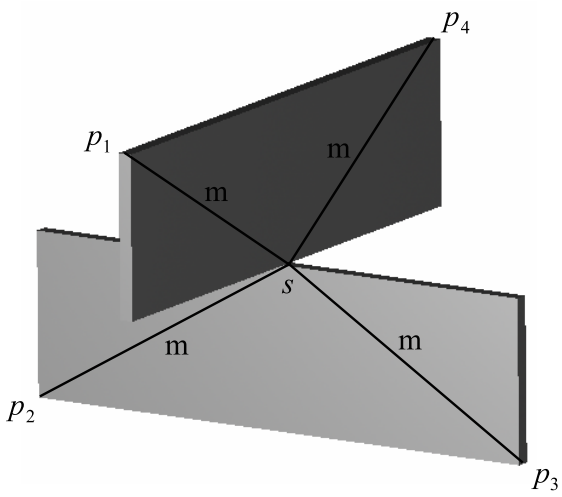

Figure 8.7: Steiner point with bi-vertically coplanar incident edges.

Therefore, the sink edge must be an f-edge. By Lemma 8.1, the two b-edges must be on opposite sides of $\mathcal{H}_s$. Consequently, at least one of the b-edges must be on the same side of $\mathcal{H}_s$ as the sink edge, which is not possible by Lemma 8.3. ∎

We now eliminate five more labellings.

Lemma 8.6. *Let T be a gradient-constrained MGA in three-space and let s be a Steiner point in T. Then the labelling of s is not (fmbb), (fbbb), (mmbb), (mbbb) or (bbbb).*

Proof. In each of the five cases, there must be either an m-edge and a b-edge, or two b-edges, on the same side of $\mathcal{H}_s$, which is not possible by Lemma 8.1. ∎

In the next lemma, we examine the labelling (mmmb).

Lemma 8.7. *Let T be a gradient-constrained MGA in three-space and let s be a Steiner point in T with incident sink edge sp_4. If sp_4 is a b-edge, then the labelling of s is not (mmmb).*

Proof. By Lemma 8.1, the three m-edges must be on the opposite side of $\mathcal{H}_s$ to the b-edge. (Figure 8.8 (i)). Denote the m-edges by p_1s, p_2s, p_3s and their respective m-cones by $\mathcal{C}_1, \mathcal{C}_2, \mathcal{C}_3$. We can assume without loss of generality that p_1, p_2, p_3 lie on a unit circle in the horizontal plane at a vertical distance m below s, since by Lemma 7.4, the optimality of

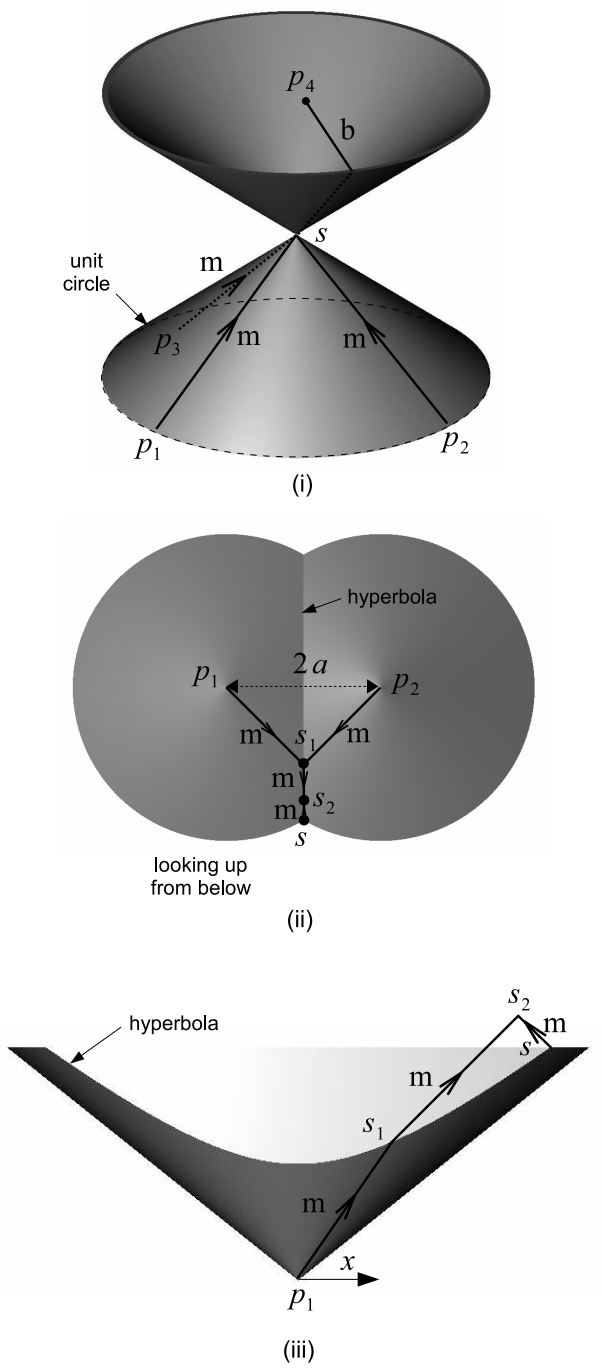

Figure 8.8: Steiner point with labelling (mmmb), where the b-edge is the sink edge. (i) Gilbert arborescence. (ii)–(iii) Hyperbola at the intersection of source m-cones, viewed from below, and along a line orthogonal to the vertical plane containing the hyperbola.

s depends only on the angles between edges, not the edge lengths. We also assume that the angle between the projections of p_1s and p_2s onto a horizontal plane is at most 120°.

The intersection of $\mathcal{C}_1$ and $\mathcal{C}_2$ is a hyperbola lying in a vertical plane through s (Figure 8.8 (ii) and (iii)). Let s_1 be a point on this hyperbola. Then p_1s_1 and p_2s_1 are m-edges, since s_1 lies on $\mathcal{C}_1$ and $\mathcal{C}_2$. Let s_2 be a second point in the vertical plane containing the hyperbola, such that s_1s_2 and ss_2 are m-edges, and s_2 is above s (Figure 8.8 (iii)).

Thus, $T_1 := p_1s \cup p_2s \cup p_3s$ and $T_2 := p_1s_1 \cup p_2s_1 \cup p_3s \cup s_1s_2 \cup ss_2$ are arborescences connecting p_1, p_2, p_3, p_4 and, since each path from p_i, $i = 1, 2, 3$ to p_4 is a geodesic under the gradient metric, the flow cost component cannot be improved, and is the same for both arborescences. Hence, the arborescence with the shorter length will have the lesser cost.

Denoting the vertical distance between s and p_4 by z_4, the length L_1 of T_1 is given by $L_1 = \sqrt{1+m^2}\left(3 + \frac{z_4}{m}\right)$. Denoting the distance between p_1 and p_2 by $2a$, and the horizontal distance from the line through p_1, p_2 to s_1 by x, the length L_2 of T_2 as a function of x is

$$L_2(x) = \sqrt{1+m^2}\left(\frac{3}{2}\sqrt{x^2+a^2} + \frac{1}{2}\sqrt{1-a^2} - \frac{1}{2}x + \frac{3}{2} + \frac{z_4}{m}\right).$$

The first derivative is

$$L_2'(x) = \sqrt{1+m^2}\left(\frac{3}{2}\frac{x}{\sqrt{x^2+a^2}} - \frac{1}{2}\right).$$

Setting $L_2'(x) = 0$, it is easy to show that $L_2(x)$ is minimised when $x = \frac{a}{\sqrt{8}}$, giving

$$\begin{aligned} L_2\left(\frac{a}{\sqrt{8}}\right) &= \sqrt{1+m^2}\left(\sqrt{2}a + \frac{1}{2}\sqrt{1-a^2} + \frac{3}{2} + \frac{z_4}{m}\right) \\ &\leq \sqrt{1+m^2}\left(3 + \frac{z_4}{m}\right). \end{aligned}$$

Since the length of T_2 is less than the length of T_1, and the flow components are the same, we conclude that T_2 is not minimal, and therefore the labelling (mmmb) is not feasibly optimal if the sink edge is a b-edge. ∎

We now state the main result in this section.

Theorem 8.2. *Let T be a gradient-constrained MGA in three-space and let s be a Steiner point*

in T. Then the labellings (fffm), (ffmm), (fmmm) and (mmmm) are feasibly optimal.

Proof. Steiner points with these labellings were obtained by a Matlab program which generates random arborescences with degree-four Steiner points, and tests whether these are MGAs by checking whether the necessary and sufficient conditions of Theorem 6.2 in Chapter 6 are satisfied. The optimal networks generated by this program were double-checked using the UNO software product. ∎

Feasible configurations for degree-four Steiner points are shown in Figure 8.9. Three different configurations for Steiner points with the labelling (ffmm) are shown. In all cases, the sink edge is indicated by arrows. The m-cones are shown to distinguish between f-, m- and b-edges. We note that the sink edge can be any of the four edges, except for the labelling (fffm), in which case the sink edge must be an f-edge.

The labellings not accounted for in this section are (fffb), (ffmb), (fmmb) and (mmmb), the last case having only been proved not feasible for the case where the b-edge is the sink edge. The following conjecture, if true, would prove that these four labellings are not feasibly optimal.

Conjecture 8.1. *Let T be a gradient-constrained MGA in three-space and let s be a Steiner point in T. If the degree of s is greater than three, then s has no incident b-edges.*

There is strong evidence to suggest that this conjecture is true. The main support for this belief is that, in three-space, a b-edge path from a source to a sink can be embedded in many different ways. Numerical experiments indicate that this path tends to be embedded using at least three zigzag components, rather than two. In this way, edges can attach to different corner points on the zigzag so as to reduce the cost of the network.

To demonstrate this, consider the following example. Let $p_1 = (-0.707, 0.707, 0)$, $p_2 = (-0.707, -0.707, 0)$, $p_3 = (1, 0, -0.5)$ be sources with respective flows $t_1 = 1, t_2 = 1$, $t_3 = 100$, and let $p_4 = (1, 0, 0.5)$ be the sink. The cost parameters are $d = h = 1$ and the maximum gradient is $m = 0.5$. It can be verified that the network shown in Figure 8.10, in which the Steiner point s has labelling (ffmm), is a gradient-constrained MGA.

If we perturb p_3 by ϵ in the negative x-direction, we notice that the topology suddenly changes to the one shown in Figure 8.11, in which $\epsilon = 0.1$. The path from p_3 to p_4 now has

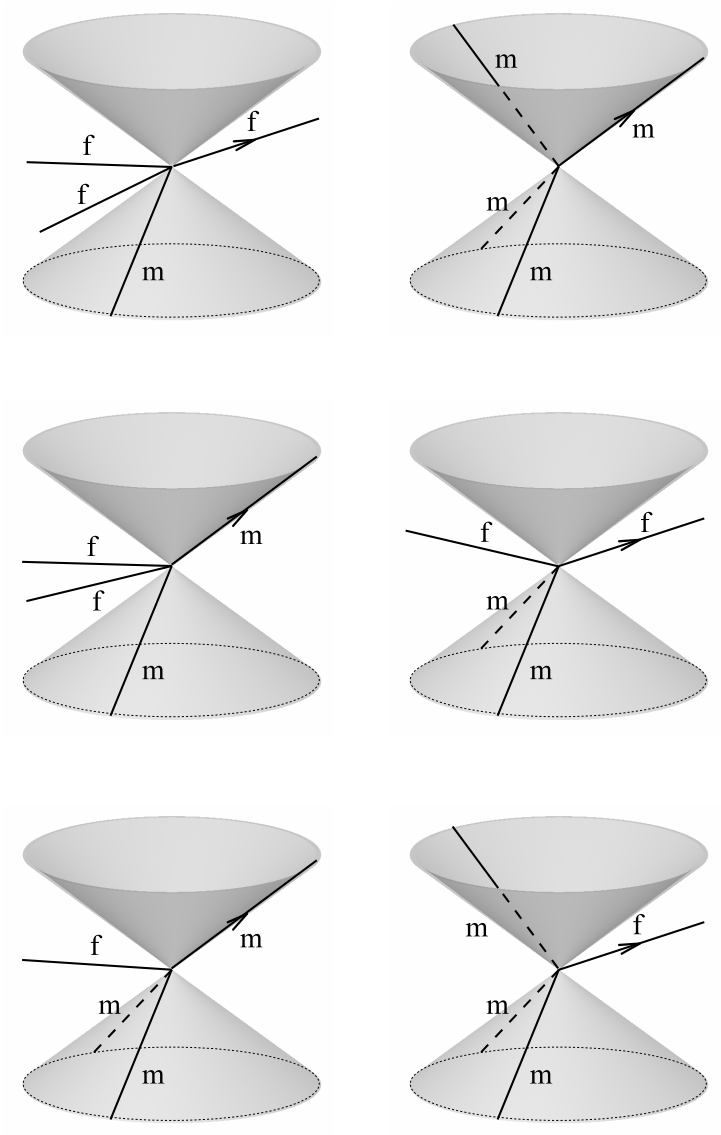

Figure 8.9: Feasibly optimal labellings for degree-four Steiner points in three-space.

the freedom to be embedded in three-space such that it has three zigzags instead of two. Consequently, the edges incident to p_1 and p_2 can connect to different corner points on the path to reduce the cost of the network. This behaviour has been frequently observed when attempting to construct MGAs with the above labellings.

8.6 Maximum degree of Steiner points

The degree of a Steiner point in a gradient-constrained Steiner minimum tree (SMT) in three dimensions is either three or four [13], subject to some constraints on m. In general there is no upper bound on the degree of a Steiner point in a minimum Gilbert network (MGN) [27]. The Steiner problem is a special case of the Gilbert arborescence problem, which is itself a special case of the Gilbert network problem. What then can we say about the degree of Steiner points in gradient-constrained MGAs in three dimensions? Is the degree limited to three or four as for gradient-constrained SMTs, is it unbounded as for general MGNs, or is it bounded from above by some finite integer value greater than four?

This has proved to be an exceedingly difficult question to answer. For some time, we conjectured that the degree is unbounded, by consideration of the arborescence in Figure 8.12 (i), in which the Steiner point s has $k-1$ incident source m-edges, where k is arbitrarily large, and the sink edge is a b-edge. In this network, each path from p_i, $i = 1, \ldots, k-1$ to p_k is a geodesic under the gradient metric. Therefore, the flow cost component cannot be improved.

The discovery of Lemma 8.7, however, revealed that the fixed cost can be improved. By placing a new Steiner point s_1 at an optimal location on the hyperbola at the intersection of two of the source m-cones, and a second Steiner point s_2 at a strategic location above s, the fixed cost is reduced while flow cost is unaffected. If ss_2 is a b-edge, the procedure can be repeated for another pair of source m-edges. From this we can state the following important result.

Theorem 8.3. *Let T be a gradient-constrained MGA in $\mathbb{R}^3$ and let s be a Steiner point in T with incident sink edge sp_k. If sp_k is a b-edge, then s has degree three, and the two source edges are*

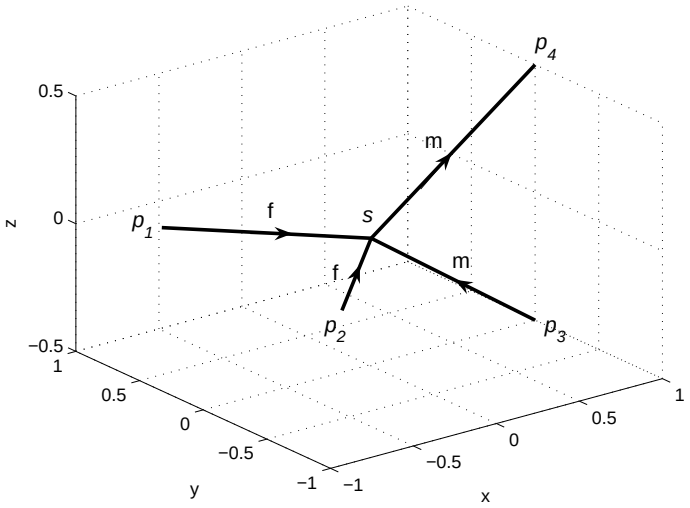

Figure 8.10: Steiner point with labelling (ffmm).

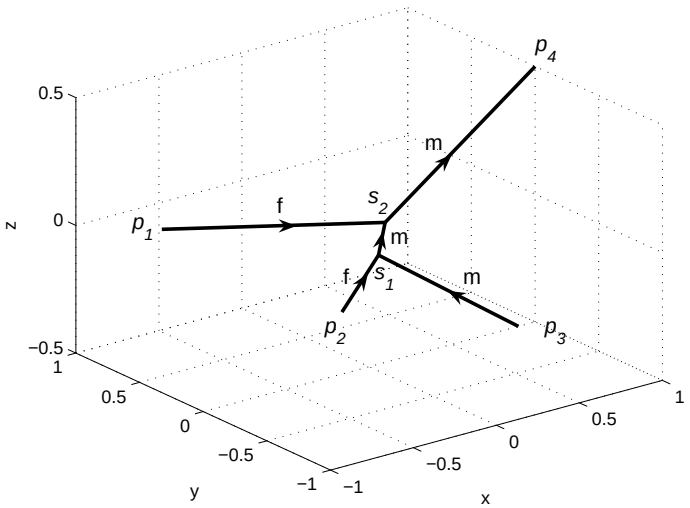

Figure 8.11: Change in topology resulting from a perturbation of a terminal.

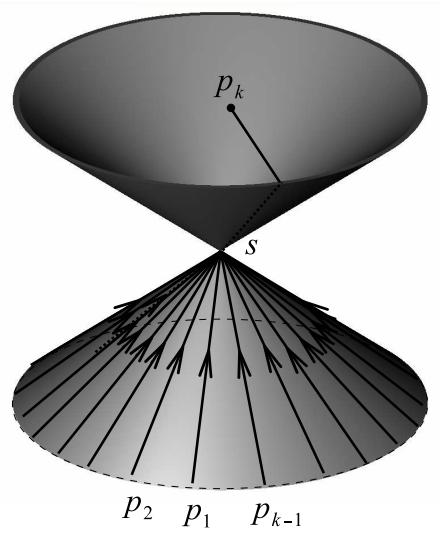

(i)

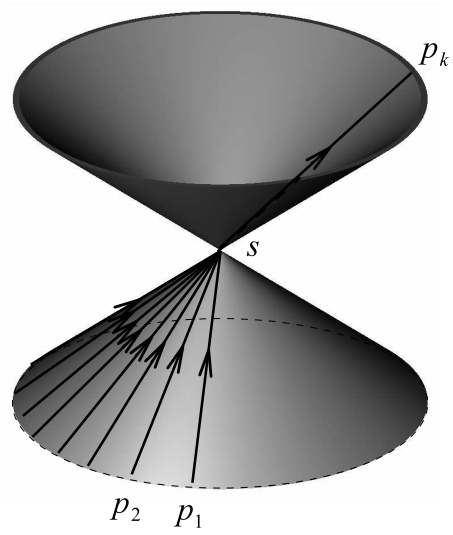

(ii)

Figure 8.12: Large-degree Steiner points, where the sink edge is (i) a b-edge, and (ii) an m-edge.

vertically coplanar m-edges on the opposite side of $\mathcal{H}_s$ to the sink edge.

Proof. By Lemma 8.2, s has no incident f-edges, because the sink edge is a b-edge. Therefore all source edges are m-edges. By repeated application of Lemma 8.7 we see that, provided the sink edge preserves its labelling, s has at most two incident source m-edges. By Lemma 8.1, these edges must be on the opposite side of $\mathcal{H}_s$ to the sink edge. If the m-edges do not lie in a vertical plane, then their associated vectors must be vertical, otherwise the three vectors cannot balance. But now for the vectors to balance, the sum of the two weights on the source edges must equal the weight on the sink edge which, under the assumption that $d > 0$, is not possible in a Gilbert arborescence with a linear cost function $w(t) = d + ht$. Hence the two m-edges must be vertically co-planar. ∎

From this result, we see that the network in Figure 8.12 (i) is not an MGA. Suppose, however, that we change the sink edge so that it is now an m-edge instead of a b-edge (Figure 8.12 (ii)). The proof of Lemma 8.7 relies on the sink edge being a b-edge, and is therefore no longer applicable. The paths from $p_i,\ i = 1, \ldots, k-1$ to p_k are still geodesics under the gradient metric, so the flow cost cannot be improved.

Can the development cost be improved? To answer this, consider the arborescence $T = p_1s \cup p_2s \cup sp_3$ in Figure 8.13 (i), where p_1, p_2 are sources with very large associated flows t_1, t_2, p_3 is the sink, s is a Steiner point, and the three edges are m-edges. Let $\mathcal{C}_1, \mathcal{C}_2, \mathcal{C}_3, \mathcal{C}_s$ denote the m-cones associated with p_1, p_2, p_3, s respectively. Then, as in the proof of Lemma 8.7, $\mathcal{C}_1 \cap \mathcal{C}_2$ is a hyperbola.

Now there are two cases. Suppose that p_1, p_2 are placed on $\mathcal{C}_s$ such that the hyperbola does not intersect $\mathcal{C}_3$ below $\mathcal{H}_s$ (Figure 8.13 (ii)). If p_1, p_2 lie on the same horizontal plane, the hyperbola associated with the two m-cones lies in a vertical plane. If this vertical plane makes an angle greater than $90°$ with the vertical plane containing the sink edge, then the hyperbola does not intersect $\mathcal{C}_3$ below $\mathcal{H}_s$. Now if s is replaced with a Steiner point s_1 on the hyperbola, s_1 has labelling (fmm), and the paths from p_1, p_2 to p_3 are no longer geodesics. If the flow cost is very large, this new network is not minimal. Hence, in this case the length of T cannot be shortened without disrupting the geodesic paths between the sources and the sink.

Now suppose that p_1, p_2 are placed on $\mathcal{C}_s$ such that the hyperbola at $\mathcal{C}_1 \cap \mathcal{C}_2$ intersects

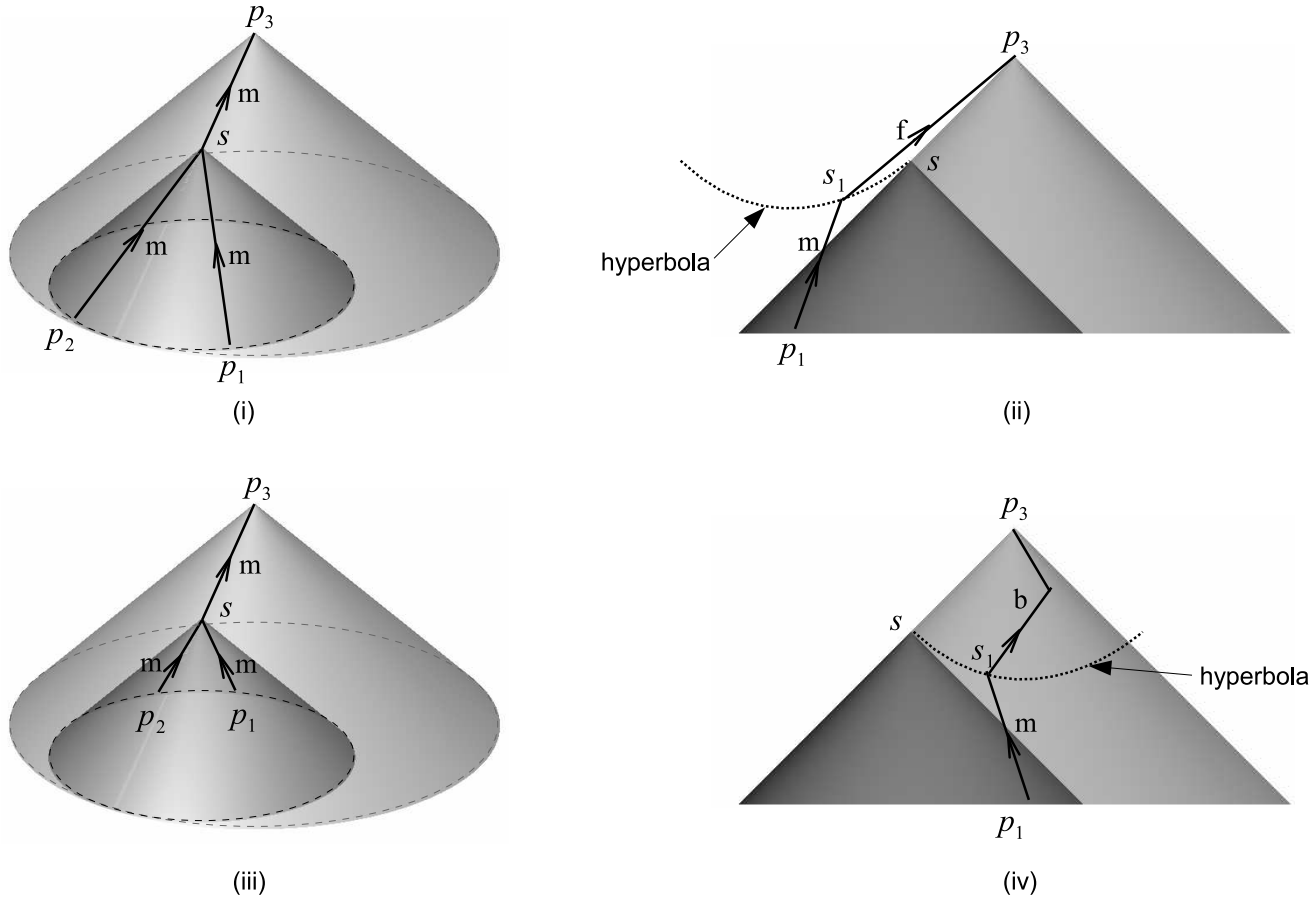

Figure 8.13: Networks for which the paths from the sources to the sink are geodesics under the gradient metric. (i)–(ii) Shortest geodesic network. (iii)-(iv) Not a shortest geodesic network.

$\mathcal{C}_3$ below $\mathcal{H}_s$. A new Steiner point s_1 on the hyperbola has labelling (mmb), and since s_1 is lower than s, the length of the new network is less than T, while the flow cost is unchanged. Thus in this case T is not minimal.

Therefore, if a Steiner point has $k-1$ source m-edges on one side of $\mathcal{H}_s$ and an m-edge sink on the other, such that the flow costs are very large compared to the fixed cost, and such that none of the hyperbolae associated with pairs of source m-cones intersect $\mathcal{C}_k$ below $\mathcal{H}_s$, then the network has the shortest length among all networks connecting $p_1, \ldots, p_k$ for which the paths from the sources to the sink are geodesics. This leads us to the following result.

Theorem 8.4. *There is no upper bound on the degree of a Steiner point in a gradient-constrained MGA in three dimensions.*

Using the UNO software product, many high-degree Steiner points satisfying the properties described above were found.

We conclude this discussion with some additional observations about networks generated in UNO for which large-degree Steiner points were achieved:

- A large-degree Steiner point can have at least two source m-edges above $\mathcal{H}_s$, provided m is sufficiently small, and the flows associated with these edges are not too large.
- If three m-edges are arranged around $\mathcal{H}_s$ such that one pair of adjacent m-cones intersects $\mathcal{C}_k$ and the other pair of adjacent m-cones does not, then the above discussion about hyperbola is valid only for the pair of m-edges subtending the smaller angle.
- From the above comment, a large-degree Steiner point can have at most one incident m-edge below $\mathcal{H}_s$ on the side of $\mathcal{V}_s$ containing the sink edge.

8.7 Hulls in gradient-constrained three-space

We conclude this chapter by briefly discussing hulls in gradient-constrained three-space. Recall from Chapter 7 that, for a set N of terminals in a vertical plane $\mathcal{P}$, there exists an MGA, T, for N lying on $\mathcal{P}$ (Lemma 7.6). Moreover, all Steiner points in T are in the

reduced hull of N, which is the interior of the convex hull of N excluding points p having the property that the Euclidean straight line segments connecting p and all terminals on at least one side of $\mathcal{V}_s$ have gradient strictly greater than m, where $\mathcal{V}_s$ is the vertical line through s (Definition 7.3, Lemma 8.8).

In three dimensions, the situation is more difficult. One complication stems from the fact that a Steiner point does not necessarily lie in the convex hull of its adjacent vertices. To see this, let $m = 1$, $p_1 = (-1, -1)$, $p_2 = (1, -1)$, $p_3 = (0, 1)$, $s = (0, 0)$, and $T = p_1s \cup p_2s \cup sp_3$. Perturbing p_3 horizontally out of the (x, z) plane, the cost of T is unchanged. The position of s is unchanged, but now it lies outside the plane of its three adjacent vertices.

It was also shown in [13] that all Steiner points in gradient-constrained SMTs lie in $\text{hull}_g(N)$, the hull of N in the gradient metric. The following generalises the definition of the *reduced hull* of a set of terminals to the three-dimensional case.

Definition 8.2. *Let N be a set of terminals in $\mathbb{R}^3$, and let* $\text{conv}(N)$ *denote the (Euclidean) convex hull of N. Then the* reduced hull *of N in the gradient metric is*

$$\begin{aligned} \text{hull}_g{}'(N) \quad := \quad & \text{conv}(N) - N - \{p \in \text{int}(\text{conv}(N)) : \exists \mathcal{P}_p \\ & \text{such that } \forall q \in N \text{ on one side of } \mathcal{P}_p,\ g(pq) > m\}, \end{aligned}$$

where $\mathcal{P}_p$ is a vertical plane through p, and a point $q \in \mathcal{P}_p$ is assumed to lie on both sides of $\mathcal{P}_p$.

In other words, the reduced hull of N is the (Euclidean) convex hull of N with a region subtracted from it, the region consisting of points in N and points p for which there exists a vertical plane $\mathcal{P}$ through p such that edges from p to every terminal on one side of $\mathcal{P}$ are b-edges.

To demonstrate this concept, suppose that N consists of the eight points at the vertices of a $1 \times 2 \times 1$ cuboid, and suppose that $m = 1$. The convex hull, gradient hull, reduced hull and region removed from the convex hull to achieve the reduced hull are shown in Figure 8.14 (i)–(iv) respectively. From the figure it seems unlikely that Steiner points can exist outside the reduced hull.

In the second example (Figure 8.15), the cuboid is turned on its side so that the longer

dimension is vertical. The convex hull, gradient hull, reduced hull and region removed from the convex hull to achieve the reduced hull are shown in Figure 8.15 (i)–(iv) respectively. Using the UNO software product we have attempted to construct examples where Steiner points lie outside the reduced hull, without success. Since we have not yet found a rigorous proof, we cannot state that all Steiner points lie in the reduced hull, and resort to the following result.

Lemma 8.8. *Let T be a gradient-constrained MGA in a vertical plane, and let s be a Steiner point in T. Then $s \in \text{hull}_g(N)$.*

It is worth noting that, in three dimensions, Steiner points can exist on the boundary of the (Euclidean) convex hull of N, and this is not possible for Steiner points in gradient-constrained MGAs in a vertical plane.

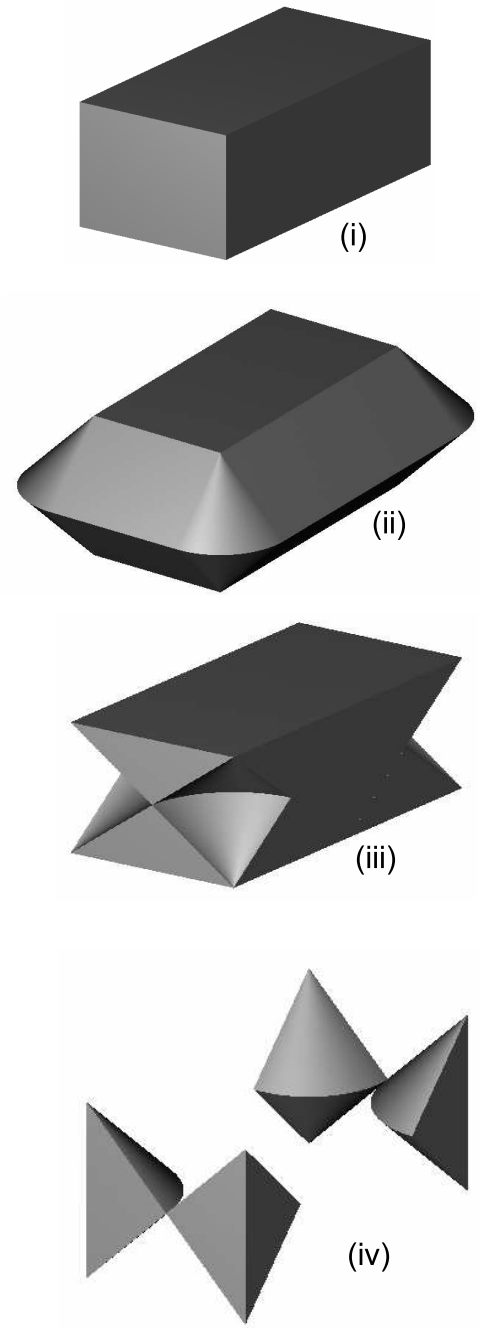

Figure 8.14: Hulls of a set of terminals at the vertices of a cuboid. (i) Convex hull. (ii) Gradient-constrained hull. (iii) Reduced hull. (iv) Region removed from convex hull to obtain reduced hull.

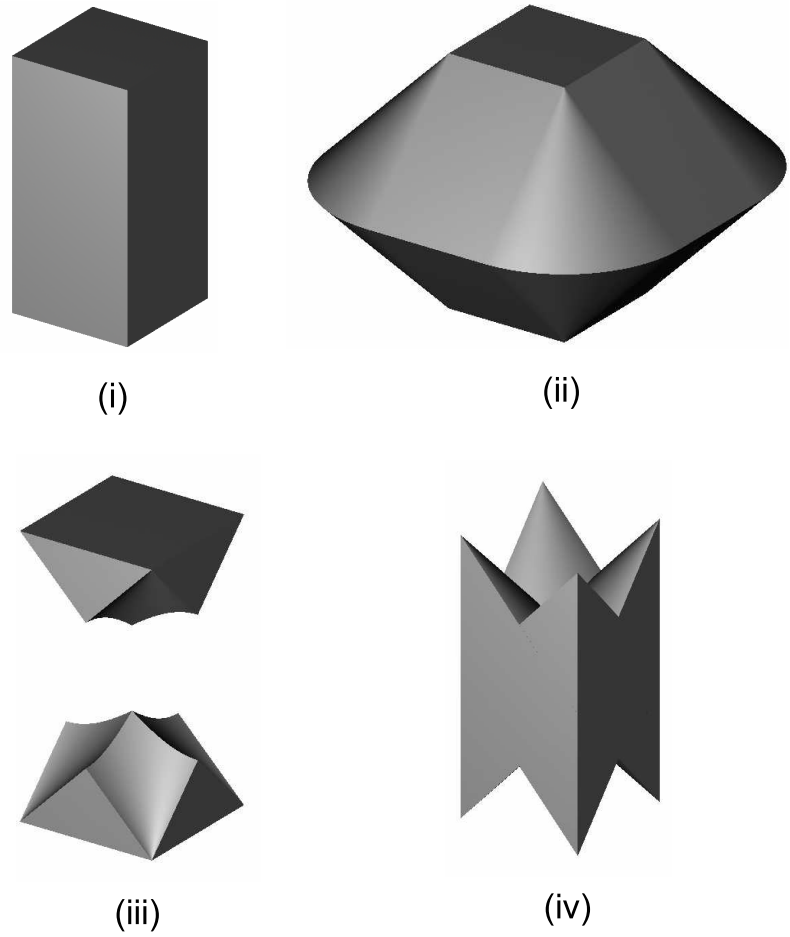

Figure 8.15: Hulls of a set of terminals at the vertices of a cuboid. (i) Convex hull. (ii) Gradient-constrained hull. (iii) Reduced hull. (iv) Region removed from convex hull to obtain reduced hull.

Part III

A Case Study

Introduction to Part III

THE Callie underground mine, located in the Tanami Desert in the Northern Territory, includes two parallel declines accessing a large orebody extending some two kilometres below the surface. As part of the strategic mine planning, it was proposed to incorporate a vertical hoisting shaft and an ore pass as an alternative to trucking material to the surface along the declines. In this work, we use network optimisation techniques to investigate the feasibility of the proposed system, and to mathematically determine the optimum positions and geometry of the shaft, ore pass and surrounding infrastructure. We propose a modelling procedure taking aspects from the Fermat-Weber problem and the Gilbert arborescence problem. We describe the implementation of the procedure into a computer program for solving the problem iteratively, and present results over a range of infrastructure and haulage costs, decline gradients and life-of-mine schedules.

Chapter 9
Callie Shaft Location Study

9.1 Introduction

9.1.1 The Tanami operations

LOCATED in the Tanami desert in the Northern Territory, 550 km north-west of Alice Springs (Figure 9.1), the Tanami operations comprise a processing facility at the Granites, two open pits and the Callie underground mine at Dead Bullock Soak, the Groundrush open pit and the Tanami mill.

Gold was discovered at Tanami in 1900, and modern mining began in 1983 following an agreement with traditional landowners. Initial production came from the open pit mines at the Granites, while current production comes from the high-grade Callie underground mine at Dead Bullock Soak.

9.1.2 Orebody

The Callie underground mine services a large orebody running approximately in an east-west direction, plunging into the ground at an angle of about 45° towards the east (Figure 9.2). The orebody is divided into two major veins (Figure 9.3).

9.1.3 Underground mine

To date, the orebody has been accessed by a single decline, called the *Callie decline*, with material having been mined to a depth of about 1000 m below the surface. Rock is ex-

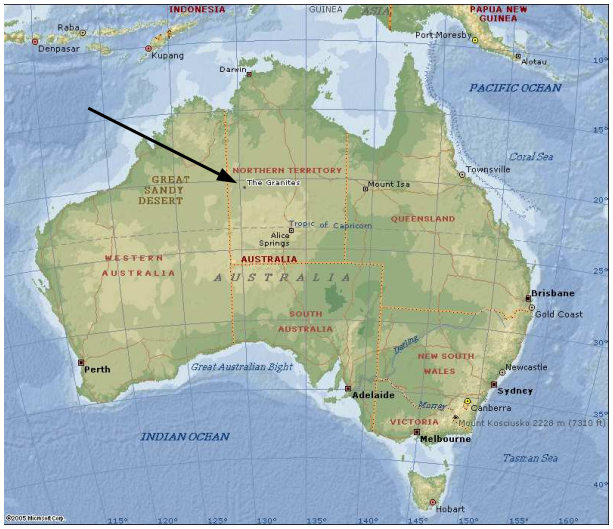

Figure 9.1: Location of the Tanami operations.

tracted from the orebody in primary stopes, which are replaced with fill material to allow adjacent secondary stopes to be subsequently extracted. Once loaded onto trucks, ore is hauled along *crosscuts* (horizontal tunnels) to the decline. Levels are at 40 m vertical intervals.

In addition to the planned extension of the Callie decline, a secondary decline, called the *Wilson Drill decline* (WDD), is to branch out from the Callie decline about 950 m below the surface (Figure 9.4). Both declines are to have fixed gradients. Levels servicing the WDD are also at 40 m vertical intervals, however they are offset from the Callie levels. The Callie decline services the *Wilson shoot*, while the WDD is to service the *Federation shoot*.

9.1.4 Hoisting shaft

As part of the strategic mine planning, it was proposed to incorporate a *vertical hoisting shaft* as an alternative to trucking material to the surface along the declines. Using this system, ore is hauled to a common tipping level, called the *haul level*, where it is crushed, loaded into a skip and hoisted to the surface via the shaft. This method can provide sig-

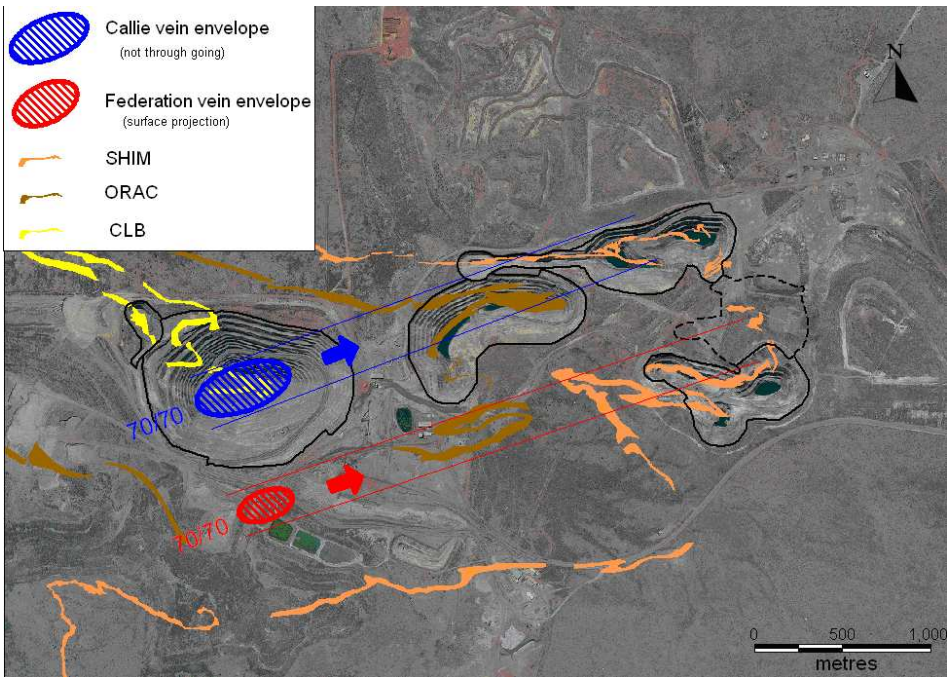

Figure 9.2: Simplified surface geology map.

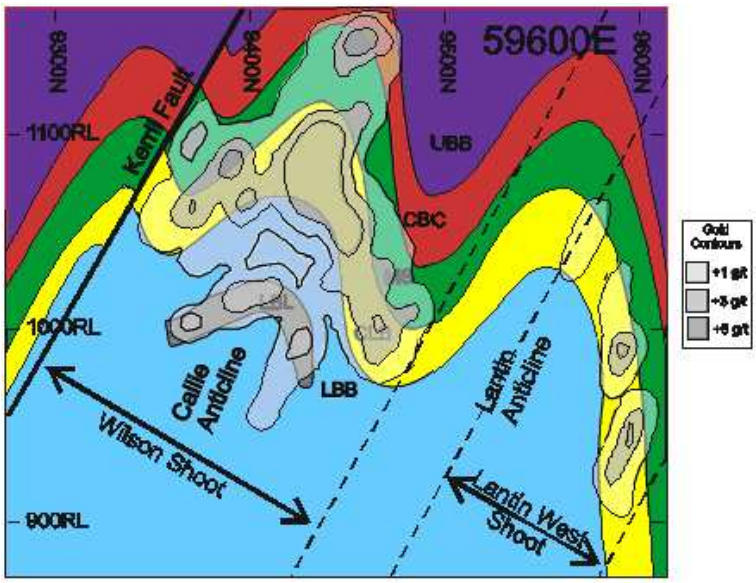

Figure 9.3: Typical cross-section through orebody (looking west).

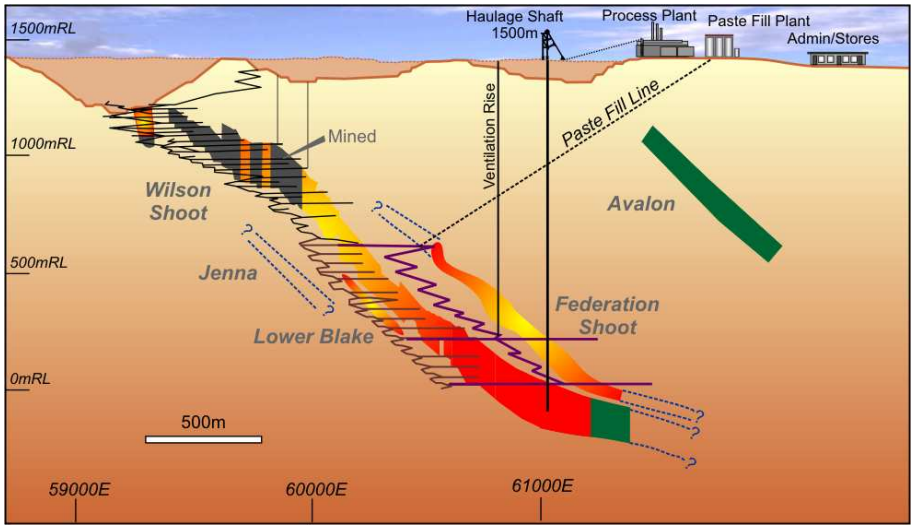

Figure 9.4: Conceptual long section.

nificant reductions in operating costs, although it requires a large capital cost associated with a hoisting shaft. A conceptual shaft loading arrangement is shown in Figure 9.5.

9.1.5 Ore pass

In addition to the shaft, it was proposed to include an *ore pass* into the mine. An ore pass is a near-vertical chute down which ore from upper levels is dropped to the haul (three levels above the shaft base, see Figure 9.5), and transported to the shaft in one of several ways:

- Ore is loaded into a truck (such as the one in Figure 9.6) by a load-haul-dump vehicle (Figure 9.7) at the bottom of an ore pass. It is then trucked from the bottom of the ore pass to the shaft.
- A load-haul-dump vehicle (Figure 9.7) trams ore directly from the base of the ore pass to the shaft.
- If the horizontal distance between the ore pass and the shaft is greater than say 300 m, a loading chute may be installed at the base of the ore pass, allowing trucks to be loaded automatically before transporting ore to the shaft.

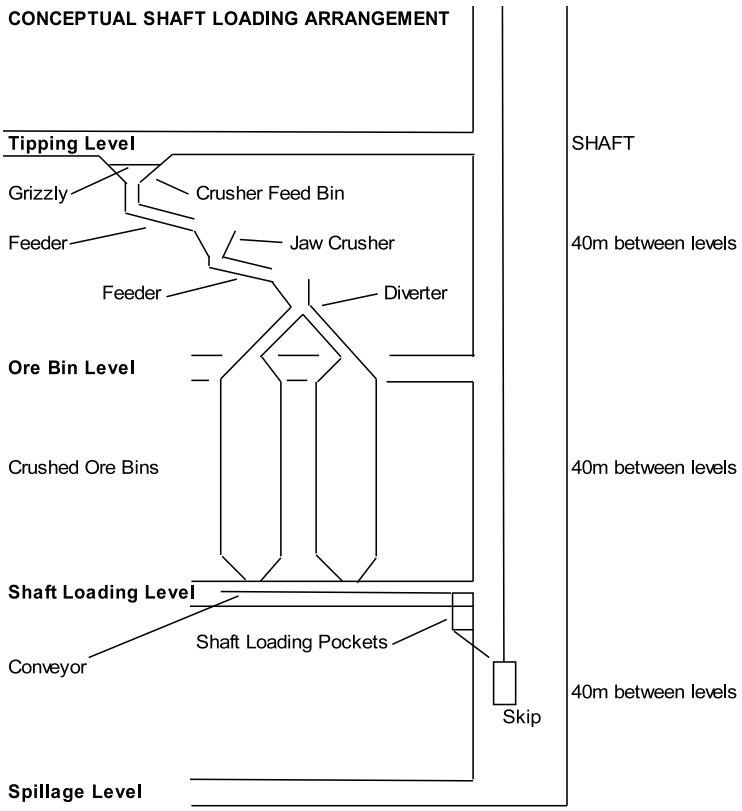

Figure 9.5: Conceptual shaft loading arrangement.

For operational reasons the ore pass is assumed to be constrained to the northing 9250N, which is about halfway between the two declines.

9.1.6 Problem description

The primary goal of this investigation is to mathematically determine:

1. the position (depth and plan coordinates) of the hoisting shaft;
2. the position (top, bottom and plan coordinates) of the ore pass and identification of the levels which access the ore pass; and
3. the geometry of the main haulage drive network at the tipping level and shaft haulage level.

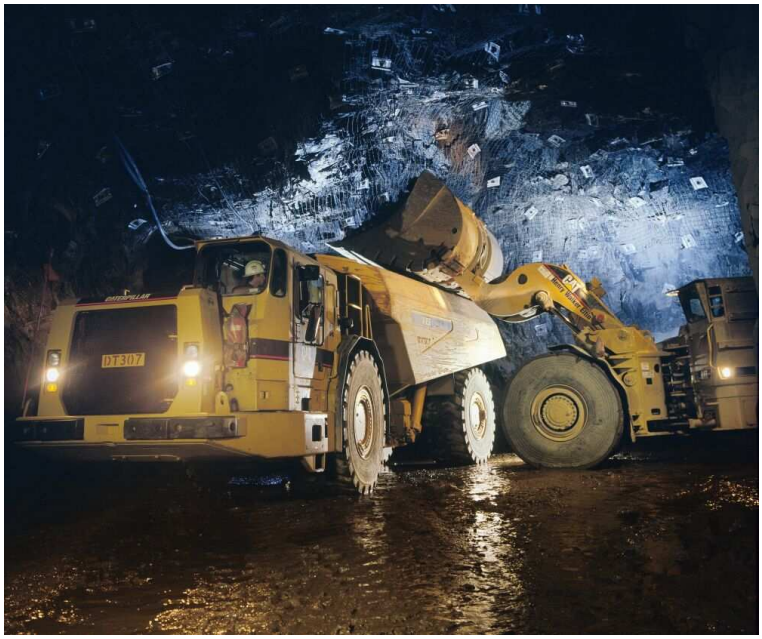

Figure 9.6: AD55 Caterpillar truck being loaded underground.

Figure 9.7: Cat R2900 load-haul-dump vehicle working underground.

9.2 Problem data

The following data, provided by Newmont Limited, is based on their 2006 ore reserves work.

9.2.1 Mine costs

Mine costs are summarised in Table 9.1.

Type	Mine component	Cost
Development	Decline	\$4020/m
	Level / main drive	\$3265/m
	Ore pass	\$1,210/m
	Shaft	\$25,000 or \$50,000 or \$75,000/m
Haulage	Decline (up) / level / main drive	\$0.75 or \$1.05/t.km
	Decline (down)	\$0.85 or \$1.20/t.km
Ore handling	Truck loading	\$2.09/t
	Crush and hoist to surface	\$2.00/t
Other	General mine services	\$16.07/t
	Ore pass fit-out	\$1,000,000

Table 9.1: Mine costs.

9.2.2 Decline gradients

Decline gradients are shown in Table 9.2.

Decline	Gradients: case 1	Gradients: case 2
Callie	1:8	1:7
WDD	1:7	1:6

Table 9.2: Decline gradients.

At the time this study was undertaken, the Callie and Wilson Drill declines were designed to about 0 RL (1400 m below the surface) with gradients 1:8 and 1:7 respectively. It is assumed that both declines will continue downwards in the same manner as the current design.

9.2.3 Access points

Access points are locations where the nominal crosscuts intersect the declines. Each access point is designated a nominal level corresponding to its approximate reduced level (RL). The surface is at approximately 1400 m RL, and access points on the Callie decline extend from 340 m RL to -660 m RL at 40 m vertical intervals (26 points), while access points on the WDD extend from 390 m RL to 70 m RL, also in 40 m vertical increments (nine points). Hence in total there are 35 access points. Their associated declines, (X,Y,Z) coordinates and nominal levels are provided in columns 1-5 of Table 9.3.

9.2.4 Schedules

Three life-of-mine (LOM) production schedules for the Callie underground mine were provided by Nadine Wetzel of Newmont. They are *base*, *probable* and *best*. The schedules were determined by Newmont as outlined in the report 'Schedule for shaft model.doc'. Details of the three schedules are provided in Table 9.4.
The predicted tonnages to be extracted from each access point, for the three cases, are provided in columns 6-8 of Table 9.3.

9.2.5 No-go zones

To avoid disruption to the shaft over the life of the mine, it must avoid impinging on the following no-go regions:

1. Orebody standoff: The shaft must not be too close to the orebody. The Vulcan file 'no_go_geol.dxf', provided by Newmont, provides a 'barrier' around the Wilson and Federation orebodies. Polygons digitised around the boundaries of the ore bodies were expanded 200 m in any direction (the two boundaries shown in Figures 9.8, 9.9 and 9.10).
2. Faults: The shaft is required to avoid faults by at least 50 m. The Vulcan file 'all_faults.dxf' provided the underground fault locations (see Figure 9.11). The main haulage drive is allowed to pass through a fault so long as it does not travel along (parallel) to it for any great length, say, no more than 15 metres at a time.

Orebody	X	Y	Z	Nominal Level	Base tonnes	Probable tonnes	Best tonnes
WIL	60256	9375	339	340	59253	59253	59253
WIL	60296	9371	299	300	296746	500000	700000
WIL	60336	9368	259	260	194808	500000	700000
WIL	60376	9364	219	220	298691	750000	700000
WIL	60415	9361	179	180	200000	750000	1050000
WIL	60455	9357	139	140	551408	1000000	1050000
WIL	60495	9354	99	100	736412	1125000	1400000
WIL	60535	9350	59	60	418845	1125000	1575000
WIL	60575	9347	19	20	500000	1000000	1225000
WIL	60615	9343	-21	-20	500000	1375000	1575000
WIL	60655	9340	-61	-60	600000	1125000	1225000
WIL	60694	9336	-101	-100	800000	1375000	1400000
WIL	60734	9333	-141	-140	600000	1125000	1575000
WIL	60774	9329	-181	-180	600000	1125000	1225000
WIL	60814	9326	-221	-220	700000	875000	1575000
WIL	60854	9322	-261	-260	500000	875000	1225000
WIL	60894	9319	-301	-300	400000	875000	1400000
WIL	60933	9315	-341	-340	500000	875000	1575000
WIL	60973	9312	-381	-380	300000	625000	1225000
WIL	61013	9308	-421	-420	200000	750000	1225000
WIL	61053	9305	-461	-460	300000	250000	1125000
WIL	61093	9301	-501	-500	100000	-	1050000
WIL	61133	9298	-541	-540	-	-	1225000
WIL	61173	9294	-581	-580	-	-	875000
WIL	61212	9291	-621	-620	-	-	1050000
WIL	61252	9287	-661	-660	-	-	350000
FED	60497	9103	398	390	110000	150000	150000
FED	60537	9103	358	350	230000	325000	325000
FED	60577	9103	318	310	240000	500000	500000
FED	60617	9103	278	270	230000	500000	500000
FED	60657	9103	238	230	230000	500000	500000
FED	60697	9103	198	190	240000	350000	500000
FED	60737	9103	158	150	120000	175000	500000
FED	60777	9103	117	110	-	-	350000
FED	60817	9103	77	70	-	-	175000

Table 9.3: Access points, nominal levels and tonnages.

	Wilson shoot			Federation shoot		
Name	Rate (Mtpa)	Quantity (Mt)	End	Rate (Mtpa)	Quantity (Mt)	End
Base	2	10	2015	0.35	1.4	2014
Probable	2.5	17.5	2018	0.5	2.5	2015
Best	3.5	30	2019	0.5	3.5	2017

Table 9.4: Base, probable and best life-of-mine schedules.

3. Surface infrastructure: The preferred area for the shaft collar is in a region south of the main entrance road. The Vulcan file 'go_surf.dxf' (the boundary shown in Figure 9.8) represents this bounded region.

Declines, haul points, 'no_go_geol.dxf' and 'go_surf.dxf' regions are shown in Figure 9.8 (plan), Figure 9.9 (section looking north) and Figure 9.10 (section looking west). Faults are shown in Figure 9.11.

9.3 Problem formulation and solution procedure

In Chapter 4, Section 4.5, we proposed a simplified procedure for determining the positions, lengths and orientations of the shaft, ore pass and main haulage drive. By this procedure, the problem was broken down into two subproblems. First, the optimum shaft depth was computed based on 'vertical' costs – decline haulage, shaft development and ore pass development – using the gradient-constrained Fermat-Weber problem. Second, a minimum-cost flow-dependent network interconnecting the declines, ore pass and shaft was constructed at the level determined by the first subproblem. The optimum network was computed based on 'horizontal' costs – haul drive development and haulage – using the Fermat-Weber problem in the Euclidean plane. In Chapter 2, Section 2.7, we showed how to find an optimum network when the shaft is allowed to lie anywhere on a straight line which, in this case, represents the boundary of the no-go region.

Although the simplified procedure seems to obtain good intuitive solutions, it does not guarantee an optimal solution for a given problem. Suppose the haul level is placed at 100 m RL based on vertical costs. Numerical tests have shown that moving the haul level to 140 m RL can reduce the cost of the network of tunnels. If the reduction in

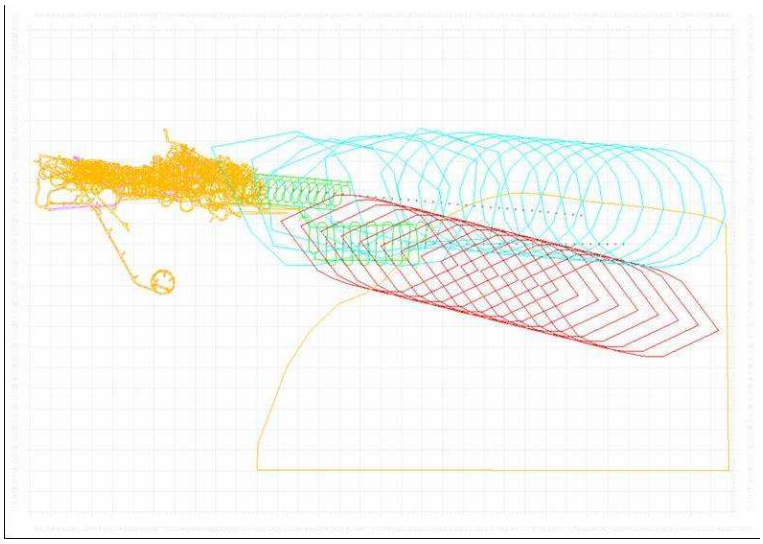

Figure 9.8: Plan view of underground mine.

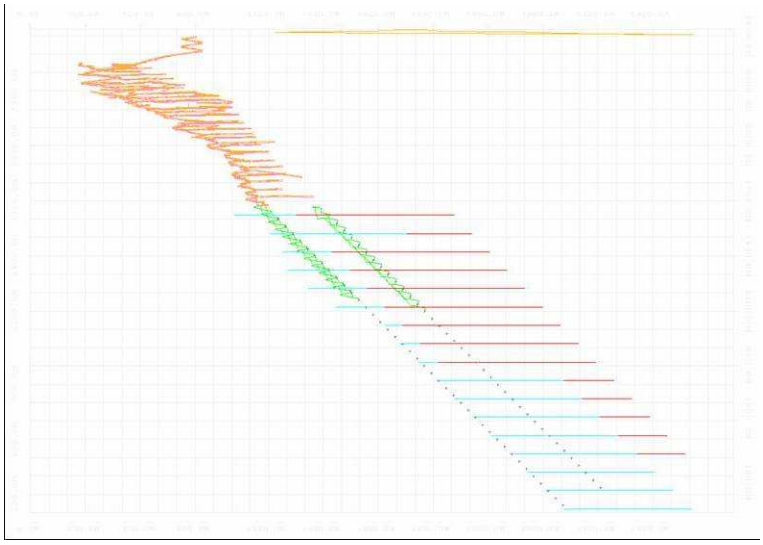

Figure 9.9: Section looking north.

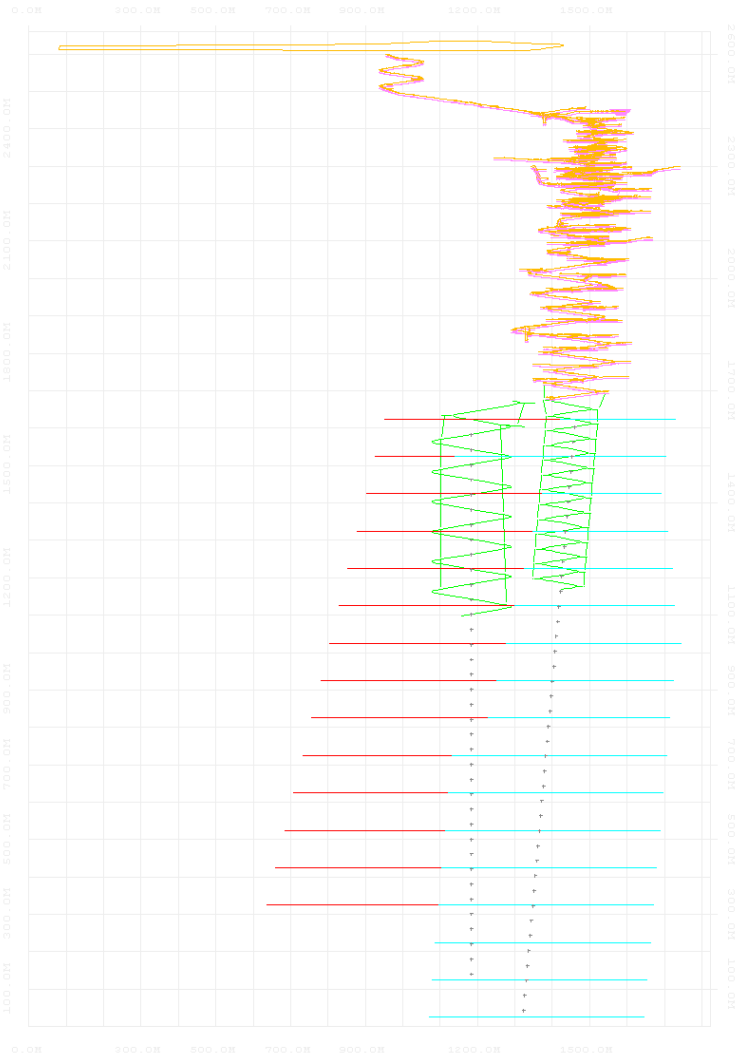

Figure 9.10: Section looking west.

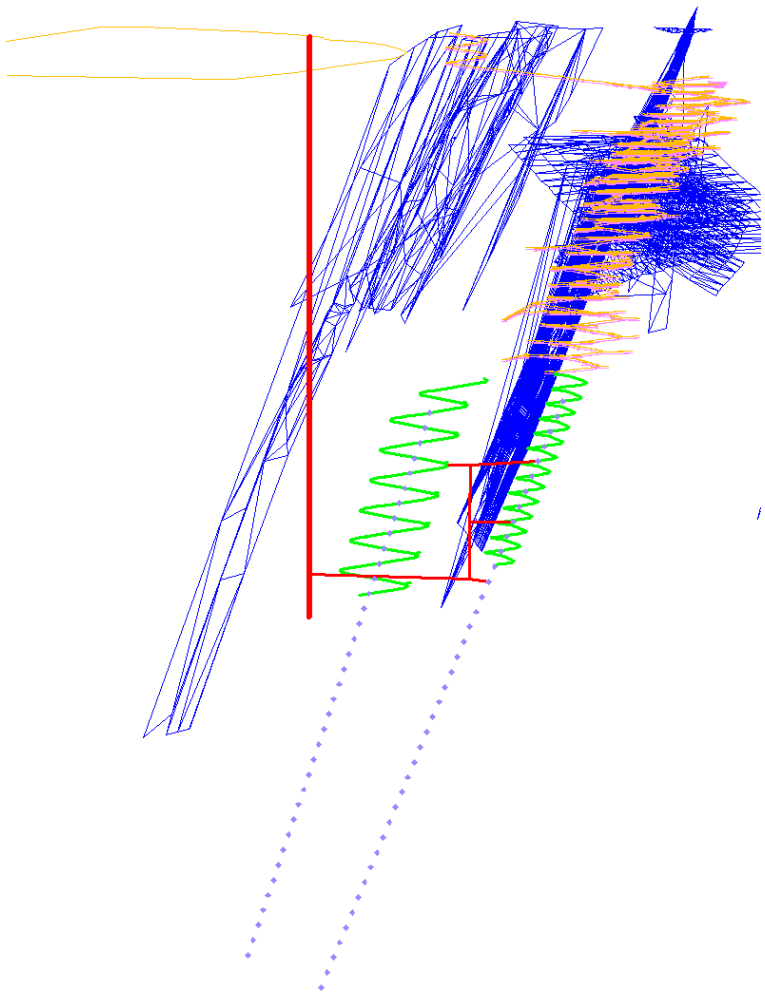

Figure 9.11: Faults (looking approximately west-south-west).

horizontal costs outweighs the increase in vertical costs, then the solution determined by the simplified procedure is not optimal.

In this chapter we propose a rigorous procedure which guarantees an optimal solution for a given problem. Refer to Figure 9.12. Placing the haulage drive at each of the 35 levels (on both declines collectively) from -660 m RL up to 390 m RL (see Figure 9.12), the vertical costs can be computed. If an ore pass is used, it is tested at every level above the haulage drive, and if an intermediate tipping point is added to the ore pass, it is also tested at every level between the haulage drive and the top of the ore pass. For each combination of haul and ore pass levels, a minimum-cost network interconnecting the declines, ore pass and shaft is computed (Figure 9.13).

Once the cost for every mine layout has been computed, the arrangement giving the lowest cost is selected as the globally optimal solution.

9.4 Results

Thirty-six tests were undertaken for each of three cases – no ore pass, one ore pass and one ore pass with two tipping points (108 tests in total). The parameters used in each case are summarised in Table 9.5. Results for the three cases are summarised in Tables 9.6, 9.7 and 9.8.

9.5 Analysis

Optimum haul levels and costs for the three ore pass configurations are compared in Table 9.9. A cost comparison chart is provided in Figure 9.14.

9.5.1 Shaft depth

A visual comparison of optimum haul levels is provided in Figure 9.15.

- The optimum haul level ranges from 390 m RL to -340 m RL (1010 m to 1740 m below the surface).

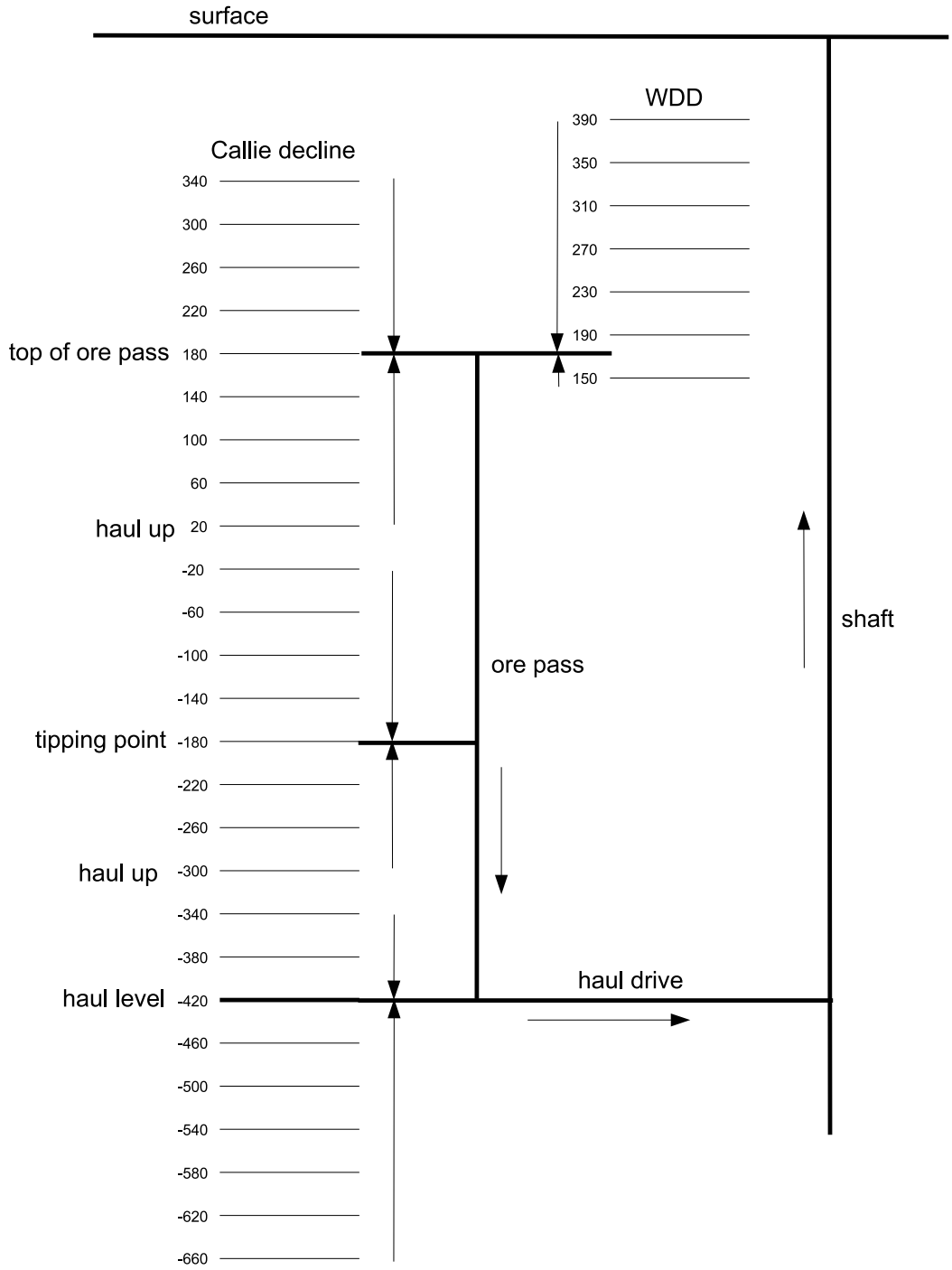

Figure 9.12: Schematic elevation of shaft and surrounding infrastructure.

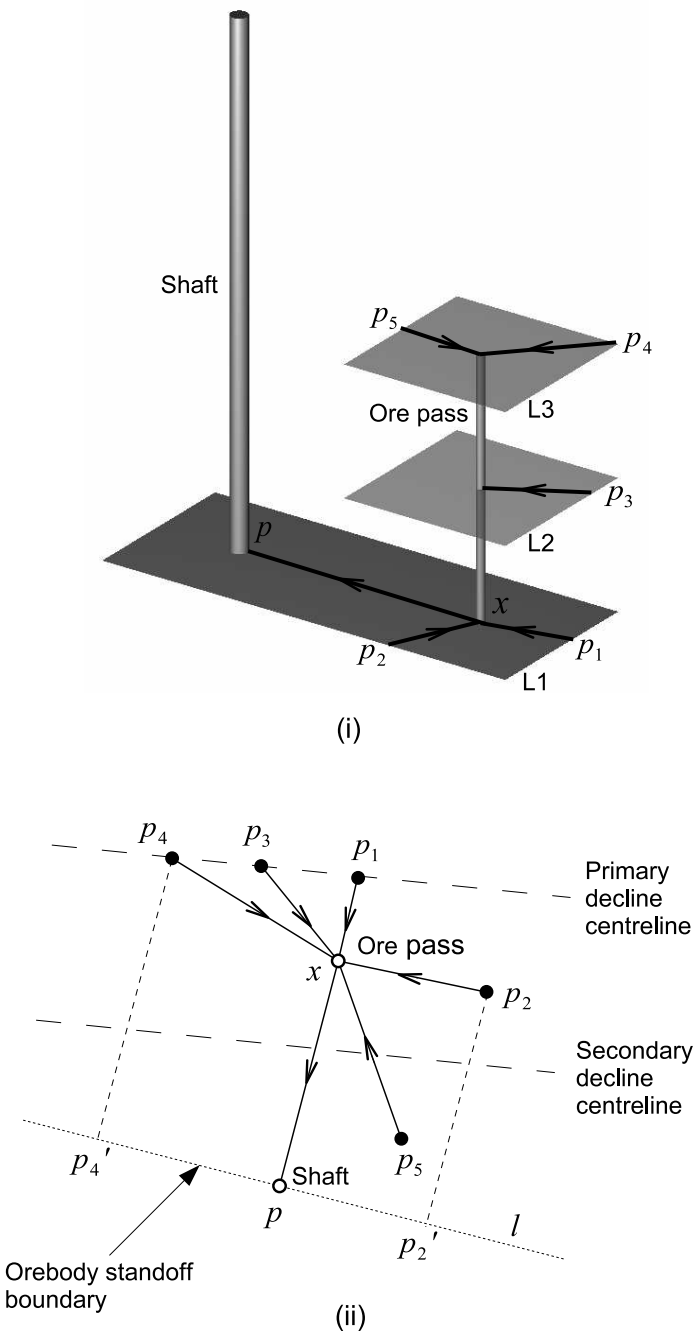

Figure 9.13: Callie underground mine. (i) Perspective view. (ii) Plan view showing horizontal network.

Case ID	Schedule	Cost rates: Shaft development $/m	Cost rates: Haulage up $/(t.km)	Cost rates: Haulage down $/(t.km)	Decline gradients: Callie	Decline gradients: WDD
BA01	Base	25,000	0.75	0.85	1:8	1:7
BA02	Base	25,000	0.75	0.85	1:7	1:6
BA03	Base	25,000	1.05	1.20	1:8	1:7
BA04	Base	25,000	1.05	1.20	1:7	1:6
BA05	Base	50,000	0.75	0.85	1:8	1:7
BA06	Base	50,000	0.75	0.85	1:7	1:6
BA07	Base	50,000	1.05	1.20	1:8	1:7
BA08	Base	50,000	1.05	1.20	1:7	1:6
BA09	Base	75,000	0.75	0.85	1:8	1:7
BA10	Base	75,000	0.75	0.85	1:7	1:6
BA11	Base	75,000	1.05	1.20	1:8	1:7
BA12	Base	75,000	1.05	1.20	1:7	1:6
PR01	Probable	25,000	0.75	0.85	1:8	1:7
PR02	Probable	25,000	0.75	0.85	1:7	1:6
PR03	Probable	25,000	1.05	1.20	1:8	1:7
PR04	Probable	25,000	1.05	1.20	1:7	1:6
PR05	Probable	50,000	0.75	0.85	1:8	1:7
PR06	Probable	50,000	0.75	0.85	1:7	1:6
PR07	Probable	50,000	1.05	1.20	1:8	1:7
PR08	Probable	50,000	1.05	1.20	1:7	1:6
PR09	Probable	75,000	0.75	0.85	1:8	1:7
PR10	Probable	75,000	0.75	0.85	1:7	1:6
PR11	Probable	75,000	1.05	1.20	1:8	1:7
PR12	Probable	75,000	1.05	1.20	1:7	1:6
BE01	Best	25,000	0.75	0.85	1:8	1:7
BE02	Best	25,000	0.75	0.85	1:7	1:6
BE03	Best	25,000	1.05	1.20	1:8	1:7
BE04	Best	25,000	1.05	1.20	1:7	1:6
BE05	Best	50,000	0.75	0.85	1:8	1:7
BE06	Best	50,000	0.75	0.85	1:7	1:6
BE07	Best	50,000	1.05	1.20	1:8	1:7
BE08	Best	50,000	1.05	1.20	1:7	1:6
BE09	Best	75,000	0.75	0.85	1:8	1:7
BE10	Best	75,000	0.75	0.85	1:7	1:6
BE11	Best	75,000	1.05	1.20	1:8	1:7
BE12	Best	75,000	1.05	1.20	1:7	1:6

Table 9.5: Test cases.

Case	Shaft X	Shaft Y	Haul level	Ore pass X	Ore pass Y	Ore pass Top	Haul up from	2nd tip	Haul up from	Costs ($M) Decline haulage	Shaft development	Ore pass development	Haulage drive development	Haulage drive haulage	Total
BA01.0	60344	8981	158	-	-	-	-	-	-	16.2	31.1	0	2.5	3.6	53.4
BA02.0	60344	8981	158	-	-	-	-	-	-	14.2	31.1	0	2.5	3.6	51.4
BA03.0	60398	8967	99	-	-	-	-	-	-	20.4	32.5	0	2.7	5.1	60.8
BA04.0	60398	8967	99	-	-	-	-	-	-	17.9	32.5	0	2.7	5.1	58.3
BA05.0	60244	9006	299	-	-	-	-	-	-	22.5	55.0	0	2.2	3.4	83.1
BA06.0	60244	9006	299	-	-	-	-	-	-	19.7	55.0	0	2.2	3.4	80.3
BA07.0	60311	8989	219	-	-	-	-	-	-	26.0	59.0	0	2.3	4.8	92.1
BA08.0	60311	8989	219	-	-	-	-	-	-	22.8	59.0	0	2.3	4.8	88.9
BA09.0	60109	9040	398	-	-	-	-	-	-	28.5	75.2	0	2.4	3.2	109.2
BA10.0	60109	9040	398	-	-	-	-	-	-	25.0	75.2	0	2.4	3.2	105.7
BA11.0	60234	9008	299	-	-	-	-	-	-	31.5	82.6	0	2.2	4.7	121.0
BA12.0	60097	9043	398	-	-	-	-	-	-	34.9	75.2	0	2.4	4.4	116.9
PR01.0	60437	8958	59	-	-	-	-	-	-	25.2	33.5	0	2.8	7.1	68.6
PR02.0	60398	8967	99	-	-	-	-	-	-	23.2	32.5	0	2.7	7.0	65.4
PR03.0	60437	8958	59	-	-	-	-	-	-	35.4	33.5	0	2.8	9.9	81.6
PR04.0	60437	8958	59	-	-	-	-	-	-	31.0	33.5	0	2.8	9.9	77.2
PR05.0	60320	8987	158	-	-	-	-	-	-	29.5	62.1	0	2.6	6.7	100.9
PR06.0	60320	8987	158	-	-	-	-	-	-	25.8	62.1	0	2.6	6.7	97.3
PR07.0	60398	8967	99	-	-	-	-	-	-	37.2	65.0	0	2.7	9.8	114.7
PR08.0	60398	8967	99	-	-	-	-	-	-	32.6	65.0	0	2.7	9.8	110.1
PR09.0	60301	8992	219	-	-	-	-	-	-	33.8	88.6	0	2.3	6.5	131.1
PR10.0	60301	8992	219	-	-	-	-	-	-	29.6	88.6	0	2.3	6.5	126.9
PR11.0	60310	8989	158	-	-	-	-	-	-	41.3	93.2	0	2.6	9.4	146.5
PR12.0	60310	8989	158	-	-	-	-	-	-	36.2	93.2	0	2.6	9.4	141.4
BE01.0	60513	8939	-21	-	-	-	-	-	-	50.9	35.5	0	2.8	11.4	100.6
BE02.0	60513	8939	-21	-	-	-	-	-	-	44.5	35.5	0	2.8	11.4	94.3
BE03.0	60552	8929	-61	-	-	-	-	-	-	70.1	36.5	0	2.8	16.2	125.6
BE04.0	60513	8939	-21	-	-	-	-	-	-	62.5	35.5	0	2.8	16.0	116.8
BE05.0	60475	8948	19	-	-	-	-	-	-	52.6	69.0	0	2.8	11.3	135.7
BE06.0	60437	8958	59	-	-	-	-	-	-	48.2	67.0	0	2.7	11.1	129.1
BE07.0	60513	8939	-21	-	-	-	-	-	-	71.4	71.0	0	2.8	16.0	161.2
BE08.0	60475	8948	19	-	-	-	-	-	-	64.7	69.0	0	2.8	15.8	152.3
BE09.0	60381	8972	77	-	-	-	-	-	-	56.5	99.2	0	2.7	11.1	169.5
BE10.0	60363	8976	139	-	-	-	-	-	-	54.9	94.6	0	2.3	10.5	162.3
BE11.0	60475	8948	19	-	-	-	-	-	-	73.8	103.6	0	2.8	15.8	195.9
BE12.0	60437	8958	59	-	-	-	-	-	-	67.6	100.6	0	2.7	15.6	186.5

Table 9.6: Results: No ore pass.

	Shaft			Ore pass							Costs ($M)				
Case	X	Y	Haul level	X	Y	Top	Haul up from	2nd tip	Haul up from	Decline haulage	Shaft development	Ore pass development	Haulage drive development	haulage	Total
BA01.1	60477	8948	19	60552	9250	219	139	-	-	10.1	34.5	0.2	2.4	4.7	53.0
BA02.1	60477	8948	19	60552	9250	219	139	-	-	8.8	34.5	0.2	2.4	4.7	51.8
BA03.1	60494	8943	-21	60571	9250	219	99	-	-	12.8	35.5	0.3	2.5	6.8	58.8
BA04.1	60494	8943	-21	60571	9250	219	99	-	-	11.2	35.5	0.3	2.5	6.8	57.3
BA05.1	60344	8981	219	60412	9250	299	259	-	-	18.3	59.0	0.1	2.4	4.4	85.3
BA06.1	60285	8996	278	60349	9250	299	299	-	-	18.7	56.1	0.0	2.6	4.3	82.8
BA07.1	60438	8958	99	60511	9250	219	158	-	-	17.9	65.0	0.1	2.4	6.3	92.8
BA08.1	60438	8958	99	60511	9250	219	158	-	-	15.7	65.0	0.1	2.4	6.3	90.6
BA09.1	60192	9019	358	60250	9250	398	398	-	-	26.2	78.2	0.0	2.7	4.4	112.6
BA10.1	60192	9019	358	60250	9250	398	398	-	-	23.0	78.2	0.0	2.7	4.4	109.3
BA11.1	60279	8997	278	60343	9250	299	299	-	-	29.9	84.2	0.0	2.6	6.0	123.7
BA12.1	60279	8997	278	60343	9250	299	299	-	-	26.2	84.2	0.0	2.6	6.0	120.0
PR01.1	60493	8944	-21	60569	9250	219	99	-	-	16.0	35.5	0.3	2.5	9.2	64.6
PR02.1	60493	8944	-21	60569	9250	219	99	-	-	14.0	35.5	0.3	2.5	9.2	62.6
PR03.1	60527	8935	-101	60606	9250	219	59	-	-	19.2	37.5	0.4	2.6	13.8	74.5
PR04.1	60495	8943	-21	60571	9250	219	99	-	-	19.7	35.5	0.3	2.5	13.0	71.9
PR05.1	60477	8948	19	60553	9250	219	139	-	-	18.0	69.0	0.2	2.4	9.1	99.8
PR06.1	60436	8958	99	60509	9250	219	158	-	-	20.1	65.0	0.1	2.4	8.6	97.3
PR07.1	60495	8943	-21	60571	9250	219	99	-	-	22.5	71.0	0.3	2.5	13.0	110.3
PR08.1	60495	8943	-21	60571	9250	219	99	-	-	19.7	71.0	0.3	2.5	13.0	107.5
PR09.1	60436	8958	99	60509	9250	219	158	-	-	22.9	97.6	0.1	2.4	8.6	132.7
PR10.1	60365	8976	179	60433	9250	299	238	-	-	25.8	91.6	0.1	2.4	8.6	129.5
PR11.1	60459	8952	59	60534	9250	219	139	-	-	28.5	100.6	0.2	2.4	12.4	145.1
PR12.1	60435	8958	99	60508	9250	219	158	-	-	28.1	97.6	0.1	2.4	12.0	141.3
BE01.1	60627	8910	-221	60712	9250	139	-61	-	-	27.5	40.5	0.4	2.7	17.0	89.2
BE02.1	60605	8916	-181	60689	9250	139	-21	-	-	25.9	39.5	0.4	2.6	16.3	85.7
BE03.1	60630	8909	-221	60715	9250	139	-61	-	-	38.6	40.5	0.4	2.6	23.9	107.1
BE04.1	60630	8909	-221	60715	9250	139	-61	-	-	33.8	40.5	0.4	2.6	23.9	102.3
BE05.1	60593	8919	-141	60676	9250	139	19	-	-	31.5	77.0	0.3	2.5	15.8	128.3
BE06.1	60570	8924	-101	60651	9250	139	19	-	-	30.2	75.0	0.3	2.5	15.2	124.2
BE07.1	60608	8915	-181	60692	9250	139	-21	-	-	41.4	79.1	0.4	2.6	22.8	147.3
BE08.1	60595	8918	-141	60678	9250	139	19	-	-	38.7	77.0	0.3	2.5	22.2	141.9
BE09.1	60570	8924	-101	60651	9250	139	19	-	-	34.4	112.6	0.3	2.5	15.2	166.0
BE10.1	60529	8935	-21	60608	9250	139	59	-	-	36.6	106.6	0.2	2.5	14.3	161.1
BE11.1	60595	8918	-141	60678	9250	139	19	-	-	44.2	115.6	0.3	2.5	22.2	185.9
BE12.1	60571	8924	-101	60653	9250	139	19	-	-	42.3	112.6	0.3	2.5	21.3	179.9

Table 9.7: Results: Ore pass with one tipping point.

	Shaft			Ore pass							Costs ($M)				
Case	X	Y	Haul level	X	Y	Top	Haul up from	2nd tip	Haul up from	Decline haulage	Shaft development	Ore pass development	Haulage drive development	haulage	Total
BA01.2	60491	8944	-21	60568	9250	219	158	99	59	8.5	35.5	0.3	2.5	4.8	52.6
BA02.2	60491	8944	-21	60568	9250	219	158	99	59	7.4	35.5	0.3	2.5	4.8	51.6
BA03.2	60523	8936	-101	60602	9250	219	139	59	-21	9.1	37.5	0.4	2.6	7.2	57.7
BA04.2	60494	8943	-21	60571	9250	219	158	99	59	10.4	35.5	0.3	2.5	6.8	56.5
BA05.2	60344	8981	219	60412	9250	299	278	259	238	18.2	59.0	0.1	2.4	4.4	85.2
BA06.2	60324	8986	259	60390	9250	299	299	278	278	17.8	57.0	0.0	2.5	4.4	82.8
BA07.2	60438	8958	99	60511	9250	219	198	158	139	17.8	65.0	0.1	2.4	6.3	92.8
BA08.2	60438	8958	99	60511	9250	219	198	158	139	15.6	65.0	0.1	2.4	6.3	90.6
BA09.2	60231	9009	318	60291	9250	358	358	339	339	23.7	81.2	0.0	2.8	4.5	113.2
BA10.2	60231	9009	318	60291	9250	358	358	339	339	20.8	81.2	0.0	2.8	4.5	110.2
BA11.2	60321	8987	259	60387	9250	299	299	278	278	28.5	85.6	0.0	2.5	6.1	123.7
BA12.2	60321	8987	259	60387	9250	299	299	278	278	25.0	85.6	0.0	2.5	6.1	120.2
PR01.2	60525	8936	-101	60603	9250	219	139	59	-21	11.7	37.5	0.4	2.6	9.9	63.0
PR02.2	60525	8936	-101	60603	9250	219	139	59	-21	10.2	37.5	0.4	2.6	9.9	61.5
PR03.2	60527	8935	-101	60606	9250	219	139	59	-21	16.3	37.5	0.4	2.6	13.8	71.6
PR04.2	60527	8935	-101	60606	9250	219	139	59	-21	14.3	37.5	0.4	2.6	13.8	69.6
PR05.2	60493	8944	-21	60569	9250	219	158	99	59	15.0	71.0	0.3	2.5	9.2	99.0
PR06.2	60477	8948	19	60553	9250	219	179	139	99	15.3	69.0	0.2	2.4	9.1	97.1
PR07.2	60495	8943	-21	60571	9250	219	158	99	59	21.0	71.0	0.3	2.5	13.0	108.8
PR08.2	60495	8943	-21	60571	9250	219	158	99	59	18.4	71.0	0.3	2.5	13.0	106.2
PR09.2	60436	8958	99	60509	9250	219	198	158	139	22.8	97.6	0.1	2.4	8.6	132.6
PR10.2	60348	8980	158	60415	9250	299	259	219	198	24.1	93.2	0.2	2.5	8.5	129.4
PR11.2	60495	8943	-21	60571	9250	219	158	99	59	21.0	106.6	0.3	2.5	13.0	144.3
PR12.2	60435	8958	99	60508	9250	219	198	158	139	28.0	97.6	0.1	2.4	12.0	141.2
BE01.2	60639	8907	-261	60724	9250	139	59	-61	-141	22.0	41.5	0.5	2.7	17.5	85.3
BE02.2	60639	8907	-261	60724	9250	139	59	-61	-141	19.3	41.5	0.5	2.7	17.5	82.6
BE03.2	60667	8900	-341	60755	9250	139	19	-101	-221	26.7	43.5	0.6	3.0	26.3	101.0
BE04.2	60642	8907	-261	60728	9250	139	59	-61	-141	27.1	41.5	0.5	2.7	24.6	97.4
BE05.2	60593	8919	-141	60676	9250	139	77	19	-61	29.8	77.0	0.3	2.5	15.8	126.5
BE06.2	60593	8919	-141	60676	9250	139	77	19	-61	26.1	77.0	0.3	2.5	15.8	122.8
BE07.2	60642	8907	-261	60728	9250	139	59	-61	-141	30.9	83.1	0.5	2.7	24.6	142.8
BE08.2	60608	8915	-181	60692	9250	139	59	-21	-101	33.0	79.1	0.4	2.6	22.8	138.9
BE09.2	60526	8936	-61	60604	9250	219	139	77	19	35.5	109.6	0.3	2.5	15.8	164.7
BE10.2	60502	8942	-21	60579	9250	219	158	99	59	34.7	106.6	0.3	2.5	15.1	160.2
BE11.2	60608	8915	-181	60692	9250	139	59	-21	-101	37.7	118.6	0.4	2.6	22.8	183.1
BE12.2	60595	8918	-141	60678	9250	139	77	19	-61	36.5	115.6	0.3	2.5	22.2	178.2

Table 9.8: Results: Ore pass with two tipping points.

Case	No ore pass Haul level	No ore pass Cost $M	Ore pass with one tipping point Haul level	Ore pass with one tipping point Cost $M	Ore pass with two tipping points Haul level	Ore pass with two tipping points Cost $M	Best option
BA01	158	53.4	19	53.0	-21	52.6	ore pass with two tipping points
BA02	158	51.4	19	51.8	-21	51.6	no ore pass
BA03	99	60.8	-21	58.8	-101	57.7	ore pass with two tipping points
BA04	99	58.3	-21	57.3	-21	56.5	ore pass with two tipping points
BA05	299	83.1	219	85.3	219	85.2	no ore pass
BA06	299	80.3	278	82.8	259	82.8	no ore pass
BA07	219	92.1	99	92.8	99	92.8	no ore pass
BA08	219	88.9	99	90.6	99	90.6	no ore pass
BA09	398	109.2	358	112.6	318	113.2	no ore pass
BA10	398	105.7	358	109.3	318	110.2	no ore pass
BA11	299	121.0	278	123.7	259	123.7	no ore pass
BA12	398	116.9	278	120.0	259	120.2	no ore pass
PR01	59	68.6	-21	64.6	-101	63.0	ore pass with two tipping points
PR02	99	65.4	-21	62.6	-101	61.5	ore pass with two tipping points
PR03	59	81.6	-101	74.5	-101	71.6	ore pass with two tipping points
PR04	59	77.2	-21	71.9	-101	69.6	ore pass with two tipping points
PR05	158	100.9	19	99.8	-21	99.0	ore pass with two tipping points
PR06	158	97.3	99	97.3	19	97.1	ore pass with two tipping points
PR07	99	114.7	-21	110.3	-21	108.8	ore pass with two tipping points
PR08	99	110.1	-21	107.5	-21	106.2	ore pass with two tipping points
PR09	219	131.1	99	132.7	99	132.6	no ore pass
PR10	219	126.9	179	129.5	158	129.4	no ore pass
PR11	158	146.5	59	145.1	-21	144.3	ore pass with two tipping points
PR12	158	141.4	99	141.3	99	141.2	ore pass with two tipping points
BE01	-21	100.6	-221	89.2	-261	85.3	ore pass with two tipping points
BE02	-21	94.3	-181	85.7	-261	82.6	ore pass with two tipping points
BE03	-61	125.6	-221	107.1	-341	101.0	ore pass with two tipping points
BE04	-21	116.8	-221	102.3	-261	97.4	ore pass with two tipping points
BE05	19	135.7	-141	128.3	-141	126.5	ore pass with two tipping points
BE06	59	129.1	-101	124.2	-141	122.8	ore pass with two tipping points
BE07	-21	161.2	-181	147.3	-261	142.8	ore pass with two tipping points
BE08	19	152.3	-141	141.9	-181	138.9	ore pass with two tipping points
BE09	77	169.5	-101	166.0	-61	164.7	ore pass with two tipping points
BE10	139	162.3	-21	161.1	-21	160.2	ore pass with two tipping points
BE11	19	195.9	-141	185.9	-181	183.1	ore pass with two tipping points
BE12	59	186.5	-101	179.9	-141	178.2	ore pass with two tipping points

Table 9.9: Summary and comparison.

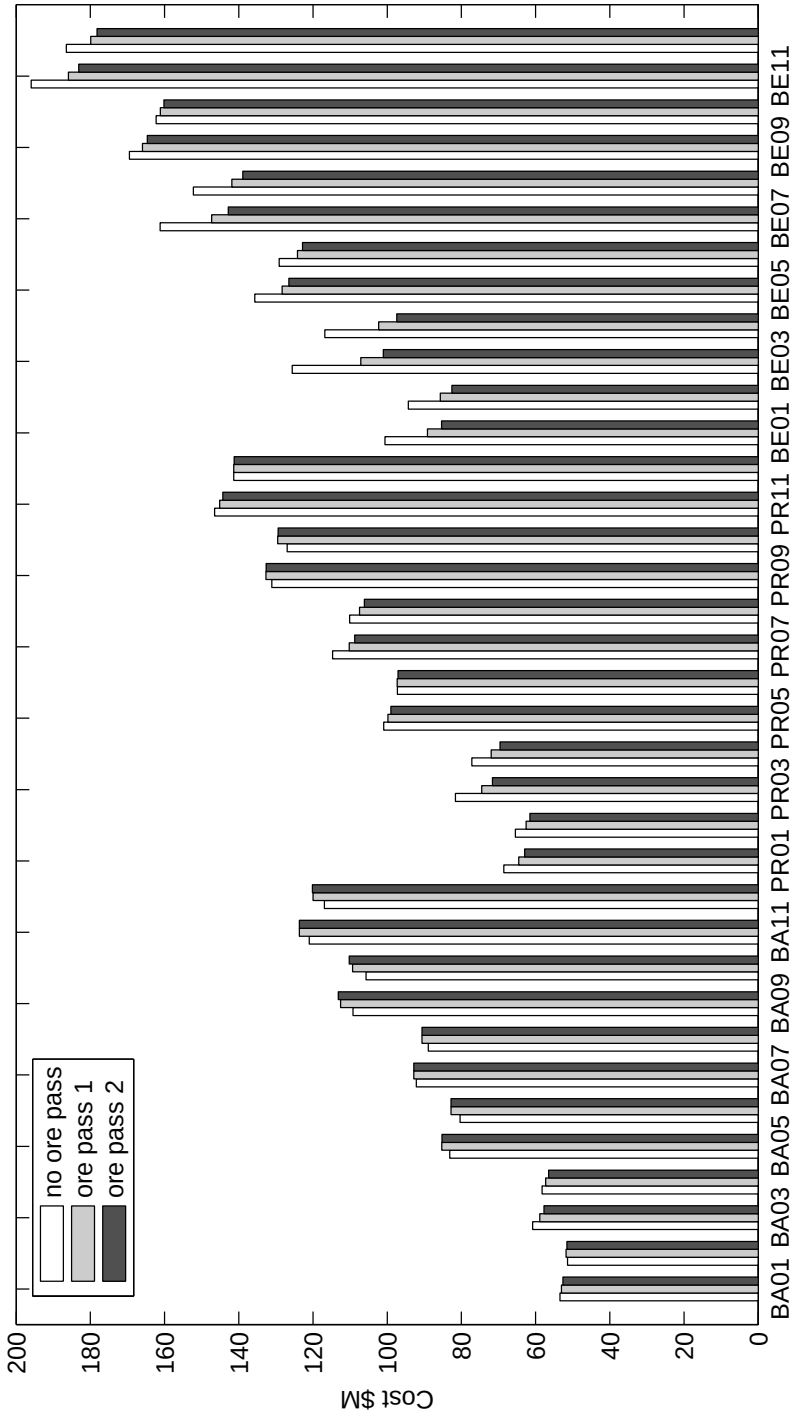

Figure 9.14: Cost comparison chart for optimum solutions.

- For the 'base' schedule, the optimum haul level ranges from 390 m RL to -60 m RL, over 450 vertical metres.
- For the 'probable' schedule, the optimum haul level ranges from 350 m RL to -220 m RL, over 570 vertical metres.
- For the 'best' schedule, the optimum haul level ranges from 310 m RL to -340 m RL, over 650 vertical metres.

9.5.2 Ore pass vs no ore pass

- If an ore pass is justified, it is always economical for it to have two tipping points.
- For the 'base' schedule, an ore pass is not justified, except if the shaft development is $\$25,000/\text{m}$, in which case it is generally more economical to include an ore pass with two tipping points.
- For the 'probable' schedule, an ore pass with two tipping points is justified in all cases except PR08 and PR09 ($\$75,000/\text{m}$ shaft development, $\$0.75/(\text{t.km})$ haulage up, $\$0.85/(\text{t.km})$ haulage down). In these latter cases an ore pass is not justified.
- For the 'best' schedule, an ore pass with two tipping points is always justified.

9.5.3 Shaft and ore pass optimum plan locations

A visual comparison of optimum shaft and ore pass plan locations is provided in Figure 9.16.

- The shaft optimally lies on the orebody standoff boundary between points (60097, 9043) and (60667, 8900), over 588 metres.
- The ore pass optimally lies on 9250N between 60250E and 60755E, over 505 metres.

9.5.4 Breakdown of costs

A breakdown of costs, averaged over all 108 tests, is provided in Figure 9.17. The pie chart shows that shaft development is by far the most significant cost component, followed by decline haulage. This explains why varying the shaft development from

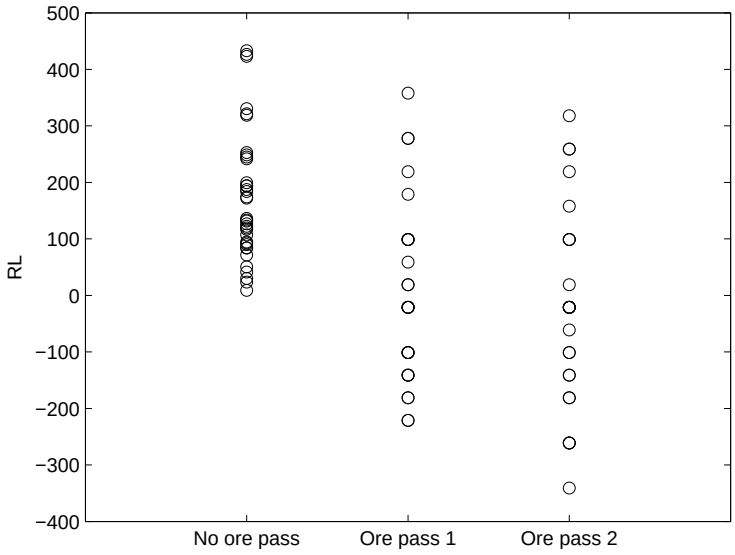

Figure 9.15: Optimum haul levels.

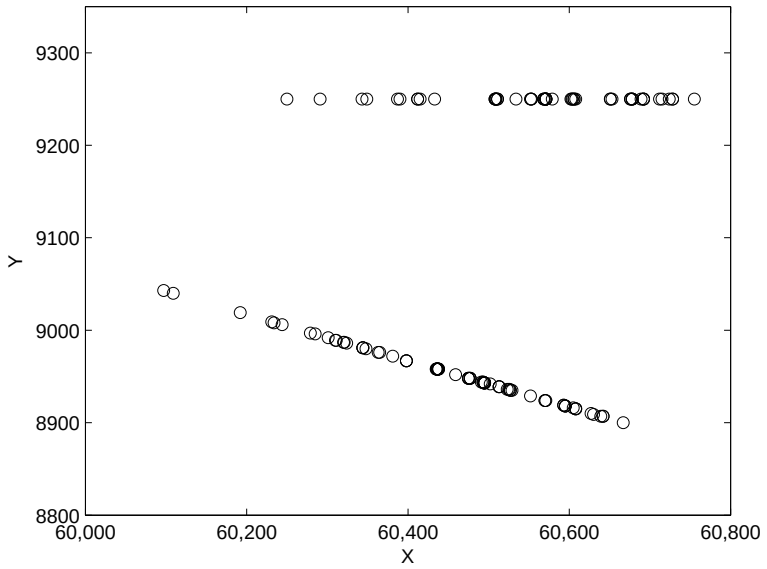

Figure 9.16: Optimum shaft and ore pass locations.

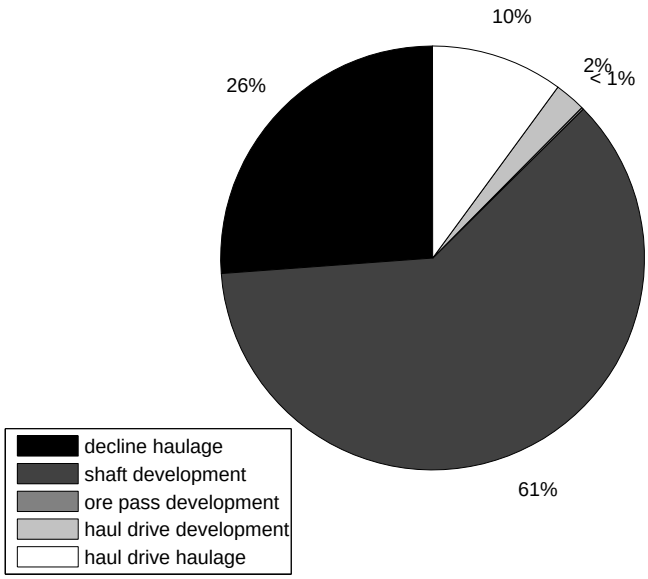

Figure 9.17: Breakdown of costs.

$25,000/m to $50,000/m to $75,000/m has such a significant impact on the shaft depth and the total cost of the mine.

9.5.5 Effects of parameters

We now discuss the effects of changing various parameters on the output of the model.

Shaft development

Table 9.10 summarises optimum haul levels based on shaft development. From the table we make the following observations:

- On average, increasing the shaft development from $25,000/m to $50,000/m causes the optimum haul level to move up by three 40 m levels.
- On average, increasing the shaft development from $50,000/m to $75,000/m causes the optimum haul level to move up by one 40 m level.

Ore pass	Schedule	Optimum haul level range $25,000/m	$50,000/m	$75,000/m
No ore pass	Base	100 to 150	220 to 300	300 to 390
	Probable	60 to 100	100 to 150	150 to 200
	Best	60 to 100	100 to 150	150 to 200
Ore pass 1	Base	-20 to 20	100 to 270	270 to 350
	Probable	-100 to -20	-20 to 100	60 to 180
	Best	-220 to -180	-180 to -100	-180 to -100
Ore pass 2	Base	-100 to -20	100 to 260	260-310
	Probable	-100	-20 to 20	-20 to 150
	Best	-340 to -260	-260 to -140	-180 to -20

Table 9.10: Optimum haul levels based on shaft development costs.

Thus, increasing the shaft development causes a significant decrease in the shaft depth, because the resulting increase in decline haulage is outweighed by the decrease in shaft development.

Ore pass

The following effects of including an ore pass in the model can also be seen from Table 9.10:

- On average, including an ore pass with one tipping point causes the optimum haul level to move down by three levels.
- On average, including an ore pass with two tipping points causes the optimum haul level to move down by seven levels.
- Including an ore pass provides additional savings by reducing decline haulage.
- Provision of a second tipping point introduces further savings.

Providing an ore pass causes the optimum haul level to become lower. This is because decline haulage is fixed for levels serviced by the ore pass, i.e. the cost of decline haulage for these levels is independent of the shaft depth, and is ignored in the model. Hence the shaft tipping level must be lowered to account for the unbalanced haulage, shaft and ore pass vectors. Including additional tipping points causes the shaft depth to increase further. The more ore is dropped down the ore pass, the deeper the shaft will be.

Gradients

The effect of increasing the Callie and WDD gradients from 1:7 and 1:6 to 1:8 and 1:7 respectively is to increase decline haulage costs. If decline haulage costs were very large compared to shaft development, the ore pass and shaft tipping levels would tend to space themselves out over the depth of the mine, so as to minimise the average haulage distance. Consequently the shaft depth would increase. In this study, shaft development is very large compared to decline haulage, and the effect of increasing gradients has little or no effect.

The following observations were noted when the model was run with decline gradients set to zero:

- No ore pass: optimum haul level is 180 m RL.
- Ore pass with one tipping point: optimum haul level is -460 m RL; top of ore pass is 180 m RL; haul up from -180 m RL.
- Ore pass with two tipping points: optimum haul level is -160 m RL; top of ore pass is 180 m RL (haul up from -20 m RL); second tipping point is at -180 m RL (haul up from -300 m RL).

It can be verified that, in all three cases, the haul and ore pass levels have positioned themselves so as to minimise the total haulage cost.

Haulage costs

On average, increasing the decline haulage costs from \$0.75/t.km and \$0.85/t.km for upwards and downwards haulage to \$1.05/t.km and \$1.20/t.km respectively has the effect of lowering the optimum haul level by one 40 m level. The reasons are similar to the reasons for the gradient effects.

9.6 Recommendation

9.6.1 Recommended solutions

Recommended solutions are provided in Table 9.11.

Case	Ore pass?	Shaft X	Shaft Y	Haul level	Ore pass X	Ore pass Y	Ore pass Top	Haul up from	2nd tip	Haul up from	Costs ($M) Decline haulage	Shaft development	Ore pass development	Haulage drive development	Haulage drive haulage	Total
BA01	ore pass 2	60491	8944	-21	60568	9250	219	158	99	59	8.5	35.5	0.3	2.5	4.8	52.6
BA02	no ore pass	60344	8981	158	-	-	-	-	-	-	14.2	31.1	0.0	2.5	3.6	51.4
BA03	ore pass 2	60523	8936	-101	60602	9250	219	139	59	-21	9.1	37.5	0.4	2.6	7.2	57.7
BA04	ore pass 2	60494	8943	-21	60571	9250	219	158	99	59	10.4	35.5	0.3	2.5	6.8	56.5
BA05	no ore pass	60244	9006	299	-	-	-	-	-	-	22.5	55.0	0.0	2.2	3.4	83.1
BA06	no ore pass	60244	9006	299	-	-	-	-	-	-	19.7	55.0	0.0	2.2	3.4	80.3
BA07	no ore pass	60311	8989	219	-	-	-	-	-	-	26.0	59.0	0.0	2.3	4.8	92.1
BA08	no ore pass	60311	8989	219	-	-	-	-	-	-	22.8	59.0	0.0	2.3	4.8	88.9
BA09	no ore pass	60109	9040	398	-	-	-	-	-	-	28.5	75.2	0.0	2.4	3.2	109.2
BA10	no ore pass	60109	9040	398	-	-	-	-	-	-	25.0	75.2	0.0	2.4	3.2	105.7
BA11	no ore pass	60234	9008	299	-	-	-	-	-	-	31.5	82.6	0.0	2.2	4.7	121.0
BA12	no ore pass	60097	9043	398	-	-	-	-	-	-	34.9	75.2	0.0	2.4	4.4	116.9
PR01	ore pass 2	60525	8936	-101	60603	9250	219	139	59	-21	11.7	37.5	0.4	2.6	9.9	63.0
PR02	ore pass 2	60525	8936	-101	60603	9250	219	139	59	-21	10.2	37.5	0.4	2.6	9.9	61.5
PR03	ore pass 2	60527	8935	-101	60606	9250	219	139	59	-21	16.3	37.5	0.4	2.6	13.8	71.6
PR04	ore pass 2	60527	8935	-101	60606	9250	219	139	59	-21	14.3	37.5	0.4	2.6	13.8	69.6
PR05	ore pass 2	60493	8944	-21	60569	9250	219	158	99	59	15.0	71.0	0.3	2.5	9.2	99.0
PR06	ore pass 2	60477	8948	19	60553	9250	219	179	139	99	15.3	69.0	0.2	2.4	9.1	97.1
PR07	ore pass 2	60495	8943	-21	60571	9250	219	158	99	59	21.0	71.0	0.3	2.5	13.0	108.8
PR08	ore pass 2	60495	8943	-21	60571	9250	219	158	99	59	18.4	71.0	0.3	2.5	13.0	106.2
PR09	no ore pass	60301	8992	219	-	-	-	-	-	-	33.8	88.6	0.0	2.3	6.5	131.1
PR10	no ore pass	60301	8992	219	-	-	-	-	-	-	29.6	88.6	0.0	2.3	6.5	126.9
PR11	ore pass 2	60495	8943	-21	60571	9250	219	158	99	59	21.0	106.6	0.3	2.5	13.0	144.3
PR12	ore pass 2	60435	8958	99	60508	9250	219	198	158	139	28.0	97.6	0.1	2.4	12.0	141.2
BE01	ore pass 2	60639	8907	-261	60724	9250	139	59	-61	-141	22.0	41.5	0.5	2.7	17.5	85.3
BE02	ore pass 2	60639	8907	-261	60724	9250	139	59	-61	-141	19.3	41.5	0.5	2.7	17.5	82.6
BE03	ore pass 2	60667	8900	-341	60755	9250	139	19	-101	-221	26.7	43.5	0.6	3.0	26.3	101.1
BE04	ore pass 2	60642	8907	-261	60728	9250	139	59	-61	-141	27.1	41.5	0.5	2.7	24.6	97.0
BE05	ore pass 2	60593	8919	-141	60676	9250	139	77	19	-61	29.8	77.0	0.3	2.5	15.8	126.4
BE06	ore pass 2	60593	8919	-141	60676	9250	139	77	19	-61	26.1	77.0	0.3	2.5	15.8	122.7
BE07	ore pass 2	60642	8907	-261	60728	9250	139	59	-61	-141	30.9	83.1	0.5	2.7	24.6	142.0
BE08	ore pass 2	60608	8915	-181	60692	9250	139	59	-21	-101	33.0	79.1	0.4	2.6	22.8	138.0
BE09	ore pass 2	60526	8936	-61	60604	9250	219	139	77	19	35.5	109.6	0.3	2.5	15.8	164.2
BE10	ore pass 2	60502	8942	-21	60579	9250	219	158	99	59	34.7	106.6	0.3	2.5	15.1	160.2
BE11	ore pass 2	60608	8915	-181	60692	9250	139	59	-21	-101	37.7	118.6	0.4	2.6	22.8	181.8
BE12	ore pass 2	60595	8918	-141	60678	9250	139	77	19	-61	36.5	115.6	0.3	2.5	22.2	177.6

Table 9.11: Recommended solutions by case.

9.6.2 Possible improvements to the model

The provision of more than two tipping points could potentially result in further savings, although the additional cost of developing tunnels from the declines to the ore pass must be considered. Moreover, experiments have indicated that having two ore passes, one for each decline, reduces haulage and development costs associated with the haulage drive which, on average, account for about 12% of the total variable cost of the mine.

Confining the ore pass to be fixed on the northing between the two declines has the effect of increasing the main haulage drive development and haulage costs. The increase, however, is not significant.

Chapter 10

Conclusion

10.1 Overview

GRADIENT-CONSTRAINED flow-dependent networks and their application to underground mining were studied. Two problems were considered: the Fermat-Weber problem, which asks for a point minimising the sum of weighted distances to a set of given points, and the Gilbert arborescence problem, which asks for a minimum-cost flow-dependent network interconnecting given sources and a unique sink. The problems were studied in three settings: Euclidean space, Minkowski spaces and gradient-constrained space. Aspects from both problems were used to mathematically determine an optimum location and depth of a vertical hoisting shaft in the Callie underground mine.

10.2 Summary of new contributions

In this section we repeat the list of the new contributions of this thesis. This list was originally presented in Chapter 1. Contributions are listed in order of appearance, with section numbers indicating where the point is first discussed in the thesis. Published, submitted and forthcoming papers are shown in parentheses.

10.2.1 The Fermat-Weber problem

Euclidean space

1. A new characterisation of Fermat-Weber points for collinear sets of given points was developed (Section 2.3).
2. New results were derived for the case where the given points form the vertices of a convex polygon, and certain pairs of weights are equal (Section 2.5).
3. A previously unstudied variant of the Fermat-Weber problem in the plane was introduced, whereby one of the given points is allowed to lie anywhere on an infinite line in the plane. The problem was applied to a subproblem of the Callie shaft location study (Section 2.7).

Minkowski spaces [84]

1. Practical methods were developed for determining the dual ball for a given unit ball (Section 3.2.1).
2. The term *balanced double cluster* was introduced to depict weighted sets of given points satisfying special properties. It was shown that if a Fermat-Weber point for a set N of given points lies outside the convex hull of N, then N is a balanced double cluster (Section 3.4.2).
3. The term *balanced concurrent segments* was introduced to depict weighted sets of given points satisfying special properties. It was shown that if a set N of given points can be matched up to form balanced concurrent segments, then the intersection of these segments is the set of Fermat-Weber points for N (Section 3.5.1).
4. The study of the Fermat-Weber problem for a given set of weighted *cogeodesic* points was initiated. A new characterisation of Fermat-Weber points for weighted collinear and cogeodesic sets was developed (Section 3.5.2).
5. A new geometric property of the solution to the weighted three-point problem in the plane was discovered (Section 3.6).

Gradient-constrained space [14], [84]

1. The *gradient-constrained Fermat-Weber problem* was introduced (Section 4.1).
2. For the first time, gradient-constrained space was treated as a Minkowski space. The unit ball, dual ball and dual norm were derived, and a practical method for determining sets of norming functionals was developed (Section 4.2).
3. A new gradient descent algorithm was developed for solving the problem iteratively. The algorithm was implemented into a software product (Section 4.3).
4. Convergence was proved for the two- and three-dimensional cases (Section 4.4).
5. The problem was applied to a simplified version of the Callie shaft location study (Section 4.5).

10.2.2 The Gilbert arborescence problem

Euclidean space [81]

1. A new title, the *Gilbert arborescence problem*, was given to the special case of the Gilbert network problem in which flows are from given sources to a unique sink. At present, this problem has been studied only in a handful of papers (Section 5.1).
2. It was shown that a minimum Gilbert arborescence has a tree topology, i.e. it has no cycles or crossing edges (Section 5.3).
3. Necessary and sufficient conditions for a Steiner point to be locally minimal with respect to its adjacent vertices were established (Section 5.4).
4. It was shown that the degree of all Steiner points in minimum Gilbert arborescences in the Euclidean plane is three (Section 5.5).
5. Good progress was made on proving the conjecture that the degree of Steiner points in minimum Gilbert arborescences in Euclidean three-space is three (Section 5.6).
6. Expressions for the optimum angles between edges incident to a Steiner point were determined. The notions of *critical and absorbing angles* were generalised to the Gilbert arborescence problem (Section 5.7).
7. Exact and approximate algorithms for solving the Gilbert arborescence problem in

Euclidean space were discussed (Section 5.8).

Minkowski spaces [80]

1. The study of the Gilbert arborescence problem in Minkowski spaces was initiated. (Section 6.1).
2. Concepts of parenthesisations, abstract Steiner trees and reduced Minkowski addition were generalised to the weighted case (Section 6.3).
3. Necessary and sufficient conditions for a terminal to be locally minimal with respect to its adjacent vertices were established (Section 6.4).
4. Necessary and sufficient conditions for a Steiner point to be locally minimal with respect to its adjacent vertices were established (Section 6.5).

Gradient-constrained vertical plane [82]

1. The *gradient-constrained Gilbert arborescence problem* (in a vertical plane) was introduced (Section 7.1).
2. A range of fundamental properties of gradient-constrained minimum Gilbert arborescences (in a vertical plane) was established. In particular, it was shown that the degree of Steiner points is either three or four (Section 7.3).
3. It was shown that a degree-three Steiner point has seven feasibly optimal labellings: (fff), (ffm), (ffb), (fmm), (fmb), (mmm) and (mmb) (Section 7.4).
4. It was shown that a degree-four Steiner point has three feasibly optimal labellings: (ffmm), (fmmm) and (mmmm) (Section 7.5).
5. The *reduced hull* of a set N of terminals was defined. It was shown that all Steiner points lie in the reduced hull of N (Section 7.6).

Gradient-constrained three-space [82]

1. The *gradient-constrained Gilbert arborescence problem* (in three-space) was introduced (Section 8.1).

2. A range of fundamental properties of gradient-constrained minimum Gilbert arborescences (in three-space) was established (Section 8.3).
3. It was shown that a degree-three Steiner point has seven feasibly optimal labellings: (fff), (ffm), (ffb), (fmm), (fmb), (mmm) and (mmb) (Section 8.4).
4. It was shown that a degree-four Steiner point has four feasibly optimal labellings: (fffm), (ffmm), (fmmm) and (mmmm) (Section 8.5).
5. It was shown that there is no upper bound on the degree of Steiner points (Section 8.6).

10.2.3 Callie shaft location study [83]

1. Aspects from the Fermat-Weber problem and the Gilbert arborescence problem were used to develop a network model for the Callie underground mine (Section 9.1).
2. An algorithm was developed to mathematically determine an optimum location and depth of a vertical hoisting shaft in the Callie underground mine. The algorithm was implemented into a software product (Section 9.3).
3. Results were analysed over a range of infrastructure and haulage costs, decline gradients and life-of-mine schedules (Section 9.5).

10.3 Future research

Some ideas for further research relating to material presented in this thesis are provided below.

10.3.1 Gradient-constrained problems for $m > 1$

Many of the fundamental properties of gradient-constrained networks established in this thesis have been obtained under the assumption that $m \leq 1$. The properties of gradient-constrained networks for $m > 1$ are quite different. We have already made some progress on this topic. We have shown that the labellings (ffb) and (ffm) are feasibly optimal for

degree-three Steiner points in gradient-constrained Steiner minimum trees, even for trees in the vertical plane. Also, it seems that for $m > \sqrt{3}$ the labelling (fmm) is no longer feasibly optimal.

10.3.2 Flow-dependent networks with general cost functions

Throughout our work on flow-dependent networks we have assumed that the cost of an edge is a function of flow, where the function satisfies several stated conditions for Gilbert networks. It would be interesting to investigate flow-dependent networks whose cost functions do not satisfy these conditions, such as networks with the function $w(t) = d + ht^2$. It seems likely that the fundamental properties of flow-dependent networks with these cost functions would be markedly different to the properties of networks whose cost functions satisfy the conditions for Gilbert networks.

Appendix A

Mathematical Symbols

d	development cost per unit length, typically in \$/m
e	an edge in a network
$f(\cdot)$	the Fermat-Weber function
$g(\cdot)$	the absolute value of the gradient of an edge or line
h	haulage cost per unit mass per unit length, typically in \$/(t.km)
k	the number of given points or terminals
l	the length of an edge, line or geodesic
m	maximum gradient
n	the dimension of a space
o	the origin
p, q	given points or terminals
s	a Steiner point
t	a quantity of ore, typically in tonnes
$\mathbf{u}$	a unit normal vector
$\mathbf{v}$	a weighted scaled unit normal vector
$w(\cdot)$	a cost function satisfying the conditions for Gilbert networks
x, y, z	Catersian coordinate system, where the z-axis is vertical

A	a set of norming functionals
B	a unit ball
B^*	a dual ball
$C(\cdot)$	the cost of a network
D	a diagonal line
E	the set of edges in a network
H	a hyperplane
L	a line
N	a set of given points or terminals
S	a half-space
T	a network with a tree topology
$\mathcal{C}$	a cone whose generating lines have maximum gradient
$\mathcal{H}_s$	the horizontal plane through a Steiner point s
$\mathcal{V}_s$	a special vertical plane through a Steiner point s
$\mathcal{P}$	an arbitrary vertical plane
α, β, γ	angles, where α is typically $\tan^{-1}(m)$
δ	the distance from o to a supporting hyperplane of B
ϵ	a precision
$\rho(\cdot, \cdot)$	a metric
ϕ	a norming functional
ψ	the acute angle between an m-edge and an m-edge vector
Σ	a set of operands
$\langle\Sigma\rangle$	a parenthesisation of Σ
$\mathbb{R}^n$	n-dimensional Euclidean space
$\|\cdot\|$	a norm
$\lvert\cdot\rvert$	Euclidean distance
$\lvert\cdot\rvert_g$	the norm from which the gradient metric is derived

Appendix B
Useful Identities

Let m be a maximum allowable gradient satisfying $0 < m \leq 1$, and let $\alpha = \tan^{-1}(m)$. The following relationships between m and α are easily obtainable using simple trigonometry.

Identities involving α:

$$\sin\alpha = \frac{m}{\sqrt{1+m^2}} = \frac{1}{\sqrt{1+m^{-2}}} \tag{B.1}$$

$$\cos\alpha = \frac{1}{\sqrt{1+m^2}} = \frac{1}{m\sqrt{1+m^{-2}}} \tag{B.2}$$

$$\tan\alpha = m \tag{B.3}$$

Identities involving 2α:

$$\sin(2\alpha) = \frac{2m}{1+m^2} = \frac{2}{m(1+m^{-2})} \tag{B.4}$$

$$\cos(2\alpha) = \frac{1-m^2}{1+m^2} = \frac{m^{-2}-1}{1+m^{-2}} \tag{B.5}$$

$$\tan(2\alpha) = \frac{2m}{1-m^2} = \frac{2}{m^{-2}-1} \tag{B.6}$$

Bibliography

[1] M. Alfaro, M. Conger, K. Hodges, A. Levy, R. Kochar, L. Kuklinski, Z. Mahmood, and K. von Haam, "The structure of singularities in Φ-minimizing networks in $\mathbf{R}^2$," *Pacific Journal of Mathematics*, vol. 149, no. 2, pp. 201–210, 1991.

[2] C. Alford, M. Brazil, and D. H. Lee, "Optimisation in underground mining," in *Handbook on Operations Research in Natural Resources*. New York: Springer-Verlag, 2007, pp. 561–577.

[3] C. Bajaj, "The algebraic degree of geometric optimization problems," *Discrete and Computational Geometry*, vol. 3, no. 2, pp. 177–191, 1988.

[4] S. Bhaskaran and F. J. M. Salzborn, "Optimal design of gas pipeline networks," *The Journal of the Operational Research Society*, vol. 30, no. 12, pp. 1047–1060, 1979.

[5] S. Boyd and L. Vandenberghe, *Convex Optimization*. New York: Cambridge University Press, 2004.

[6] S. Boyd, L. Xiao, and A. Mutapcic, "Subgradient methods," Oct. 2003, Notes for EE392o, Stanford University. [Online]. Available: http://www.stanford.edu/class/ee392o/subgrad_method.pdf

[7] M. Brazil, P. A. Grossman, D. H. Lee, J. H. Rubinstein, D. A. Thomas, and N. C. Wormald, "Constrained path optimisation for underground mine layout," in *International Conference of Applied and Engineering Mathematics*, London, Jul. 2007, pp. 856–861.

[8] M. Brazil, D. H. Lee, J. H. Rubinstein, D. A. Thomas, J. F. Weng, and N. C. Wormald, "Network optimisation of underground mine design," in *The Australasian Institute of Mining and Metallurgy Proceedings*, vol. 305, no. 1, 2000, pp. 57–65.

[9] ——, "A network model to optimise cost in underground mine design," *Transactions of the South African Institute of Electrical Engineers*, vol. 93, no. 2, pp. 97–103, 2002.

[10] ——, "Optimisation in the design of underground mine access," in *Orebody Modelling and Strategic Mine Planning: Uncertainty and Risk Management*, ser. Spectrum Series, R. Dimitrakopoulos, Ed., vol. 14. Australasian Institute of Mining and Metallurgy, 2005, pp. 121–124.

[11] M. Brazil, D. H. Lee, M. van Leuven, J. H. Rubinstein, D. A. Thomas, and N. C. Wormald, "Optimising declines in underground mines," in *Mining Technology: Transactions of the Institute of Mining and Metallurgy, Section A*, vol. 112, 2003, pp. 164–170.

[12] M. Brazil, B. K. Nielsen, D. A. Thomas, M. G. Volz, and M. Zachariasen, "Geometric constructions of weighted Euclidean Steiner trees with given full topologies," working paper.

[13] M. Brazil, J. H. Rubinstein, D. A. Thomas, J. F. Weng, and N. C. Wormald, "Gradient-constrained minimum networks. I. Fundamentals," *Journal of Global Optimization*, vol. 21, no. 2, pp. 139–155, 2001.

[14] M. Brazil, J. H. Rubinstein, and M. Volz, "The gradient-constrained Fermat-Weber problem for underground mine design," in *Proceedings of the 18th National ASOR Conference and 11th Australian Optimisation Day*, L. Caccetta and V. Rehbock, Eds., Perth, Sep. 2005, pp. 16–23.

[15] M. Brazil and D. A. Thomas, "Network optimization for the design of underground mines," *Networks*, vol. 49, no. 1, pp. 40–50, 2007.

[16] M. Brazil, D. A. Thomas, and J. F. Weng, "Gradient-constrained minimum networks. II. Labelled or locally minimal Steiner points," submitted 2005.

[17] ——, "Gradient-constrained minimal Steiner trees," in *Network Design: Connectivity and Facilities Location*, ser. DIMACS Series in Discrete Mathematics and Theoretical Computer Science, P. M. Pardalos and D. Du, Eds. American Mathematical Society, 1998, vol. 40, pp. 23–38.

[18] M. Brazil, D. A. Thomas, J. F. Weng, J. H. Rubinstein, and D. H. Lee, "Cost optimisation for underground mining networks," *Optimization and Engineering*, vol. 6, no. 2, pp. 241–256, 2005.

[19] M. Brazil and M. Zachariasen, "Steiner trees for fixed orientation metrics," *Journal of Global Optimization*, to appear 2008.

[20] J. Brimberg, "The Fermat-Weber location problem revisited," *Mathematical Programming*, vol. 71, no. 1, pp. 71–76, 1995.

[21] J. Brimberg, H. Juel, and A. Schöbel, "Linear facility location in three dimensions—models and solution methods," *Operations Research*, vol. 50, no. 6, pp. 1050–1057, 2002.

[22] G. D. Chakerian and M. A. Ghandehari, "The Fermat problem in Minkowski spaces," *Geometriae Dedicata*, vol. 17, no. 3, pp. 227–238, 1985.

[23] R. Chandrasekaran and A. Tamir, "Open questions concerning Weiszfeld's algorithm for the Fermat-Weber location problem," *Mathematical Programming*, vol. 44, pp. 293–295, 1989.

[24] D. Cieslik, *Steiner Minimal Trees*. The Netherlands: Kluwer Academic Publishers, 1998.

[25] E. J. Cockayne, "On the Steiner problem," *Canadian Mathematical Bulletin*, vol. 10, pp. 431–450, 1967.

[26] R. Courant and H. Robbins, *What is Mathematics?* New York: Oxford University Press, 1941.

[27] C. L. Cox, "Flow-dependent networks: Existence and behavior at Steiner points," *Networks*, vol. 31, no. 3, pp. 149–156, 1998.

[28] Z. Drezner and H. W. Hamacher, Eds., *Facility Location : Applications and Theory*. Berlin: Springer, 2004.

[29] D.-Z. Du, B. Gao, R. L. Graham, Z.-C. Liu, and P.-J. Wan, "Minimum Steiner trees in normed planes," *Discrete and Computational Geometry*, vol. 9, no. 1, pp. 351–370, 1993.

[30] D.-Z. Du and F. K. Hwang, "Reducing the Steiner problem in a normed space," *SIAM Journal on Computing*, vol. 21, no. 6, pp. 1001–1007, 1992.

[31] R. Durier and C. Michelot, "Geometrical properties of the Fermat-Weber problem," *European Journal of Operational Research*, vol. 20, no. 3, pp. 332–343, 1985.

[32] ——, "On the set of optimal points to the Weber problem: further results," *Transportation Science*, vol. 28, no. 2, pp. 141–149, 1994.

[33] H. Edelsbrunner and T.-S. Tan, "A quadratic time algorithm for the minmax length triangulation," *SIAM Journal on Computing*, vol. 22, no. 3, pp. 527–551, 1993.

[34] E. N. Gilbert, "Minimum cost communication networks," *The Bell System Technical Journal*, vol. 46, pp. 2209–2227, 1967.

[35] E. N. Gilbert and H. O. Pollak, "Steiner minimal trees," *SIAM Journal on Applied Mathematics*, vol. 16, no. 1, pp. 1–29, 1968.

[36] I. Gódor, "Special properties of the Fermat-problem applied to local topology optimization," *Periodica Polytechnica: Electrical Engineering Series*, vol. 48, no. 3–4, pp. 119–132, 2004.

[37] I. Greenberg and R. A. Robertello, "The three factory problem," *Mathematics Magazine*, vol. 38, no. 2, pp. 67–72, 1965.

[38] S. Gueron and R. Tessler, "The Fermat-Steiner problem," *The American Mathematical Monthly*, vol. 109, no. 5, pp. 443–451, 2002.

[39] M. Hanan, "On Steiner's problem with rectilinear distance," *SIAM Journal on Applied Mathematics*, vol. 14, no. 2, pp. 255–265, 1966.

[40] F. K. Hwang, "A linear time algorithm for full Steiner trees," *Operations Research Letters*, vol. 4, no. 5, pp. 235–237, 1986.

[41] ——, "A primer of the Euclidean Steiner problem," *Annals of Operations Research*, vol. 33, pp. 73–84, 1991.

[42] F. K. Hwang, D. S. Richards, and P. Winter, *The Steiner Tree Problem*, ser. Annals of Discrete Mathematics. North Holland: Elsevier Science Publishers, 1992, vol. 53.

[43] F. K. Hwang and J. F. Weng, "The shortest network under a given topology," *Journal of Algorithms*, vol. 13, no. 3, pp. 468–488, 1992.

[44] G. Jalal and J. Krarup, "Geometrical solution to the Fermat problem with arbitrary weights," *Annals of Operations Research*, vol. 123, no. 1–4, pp. 67–104, 2003.

[45] V. Jarník and O. Kossler, "O minimálních grafech obsahujících n daných bodu," *Ćas. Pêstování Mat.*, vol. 63, pp. 223–235, 1934.

[46] H. Juel and R. F. Love, "The solution of location problems with certain existing facility structures," *Canadian Journal of Operational Research and Information Processing*, vol. 21, no. 2, pp. 145–150, 1983.

[47] J. Krarup and S. Vajda, "On Torricelli's geometrical solution to a problem of Fermat," *IMA Journal of Management Mathematics*, vol. 8, no. 3, pp. 215–224, 1997.

[48] H. W. Kuhn, "Locational problems and mathematical programming," in *Colloquium on the Application of Mathematics to Economics*, A. Prekopa, Ed. Budapest: Akademiai Kiado, 1963, pp. 235–242.

[49] ——, "On a pair of dual nonlinear programs," in *Methods of Nonlinear Programming*, J. Abadie, Ed. North Holland: North Holland Publishing, 1967, pp. 37–54.

[50] ——, "A note on Fermat's problem," *Journal Mathematical Programming*, vol. 4, no. 1, pp. 98–107, 1973.

[51] ——, ""Steiner's" problem revisited," in *Studies in Optimization*, ser. Studies in Mathematics, G. B. Dantzig and B. C. Eaves, Eds., 1974, vol. 10, pp. 52–70.

[52] H. W. Kuhn and R. E. Kuenne, "An efficient algorithm for the numerical solution of the generalized Weber problem in spatial economics," *Journal of Regional Science*, vol. 4, no. 2, pp. 21–33, 1962.

[53] Y. S. Kupitz and H. Martini, "Geometric aspects of the generalized Fermat-Torricelli problem," in *Intuitive Geometry*, ser. Bolyai Society Mathematical Studies, I. Bárány and K. Boroczky, Eds. Budapest: Janos Bolyai Mathematical Society, 1997, vol. 6, pp. 55–127.

[54] G. R. Lawlor and F. Morgan, "Paired calibrations applied to soap films, immiscible fluids, and surfaces and networks minimizing other norms," *Pacific Journal of Mathematics*, vol. 166, no. 1, pp. 55–83, 1994.

[55] D. H. Lee, "Some industrial case studies of Steiner trees," unpublished paper presented at NATO Workshop on Topological Network Design, Denmark, 1989.

[56] ——, "Low cost drainage networks," *Networks*, vol. 6, pp. 351–371, 1976.

[57] H. Lerchs and I. F. Grossmann, "Optimum design of open-pit mines," *Transactions of the Canadian Institute of Mining and Metallurgy*, vol. LXVIII, pp. 17–24, 1965.

[58] Y. Lizotte and J. Elbrond, "Optimal layout of underground mining levels," *The Canadian Institute of Mining, Metallurgy and Petrolium Bulletin*, vol. 78, no. 873, pp. 41–48, 1985.

[59] *VULCAN Basics*, V6_ITM06, Maptek Pty Limited, 2007.

[60] H. Martini, K. J. Swanepoel, and G. Weiss, "The Fermat-Torricelli problem in normed planes and spaces," *Journal of Optimization Theory and Applications*, vol. 115, no. 2, pp. 283–314, 2002.

[61] Z. A. Melzak, "On the problem of Steiner," *Canadian Mathematical Bulletin*, vol. 4, pp. 143–148, 1961.

[62] F. Plastria, "Four-point Fermat location problems revisited. New proofs and extensions of old results," *IMA Journal of Management Mathematics*, vol. 17, no. 4, pp. 387–396, 2006.

[63] K. Prendergast, "Steiner ratio for gradient constrained networks," Ph.D. dissertation, Department of Electrical and Electronic Engineering, The University of Melbourne, Australia, Apr. 2006.

[64] K. Prendergast, D. A. Thomas, and J. F. Weng, "Optimum Steiner ratio for gradient-constrained networks connecting three points in 3-space," *Networks*, submitted 2006.

[65] R. T. Rockafellar, *Convex Analysis*. Princeton, New Jersey: Princeton University Press, 1970.

[66] J. H. Rubinstein, "Issues about weighted networks," 2005, unpublished research note.

[67] J. H. Rubinstein and D. A. Thomas, "A variational approach to the Steiner network problem," *Annals of Operations Research*, vol. 33, pp. 481–499, 1991.

[68] D. Sankoff and P. Rousseau, "Locating the vertices of a Steiner tree in an arbitrary metric space," *Mathematical Programming*, vol. 9, pp. 240–246, 1975.

[69] N. Z. Shor, *Minimization Methods for Non-Differentiable Functions*. Berlin; New York: Springer-Verlag, 1985.

[70] K. J. Swanepoel, "Vertex degrees of Steiner minimal trees in ℓ_p^d and other smooth Minkowski spaces," *Discrete and Computational Geometry*, vol. 21, pp. 437–447, 1999.

[71] ——, "Balancing unit vectors," *Journal of Combinatorial Theory Series A*, vol. 89, no. 1, pp. 105–112, 2000.

[72] ——, "The local Steiner problem in normed planes," *Networks*, vol. 36, pp. 104–113, 2000.

[73] ——, "The local Steiner problem in finite-dimensional normed spaces," *Discrete and Computational Geometry*, vol. 37, no. 3, pp. 419–442, 2007.

[74] D. A. Thomas, M. Brazil, D. H. Lee, and N. C. Wormald, "Network modelling of underground mine layout: Two case studies," *International Transactions in Operational Research*, vol. 14, no. 2, pp. 143–158, 2007.

[75] D. A. Thomas and J. F. Weng, "Minimum cost flow-dependent communication networks," *Networks*, vol. 48, no. 1, pp. 39–46, 2006.

[76] ——, "Gradient-constrained minimum networks: An algorithm for computing Steiner points," *Journal of Discrete Optimization*, submitted 2006.

[77] A. C. Thompson, *Minkowski Geometry*, ser. Encyclopedia of Mathematics and its Applications. Cambridge; New York: Cambridge University Press, 1996, vol. 63.

[78] D. Trietsch, "Minimal Euclidean networks with flow dependent costs — The generalized Steiner case," May 1985, Discussion Paper No. 655.

[79] W. J. van de Lindt, "A geometrical solution of the three factory problem," *Mathematics Magazine*, vol. 39, no. 3, pp. 162–165, 1966.

[80] M. G. Volz, M. Brazil, and D. A. Thomas, "Flow-dependent networks in Minkowski spaces," Forthcoming.

[81] ——, "The Gilbert arborescence problem in Euclidean space," Forthcoming.

[82] ——, "Gradient-constrained flow-dependent networks," Forthcoming.

[83] ——, "Strategic optimisation of a vertical hoisting shaft in the Callie underground mine," Forthcoming.

[84] ——, "The gradient-constrained Fermat-Weber problem," *Geometriae Dedicata*, submitted July 2008.

[85] A. Weber, *Uber den Standort der Industrien.* Tubingen: Verlag J. C. B. Mohr, 1909, (Translation by C. J. Friedrich: *Theory of the Location of Industries*, Chicago: University of Chicago Press, 1929).

[86] E. Weiszfeld, "Sur le point pour lequel la somme des distances de n points donnés est minimum," *Tohoku Mathematical Journal*, vol. 43, pp. 355–386, 1937.

[87] C. Witzgall, "Optimal location of a central facility: Mathematical models and concepts," National Bureau of Standards, Tech. Rep. 8388, 1964.

[88] G. L. Xue, G.-H. Lin, and D.-Z. Du, "Grade of service Steiner minimum trees in the Euclidean plane," *Algorithmica*, vol. 31, pp. 479–500, 2001.

[89] C. Zalinescu, *Convex Analysis in General Vector Spaces*. Singapore; New Jersey: World Scientific, 2002.